TECNOLÓGICO DE MONTERREY, CAMPUS CIUDAD DE MÉXICO

DOCTORAL THESIS

Sliding Mode Control for Doubly Fed Induction Machine

Author:
Iván Villanueva

Advisor:
Dr. Pedro Ponce

Co-advisor:
Dr. Arturo Molina

A thesis submitted in fulfillment of the requirements for the degree of Doctor of Philosophy

in the

Mechatronic Engineering Systems and Product Innovation

Escuela de Ingeniería y Ciencias

December 1, 2017

Declaration of Authorship

I, Iván Villanueva, declare that this thesis titled, "Sliding Mode Control for Doubly Fed Induction Machine" and the work presented in it are my own. I confirm that:

- This work was done wholly or mainly while in candidature for a research degree at this University.
- Where any part of this thesis has previously been submitted for a degree or any other qualification at this University or any other institution, this has been clearly stated.
- Where I have consulted the published work of others, this is always clearly attributed.
- Where I have quoted from the work of others, the source is always given. With the exception of such quotations, this thesis is entirely my own work.
- I have acknowledged all main sources of help.
- Where the thesis is based on work done by myself jointly with others, I have made clear exactly what was done by others and what I have contributed myself.

Signed:

Date:

"Optimism is the faith that leads to achievement; nothing can be done without hope and confidence."

Helen Keller

TECNOLÓGICO DE MONTERREY, CAMPUS CIUDAD DE MÉXICO

Abstract

Escuela de Ingeniería y Ciencias

Doctor of Philosophy

Sliding Mode Control for Doubly Fed Induction Machine

by Iván Villanueva

The objective of this thesis is to provide robust control methods for Doubly Fed Induction Generator (DFIG) mainly used for wind energy conversion systems (WECS). The controller deals with the power electronic stage needed to control the electric machine. Due to the high sensibility of this machine against disturbances the systems requires an accurate controller that allows to follow the stator power regulation despite the presence of disturbances.

DFIG-based WECS are highly sensible to stator voltage perturbations because the stator is directly connected to the electric grid. The offered controller can regulate torque and reactive power even during low depth voltage dips by injecting negative sequence current without the necessity of sequence components separation of the rotor current.

The proposed control system is based on Sliding-Mode Control (SMC), offering a fast-dynamic response and providing insensitivity to matched and bounded disturbance/uncertainties. The naturally discontinuous control signals of SMC can be used for direct switching of power electronic devices avoiding modulation and making the control system simple and robust. Furthermore, the controller does not depend on electric machine's parameters and it is decoupled by means of reference frame orientation.

The switching frequency is analyzed using a frequency-domain method known as Tsypkin's locus, therefore it is possible to calculate a hysteresis width which will maintain the switching frequency inside safe operational range preventing to exceed the maximum switching frequency of semiconductor devices.

The dynamic response of the control system under balanced and unbalanced voltage faults is enhanced by the application of demagnetizing current for fast natural flux clearance. The demagnetizing current is supplied using the original controller by modifying the torque and reactive power references.

The operation of the controller and the ideas presented in this thesis have been verified through simulations made in National Instruments™ LabVIEW and Matlab Simulink®.

Acknowledgements

This research project has been carried out at the mechatronics engineering systems and product innovation development group at Tecnologico de Monterrey, Mexico City Campus. Thanks to the financial support from grant 266632 “Bi-national Laboratory on Smart Sustainable Energy Management and Technology Training” from CONACYT.

I would like to thank my advisors Dr. Pedro Ponce and Dr. Arturo Molina for their unfailing support, assistance, inspiration and encouragement. I also would like to express my gratitude to Dr. Antonio Rosales whose valuable help has greatly contributed to the culmination of this thesis work.

I would like to thank my fellow doctoral students and postdoctoral researchers for they feedback, cooperation and friendship.

Finally, I must express my profound gratitude to my parents Gil Villanueva and Lina Rosas for their love and support along the way.

Contents

List of Figures

List of Abbreviations

DFIG	**D**oubly **F**ed **I**nduction **G**eneration
SMC	**S**liding **M**ode **C**ontrol
WECS	**W**ind **E**nergy **C**onversion **S**ystem
RES	**R**enewable **E**nergy **S**ources
IM	**I**nduction **M**achine
SCIG	**S**quirrel **C**age **I**nduction **G**enerator
WRIG	**W**ound **R**otor **I**nduction **G**enerator
PMSG	**P**ermanent **M**agnet **S**ynchronous **G**enerator
EESG	**E**lectrically **E**xited **S**ynchronous **G**enerator
VSWT	**V**ariable **S**peed **W**ind **T**urbine
FSWT	**F**ixed **S**peed **W**ind **T**urbine
EMF	**E**lectro **M**otive **F**orce
RSC	**R**otor-**S**ide **C**onverter
GSC	**G**rid-**S**ide **C**onverter
PI	**P**roportional, **I**ntegral
DTC	**D**irect **T**orque **C**ontrol
DPC	**D**irect **P**ower **C**ontrol
FRT	**F**ault **R**ide **T**hrough
HAWT	**H**orizontal **A**xis **W**ind **T**urbine
LSS	**L**ow **S**peed **S**haft
HSS	**H**igh **S**peed **S**haft
IGBT	**I**nsulated **G**ate **B**ipolar **T**ransistor
PLL	**P**hase **L**ocked **L**oop
PWM	**P**ulse **W**idth **M**odulation
SVM	**S**pace **V**ector **M**odulation
GVO	**G**rid **V**oltage **O**riented
FESS	**F**lywheel **E**nergy **S**torage **S**ystem

List of Symbols

v	Voltage	[V]
i	Current	[A]
λ	Magnetic Flux	[Wb]
s, r	Stator, rotor subindex	
d, q	Direct, quadrature reference frame subindex	
α, β	Alpha, beta reference frame subindex	
L_m	Magnetic inductance	[H]
L_{ls}	Stator leakage inductance	[H]
L_s	Stator inductance	[H]
L_{lr}	Rotor leakage inductance	[H]
L_r	Rotor inductance	[H]
P	Number of pole pairs	
P_s, Q_s	Stator active, reactive power	[W,VAr]
T_{em}	Electromagnetic torque	[N·m]
ω_s	Synchronous speed	[rad/s]
θ_{sf}	Stator flux angular position	[rad]
ω_m	DFIG's electrical angular speed	[rad/s]
Ω_m	Mechanical speed at HSS	[rad/s]
ω_L	Mechanical speed at LSS	[rad/s]
θ_m	Rotor mechanical angle	[rad]
s	Slip	
ω_r	Rotor electrical speed	[rad/s]
K_e	Kinetic energy	[J]
P_{wt}	Aerodynamic power	[W]
T_{wt}	Aerodynamic torque	[N·m]
C_P	Power coefficient	
γ	Pitch angle	[°]
Λ	Tip-speed ratio	
ρ	Air density	[kg/m^3]
A	Turbine transverse area	[m^2]
r	Turbine radius	[m]
V	Wind speed	[m/s]
η	gearbox ratio	
J_{wt}	Wind turbine inertia	[kg·m^2]
J_g	Electric generator inertia	[kg·m^2]
D_{wt}	Damping coefficient at rotor shaft	[N·m·s]
D_g	Damping coefficient at generator shaft	[N·m·s]
K_S	Spring torsional stiffness	[N·m]
D_S	Spring damping coefficient	[N·m·s]

To my parents.

Chapter 1

Introduction

1.1 Background

Renewable energy has experienced a remarkable expansion during the last years. Most economically developed countries have created plans to accelerate the development and deployment of renewable energy sources [1]. The priority is to reduce prices in technologies, installation and maintenance so renewable could withstand traditional sources prices without the necessity of government financing.

Among Renewable Energy Sources (RES), wind energy represents the most important energy source in terms of installed capacity (not considering hydro power) and it is the leading source of new power generating capacity in Europe, United States and the second largest in China [1]. In 2015 the new global installed capacity increased approximately 64 GW, a new record. In 2016 the increment was about 54 GW for a global total of approximately 487 GW [1], [2].

Nowadays, the major fuels for primary energy productions are oil, natural gas and coal. During 2015, 309.6 TWh of energy were generated in Mexico from which approximately 50% of the total energy was generated by combined cycle, followed by 13 % by traditional thermoelectric plants, 11 % by coal, 10 % generated by hydroelectric, 4% by nuclear, 4% by gas turbines, 2 % by geothermal, 3% by wind and less than 1% solar [3]. In figure 1.1 it is displayed the contribution percentage of each generation technology during 2015. With the low contribution of RES (not considering hydroelectric), they can be relegated to negative loads since the traditional generation units are much larger. The renewable energy potential in Mexico is high, the probed potential of power generation through biomass, solar and wind are 3.3, 25.1 and 25.1 TWh/year respectively [4]. Moreover, the Mexican government has the objective of achieving 35 % of electric energy generated by renewable sources by 2024 [5], [6].

The Mexican government electric energy subsidy has risen 45% this year for a budget of 43 billion Mexican pesos (approximately 2.39 billion dollars) [7], despite the subsidy, the average domestic rates are 25% higher than in the United States because the prices of production are very high [8]. With the government subside used to maintain the domestic prices low it could be possible to support the development and installation of RES to reduce the generation prices caused by fuel-oil based generators [8].

When the penetration of RES to the electric grid is large, strict technical requirements are necessary for supporting the electric grid in case of contingency. In European countries, the regulation typically known as "grid codes" are necessary for

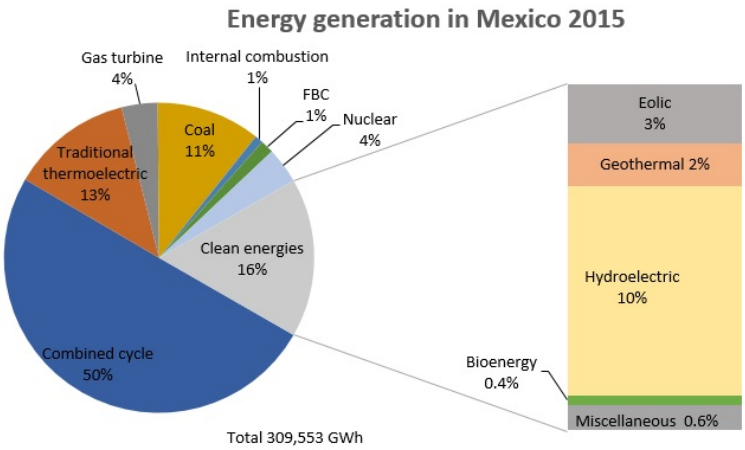

FIGURE 1.1: Electric generation in Mexico during 2015, adapted from [3].

TABLE 1.1: Drive train wind turbines classification.

Type	Features		
	Generator	Power Converter	Transmission
A	SCIG	Without	Geared, high-speed at the machine
B	WRIG	Without	Geared, high-speed at the machine
C	DFIG	Partially rated	Geared, high-speed at the machine
D	PMSG	Full	Direct-drive, low-speed at the machine
E	PMSG / EESG	Full	Geared, medium/high speed at the machine
F	SCIG	Full	Geared, high speed at the machine

connecting new generation units with the electric grid. Grid codes cover topics as voltage operating range, power factor regulation, frequency operating range and grid support capability and fault ride-through capability [9], [10].

Wind energy cost widely varies with the wind resource, regulatory and fiscal framework, capital cost and other miscellaneous factors. On 2016 there were record low bids in tenders in Chile, India, Mexico and Morocco, furthermore, offshore wind was the most cost-effective option for new grid-based power in many markets including Brazil, Canada, Mexico, Morocco, South Africa, Turkey, Australia, China, Europe and United States [11].

Wind turbines can be classified depending on the drive train configuration and the electric generator used, i.e. Squirrel Cage Induction Generator (SCIG), Wound Rotor Induction Generator (WRIG), Doubly Fed Induction Generator (DFIG), Permanent Magnet Synchronous Generator (PMSG) and Electrically Excited Synchronous Generator (EESG); with geared or direct driven transmission trains. In Table 1.1 it is shown the classification of wind turbines by drive train configuration [1].

Fixed Speed Wind Turbines (FSWT) cover type A and type B turbines, type A is the most primitive version of modern wind turbines, operating at constant speed using either stall or pitch control and having only one optimal operation point. Type

B has a little more expanded speed range but it requires large resistors having significant power losses and increased maintenance schedule because of the brushes. These configurations cannot fulfill the requirements of grid codes and are not recommended for large wind turbines due to the difficulties limiting mechanical loads and drive train oscillation [12]. In the recent years almost no new FSWT were installed [1].

Variable Speed Wind Turbines (VSWT) are more economically viable in the long term because they can operate at maximum power point tracking but require a power converter and control system. Since 2000, DFIG became the most commonly used generator in WECS due to the benefits of variable-speed operation requiring only a partial-rated converter, but this topology uses slip rings, which increases maintenance [12]. Type D, and F are robust in construction and have a larger operational speed, however, the required full-size converter and for permanent magnet machines the rare earth elements make configurations type D and E a very expensive. Siemens has launched type F wind turbines with great success especially in offshore applications. The SCIG is well known for its robustness, low maintenance and simplicity, however, this topology consumes reactive power which must be supplied by the power converter.

Nowadays most of the units in operation are based on type C configuration and the new installed onshore units cover near 50% of the installed capacity using type C turbines in Europe and 75% in the rest of the world [1]. Although type C wind turbine is the most economical solution, the direct connection of the stator with the electric grid makes this configuration very sensitive to voltage perturbations [13]–[15].

When an abrupt voltage variation appears in the stator of a DFIG, the stator flux is directly affected. Depending on the type of fault and its starting time, the stator flux can be separated in two, a permanent flux due to the voltage applied and a natural flux, which naturally decays exponentially with the time constant of the machine [16]. If not attention is taken to the natural flux, very large voltages may be induced in the rotor windings. When the induced electromotive force is larger than the DC-link voltage, it is said that the converter is saturated and it can be severely affected by the uncontrolled current flowing though the rotor windings.

Feedback control is an useful alternative to improve the performance of DFIG generators in presence of electric faults since it is possible to face low depth faults without disconnecting the generator from the grid [17], [18]. SMC is a robust control technique capable to provide insensitivity against bounded disturbance/uncertainties and finite-time convergence [19]. Furthermore, the discontinuous nature of SMC fits with the direct control of power converters, avoiding modulation of the control signal.

1.2 Review of related works

DFIG has the main advantage of partially rated converter, typically less than 30 % of the nominal power of the machine, since the rotor needs bidirectional power flow, a back-to-back power converter configuration is used. The Rotor-Side converter (RSC)

controls stator active and reactive power, while the Grid-Side converter (GSC) regulates DC-link voltages and unity power factor operation.

Control of DFIG are typically based on vector control oriented in either the stator flux or grid voltage direction. The orientation decouples rotor current into active power (or torque) and reactive power control loops. The regulation of the rotor current is normally made using Proportional Integral (PI) controllers. The reference rotor current is obtained from a cascaded control loop which regulates active and reactive power. This relatively simple control structure has the disadvantages of tedious tuning of PI controllers because the system is complex and non-linear. The performance of PI controllers depends greatly on the correct machine parameters estimation which may change with the temperature of the machine or saturation of the magnetic core [20]. The output control signal is continuous and needs to be modulated to be injected to the electric machine by the rotor-side power converter.

Other well known control strategy is known as Direct Torque Control (DTC) introduced by T. Noguchi and I. Takahashi [21], [22] and M. Depenbrock [23] in 1984 for the induction machine. Latter Direct Power Control (DPC) was developed by T. Noguchi [24] using the same principles of DTC. DPC was adapted for the DFIG by L. Xu in 2006 [25]. DTC has fast dynamic response, simple structure and it is robust against parameter variations. The desired references are controlled directy with hysteresis controllers and a switching table which dictates the desired switching state. However, the switching frequency of this technique is variable and normally thumb rules are used to select the hysteresis width value.

Although vector control and DTC have good performance under normal conditions, DFIG is particularly sensitive to voltage variations. When the stator flux is altered, the interaction with the rotor flux can create torque oscillations that may severely affect blades shaft and transmission system. For direct control techniques, if the rotor-side controller is not designed to work under disturbances the stator currents may become non-sinusoidal compromising stability of the electric grid [26]. The capacity to withstand voltage variations and provide grid support during and after a fault is called Fault Ride Through (FRT) capability and it is a requirement to interconnect new generation units to the electric grid [9]. In Figure 1.2, different FRT techniques for DFIG are summarized.

1.2.1 FRT capability solutions using vector control

An study of the voltage recovery after short circuit faults of grid connected DFIG is presented in [49]. The first attempt to mitigate active and reactive power fluctuations was done by T. Brekken [50] using a high gain compensation controller, it is known that the torque disturbance will appear at twice the grid frequency, therefore a compensation control with a gain bandwidth designed at 100 Hz was implemented reducing torque and reactive power oscillation. It was also demonstrated by experimentation that "reducing the reactive power pulsation dramatically improves the unbalance of the stator current".

The theoretical analysis of the behavior of DFIG under unbalanced condition was developed using synchronous components theory by López J. et al. [16] in which is demonstrated that the negative sequence component is the origin of active and reactive power oscillation during unbalanced conditions, and that natural flux is a

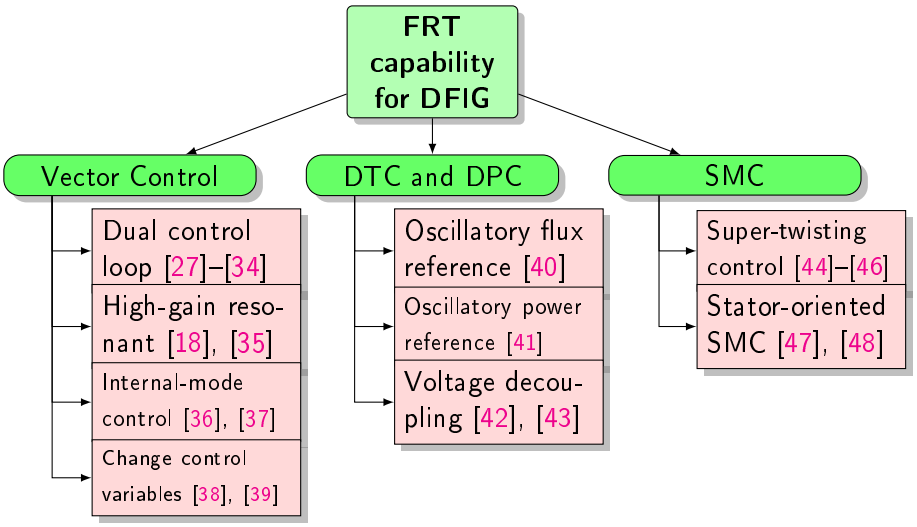

FIGURE 1.2: FRT classification for DFIG.

transient which appears because stator flux cannot abruptly change. With independent control of negative and positive sequence rotor current it is possible to achieve several control objectives depending on the priorities of the designer e.g. reduce stator current unbalance, eliminate torque oscillations, active power oscillation and reduce rotor current unbalance [15].

There are several examples of dual sequence vector control using filters for decoupling positive and negative sequence current applying traditional PI control [27]–[32] and linear quadratic regulator control [33], [34]. Although theoretically oscillation can be perfectly canceled, filtering generates a delay of the current signals, furthermore, PI controller tunning is tedious and highly dependent on system parameters. Therefore there are other solutions for example, using high gain resonant controllers for symmetrical [51] and asymmetrical faults [18], [35]. A fuzzy logic system trained using genetic algorithms is presented in [52]. A supervisory controller which uses a hysteresis-based controller if a fault is detected, otherwise traditional PI is implemented [53], [54]. Internal mode control for enhancing the dynamic behavior of the machine under fault conditions [36], [37]. Controlling power angle instead of the traditional references [38]. Rotor flux tracking instead of active power [39].

The natural flux may cause high oscillatory rotor voltages and currents, the PI control bandwidth were analyzed in [55] for avoiding unstability during voltage sags, however, rotor voltage demand is very high and could not be supported by the RSC. One way to eliminate natural flux is use demagnetizing current and then continue with the support to the electric grid [56]–[58]. When the required demagnetizing current is larger than the maximum rotor current, hardware solutions (crowbar for example) are necessary for avoiding permanent damage to the RSC. The concept of virtual rotor resistance was introduced in [59] to limit the rotor current without using a crowbar.

1.2.2 FRT capability solutions using direct control methods

Direct control techniques could be considered a special type of SMC, in [60] it was demonstrated that DTC for Induction Machine (IM) can be derived using singular perturbation method and a first order SMC. The IM has different time-scale properties for the torque and flux regulator therefore, analyzing the IM via singular perturbation method both references can be controlled independently.

DTC and DPC are robust methods which are able to maintain the power references even under unbalanced conditions without sequence component extraction. However, if the rotor flux is maintained constant (DTC will indeed maintain flux constant), the stator current will be severely affected. On the other hand, it is impossible to cancel out torque and active power oscillations at the same time [26], so DPC is not a good solution during grid faults since it will provoke high frequency torque oscillation which may severely affect the drive train specially for large wind turbines.

In [40], [41] the power references are modified in such way that the rotor flux reference is oscillatory for DTC while the active power reference is oscillatory for DPC with the idea of maintain torque and active power constant during unbalanced conditions. It has been demonstrated that maintaining a constant ratio between rotor and stator fluxes is a good way to enhance sinusoidal current exchange with the electric grid [26].

On the other hand, in [42], [43] the stator voltage is decoupled in symmetrical components and different control objectives like constant sinusoidal stator current, constant electromagnetic torque and constant active power are considered. The control strategy is simpler than vector control since the rotor current is not decoupled in symmetrical components and no modulation is required.

1.2.3 FRT capability solutions using SMC

SMC has arisen as an alternative robust control strategy which can be used in several electromechanical systems [61]. The natural outputs of SMC are discontinuous as many relayed based systems, for example power converters. Therefore is a good alternative for electric machines control. In this subsection a review of the most important works using SMC for control of DFIG is presented.

In [44]–[46] continous second order sliding mode controllers are presented and tested under unbalanced conditions, however the modulation stage is not considered and the natural flux is also omitted, therefore it is not possible to validate the effectiveness of the presented strategy in a real situation.

Another proposal is to use the discontinuous control signal of SMC for direct switching of the power converter. In [47], [48] is presented a stator-oriented SMC for DFIG which is tested under unbalanced and harmonic distorted grid, the controller is robust enough to regulate the references even during voltage disturbances, however, the natural flux is ignored. If the natural flux transient response it is not studied, the controller may cause unstable conditions due to lack of natural flux damping.

1.3 Motivation

Most vector control strategies for enhancing FRT capability of DFIG require sequence decoupling in both stator voltage and rotor current, worse yet, the decoupling is made using band-pass filter which generates delays in the controlled variable affecting the performance of the control system.

Although there are other proposals using internal mode control and high-gain resonant controllers for avoiding decoupling in rotor current, the regulators are highly dependent on system parameters, which may vary with temperature, saturation of the electric machine core, etc. Besides, vector control strategies require modulation techniques to be implementable in a power converter, adding complexity and not-modeled dynamics to the control system.

The control objectives of DTC and DPC are harmful for the operation of the machine under unbalanced conditions. In case of DTC, to maintain the rotor flux magnitude constant while the stator flux is perturbed generates non-sinusoidal current exchange with the electric grid. DPC on the other hand, provokes torque oscillation by forcing the active power to be constant. Therefore DTC and DPC are not suitable to work under unbalanced conditions in their original form.

SMC for DFIG has been presented oriented to the stator, this orientation implies coupling of the control objectives making difficult to limit the switching frequency of the power converter. Additionally, the natural flux damping may be compromised by the control objectives, which has been ignored in the previous SMC-based proposals.

1.4 Proposal summary

The main objective of this thesis is enhance DFIG behavior under both balanced and unbalanced stator voltage perturbation. A Grid-Voltage-Oriented (GVO) SMC is proposed, the orientation is made for decoupling active and reactive power like vector control. Moreover, the controller is not dependent on system parameters, does not need modulation, has simple structure, it is robust against bounded system disturbances and can control torque and reactive power under unbalanced conditions without sequence decomposition of the rotor current.

The grid-voltage controller is stable in all the regimen of operation of the electric machine making the proposal useful for supporting the electric grid by injecting reactive power in case of contingencies.

The controller uses a hysteresis-based comparator to reduce commutation frequency of the power converter. The controller is characterized in both, the time domain using the equivalent control concept and an adaptable hysteresis width and in the frequency domain using Tsypkin's method to calculate the commutation frequency of the power converter ensuring safe operation during all the operational zones of the electric machine. The frequency domain solution does not require additional sensors giving a well-founded selection of the hysteresis width of the control system.

The proposed SMC is tested considering balanced and unbalanced voltage dips faults. Depending on the voltage dip type and the dip starting time, a transient natural flux may appear in the stator, therefore the torque and reactive power references are modified to inject a demagnetizing current for restoring stator flux. The proposal offers a simple and robust DFIG controller with FRT capability.

The operation of the controller and the ideas presented in this thesis have been verified through simulations made in National Instruments™ LabVIEW and Matlab Simulink®.

Simulations were performed in

1.5 List of publications

Some of the results presented in this thesis have been published in the following works:

Villanueva, I., Torres, E., Balderas, D., Ponce, P., & Molina, A. (2017). Supervisory controller for smoothing wind turbine power output based on FESS using ANNs for short-term ahead prediction. *Journal of Modern Power Systems and Clean Energy*. Springer. **Manuscript under review.**

Villanueva, I., Ponce, P., & Molina, A. (2015). Interval type 2 fuzzy logic controller for rotor voltage of a doubly-fed induction generator and pitch angle of wind turbine blades. *IFAC-PapersOnLine*, 48(3), 2195-2202.

Villanueva, I., Ponce, P., Molina, A., & MacCleery, B. (2016). Grid-side inverter thermal cycling analysis of 1.6 MW Doubly-Fed Induction Generation wind turbine and life-time estimation. In *Power Electronics (CIEP), 2016 13th International Conference on* (pp. 329-334). IEEE.

Villanueva, I., Rosales, A., Ponce, P., & Molina, A. (2017).Grid-Voltage-Oriented Sliding Mode Control for DFIG Under Balanced and Unbalanced Grid Faults. *IEEE Transactions on Sustainable Energy*. IEEE.

Villanueva, I., Rosales, A., Ponce, P., & Molina, A. (2017). Stator-flux-oriented sliding mode controller for DFIG with variable hysteresis loop for limiting switch frequency of rotor-side power converter. *In Industrial Technology (ICIT), 2017 IEEE International Conference on* (pp. 213-218). IEEE.

Villanueva, I., Rosales, A., Ponce, P., & Molina, A. (2017). Frequency domain characterization of statator-flux-oriented SMC for DFIG using Tsypkin's Method. *Electrical Engineering, Computer Science and Automatic Control (CCE), 2017 IEEE International Conference on*. IEEE. **Accepted, unpublished.**

Villanueva, I., Rosales, A., Ponce, P., & Molina, A. (2017). Stator Flux Oriented Sliding Mode Control for Doubly Fed Induction Generator. In *Adaptive Robust Control and its Application*. InTech. **Chapter accepted, unpublished.**

1.6 Thesis structure

This thesis is organized as follows:

- Chapter 1 introduces the thesis, a review of the most important strategies for enhance FRT capability is presented. The main issues of the previous proposals are highlighted in the motivation subsection and the solution based on SMC is briefly described.

- Chapter 2 presents the dynamic model of DFIG-based wind turbines and describes the classical proposals based on vector control and DTC. At the end the behavior of DFIG under unbalanced grid voltage is studied.

- Chapter 3 presents some author's research works based on vector control. The manuscripts presents a general modeling and control of a DFIG-based wind turbine.

- Chapter 4 presents a novel control strategy based on SMC for DFIG. The proposed controller is tested under unbalanced grid conditions and characterized in the time and frequency domain.

- Chapter 5 concludes this research work highlighting the contributions of the presented manuscripts, giving a general conclusion of the proposal and suggesting related future research.

Chapter 2

Dynamic Modeling and Control of Wind Energy Conversion Systems

The pioneers models of wind turbines were based on squirrel cage induction machine and stall-pitch control, this turbines were developed in the 1970's and widely used during the next two decades until the advantages of variable-speed wind turbines became evident [12].

Horizontal Axis Wind Turbines (HAWT) are widely used in the wind industry because they have greater efficiency compared with other configurations. HAWT have a rotor with mounted blades for converting aerodynamic lifting force into torque. Most HAWT have a gearbox which turns the slow rotational speed of the rotor and blades into a high-speed rotation more suitable for electric generators. Some models include a yaw control system to orient the turbine in the wind direction. In Figure 2.1 is displayed a generic structure of a HAWT.

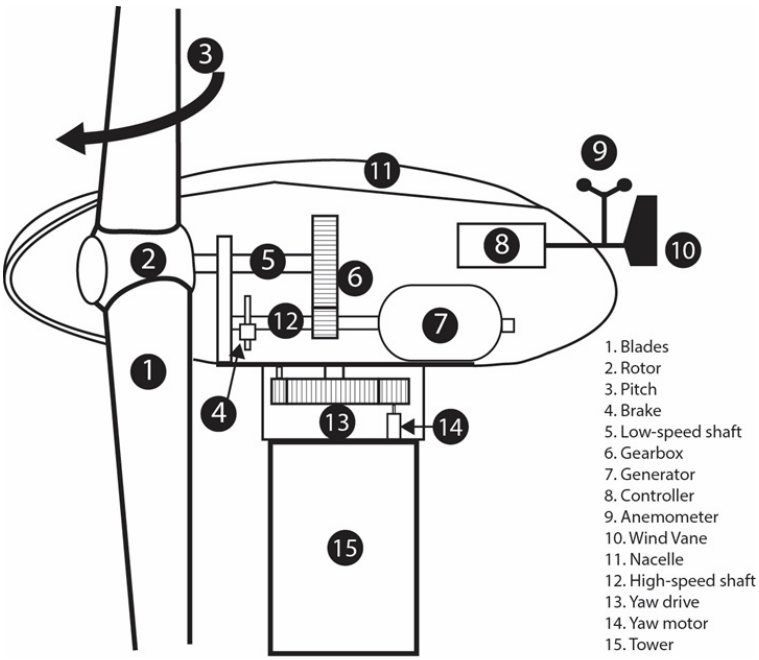

FIGURE 2.1: General structure of a HAWT

The power available in the wind is a function of the cube of the wind speed. The air power is obtaining considering the kinetic energy available in the air particles ($K_e = \frac{1}{2}mV^2$) and the air mass with a density equal to ρ flowing through a surface

of area A. The aerodynamic power available for extraction from the wind can be calculated using the well known equation:

$$P_{wt} = \frac{1}{2} C_P(\Lambda, \gamma) \rho A V^3 \tag{2.1}$$

where C_P is the power coefficient, which is the fraction of the total energy that can be extracted from the wind, the maximum achievable value is known as the Lenchester-Betz limit and has a value of $16/27 = 0.593$ [62], modern wind turbines have power coefficients near 0.4. The power coefficient is a function of the tip-speed ratio (Λ) and the pitch angle (γ). Note that the radius is selected depending on the desired power of the wind turbine and the average speed of the location. The manufacturers design their wind turbines for specific wind classes. Wind classes are determined by the average wind speed, the extreme 50-year gusts and the wind turbulence. Wind classes are defined in the IEC 61400-1 [63].

The tip speed ratio is defined as the speed at blade's tip divided by the wind speed perpendicular to the turbine:

$$\Lambda = \frac{\Omega_m r}{\eta V} \tag{2.2}$$

where Ω_m is the rotational speed of the high-speed shaft, r is the radius of the blades and η is the gearbox ratio.

2.1 Blades model

It is well known that the lifting force of the wind turbine blades is responsible of the torque applied to the rotor. It is necessary to maintain the tip speed ratio at the optimal value to maximize the lifting force of the blades and extract the maximum energy from the wind. Nevertheless, if the extracted power is larger than the nominal power of the wind turbine, it is necessary to limit power extraction for avoiding damage to the turbine, there are two ways to limit the power extraction, one is by designing of the blades to stall when the wind speed is beyond the nominal which is called active stall control and the other way is by installing actuators to change the angle between the chord line of the blade and the relative wind direction, which is called pitch control [64]. Pitch control is the most commonly used method for large wind generators. An accepted model for the power coefficient is the following [65]:

$$C_P = c_1 \left[c_2 \chi - c_3 \gamma - c_4 \gamma^x - c_5 \right] e^{-c_6 \chi} \tag{2.3}$$

$$\chi = \frac{1}{\Lambda + 0.08\gamma} - \frac{0.035}{1 + \gamma^3} \tag{2.4}$$

where $c_1 - c_6$ and x are coefficients obtained from experimental results. Λ and γ are the tip speed ratio and the pitch angle respectively. Figure 2.2 shows the power coefficient for a blade with the parameters presented in Apendix A, the optimal tip speed ratio is 8 and the nominal pitch angle is zero degrees:

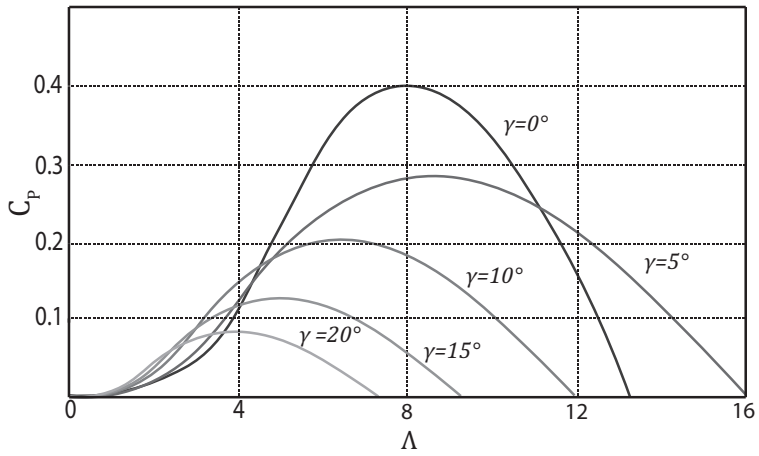

FIGURE 2.2: Power-coefficient of the blades model.

2.2 Transmission system

The mechanical power extracted by the wind turbine needs to be transmitted to the electric generation to convert mechanical into electrical energy. The transmission system can be seen as a two input, one output system, where the inputs are the aerodynamic torque T_{wt} and electromagnetic torque T_{em} and the output is the mechanical speed Ω_m. The considerations taken for this work are power losses due to friction proportional to the mechanical speed and 100% efficiency in the torque-speed conversion.

2.2.1 Rigid drive train model

The most simple case is to consider a rigid coupling between speed multipliers, in this case the transmission system can be modeled as a first-order equation, refereed to either the Low-Speed Shaft (LSS) or the High-Speed Shaft (HSS) [66].

In Figure 2.3 it is displayed a representation of a simple rigid drive train model considering blades angular inertia, power losses due to friction, a torque-speed converter and inertia of the generator.

Due to the speed multiplier the HSS speed is increased η times while the torque is reduced η times, the power is maintained constant and the transmission model can be expressed rendered either at HSS (see equation 2.5) or at LSS (see equation 2.6):

$$J_H \frac{d\Omega_m}{dt} = \frac{1}{\eta} T_{wt} - T_{em} - D_H \Omega_m \tag{2.5}$$

$$\frac{J_L}{\eta} \frac{d\Omega_m}{dt} = T_{wt} - \eta T_{em} - \frac{D_L}{\eta} \Omega_m \tag{2.6}$$

where T_{wt} is the aerodynamic torque, η is the gearbox ratio, T_{em} the electromagnetic torque and Ω_m the mechanical speed at the HSS.

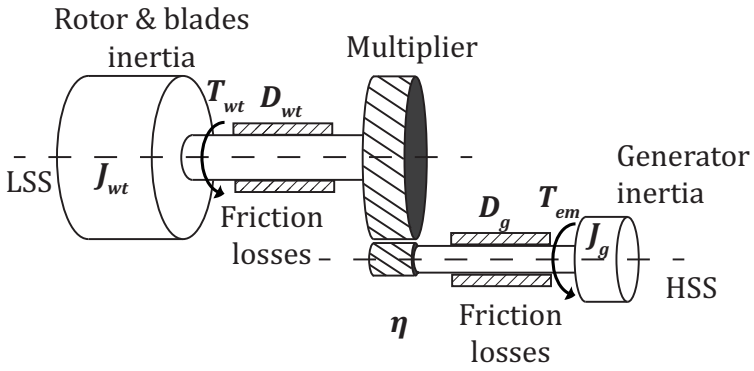

FIGURE 2.3: Rigid transmission train model

The total inertia and damping coefficients rendered at HSS (J_H, D_H) and LSS (J_L, D_L) are computed as follows:

$$J_H = \frac{1}{\eta^2} J_{wt} + J_g \tag{2.7}$$

$$D_H = \frac{1}{\eta} D_{wt} + D_g \tag{2.8}$$

$$J_L = \eta^2 J_g + J_{wt} \tag{2.9}$$

$$D_L = \eta D_g + D_{wt} \tag{2.10}$$

The resulting system is a first-degree linear equation usually known as "single-mass WECS model".

2.2.2 Flexible drive train model

In Figure 2.4 it is displayed a representation of a flexible drive train model considering blades angular inertia, power losses due to friction, the torque-speed converter, shaft stiffness and inertia of the generator.

When the mechanical torsion due to the shaft stiffness is considered, the generator

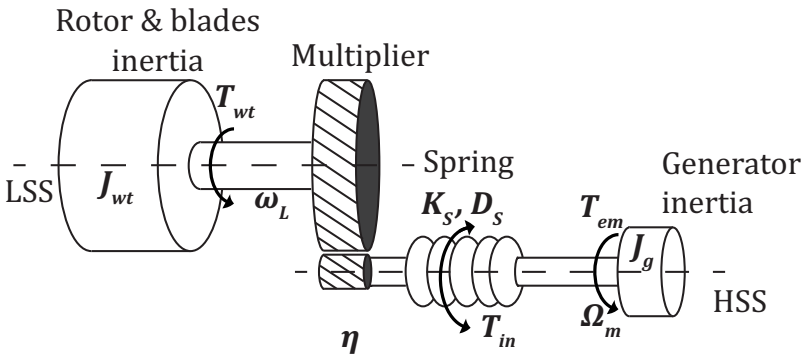

FIGURE 2.4: Flexible transmission train model

and blade's rotor will have different rotational speed which cannot be simply related with the gearbox ratio. For solving this issue the system is analyzed using an imaginary torque inside the shaft T_{in}, then the dynamics of the system can be represented

with the following set of equations [66]:

$$\frac{d\omega_L}{dt} = \frac{1}{J_{wt}} T_{wt} - \frac{\eta}{J_{wt}} T_{in} \tag{2.11}$$

$$\frac{d\Omega_m}{dt} = \frac{1}{J_g} T_{in} - \frac{1}{J_g} T_{em} \tag{2.12}$$

$$\frac{dT_{in}}{dt} = K_S(\eta\omega_L - \Omega_m) + D_S(\eta\frac{d\omega_L}{dt} - \frac{d\Omega_m}{dt}) \tag{2.13}$$

where T_{wt} is the aerodynamic torque, η is the gearbox ratio, T_{em} the electromagnetic torque, Ω_m the mechanical speed at the HSS, ω_L the mechanical speed at the LSS, K_S the spring stiffness and D_S the spring damping coefficient.

Equations (2.11) to (2.13) can be represented as a state-space model, with states $\mathbf{x_m} = [\omega_L\ \Omega_m\ T_{in}]^T$, inputs $\mathbf{u_m} = [T_{wt}\ T_{em}]^T$ and outputs $\mathbf{y_m} = [\omega_L\ \Omega_m]^T$:

$$\dot{\mathbf{x_m}} = \begin{bmatrix} 0 & 0 & -\frac{\eta}{J_{wt}} \\ 0 & 0 & \frac{1}{J_g} \\ \eta K_S & -K_S & -D_S\left(\frac{\eta^2}{J_{wt}} + \frac{1}{J_g}\right) \end{bmatrix} \mathbf{x_m} + \begin{bmatrix} \frac{1}{J_{wt}} & 0 \\ 0 & -\frac{1}{J_g} \\ \frac{\eta D_S}{J_{wt}} & \frac{D_S}{J_g} \end{bmatrix} \mathbf{u_m}; \quad \mathbf{y_m} = \begin{bmatrix} 1 & 0 & 0 \\ 0 & 1 & 0 \end{bmatrix} \mathbf{x_m} \tag{2.14}$$

2.3 Doubly-fed induction generator dynamic model

The DFIG is a special type of induction machine that has been extensively used in wind applications because the required power electronics are reduced in size (typically 30% of nominal power) and the range of speed control is sufficient for maximum power tracking of a wide range of wind speeds. The only difference between a traditional squirrel cage induction machine dynamic model and DFIG dynamic model is the inclusion of voltage at the rotor terminals (v_{rq} and v_{rd}) which are injected by the rotor-side power converter in case of the DFIG, on the other hand for the induction machine ($v_{rq} = v_{rd} = 0$). The dynamic model in an arbitrary reference frame rotating at a speed equal to "ω" can be expressed with the following equations [67]:

$$v_{sd} = R_s i_{sd} + \frac{d\lambda_{sd}}{dt} - \omega\lambda_{sq} \tag{2.15}$$

$$v_{sq} = R_s i_{sq} + \frac{d\lambda_{sq}}{dt} + \omega\lambda_{sd} \tag{2.16}$$

$$v_{rd} = R_r i_{rd} + \frac{d\lambda_{rd}}{dt} - (\omega - \omega_m)\lambda_{rq} \tag{2.17}$$

$$v_{rq} = R_r i_{rq} + \frac{d\lambda_{rq}}{dt} + (\omega - \omega_m)\lambda_{rd} \tag{2.18}$$

where λ is magnetic linkage flux, the subscript d and q are the corresponding component in the d-q reference frame and s and r are the subscripts of stator and rotor respectively. The electrical angular speed ω_m is directly proportional to the mechanical speed (Ω_m) and the number of pole pairs of the machine (P):

$$\omega_m = P\Omega_m \tag{2.19}$$

Neither magnetic saturation of the materials, machine parameters changing due to temperature nor losses in the machine core are considered in the presented model.

The fluxes are dependent on the current and inductance values:

$$\lambda_{sd} = (L_{ls} + L_m)\, i_{sd} + L_m i_{rd} \tag{2.20}$$

$$\lambda_{sq} = (L_{ls} + L_m)\, i_{sq} + L_m i_{rq} \tag{2.21}$$

$$\lambda_{rd} = (L_{lr} + L_m)\, i_{rd} + L_m i_{sd} \tag{2.22}$$

$$\lambda_{rq} = (L_{lr} + L_m)\, i_{rq} + L_m i_{sq} \tag{2.23}$$

where L_{ls} and L_{lr} are the stator and rotor leakage inductance respectively and L_m is the magnetization inductance. The stator flux is the sum of the leakage and the mutual flux, then the stator total inductance (Ls) is:

$$L_s = L_{ls} + L_m \tag{2.24}$$

similarly the rotor inductance (L_r) is:

$$L_r = L_{lr} + L_m \tag{2.25}$$

Equations (2.15) to (2.18) can be represented as an equivalent electric circuit (see Figure 2.5).

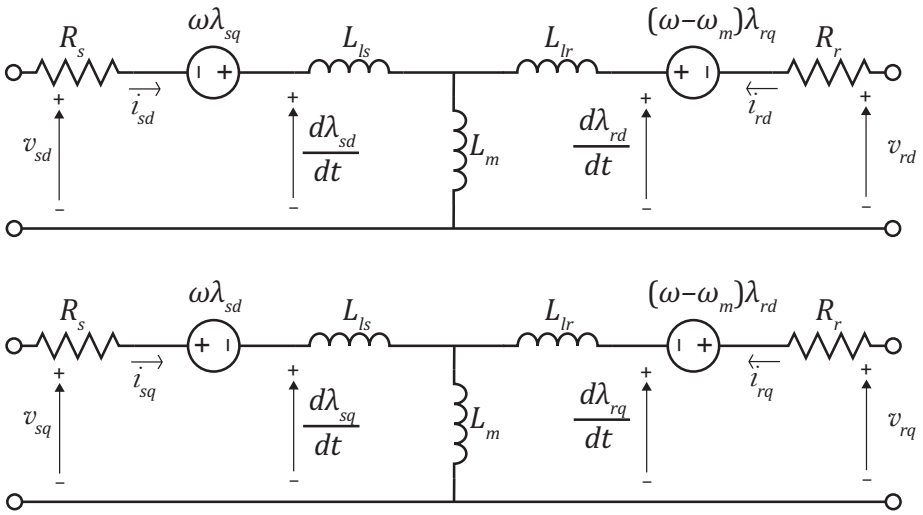

FIGURE 2.5: DFIG equivalent circuit in an arbitrary dq reference frame.

The active and reactive power can be obtained using the voltages and currents measured at the terminals of the electric machine [26].

$$P_s = \frac{3}{2}\left(v_{sd} i_{sd} + v_{sq} i_{sq}\right) \tag{2.26}$$

$$P_r = \frac{3}{2}\left(v_{rd}i_{rd} + v_{rq}i_{rq}\right) \tag{2.27}$$

$$Q_s = \frac{3}{2}\left(v_{sq}i_{sd} - v_{sd}i_{sq}\right) \tag{2.28}$$

$$Q_r = \frac{3}{2}\left(v_{rq}i_{rd} - v_{rd}i_{rq}\right) \tag{2.29}$$

The electromagnetic torque can be obtained from the interaction between stator flux and rotor current:

$$T_{em} = \frac{3PL_m}{2L_s}\,\mathrm{Im}(\vec{\lambda}_s \cdot \vec{i}_r^{\,*}) = \frac{3PL_m}{2L_s}(\lambda_{sq}i_{rd} - \lambda_{sd}i_{rq}) \tag{2.30}$$

where the operator $\vec{x}^*$ is the complex conjugate of vector $\vec{x}$, which has the form: $\vec{x} = x_d + jx_q$.

Another common way to express T_{em} is obtained from substituting equations (2.20) and (2.21) in (2.30).

$$T_{em} = \frac{3PL_m}{2}(i_{rd}i_{sq} - i_{rq}i_{sd}) \tag{2.31}$$

2.3.1 State-space representation of DFIG

From equations (2.15) to (2.23) at a synchronous-speed rotating reference frame ($\omega = \omega_s$), it is possible to obtain a state-space representation of the current magnitudes (for further details see [26]):

$$\dot{\mathbf{x}} = A\mathbf{x} + B\mathbf{u}; \quad \mathbf{y} = C\mathbf{x} \tag{2.32}$$

where $\mathbf{x} = [i_{sd}\ i_{sq}\ i_{rd}\ i_{rq}]^T$, $\mathbf{u} = [v_{sd}\ v_{sq}\ v_{rd}\ v_{rq}]^T$

$$A = \left(\tfrac{1}{\sigma L_s L_r}\right)\begin{bmatrix} -R_sL_r & \omega_m L_m^2 + \omega_s\sigma L_sL_r & R_rL_m & \omega_m L_mL_r \\ -\omega_m L_m^2 - \omega_s\sigma L_sL_r & -R_sL_r & -\omega_m L_mL_r & R_rL_m \\ R_sL_m & -\omega_m L_sL_m & -R_rL_s & -\omega_m L_rL_s + \omega_s\sigma L_sL_r \\ \omega_m L_sL_m & R_sL_m & \omega_m L_rL_s - \omega_s\sigma L_sL_r & -R_rL_s \end{bmatrix}$$

$$B = \left(\tfrac{1}{\sigma L_s L_r}\right)\begin{bmatrix} L_r & 0 & -L_m & 0 \\ 0 & L_r & 0 & -L_m \\ -L_m & 0 & L_s & 0 \\ 0 & -L_m & 0 & L_s \end{bmatrix}$$

$$C = \begin{bmatrix} 0 & 0 & 1 & 0 \\ 0 & 0 & 0 & 1 \end{bmatrix}$$

where $\sigma = 1 - L_m^2/(L_sL_r)$, commonly known as leakage coefficient. It is important to mention than the system expressed in equation 2.32 is non linear due to the mechanical speed ω_m, which is a function of the electromagnetic torque, dependent on the states (see equation (2.31)).

2.4 Wind turbine control strategy

The general control strategy of a DFIG-based wind turbine is displayed in figure 2.6. There are two control loops, the external one is in charge of giving the references of active and reactive power to the rotor-side controller and the DC-link voltage and reactive power to the grid-side controller. A rotor-speed-based regulation may be

used to extract the maximum power from the wind. There are also other possibilities based on the grid necessities [68]–[70].

The internal control loop regulates the stator active and reactive power using the RSC and maintains the DC-link voltage constant and the converter reactive power using the GSC.

The internal control of the RSC is the field of study of this thesis. The references are considered to be given by the external control loop and the DC-link is considered to be constant. In the following sections the classical RSC control methods are briefly described.

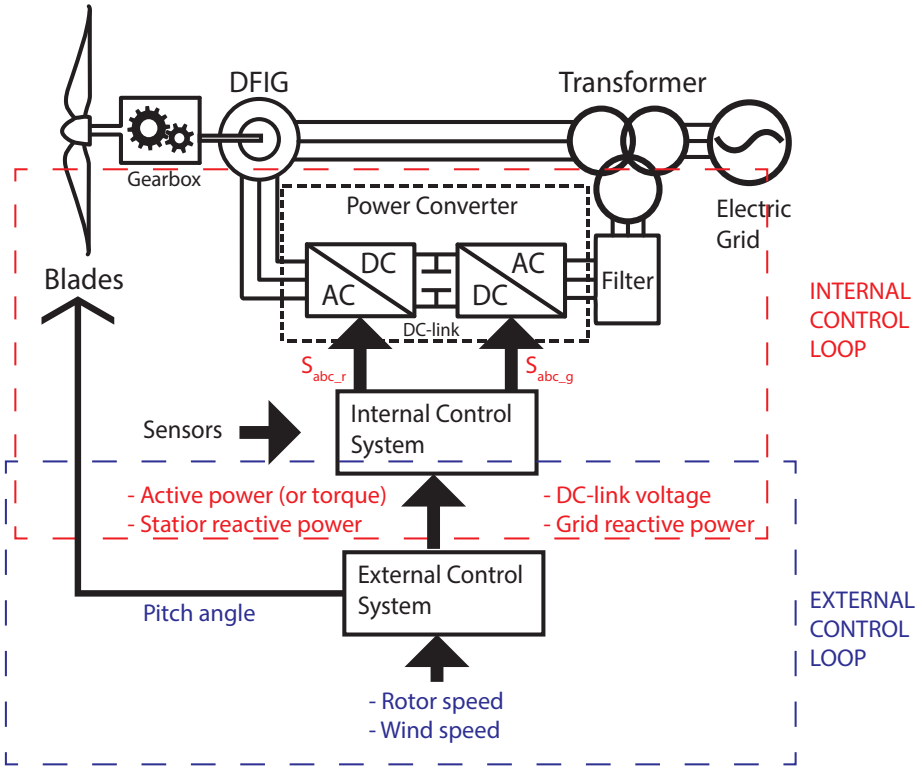

FIGURE 2.6: Internal and external control loops for DFIG-based wind turbines.

2.5 Field orientated control of DFIG

For VSWTs control system is unavoidable and plays an important role in the efficiency of the wind energy extraction, the rotor-side converter controller controls torque (or active power) and the stator reactive power. On the other hand, the grid-side converter maintains DC bus at constant voltage and controls the converter reactive power, allowing unitary power factor operation of the system or even inject reactive power to the electric grid.

Field orientation is a common technique used to control AC electric machinery, the basic idea is to represent the machine in a rotating reference frame which allows not only to decouple active and reactive power in two different control loops, but also to see the controlled variables (generally currents) as DC signals, which are

much easier to control than AC signals. The counterpart is that the control loop used to regulate the currents to the desired value is highly dependent on system parameters and modulation is required since the control signal is continuous and the converter has only limited commutation states.

In Figure 2.7 it is represented the basic scheme of a DFIG-based wind turbine. The power signals are injected via power converters, therefore it is necessary to generate pulse-width modulated signals according to the desired reference values.

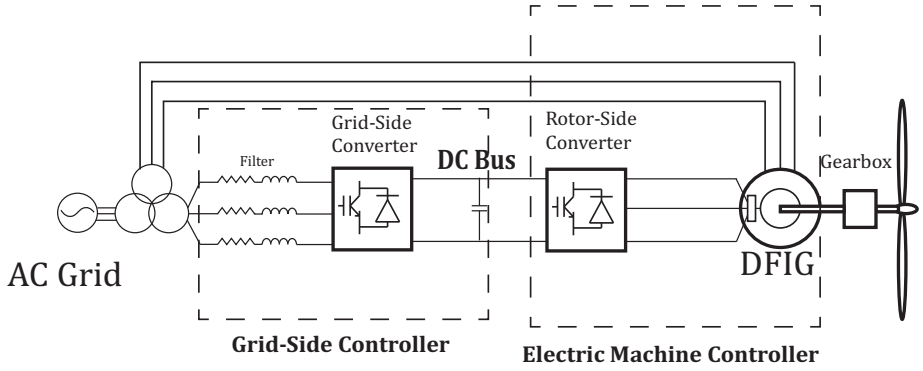

FIGURE 2.7: DFIG based WECS basic scheme.

2.5.1 Field orientation principle

For DFIG the stator is directly connected to the electric grid while the rotor is fed through a power converter. The decoupled control is achieved aligning the "direct" d axis with the stator flux. If the voltage drop due to the stator resistance is neglected, the stator voltage and stator flux vectors will be 90 degrees appart each other (see equation (2.15) and (2.16)), then $v_{sd} = 0$ and $\lambda_{sq} = 0$. The stator voltage will be indirectly aligned with the "quadrature" q axis. Solving equations (2.20) and (2.21) for stator current considering that $\lambda_{sq} = 0$:

$$i_{sd} = \frac{\lambda_{sd}}{L_s} - \frac{L_m}{L_s} i_{rd} \tag{2.33}$$

$$i_{sq} - \frac{L_m}{L_s} i_{rq} \tag{2.34}$$

Substituting equations (2.33) and (2.34) in equations (2.26) and (2.28):

$$P_s = \frac{3}{2}\left(\cancelto{0}{v_{sd} i_{sd}} + v_{sq} i_{sq}\right) = \frac{-3L_m}{2L_s}(v_{sq}\boldsymbol{i_{rq}}) \tag{2.35}$$

$$Q_s = \frac{3}{2}\left(v_{sq} i_{sd} - \cancelto{0}{v_{sd} i_{sq}}\right) = \frac{3 v_{sq}\lambda_{sd}}{2L_s} - \frac{3L_m}{2L_s}(v_{sq}\boldsymbol{i_{rd}}) \tag{2.36}$$

Usually, it is preferred to control electromagnetic torque instead of stator power. T_{em} is directly related with the rotor speed control necessary to maintain tip-speed ratio at the optimal value. Substituting equation (2.34) in equation (2.30)

$$T_{em} = \frac{3PL_m}{2L_s}(\cancelto{0}{i_{rd}\lambda_{sq}} - i_{rq}\lambda_{sd}) = \frac{-3PL_m}{2L_s}(\lambda_{sd}\boldsymbol{i_{rq}}) \tag{2.37}$$

From equations (2.36) and (2.37) or (2.35) it is easy to solve for the desired rotor current in its "d,q" components:

$$i_{rd}^{*} = \frac{\lambda_{sd}}{L_m} - \frac{2L_s}{3L_m v_{sq}} Q_s^{*} \tag{2.38}$$

$$i_{rq}^{*} = -\frac{2L_s}{3PL_m\lambda_{sd}} T_{em}^{*}; \quad i_{rq}^{*} = -\frac{2L_s}{3L_m v_{sq}} P_s^{*} \tag{2.39}$$

Equations (2.38) and (2.39) were obtained from a simplified equation which neglects the voltage drop due to stator resistance, furthermore, the parameters uncertainties and variation during the operation of the machine could provoke that the actual active (or torque) and reactive power will not exactly be the desired values. For solving this issue, an external control loop could be used regulating the desired stator power [71].

The general scheme of a field oriented controller for DFIG is presented in Figure 2.8, from the desired active and reactive power it is possible to calculate the desired rotor current, then a current regulation loop is used for rotor current tracking, traditionally, PI control is used for the current regulation loops, although the use of any other continuous control techniques is also possible. We are supposing that rotor current and mechanical position of the rotor θ_m are known. The stator flux and rotor position measurement or estimation are required to orient rotor current in the stator flux direction (for further details on vector orientation see Appendix B). Perturbation rejection terms v_{rd2} and v_{rq2} could be included to enhance the dynamic response of the control system [72].

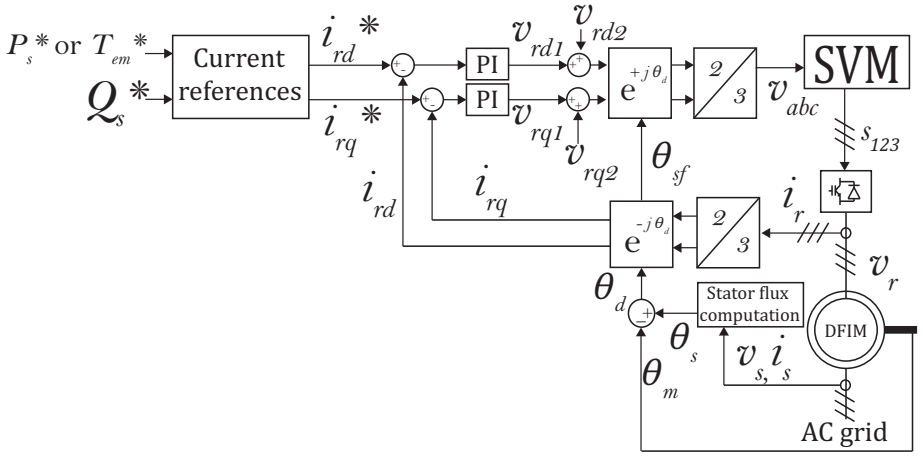

FIGURE 2.8: Field oriented control scheme for DFIG.

2.5.2 Current regulation loops

The rotor voltage in a synchronous rotating reference frame can be obtained from equations (2.17) and (2.18):

$$v_{rd} = R_r i_{rd} + \frac{d\lambda_{rd}}{dt} - \omega_r \lambda_{rq} \tag{2.40}$$

$$v_{rq} = R_r i_{rq} + \frac{d\lambda_{rq}}{dt} + \omega_r \lambda_{rd} \tag{2.41}$$

where $\omega_r = \omega_s - \omega_m$, that is known as the rotor electrical speed.

On the other hand, by substituting equations (2.33) and (2.34) in (2.22) and (2.23), the following expressions are obtained:

$$\lambda_{rd} = \sigma L_r i_{rd} + \frac{L_m}{L_s}\lambda_{sd} \tag{2.42}$$

$$\lambda_{rq} = \sigma L_r i_{rq} \tag{2.43}$$

where σ is the leakage coefficient ($\sigma = 1 - L_m^2/(L_s L_r)$).

The relationship between rotor voltages and currents can be obtained by substituting equations (2.42) and (2.43) in (2.40) and (2.41):

$$v_{rd} = R_r i_{rd} + \sigma L_r \frac{di_{rd}}{dt} + \frac{L_m}{L_s}\cancelto{0}{\frac{d\lambda_{sd}}{dt}} - \omega_r \sigma L_r i_{rq} \tag{2.44}$$

$$v_{rq} = R_r i_{rq} + \sigma L_r \frac{di_{rq}}{dt} + \frac{\omega_r L_m}{L_s}\lambda_{sd} + \omega_r \sigma L_r i_{rd} \tag{2.45}$$

If the electric machine is operating under normal conditions, the flux is constant in time, therefore the derivate of the flux in time is zero. Additionally, we can see that there is a cross term dependent on the rotor electrical speed ω_r, when the machine is operating at synchronous speed ($\omega_r = 0$), those terms are zero and the relation between the stator current and rotor voltage could be modeled as first order system with the transfer function: $H(s) = \frac{1}{\sigma L_r s + R_r}$.

For simplifying the controller design, it is common to compensate the cross terms so the current regulator do not have to deal with them [72] (see Figure 2.8):

$$v_{rd2} = -\omega_r \sigma L_r i_{rq} \tag{2.46}$$

$$v_{rq2} = \omega_r (\sigma L_r i_{rd} + \frac{L_m \lambda_{sd}}{L_s}) \tag{2.47}$$

with those terms being compensated, it is easy to design the regulator considering that the plant is seen as a first order system. In Figure 2.8 the controllers are considered to be traditional PI regulators, but any other strategy can be used instead.

2.6 Direct control techniques for DFIG

Specifically, Direct Torque control and Direct Power Control. DTC was originally proposed for the IM in 1984 [21]–[23], later DPC emerged from some modifications of DTC [24]. The controller schemes presented in this section are the simplest versions of the direct control techniques adapted in 2006 for the DFIG configuration [25].

2.6.1 Direct torque control

DTC is based on control of two variables: the torque and rotor flux amplitude. In steady state, the stator and rotor fluxes rotate at the same speed. Since the reference frame used by DTC is dependent on the mechanical speed, the stator and rotor fluxes can rotate either clockwise (at sub-synchronous speed) and counterclockwise (at super-synchronous speed).

The principle of operation of DTC is based on the interaction between rotor and stator fluxes. From equation (2.30), it is possible to obtain a torque expression between rotor and stator flux by substituting equations (2.20) to (2.23) and doing some algebraic manipulation. The resulting equation is:

$$T_{em} = \frac{3PL_m}{2\sigma L_r L_s} \mathrm{Im}(\vec{\lambda}_r \cdot \vec{\lambda}_s) = \frac{3PL_m}{2\sigma L_r L_s} \|\vec{\lambda}_s\| \|\vec{\lambda}_r\| \sin(\delta) \tag{2.48}$$

where δ is the angle between stator and rotor flux vectors.

Since the rotor is directly fed by the rotor-side converter, the rotor flux vector can be controlled by the injection of voltage vectors, in a similar way that the stator flux is controlled in traditional vector control for IMs.

A switching logic table is used to select the desired vector which will regulate the control variables. In figure 2.9 it is shown the control diagram of DTC for DFIG.

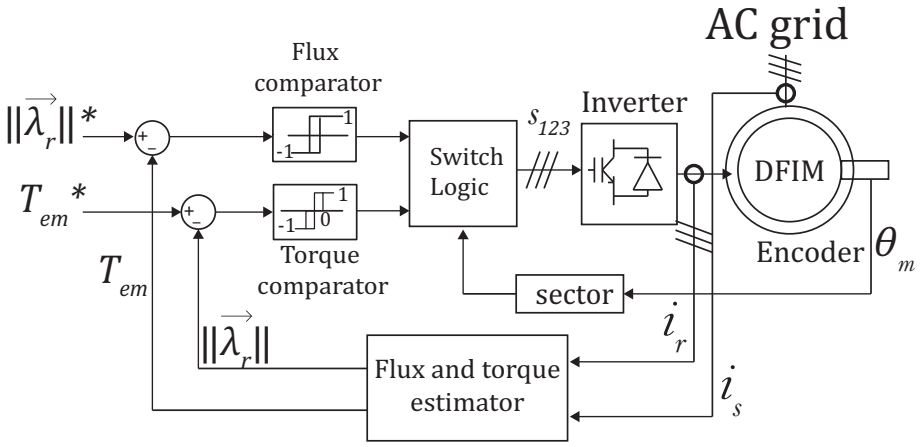

FIGURE 2.9: Direct Torque Control for DFIG.

2.6.2 Direct power control

DPC is a variation of DTC which regulates a more useful variable which is the reactive power. The basic principle for this technique is the fact that the active and reactive power can be decoupled by the components of the interaction between stator and rotor fluxes. From the DFIG dynamic models equations it is possible to obtain the following expressions:

$$P_s = \frac{3L_m}{2\sigma L_r L_s} \omega_s \left\|\vec{\lambda}_s\right\| \left\|\vec{\lambda}_r\right\| \sin\delta \tag{2.49}$$

$$Q_s = \frac{3\omega_s \left\|\vec{\lambda}_s\right\|}{2\sigma L_s}\left(\frac{L_m}{L_r}\left\|\vec{\lambda}_s\right\| - \left\|\vec{\lambda}_r\right\|\cos\delta\right) \tag{2.50}$$

From equations (2.49) and (2.50) it can be concluded that the stator active and reactive power can be controlled by the sine and cosine components of the angle between stator and rotor fluxes (δ). In a similar way than DTC, a comparator-based control system can be used with a switching logic table that dictates the switching vector that will control both variables at the same time. In Figure 2.10 it is shown the basic scheme of DPC for DFIG.

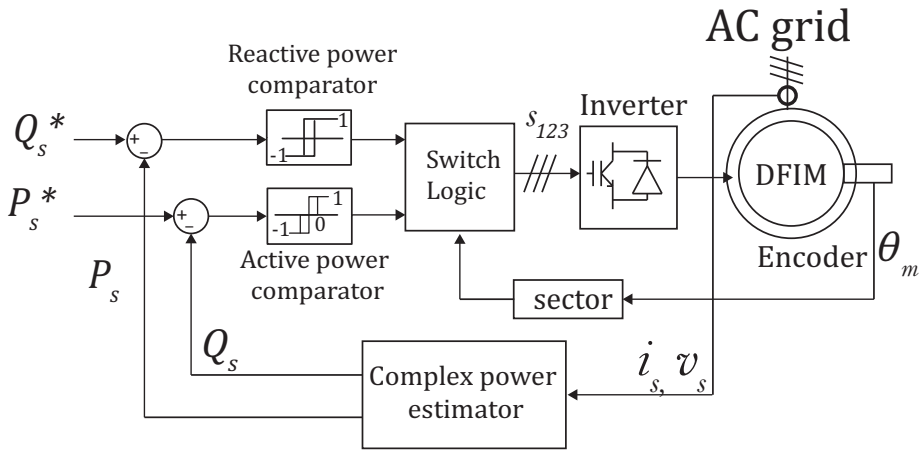

FIGURE 2.10: Direct Power Control for DFIG.

2.7 Behavior of DFIG under voltage disturbances

In this section two important phenomena which occurs during asymmetrical voltage dips are presented, the first one is related with the oscillations in torque and reactive power due to the interaction between positive and negative sequence components of currents and voltages. Section 2.7.1 demonstrate that it is not possible to cancel stator active power oscillations and electromagnetic torque oscillations at the same time, therefore, it is preferable to eliminate torque oscillations since they may affect the mechanical components of a wind turbine.

Section 2.7.2 presents the behavior of the stator flux during stator voltage faults, the concept of natural flux and the demagnetization current principle.

2.7.1 Complex power and torque under unbalanced conditions

The active and reactive power can be obtained from electrical quantities from the stator reference frame:

$$P_s = \frac{3}{2}\,\mathrm{Re}(\vec{v}_s\vec{i}_s^{\,*}) = \frac{3}{2}(v_{s\alpha}i_{s\alpha} + v_{s\beta}i_{s\beta}) \tag{2.51}$$

$$Q_s = \frac{3}{2}\,\mathrm{Im}(\vec{v}_s\vec{i}_s^{\,*}) = \frac{3}{2}(v_{s\beta}i_{s\alpha} - v_{s\alpha}i_{s\beta}) \tag{2.52}$$

where the operator $\vec{x}^*$ is the complex conjugate.

In case of unbalanced conditions, the symmetrical components methods can be used for simplifying analysis, since zero sequence do not produce complex power, only positive and negative sequences are analyzed:

$$\vec{v_s} = \vec{v_{s1}} + \vec{v_{s2}} = v_{s\alpha 1} + v_{s\alpha 2} + j(v_{s\beta 1} + v_{s\beta 2}) \tag{2.53}$$

$$\vec{i_s} = \vec{i_{s1}} + \vec{i_{s2}} = i_{s\alpha 1} + i_{s\alpha 2} + j(i_{s\beta 1} + i_{s\beta 2}) \tag{2.54}$$

Substituting (2.53) and (2.54) in equations (2.51) and (2.52) yields:

$$\begin{aligned} P_s = \overbrace{\frac{3}{2}(v_{s\alpha 1}i_{s\alpha 1} + v_{s\beta 1}i_{s\beta 1})}^{P_{s11}} + \overbrace{\frac{3}{2}(v_{s\alpha 1}i_{s\alpha 2} + v_{s\beta 1}i_{s\beta 2})}^{P_{s12}} \\ + \underbrace{\frac{3}{2}(v_{s\alpha 2}i_{s\alpha 1} + v_{s\beta 2}i_{s\beta 1})}_{P_{s21}} + \underbrace{\frac{3}{2}(v_{s\alpha 2}i_{s\alpha 2} + v_{s\beta 2}i_{s\beta 2})}_{P_{s22}} \end{aligned} \tag{2.55}$$

$$\begin{aligned} Q_s = \overbrace{\frac{3}{2}(v_{s\beta 1}i_{s\alpha 1} - v_{s\alpha 1}i_{s\beta 1})}^{Q_{s11}} + \overbrace{\frac{3}{2}(v_{s\beta 1}i_{s\alpha 2} - v_{s\alpha 1}i_{s\beta 2})}^{Q_{s12}} \\ + \underbrace{\frac{3}{2}(v_{s\beta 2}i_{s\alpha 1} - v_{s\alpha 2}i_{s\beta 1})}_{Q_{s21}} + \underbrace{\frac{3}{2}(v_{s\beta 2}i_{s\alpha 2} - v_{s\alpha 2}i_{s\beta 2})}_{Q_{s22}} \end{aligned} \tag{2.56}$$

On the other hand, electromagnetic torque can be obtained using the well known equation:

$$\tau_e = \frac{3P}{2}\,\mathrm{Im}(\vec{\lambda_s}\,\overline{\vec{i_s}}) \tag{2.57}$$

Using the symmetrical components theory, an unbalance condition can be modeled with invariant positive and negative sequence components, therefore at steady state the derivate terms of equations (2.15) and (2.16) are zero leading to the following positive and negative stator flux components:

$$\vec{\lambda_{s1}} = \frac{\vec{v_{s1}} - R_s\vec{i_{s1}}}{j\omega_s} \tag{2.58}$$

$$\vec{\lambda_{s2}} = \frac{\vec{v_{s2}} - R_s\vec{i_{s2}}}{-j\omega_s} \tag{2.59}$$

Substituting equations (2.58) and (2.59) in (2.57)

$$\tau_e = \frac{3p}{2\omega_s}\,\mathrm{Re}[\vec{v_{s1}}\vec{i_{s1}}^* + \vec{v_{s1}}\vec{i_{s2}}^* - \vec{v_{s2}}\vec{i_{s1}}^*\vec{v_{s2}}\vec{i_{s2}}^* + R_s(\vec{i_{s2}}^2 - \vec{i_{s1}}^2)] \tag{2.60}$$

Comparing equation (2.60) with equation (2.55) it is easy to see that the same terms appear in both equations:

$$\tau_e = \frac{p}{\omega_s}(P_{s11} + P_{s12} - P_{s21} - P_{s22}) + k_{i21}(|\vec{i_{s2}}|^2 - |\vec{i_{s1}}|^2)] \tag{2.61}$$

where $k_{i21} = \frac{3PR_s}{\omega_s}$.

The terms P_{s12} and P_{s21} are the cause of oscillation in torque and power when an unbalanced voltage dip occurs. Since the condition for canceling torque oscillations ($P_{s12} = P_{s21}$) is opposite to the condition for canceling active power oscillations ($P_{s12} = -P_{s21}$) it is not possible to cancel both at the same time. It is preferable to cancel torque oscillations, otherwise the mechanical components may be severely damaged. On the other hand, in order to cancel reactive power oscillations, the following condition must be met $Q_{s12} + Q_{s21} = 0$.

2.7.2 Stator flux evolution in time under stator voltage dips

In [16] the dynamic behavior of DFIG under voltage dips is studied in detail. Here only a brief explanation of the natural flux evolution in time and the demagnetizing principle is presented.

The stator flux derivative seen in a stationary reference frame can be obtained with equations (2.15), (2.16) (2.20) and (2.21). Considering that the stator volage is faulted, $\vec{v}_s = \vec{v}_{sfault}$ the dynamic equation of the stator flux is:

$$\frac{d\vec{\lambda}_s}{dt} = \vec{v}_{sfault} - \frac{R_s}{L_s}\vec{\lambda}_s + \frac{L_m}{L_s}R_s\vec{i}_r \tag{2.62}$$

Neglecting rotor current and considering that the fault voltage can be decoupled in symmetrical components (see Apendix A, for further details on Fortescue's transform) $\vec{v}_{sfault} = \vec{v_s^+} + \vec{v_s^-}$. The stator flux has the following dynamic behavior [73]:

$$\vec{\lambda}_s(t) = \vec{\lambda_{sn}}(0)e^{-\frac{R_s}{L_s}t} + \frac{\vec{v_s^+}}{j\omega_s}e^{j\omega_s t} - \frac{\vec{v_s^-}}{j\omega_s}e^{-j\omega_s t} \tag{2.63}$$

The first term is the natural flux which decays exponentially if the rotor current is neglected. On the other hand, the forced flux due to the remaining voltage applied to the stator has two components, one rotating in synchronous speed due to the positive sequence component of the faulted voltage and the other one rotating in the opposite direction due to the negative sequence component of voltage.

Considering a balanced voltage dip in the stator, the negative voltage component will be zero and the stator flux evolution in time will be composed by a forced voltage due to the positive sequence component and a transient natural flux which decays exponentially with the time constant $\tau_{sn} = \frac{L_s}{R_s}$. In Figure 2.11 the evolution of a three phase voltage dip is presented in a polar graph.

On the other hand, the evolution of the stator flux will be composed by a positive and a negative forced solution and the transient natural flux for unbalanced voltage dips. Depending on the starting time of the fault the natural flux may exist or not. For example, for a voltage dip in phase "a" if the fault start at $t = nT$ or $t = \frac{4n+2}{4}T$, where T is the oscillation period and $n \in \mathbb{N}$, the natural flux will be zero, while for a fault starting at $t = \frac{4n+1}{4}T$, or $t = \frac{4n+3}{4}T$, the natural flux will be maximum. In Figure 2.12, it is displayed the stator flux evolution for the ideal case (no natural flux) and in Figure 2.13, it is displayed the natural flux evolution for the worst case (maximum natural flux).

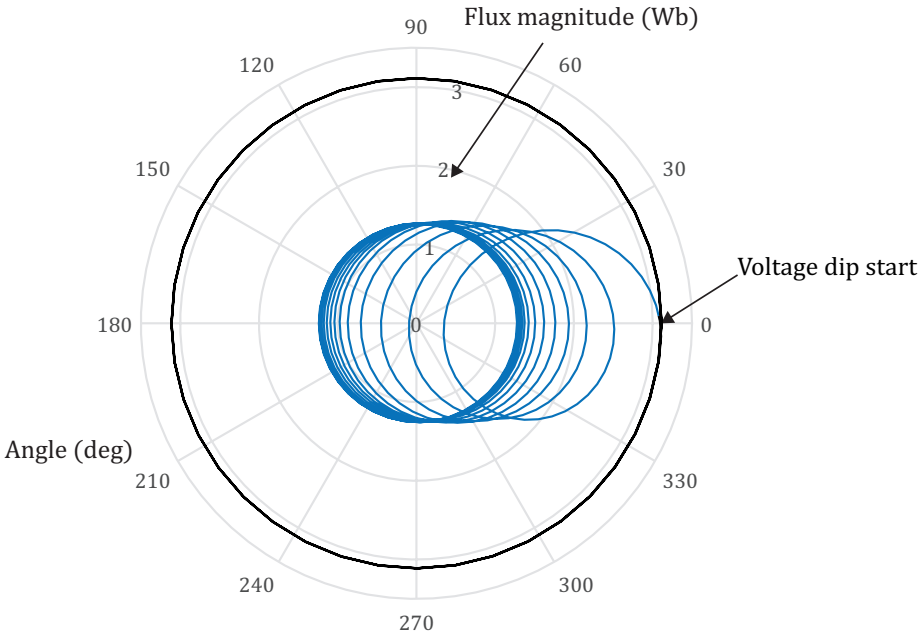

FIGURE 2.11: Stator flux evolution in time for a 60% three-phase voltage dip.

The natural flux is a component appearing due to instantaneous voltage dips, since the stator flux cannot change abruptly. The natural flux induces a large voltage in the rotor and may cause lost of control of the electric machine. Therefore, the concept of demagnetizing current [56]–[58] is used in order to counteract the natural flux and return the electric machine to a stable state, preventing further deformation of stator and rotor currents.

A rotor current could be applied to eliminate natural flux [56]:

$$\vec{i_{rn}} = -\frac{L_m}{L_s L_r'} k_d \vec{\lambda_{sn}} \tag{2.64}$$

enhancing the dynamic behavior of the DFIG by eliminating faster the natural flux.

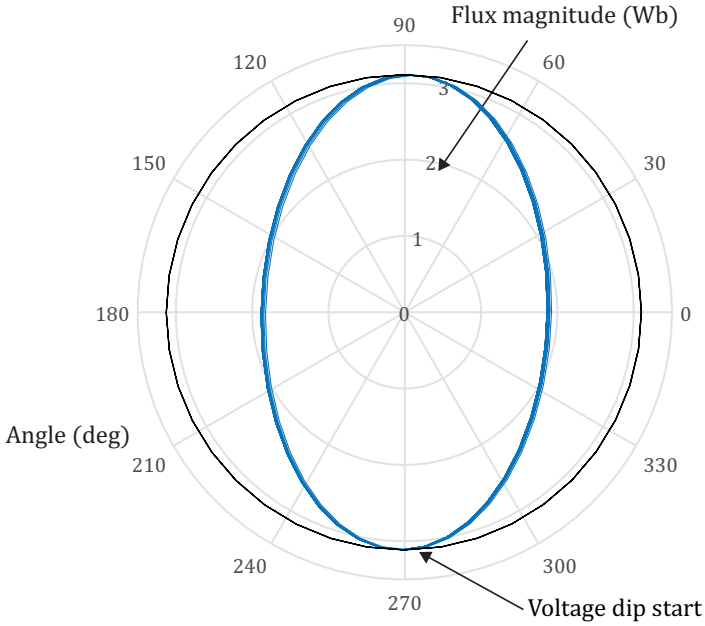

FIGURE 2.12: Stator flux evolution in time for a 60% voltage dip in phase "a" starting at $t = nT$.

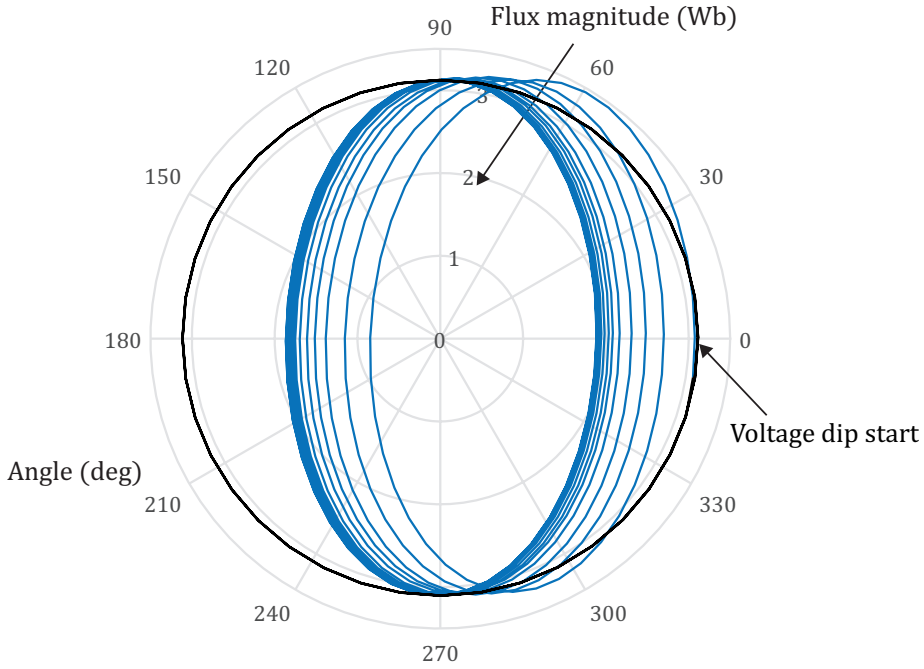

FIGURE 2.13: Stator flux evolution in time for a 60% voltage dip in phase "a" starting at $t = \frac{4n+1}{4}T$.

Chapter 3

Vector control publications

This chapter presents general works that simulate the complete wind turbine and some important aspects to take into account during the operation of the system.

In section 3.1, the external control loop of the wind turbine is discussed considering real wind profiles extracted from [74]. Then in 3.2, a pitch angle controller that limits the power extraction of the wind turbine is presented and tested under a highly variable wind profile. Finally, the thermal aspects of the power converter and life-time estimation methods of semiconductor devices are studied in section 3.3.

Figure 3.1 displays the scientific production concerning the general aspects of the operation of a wind turbine in a diagram.

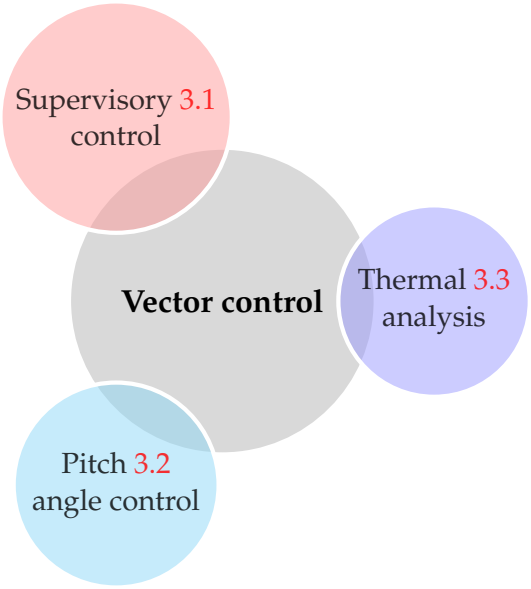

FIGURE 3.1: Vector-control-based scientific production.

3.1 Supervisory controller using short-term ahead prediction

Villanueva, I., Torres, E., Balderas, D., Ponce, P., & Molina, A. (2017). Supervisory controller for smoothing wind turbine power output based on FESS using ANNs for short-term ahead prediction. *Journal of Modern Power Systems and Clean Energy*. Springer. **Manuscript under review.**

In this paper it is presented a general structure of a DFIG coupled with an energy storage system based on a Flywheel. The control used is based on the maximization of the energy extraction. A flywheel is used to reduce active power fluctuation. The power reference of the flywheel is obtained using a fuzzy logic controller and a short-term ahead prediction using Artificial Neural Networks.

Noname manuscript No.
(will be inserted by the editor)

Supervisory Controller for Smoothing Wind Turbine Power Output based on FESS using ANNs for Short-Term Ahead Prediction

the date of receipt and acceptance should be inserted later

Abstract One of the most challenging aspects concerning the increasing penetration of Eolic generation is the highly uncertain nature of wind, which may be the origin of several problems related with output power quality, system stability and poor reliability of wind energy generation. Include an Energy Storage System (ESS) is a common solution to mitigate the negative effects of power fluctuation in renewable generators. The use of Flywheels Energy Storage Systems (FESSs) is an attractive solution in wind applications. This paper presents a fuzzy logic supervisory controller for management stored energy in a FESS. The controller inputs are the extracted wind power, the rotational speed of the FESS and a predicted slope angle of the wind profile obtained using Artificial Neural Networks (ANNs). The results verify the effectiveness of the proposed supervisory controller by comparing the mean and standard deviation of the simulation output power against the most popular fuzzy logic controller.

Keywords Doubly-fed induction generator · flywheel energy storage system · artificial neural networks · supervisory control · variable-speed wind turbine.

1 Introduction

Despite the recent oil prices drop, wind energy was the leading source of new power generating capacity in Europe and United States in 2015, and the second largest in China, increasing 64 GW of installed capacity in 2015 and 54 GW during 2016 for a global total of approximately 487 GW [21].

Most power grid codes focus on reactive power control, frequency response, fault ride through capability and allowable voltage levels [54]. A grid with high proportion of renewable energy sources may suffer from frequency and voltage variations due to the intermittent nature from primary energy sources; hence, including ESS can be used to improve the quality of output power.

Flywheels are widely used in wind generation because they have long cycle life with insensitivity to depth of discharge, high energy density, wide operating temperature range and low environmental impact. Some relevant works present the usage of flywheels in wind farms [18,12], wind-diesel generator systems [14, 8] and micro-grid integration [6,26].

Supervisory control can be used to compute a power reference for an electric machine coupled mechanically with a flywheel. Typically fuzzy logic controllers are used [7,11,29,32,33,46,53,52] due to their intuitive programming process and good performance. Other proposals use Artificial Neural Networks (ANNs) [2] and classical control schemes [40,13]. Most proposals use flywheel speed and wind turbine power to calculate the power reference. Short-term ahead prediction of wind speed has been implemented using a linear regression model, after that, the additional data was used in a simple supervisory controller [28].

Wind prediction has been implemented using different types of artificial intelligence techniques such as autoregressive models [43,44], Supported Vector Machines (SVM) [42] as well as different types of ANNs [36]. Among these methods, ANNs have been widely used for short-term ahead prediction [30,27], for prediction on different towers [36], as well as wind power estimation using 14 previous hours [15] and can be used to predict tendencies of wind speed fluctuations consequently reducing power fluctuations.

In this work, it is proposed a new fuzzy logic supervisory controller, considering the flywheel speed, the power extracted by the Eolic generator and wind speed tendency (slope angle) prediction using ANNs. The supervisory control uses wind tendency to give additional information to the supervisory system preventing a future scenario for smoothing the power output further compared with the traditional scheme of supervisory controllers [11,29,32,33,52], which is by far the most popular solution.

2 System Model

The studied model consists on a variable speed wind turbine based on a Doubly Fed Induction Generator (DFIG) (2.4 MW). The stator of the electric machine is connected to the AC grid, while the rotor is being fed through a back-to-back converter. The FESS is coupled with an Induction Machine (IM) (1.6 MW) and a full size converter is used to feed the stator (Figure 1).

Vector model is the most common representation to control DFIG [48]. A stator-flux oriented vector controller is used for the DFIG, for details about the controller used see [49], the required voltage is send to the electric machine using space vector modulation, the parameters of the current regulator loop within the controller are presented in the Appendix. The vector controller uses a power estimator to calculate the reference power that the turbine could extract based on the mechanical speed of the turbine (ω_{mec}), and that power is set as the stator real power reference. The reactive power reference is kept equal to zero.

The flywheel is controlled using Direct Torque Control (DTC). It is advantageous to use DTC over vector control when it is necessary to change quickly between motoring and generation regions [10].

Both machines share the same grid-side converter, which is in charge of maintaining the DC link constant. The details about the grid-side vector control are published in [1].

The tendency predictor uses the values of the measured wind speed (W_S) to predict the future values.

The electric machine and power estimator model are presented in section 3; the ANNs predictor block is presented in detail in section 4; the fuzzy logic supervisory controller in section 5; results in section 6 and finally the conclusions.

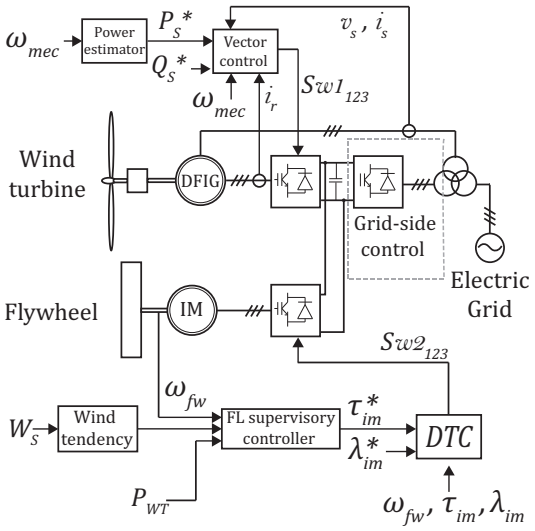

Fig. 1: Studied system model

3 Wind Generator Model

The power extracted from the wind can be calculated using:

$$P_{WT} = \frac{1}{2} C_P(\Lambda, \theta) \rho A W_S^3 \tag{1}$$

where C_P is the power coefficient which is a function of the tip-speed ratio (Λ) and the pitch angle (θ), (ρ) is the air density, (A) is the transverse area of the turbine and (W_S) is the wind speed normal to the rotor's plane. The tip speed ratio is defined as follows:

$$\Lambda = \frac{\omega_{mec} R}{W_S} \tag{2}$$

where ω_{mec} is the rotational speed of the wind turbine in $\frac{rad}{s}$ and R is the blades radius.

3.1 Blades Model

An accepted model for the power coefficient is the following [39]:

$$C_P = c_1 \left[c_2 c_7 - c_3 \theta - c_4 \theta^x - c_5 \right] e^{-c_6 c_7} \tag{3}$$

$$c_7 = \frac{1}{\Lambda + 0.08\theta} - \frac{0.035}{1 + \theta^3} \tag{4}$$

where $c_1 - c_6$ and x are coefficients obtained from experimental results. Λ and θ are the tip speed ratio and the pitch angle respectively. Figure 2 shows the power coefficient of the studied turbine (see appendix for details, the value of "x" is not presented because $c_4 = 0$):

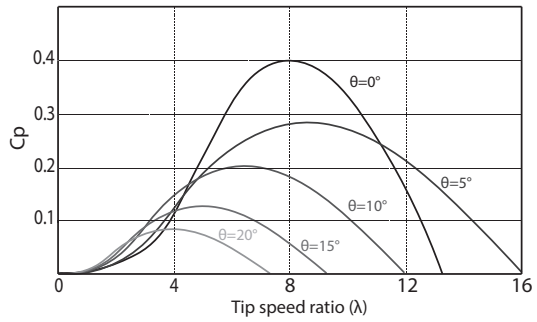

Fig. 2: Power-coefficient of the blades model. The optimal tip-speed ratio is equal to 8.

3.2 Doubly Fed Induction Generator and Induction Machine

The DFIG is a special type of induction generator that has been extensively used in wind applications because the required power electronics are reduced in size (typically 30% of nominal power) and the range of speed control is sufficient for maximum power tracking of a wide range of wind speeds. The dynamic models of DFIG and IM are very similar, in case of DFIG there is a voltage at the rotor terminals (v_{qr} and v_{dr}) which is injected by the rotor-side converter. On the other hand, for the IM the rotor conductors are short-circuited, therefore $v_{qr} = v_{dr} = 0$. The dynamic model of both machines in an arbitrary reference frame rotating at a speed equal to ω can be expressed with the following equations [47]:

$$v_{qs} = \frac{d\lambda_{qs}}{dt} + \omega\lambda_{ds} + R_s i_{qs} \tag{5}$$

$$v_{ds} = \frac{d\lambda_{ds}}{dt} - \omega\lambda_{qs} + R_s i_{ds} \tag{6}$$

$$v_{qr}^{'} = \frac{d\lambda_{qr}^{'}}{dt} + (\omega - \omega_r)\lambda'_{dr} + R'_r i'_{qr} \tag{7}$$

$$v_{dr}^{'} = \frac{d\lambda_{dr}^{'}}{dt} - (\omega - \omega_r)\lambda'_{qr} + R'_r i'_{dr} \tag{8}$$

where λ is magnetic linkage flux, the subscript d and q are the corresponding component in the d-q reference frame and s and r are the subscripts of stator and rotor respectively, ω_r is the mechanical speed at the DFIG shaft, which can be related by the gearbox ratio with a linear equation $\omega_r = \nu\omega_{mec}$, where ν is the gearbox ratio. Neither magnetic saturation of the materials, machine parameters changing due to temperature nor losses in the machine core are considered.

The fluxes are dependent on the current and inductance values:

$$\lambda_{ds} = (L_{ls} + L_m)\, i_{ds} + L_m i_{dr}^{'} \tag{9}$$

$$\lambda_{qs} = (L_{ls} + L_m)\, i_{qs} + L_m i_{qr}^{'} \tag{10}$$

$$\lambda'_{dr} = (L'_{lr} + L_m)\, i_{dr}^{'} + L_m i_{ds} \tag{11}$$

$$\lambda'_{qr} = (L'_{lr} + L_m)\, i_{qr}^{'} + L_m * i_{qs} \tag{12}$$

The electromagnetic torque can be obtained by:

$$T_E = \frac{3P}{4} L_m (i_{dr}^{'} i_{qs} - i_{qr}^{'} i_{ds}) \tag{13}$$

3.3 Flywheel

The flywheel stores kinetic energy in a rotating inertia. The energy storage in the flywheel is limited by the mechanical stress through centrifugal force at high speed.

$$E = 0.5 J_{FW} \omega_{fw}^2 \tag{14}$$

where J_{FW} is the moment of inertia of the flywheel ($kg.m^2$), and ω_{fw} is the angular velocity ($radians/s$).

4 Wind Tendency Predictor Based on Artificial Neural Networks

Because of wind variability, predicting exact wind velocities with a short time interval is quite complex; instead, it is intended that the system predicts wind tendencies. In order to predict these tendencies, two types of Artificial Neural Networks (ANNs) were designed to make a prediction five minutes ahead, using a one hour window. The adaptation intends to minimize the difference between the system output and the expected output obtained from the network. Once the network has been trained, it can be used to make predictions using new information. Undoubtedly, their ability to learn and to adapt continuously to new data allows them to track changes of signals over time.

ANNs have been used for wind prediction forecasting wind speed from different directions close to a cluster of turbines [3]. Also, ANNs have been used to predict hourly wind speed data [5,35] either in steps of $5min$ [19] or in steps over $3s$ [27].

There are many types of algorithms created for training ANN. Deep Learning (DL) algorithms and Recurrent Learning could be consider two of the most important ones [51]. DL create representation using multiple levels of abstraction [34], which can be translated into a network where each layer will create an higher level of decomposition of the previous layer. By means of these levels of abstraction, they can process images or video for visual object recognition and face detection. On the other hand, Recurrent learning (RL) are networks that

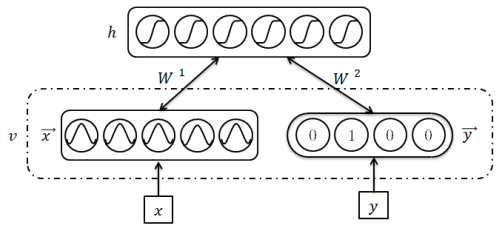

Fig. 3: Representation of the RBM with symmetrical connected weights

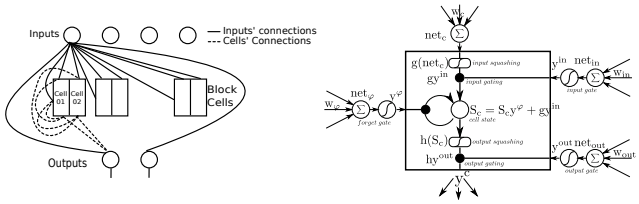

Fig. 4: LSTM with memory blocks in the hidden layer. Each memory cell has 3 gates (input, output and forget gates), which control the read, write and forget states of the cell. The functions g and h squash the cell input and output respectively.

uses internal recurrence to create a representation of current and past information [4,9], whereby creates a form of memory. These Networks are useful for the detection of patterns or sequences, which are useful for handwritten recognition [16] or speech recognition [17].

The two ANN algorithms used to predict wind tendencies are Restricted Boltzmann Machines (RBM) [24] and Long-Short Time Memory (LSTM) [25]. These algorithms were chosen since they have proven their effectiveness for data predicting [50], text classification [31], handwriting recognition [16,45], and speech recognition [17]. Also, they have hardly ever been used to predict wind changes [37], which makes it appealing to observe their behavior predicting wind tendencies.

A small summary of one of the most used algorithms is given, which later will be use for comparison.

4.1 Restricted Boltzmann Machines

RBMs is a two-layer neural network, with a set of *visible* units $\mathbf{v} = (v_1, \cdots, v_i)$ and *hidden* units $\mathbf{h} = (h_1, \cdots, h_j)$ that are connected with symmetric weights (see Figure 3). In a common RBM, the visible units represent the data modelling their dependencies, while the hidden units, are known as feature extractors, which make the representation built by the system. The probability $p(\mathbf{v}, \mathbf{h}; \Theta) \propto e^{-E(\mathbf{v},\mathbf{h};\Theta)}$ is known as the Boltzmann distribution with energy function: $E(\mathbf{v}, \mathbf{h}; \Theta) = -\mathbf{h}^T\mathbf{W}\mathbf{v} - \mathbf{b}^T\mathbf{v} - \mathbf{a}^T\mathbf{h}$ with $\mathbf{W}$ as the symmetric weights, $\mathbf{b}$ and $\mathbf{a}$ as the bias of the visible and hidden units respectively, and $\Theta = (\mathbf{W}, \mathbf{b}, \mathbf{a})$. The two conditional distributions over the variables, hidden given the visible $p(h_j = 1|\mathbf{v}) = \sigma_h(a_j + \sum_i v_i w_{ij})$ and visible given the hidden, $p(v_i = 1|\mathbf{h}) = \sigma_v(b_i + \sum_j h_j w_{ij})$, where σ called the activation function. The most common activation function is the sigmoid function $\sigma = \frac{1}{1+e^{-x}}$.

To train the network, the algorithm called Contrastive Divergence (CD)[23] is used for fitting the probability $p(v)$ to a certain set of observations. For $w_{ij} \in \mathbf{W}$

$$\Delta w_{ij} = \epsilon \frac{\partial p(\mathbf{v})}{\partial w_{ij}} = \epsilon(\langle v_i h_j \rangle^0 - \langle v_i h_j \rangle^n)$$

with ϵ as the learning rate, $\langle v_i h_j \rangle^0$ is the correlation when a data vector is clamped on the visible units and hidden states are sampled from their conditional distribution. $\langle v_i h_j \rangle^n$ is the correlation stationary distribution after running the Markov Chain using n Gibbs samples. A similar rule can be learned to update the biases. The learning works well enough even though it does not exactly follow the log probability of the training data [23].

4.2 Long-Short Time Memory

4.3 Neural Networks Prediction Methodology

To generate the prediction of the wind velocity, the ANNs were trained with data from http://www.winddata.com/ that was sampled at $5Hz$ with different time durations. The data was averaged over steps of $5min$ and also averaged between three different sensors. The data was arranged with a window size of one hour as the training inputs ($15inputs$) and used the next value as the output. If the data smaller than one hour and five minutes, it was not considered, and the next dataset was introduced. The data was split as 80% for training and 20% for testing. The training sets were composed of mini-batches of 100 wind windows selected. The data was normalized so it would fall within the interval $[0, 1]$

The MLP had 1 hidden layer, with 100 Neurons, and was trained over 50 epochs. The weights were drawn from $N(0, 0.1^2)$. The weights and biases were updated with a learning rate of 10^{-3} and a momentum of 0.5 with an increment of 0.1 at 40% and 80% of the learning process. The activation function for the hidden and output layer was the logistic sigmoid.

The initial values to train the RBM (weights, biases and rates) were adapted from [22]. The hidden layer used the logistic function, with the number of units to be in the next order of magnitude (base 2) than the total number of visible units. The RBMs were trained over 50 epochs, each comprising CD updates derived from 10 Gibbs sampling iterations. The weights were drawn from $N(0, 0.1^2)$ for the logistic sigmoid connections, with the different biases initialized at zero. The weights and biases were updated with a learning rate of 10^{-3} and a momentum of 0.5 with an increment by 0.1 at 40% and 80% of the learning process (higher increments made the learning unstable). A cost of $2 \cdot 10^{-4}$ is imposed since this facilitates the learning process of CD by increasing the mixing rate of the Markov chain.

For the LSTM, the network consists of 50 blocks, each containing 2 cells (100 Neurons). The system was initialized with weights equal to a normally distributed random number $N(0, 0.01^2)$, and had an learning rate of 0.05. The LSTM was trained over 100 sweeps (or epochs). Logistic units were used for the system activation functions, as both,the hidden (cells in the blocks) and the output cells.

The mean absolute percentage error (MAPE) [20] was used to test the quality of the model over the whole prediction time:

$$MAPE = \frac{1}{N} \sum_{k=1}^{N} \frac{|e_t|}{x_t} \tag{15}$$

where n is the number of time periods, $e_t = x_t - \hat{x}_t$, where x_t is the actual observation for the time period t and $\hat{x}_t$ is the forecast for the same period. Besides calculating the Total MAPE, two other MAPEs were calculated. The first one is in the operation range, while the second one is not. Generally, the smaller the wind variation the lower the forecast error will be [20].

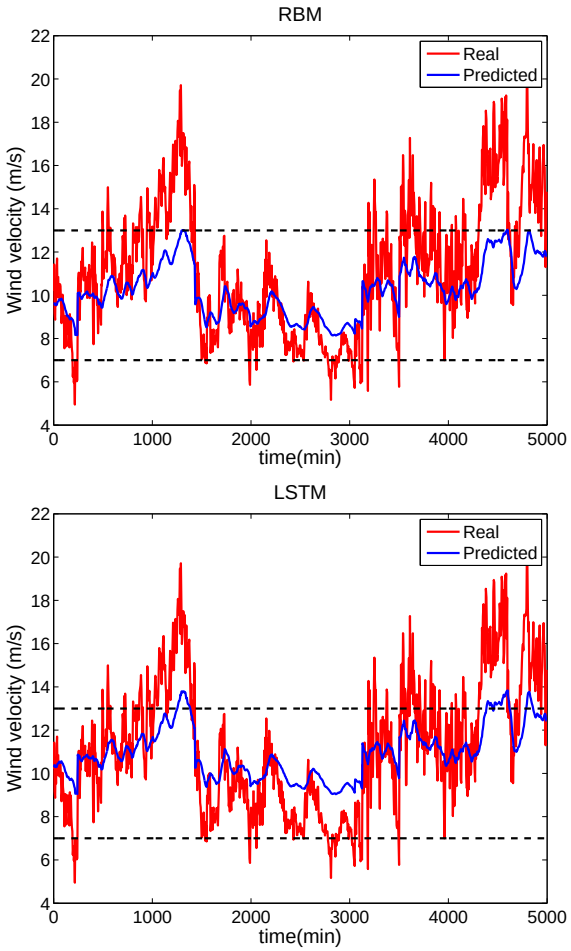

Fig. 5: Results of the prediction using RBM and LSTM

Table 1: Table of the total MAPE, the MAPE inside (in) and outside (out) of the threshold

	BP	RBM	LSTM
MAPE total	14.55%	14.30%	14.97%
MAPE(in)	9.89%	9.84%	11.68%
MAPE(out)	24.04%	24.02%	22.11%

4.4 Results

Figure 5 show the results of the prediction using the proposed methods. Notice how it follows the tendency of the real wind speed and the predicted one. A threshold is added between $(7, 13) m/s$ (dotted line) to appreciate the interval in which the method performs better.

Table 1 displays the MAPE of the different techniques, showing also the value of the MAPE inside and outside the threshold.

The results on BP are between the ones obtained from the two proposed techniques. The networks are being trained without discriminating or selecting specific bands and there is no preprocessing of the signal besides using a simple sample window, which allows the flow of information from the sensor to the control almost immediately.

5 Fuzzy Logic Supervisory Control

Fuzzy control allows programming with if-then rules, enabling experts to include their experience within the control system. Mamdani's method [41] proposed in 1974 uses synthesized linguistic rules and computes them taking the center of mass of the split membership functions to obtain a crisp output (or outputs) of the controller. This method has been effectively used in the

context of complex, not-well-defined processes and is one of the most widely used fuzzy logic systems [38].

The controller uses three input variables with membership functions of triangular and trapezoidal shapes for simplicity. The input variables are flywheel speed (Figure 6), wind turbine generation (Figure 7) and wind profile slope angle obtained from the prediction (Figure 8); meanwhile, the output membership function is referred to the power reference (see Fig. 9).

The slope angle is calculated using equation 16

$$\gamma = \arctan \frac{W_{SP}(z+2) - W_{SP}(z+1)}{T} \tag{16}$$

where γ is the slope angle, W_{SP} is the predicted wind speed z is a discrete time domain and T is the discrete signal period.

The objectives of the supervisory controller are to maintain the flywheel within maximum and minimum values and to smooth the total power delivered to the grid using the wind turbine power (P_{WT}), the flywheel speed (ω_{fw}) and the wind speed slope angle (γ). When the generated power is low, the total output power will be low enough to prevent the flywheel from decelerating below the minimum level, on the other hand when the generated power is medium or high the flywheel may charge or deliver energy depending on its rotational speed. The wind prediction slope angle gives extra information so the fuzzy logic can give a better power reference optimizing the FESS usage.

The membership limits were selected according to the maximum and minimum values that the controlled variables are allowed or can to take, for the flywheel speed, the minimum speed value is 0.8 of the synchronous speed, since the kinetic energy is a function of the squared rotational speed any value below that limit would not have enough energy to deliver it to the grid. On the other hand, the maximum flywheel speed depends on the flywheel design and the coupled electric machine. The maximum wind turbine generation limit is the nominal power (2.4 MW =1.5 pu), in this work a higher power were selected since the pitch controller do not actuate immediately, therefore the membership function domain was increased. Finally, the slope angle can only have values within the range of the arctan function.

The fuzzy rules based on input variables (Flywheel Speed, Wind Power and Wind Profile Slope Angle) are summarized in Table 2. The subsets of fuzzy membership are noted as follows: EL (Extremely low), VL (Very low), L (Low), ML (Medium low), MH (Medium high), M (Medium), H (High), VH (Very high), EH (Extremely high) and Max (Maximum). The antecedents are connected using the smallest degree of membership of the inputs (AND, minimum), while the fired rules are

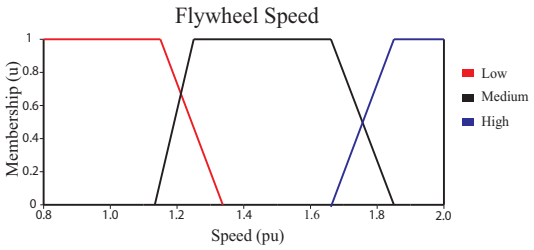

Fig. 6: Flywheel speed membership function

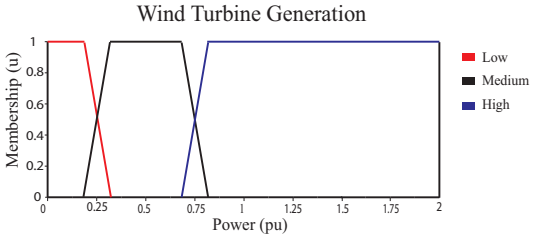

Fig. 7: Wind turbine generation membership function

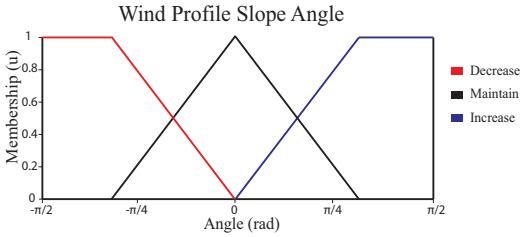

Fig. 8: Wind profile slope angle membership function

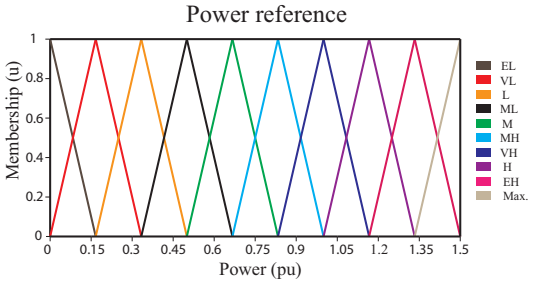

Fig. 9: Fuzzy sets for the power reference

connected using the minimum consequent implication method. Finally, the defuzzification is obtained with the center of mass method.

The output of the fuzzy logic controller is the total power of the system (wind turbine + flywheel). Since the induction machine is controlled using direct torque control, the torque reference of the electric machine is obtained using equation 17:

$$\tau_{im}^{*} = \frac{P_{ref} - P_{WT}}{\omega_{fw}} \tag{17}$$

Wind prediction slope angle - Decrease			
ω_{fw} \ P_{WT}	Low	Medium	High
Low	EL	L	M
Medium	VL	ML	MH
High	L	M	H
Wind prediction slope angle - Maintain			
Low	L	M	H
Medium	ML	MH	VH
High	M	H	EH
Wind prediction slope angle - Increase			
Low	ML	MH	VH
Medium	M	H	EH
High	MH	VH	Max.

Table 2: Fuzzy Rules

where P_{ref} is the output power reference of the supervisory controller, P_{WT} is the power delivered by the wind turbine and ω_{fw} is the flywheel angular speed.

6 Results of the wind turbine power extraction

Figure 10 represents the input wind speed of the system. The full range is within the operating zone of the wind turbine; although the nominal wind speed is 12 m/s. The pitch actuator is capable of maintaining safe operation up to a wind speed of 22 m/s, which is the cut out speed for this model (for pitch controller details see [55]). The simulation was done for 150 seconds. The electrical and mechanical characteristics of the simulated turbine are specified in the appendix.

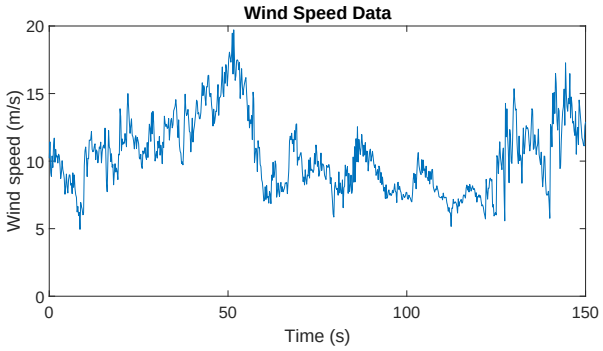

Fig. 10: Input wind speed.

The output power of the generator using the power base of the induction machine ($S_{base} = 1.6\ MVA$) is shown in Figure 11, while the rotational speed of the DFIG is shown in Figure 12.

The pitch angle controller is activated during high-speed periods in order to aerodynamically reduce the mechanical power at the shaft of the generator.

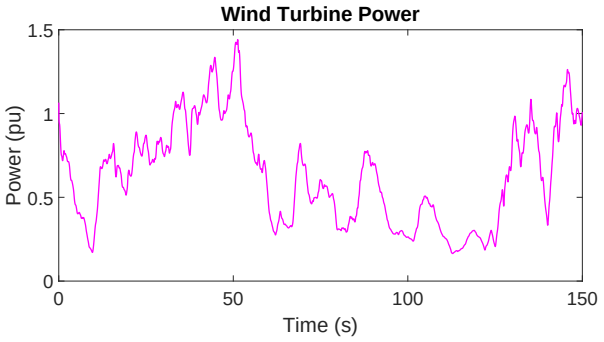

Fig. 11: Power extracted by the generator

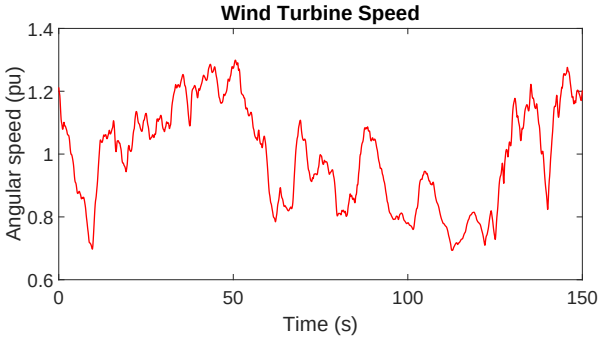

Fig. 12: Rotational speed of the DFIG

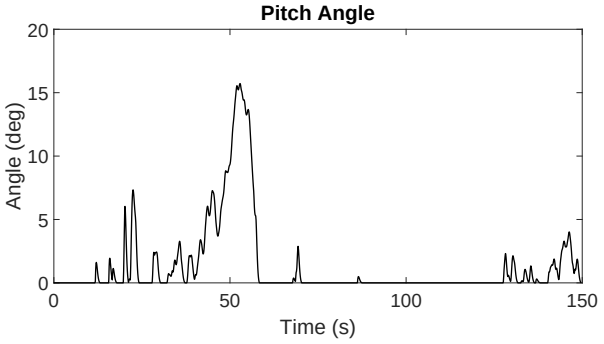

Fig. 13: Pitch angle of the blades

6.1 Results of supervisory controller

The most cited supervisory controller [33,11] was replicated (controller 1) and compared against the novel version (controller 2). The enhanced controller uses a short-term ahead prediction of 1 second, the reported results were obtained using RBM as wind speed predictor since that technique reported the lower MAPE, however, any of the presented techniques could be used obtaining very similar results .

In Figure 14 the results of the total power (generator+flywheel) are presented.

For the controller 1, the flywheel speed and reference torque for the DTC controller are shown in Figures 15

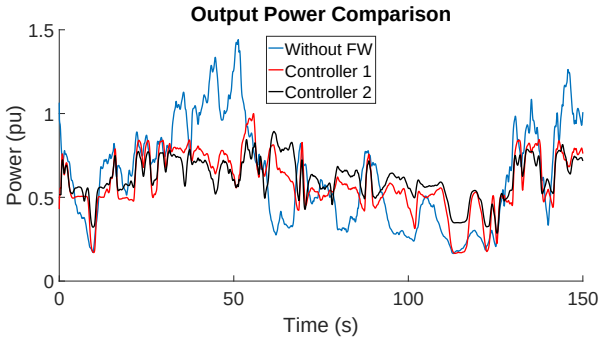

Fig. 14: Output power comparison

and 16, while for the controller 2, the same variables are shown in Figures 17 and 18.

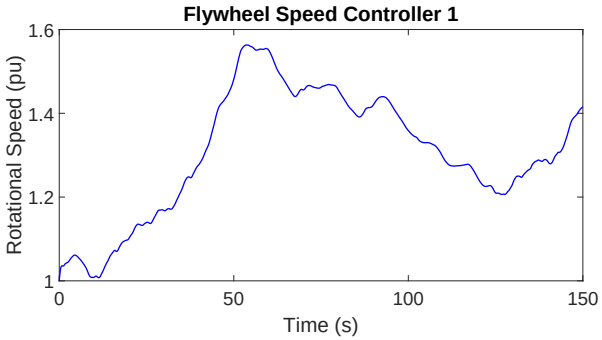

Fig. 15: Flywheel speed for controller 1

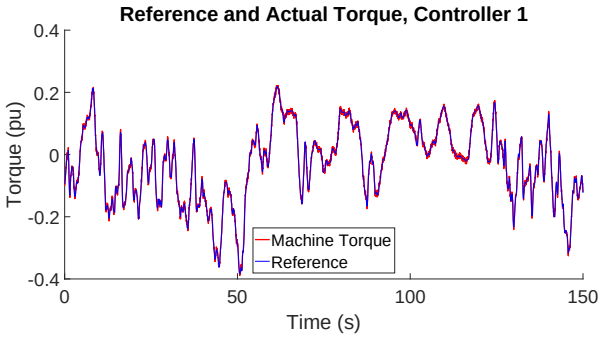

Fig. 16: Torque reference and real torque for controller 1

The mean squared error of the direct torque controller (Figures 16 and 18) is summarized in table 3.

In order to compare the proposed controller, the average and standard deviation of the output powers were calculated. The results show that the standard deviation of the output power signal decreased about 30 % with respect to the controller proposed in [33, 11], while the average power extracted remains close to the power extracted by the wind turbine alone.

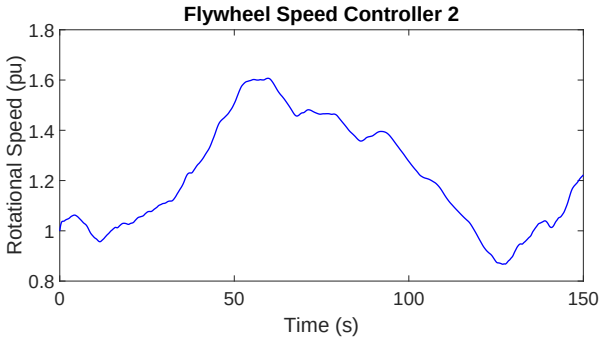

Fig. 17: Flywheel speed for controller 2

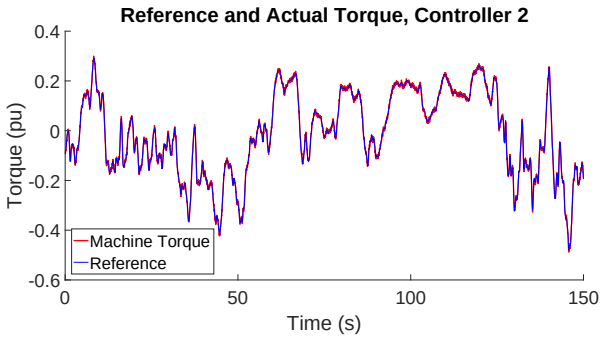

Fig. 18: Torque reference and real torque for controller 2

Table 3: DTC Mean Square Error of torque reference

Supervisory Controller	**Mean squared error**
Controller 1	3.2725 e-5
Controller 2	3.3043 e-5

Table 4: Statistical Results of Output Power

Supervisory Controller	**Average (pu)**	**Standard Deviation (pu)**
Without Controller	0.63154447	0.302308324
Controller 1	0.59154098	0.170911359
Controller 2	0.61399901	0.119457639

7 Conclusion

The main objective of this work has been to enhance the most common architecture of supervisory controllers by means of a fuzzy logic controller that works with predicted wind speed slope angle. Fuzzy logic controllers

have proven to be a suitable method for computing a power reference and inferencing the rules for proper actions for the flywheel (charge, discharge, maintain power). In this paper, a fuzzy controller that uses three inputs is proposed and proved; in the third input (wind prediction), the slope angle is used instead of the predicted value.

From the results of section 4, we can observe that the three used ANN algorithms have a good prediction of the wind tendency, which allow the implementation of ANN for short-term predicting, the additional information of the wind tendency improved the performance of the controller smoothing the output power of the system.

Furthermore, between both predicting architectures, RBM performs better than LSTM inside a certain threshold (Table 1), while on the outside it works the other way around. This effect opens a possibility to use both methods (selecting the most accurate method according to the threshold) to improve the predictions over the whole time interval.

The results demonstrate the effectiveness of the controller with respect the version that do not consider wind tendency; reducing maximum output power value from 0.9994 pu to 0.8931 pu and increasing minimum output power from 0.1654 pu to 0.2857 pu. The standard deviation of the output decreased 30 % consequently smoothing the output power of the turbine.

References

1. Abad, G., Lopez, J., Rodriguez, M., Marroyo, L., Iwanski, G.: Doubly fed induction machine: modeling and control for wind energy generation, vol. 85. John Wiley & Sons (2011)
2. Abdel-Khalik, A., Elserougi, A., Massoud, A., Ahmed, S.: A power control strategy for flywheel doubly-fed induction machine storage system using artificial neural network. Electric Power Systems Research **96**, 267–276 (2013)
3. Barbounis, T., Theocharis, J., Alexiadis, M., Dokopoulos, P.: Long-term wind speed and power forecasting using local recurrent neural network models. Energy Conversion, IEEE Transactions on **21**(1), 273–284 (2006). DOI 10.1109/TEC.2005.847954
4. Bengio, Y., Boulanger-Lewandowski, N., Pascanu, R.: Advances in optimizing recurrent networks. In: 2013 IEEE International Conference on Acoustics, Speech and Signal Processing, pp. 8624–8628. IEEE (2013)
5. Bilgili, M., Sahin, B., Yasar, A.: Application of artificial neural networks for the wind speed prediction of target station using reference stations data. Renewable Energy **32**(14), 2350–2360 (2007)
6. Bo, W., Baohui, Z., Zhiguo, H.: Control strategy for micro grid transfer between in-grid and short-time islanded states based on flywheel storage. In: Control Conference (CCC), 2013 32nd Chinese, pp. 8897–8902. IEEE (2013)
7. Cardenas, R., Pena, R., Asher, G., Clare, J.: Control strategies for enhanced power smoothing in wind energy systems using a flywheel driven by a vector-controlled induction machine. Industrial Electronics, IEEE Transactions on **48**(3), 625–635 (2001)
8. Cardenas, R., Pena, R., Clare, J., Asher, G.: Power smoothing in a variable speed wind-diesel system. In: Power Electronics Specialist Conference, 2003. PESC'03. 2003 IEEE 34th Annual, vol. 2, pp. 754–759. IEEE (2003)
9. Chung, J., Gulcehre, C., Cho, K., Bengio, Y.: Empirical evaluation of gated recurrent neural networks on sequence modeling. arXiv preprint arXiv:1412.3555 (2014)
10. Cimuca, G., Breban, S., Radulescu, M.M., Saudemont, C., Robyns, B.: Design and control strategies of an induction-machine-based flywheel energy storage system associated to a variable-speed wind generator. Energy Conversion, IEEE Transactions on **25**(2), 526–534 (2010)
11. Cimuca, G.O., Saudemont, C., Robyns, B., Radulescu, M.M.: Control and performance evaluation of a flywheel energy-storage system associated to a variable-speed wind generator. Industrial Electronics, IEEE Transactions on **53**(4), 1074–1085 (2006)
12. Daoud, M.I., Massoud, A., Ahmed, S., Abdel-Khalik, A., Elserougi, A.: Ride-through capability enhancement of VSC-HVDC based wind farms using low speed flywheel energy storage system. In: Applied Power Electronics Conference and Exposition (APEC), 2014 Twenty-Ninth Annual IEEE, pp. 2706–2712. IEEE (2014)
13. Diaz-Gonzalez, F., Bianchi, F.D., Sumper, A., Gomis-Bellmunt, O.: Control of a flywheel energy storage system for power smoothing in wind power plants. Energy Conversion, IEEE Transactions on **29**(1), 204–214 (2014)
14. El Mokadem, M., Nichita, C., Reghem, P., Dakyo, B.: Short term energy storage based on reluctance machine control for wind diesel system. In: Power Electronics and Motion Control Conference, 2006. EPE-PEMC 2006. 12th International, pp. 1585–1590. IEEE (2006)
15. Fonte, P., Silva, G.X., Quadrado, J.: Wind speed prediction using artificial neural networks. WSEAS Transactions on Systems **4**(4), 379–384 (2005)
16. Graves, A.: Generating sequences with recurrent neural networks. CoRR **abs/1308.0850** (2013)
17. Graves, A., Mohamed, A., Hinton, G.E.: Speech recognition with deep recurrent neural networks. CoRR **abs/1303.5778** (2013)
18. Greigarn, T., Garcia-Sanz, M.: Control of flywheel energy storage systems for wind farm power fluctuation mitigation. In: Energytech, 2011 IEEE, pp. 1–6. IEEE (2011)
19. Guan, C., Luh, P., Michel, L., Wang, Y., Friedland, P.: Very short-term load forecasting: Wavelet neural networks with data pre-filtering. Power Systems, IEEE Transactions on **28**(1), 30–41 (2013). DOI 10.1109/TPWRS.2012.2197639
20. Guo, Z., Zhao, W., Lu, H., Wang, J.: Multi-step forecasting for wind speed using a modified emd-based artificial neural network model. Renewable Energy **37**(1), 241–249 (2012)
21. Hernández, C.V., Telsnig, T., Pradas, A.V.: JRC wind energy status report 2016 edition (2017)
22. Hinton, G.: A practical guide to training restricted Boltzmann machines. In: G. Montavon, G. Orr, K.R. Mller (eds.) Neural Networks: Tricks of the Trade, *Lecture Notes in Computer Science*, vol. 7700, pp. 599–619. Springer Berlin Heidelberg (2012). DOI 10.1007/978-3-642-35289-8:32. URL http://dx.doi.org/10.1007/978-3-642-35289-8:32

23. Hinton, G.E.: Training products of experts by minimizing contrastive divergence. Neural Computation, 14(8): 17111800, pp. 1771–1800 (2002)
24. Hinton, G.E., Sejmowski, T.J.: Optimal perceptual interface. Proceedings of the IEEE conference on Computer Vision and Pattern Recognition, Washington, D.C., June, 1983 (1983)
25. Hochreiter, S., Schmidhuber, J.: Long short-term memory. Neural Comput. **9**(8), 1735–1780 (1997)
26. Hu, K., Liaw, C.: On the flywheel/battery hybrid energy storage system for dc microgrid. In: Future Energy Electronics Conference (IFEEC), 2013 1st International, pp. 119–125. IEEE (2013)
27. Islam, F., Al-Durra, A., Muyeen, S.: Smoothing of wind farm output by prediction and supervisory-control-unit-based fess. IEEE Transactions on Sustainable Energy **4**(4), 925–933 (2013)
28. Islam, F., Hasanien, H., Al-Durra, A., Muyeen, S.: A new control strategy for smoothing of wind farm output using short-term ahead wind speed prediction and flywheel energy storage system. In: American Control Conference (ACC), 2012, pp. 3026–3031. IEEE (2012)
29. Jerbi, L., Krichen, L., Ouali, A.: A fuzzy logic supervisor for active and reactive power control of a variable speed wind energy conversion system associated to a flywheel storage system. Electric Power Systems Research **79**(6), 919–925 (2009)
30. Kariniotakis, G., Stavrakakis, G., Nogaret, E.: Wind power forecasting using advanced neural networks models. Energy Conversion, IEEE Transactions on **11**(4), 762–767 (1996). DOI 10.1109/60.556376
31. Larochelle, H., Bengio, Y.: Classification using discriminative restricted Boltzmann machines. In: In ICML 08: Proceedings of the 25th International Conference on Machine learning. ACM (2008)
32. Leclercq, L., Robyns, B., Grave, J.: Fuzzy logic based supervisor of a flywheel energy storage system associated with wind and diesel generators. In: Proceedings of the 8th International Conference on Optimization of Electrical and Electronic Equipments-OPTIM, pp. 441–446 (2002)
33. Leclercq, L., Saudemont, C., Robyns, B., Cimuca, G., Radulescu, M.: Flywheel energy storage system to improve the integration of wind generators into a network. In: Proc. of the 5th International Symposium on Advanced Electromechanical Motion Systems, vol. 2, pp. 641–646 (2003)
34. LeCun, Y., Bengio, Y., Hinton, G.: Deep learning. Nature **521**(7553), 436–444 (2015)
35. Lee, D., Baldick, R.: Short-term wind power ensemble prediction based on gaussian processes and neural networks. Smart Grid, IEEE Transactions on **5**(1), 501–510 (2014). DOI 10.1109/TSG.2013.2280649
36. Li, S., Wunsch, D., O'Hair, E., Giesselmann, M.: Using neural networks to estimate wind turbine power generation. Energy Conversion, IEEE Transactions on **16**(3), 276–282 (2001). DOI 10.1109/60.937208
37. Liu, J.N., Hu, Y., You, J.J., Chan, P.W.: Deep neural network based feature representation for weather forecasting. In: Proceedings on the International Conference on Artificial Intelligence (ICAI), p. 1. The Steering Committee of The World Congress in Computer Science, Computer Engineering and Applied Computing (WorldComp) (2014)
38. Liu, Y., Chen, G., Ying, M.: Fuzzy logic, soft computing and computational intelligence. Berlin: Springer-Verlag (2005)
39. Lubosny, Z.: Wind turbine operation in electric power systems: advanced modeling. Springer Heidelberg (2003)
40. Lubosny, Z., Bialek, J.W.: Supervisory control of a wind farm. Power Systems, IEEE Transactions on **22**(3), 985–994 (2007)
41. Mamdani, E.H.: Application of fuzzy algorithms for control of simple dynamic plant. In: Proceedings of the Institution of Electrical Engineers, vol. 121, pp. 1585–1588. IET (1974)
42. Mohandes, M., Halawani, T., Rehman, S., Hussain, A.A.: Support vector machines for wind speed prediction. Renewable Energy **29**(6), 939 – 947 (2004)
43. Mohandes, M.A., Rehman, S., Halawani, T.O.: A neural networks approach for wind speed prediction. Renewable Energy **13**(3), 345 – 354 (1998)
44. More, A., Deo, M.: Forecasting wind with neural networks. Marine Structures **16**(1), 35–49 (2003)
45. Navdeep, J., Hinton, G.E.: Learning a better representation of speech sound waves using restricted Boltzmann machines. Proceedings of the 12th International Conference on Artificial Intelligence and Statistics (AISTATS) (2011)
46. Nobuta, M., Takahashi, R., Murata, T., Tamura, J., Sugimasa, M., Komura, A., Futami, M., Ichinose, M., Ide, K.: Cooperative operation of a wind energy conversion system with a hydrogen electrolyzer by using an adjustable speed flywheel generator. Electrical Engineering in Japan **168**(3), 19–27 (2009)
47. Ong, C.M.: Dynamic simulation of electric machinery: using MATLAB/SIMULINK, vol. 5. Prentice Hall PTR Upper Saddle River, NJ (1998)
48. Petersson, A.: Analysis, modeling and control of doubly-fed induction generators for wind turbines. Ph.D. thesis (2005)
49. Qiao, W.: Dynamic modeling and control of doubly fed induction generators driven by wind turbines. In: Power Systems Conference and Exposition, 2009. PSCE'09. IEEE/PES, pp. 1–8. IEEE (2009)
50. Salakhutdinov, R., Mnih, A., Hinton, G.: Restricted Boltzmann machines for collaborative filtering. In: Proceedings of the 24th International Conference on Machine learning, pp. 791–798. ACM (2007)
51. Schmidhuber, J.: Deep learning in neural networks: An overview. Neural Networks **61**, 85 – 117 (2015). DOI http://dx.doi.org/10.1016/j.neunet.2014.09.003. URL http://www.sciencedirect.com/science/article/pii/S0893608014002135
52. Suvire, G., Mercado, P.: Active power control of a flywheel energy storage system for wind energy applications. IET Renewable Power Generation **6**(1), 9–16 (2012)
53. Suvire, G., Mercado, P.: Combined control of a distribution static synchronous compensator/flywheel energy storage system for wind energy applications. IET Generation, Transmission & Distribution **6**(6), 483–492 (2012)
54. Tsili, M., Papathanassiou, S.: A review of grid code technical requirements for wind farms. IET Renewable Power Generation **3**(3), 308–332 (2009)
55. Villanueva, I., Ponce, P., Molina, A.: Interval type 2 fuzzy logic controller for rotor voltage of a doubly-fed induction generator and pitch angle of wind turbine blades. IFAC-PapersOnLine **48**(3), 2195–2202 (2015)

8 Appendix A

In this appendix are presented the parameters used in the simulation

System	Parameter	Value
Wind Turbine	$\rho(km/m^3)$	1.25
	$A(m^2)$	3848.45
	$\Lambda_{optimal}$	12
Blades Model	c_1	0.5
	c_2	116
	c_3	0.4
	c_4	0
	c_5	5
	c_6	21
DFIG	$R_s(pu)$	0.006014
	$R'_r(pu)$	0.01216
	$L_{ls}(pu)$	0.05783
	$L'_{lr}(pu)$	0.05783
	$L_m(pu)$	1.85083
	$S_{base}(MVA)$	2.4
Induction Machine	$R_s(pu)$	0.0275
	$R'_r(pu)$	0.0275
	$L_{ls}(pu)$	0.0833
	$L'_{lr}(pu)$	0.0833
	$L_m(pu)$	4.22
	$S_{base}(MVA)$	1.6
	$J_{FW}(kg.m^2)$	5656.85
DFIG mechanical model	$J_W(kg.m^2)$	3
	$J_G(kg.m^2)$	0.089
	ν	6.25
IM mechanical model	$J_{FW}(kg.m^2)$	5656.85
Grid-Side Control	$L_f(pu)$	0.0015
	$V^*_{DC}(V)$	1200
	V_{DC} regulator parameter	$K_p = 5$,$K_i = 0.1$
	Current regulator parameters	$K_p = 100$,$K_i = 1$
DFIG Vector control	Current regulator parameters	$K_p = 40$,$K_i = 2$

3.2 Pitch angle control using type 2 fuzzy logic

Villanueva, I., Ponce, P., & Molina, A. (2015). **Interval type 2 fuzzy logic controller for rotor voltage of a doubly-fed induction generator and pitch angle of wind turbine blades**. *IFAC-PapersOnLine*, 48(3), 2195-2202.

This paper has been presented in the 2015 IFAC Symposium on Information Control in Manufacturing (INCOM 2015) in Ottawa, Canada.

The paper presents the advantages of type 2 fuzzy logic in presence of white noise, the fuzzy logic controller is used to control the pitch angle of the wind turbine blades. The fuzzy controller is also used for the current regulation loop of the vector controller, giving the advantage of easy tunning and good performance.

Available online at www.sciencedirect.com

ScienceDirect

IFAC Papers Online
CONFERENCE PAPER ARCHIVE

IFAC-PapersOnLine 48-3 (2015) 2195–2202

Interval Type 2 Fuzzy Logic Controller for Rotor Voltage of a Doubly-Fed Induction Generator and Pitch Angle of Wind Turbine Blades

Iván Villanueva*, Pedro Ponce, Arturo Molina *****
Tecnológico de Monterrey, Mexico
* A01212854@itesm.mx
** pedro.ponce@itesm.mx
***armolina@itesm.mx

Abstract: Wind resource is highly unpredictable, intermittent and uncertain, for periods of higher speed that rated pitch angle can be controlled in order to maintain the power generation within the rank of the nominal power of the electric generator, in this paper an interval type 2 fuzzy logic controller is designed in NI LabVIEW for a non-linear model of turbines blades, after that, the controller is incorporated in a complete model of a DFIG wind turbine and another interval type 2 fuzzy controller is used for controlling the frequency and amplitude of the rotor's voltage. Finally the simulation results are shown and white noise is added for testing the performance of the controller under this condition. A comparison is made between the performance of the type-2 fuzzy logic controller, type 1 controller and a traditional PI controller tuned by trial and error method.

Keywords: Interval type 2 fuzzy logic controller, wind turbine, doubly-fed induction generator.

1. INTRODUCTION

The uncertain nature of wind makes necessary to design more powerful control systems which needs to be able to deal with any condition that could occur. High wind speed is one of them and can be either passive stall control or active pitch control. The passive stall control suffers from the disadvantage of uncertainties in aerodynamic behaviour post-stall (Burton et al., 2011), in the other hand, the active pitch control requires an actuator in order to rotate the blades but has the significant advantage of maintaining the blade stalled above the rated wind speed and therefore limit the power extracted from the wind to secure levels and continue operation.

Besides the active pitch control, the variability of the wind turbine angular speed allows a higher energy extraction, improvements in lower components stress and fewer grid connection power peak (Boukhezzar and Siguerdidjane, 2005), reducing acoustic noise of the turbine and allowing the decoupling of the active and reactive power through power electronics (Xu and Cartwright, 2006). Many simple, linear proportional-integrate-derivative (PID) controllers has been easily implemented in the field environment (Hand and Balas, 1999), but they have to be tuned and only works for an specific model of wind turbine. The gain selection of those controllers is traditionally tuned by trial and error process and the results depends on the expertise and intuition of the designated engineers.

Type 2 fuzzy sets (T2FS) are the natural expansion of type 1 fuzzy logic sets (T1FS), the bases of T2FS were introduced by Zadeh in 1975 (Zadeh, 1975). T2FS provides an additional membership function within the primary membership function, this allows T2FS to handle uncertainties and add parameters in order to increase the configurability of fuzzy sets and provide better results in operation. However, the computational cost increase exponentially with respect to T1FS, a simplification of the general T2FS is the Interval Type 2 fuzzy sets (IT2FS) where the secondary membership function has a constant value of 1. Gorzałczany (Gorzałczany, 1987) and Mendel (Liang and Mendel, 2000) established the bases of IT2FS. Many applications has been made with the IT2FS tool (Biglarbegian et al., 2011, Gorzałczany, 1987, Jammeh et al., 2009, Wu and Mendel, 2002), providing their effectiveness and capability of leading with uncertainties which can be intrinsic to the nature of the inputs to the system.

In this paper interval type 2 fuzzy sets (IT2FS) are used for the control application, the control system is based on a proportional-integral fuzzy controller and white noise is added for proving the benefits of the type 2 fuzzy sets, additionally the parameters of the wind turbine are modified for testing the usefulness of the controller during different conditions.

The IT2FS controllers are used for controlling both, the pitch angle of the blades and the frequency and amplitude of the rotor's voltage, a doubly-fed induction generator (DFIG) is considered because it has been highly proved in wind turbines applications due to the reduction in converters size which are approximately 30 % of the nominal power (Abad et al., 2011), a non-linear model of a wind turbine is used for modelling the blades, the model's used parameters has been proved in experimental rotor-torque characteristics of WKA-60 rotors (Lubosny, 2003).

10.1016/j.ifacol.2015.06.414

All the system is modelled and simulated in NI LabVIEW with the objective of a further application in an FPGA module for the control of a real DFIG with simulated loads.

The paper is organized as follow. Section 2 describes the models implemented for the simulation. Section 3 presents the designed IT2FS used for controlling the pitch angle and the electric machine. Section 4 presents the results and the comparison between a type 2 fuzzy logic PI controller, type 1 fuzzy PI controller and a traditional PI controller. Finally section 5 concludes this paper.

2. WIND TURBINE MODEL

Wind turbines are devices which objective is to extract the mechanical power of the wind and transform it into usable electric energy. The most used wind turbines are the horizontal axis ones based on the lifting force. The general structure of a horizontal wind turbine is presented in the next sub-section.

2.1 General structure of a horizontal wind turbine

On figure 1 is shown the basic structure of a horizontal axis wind turbine (HAWT). One of the most important parts are the blades which are used for mechanical power extraction from the wind, the blades are attached to the rotor which transmit the extracted power through a shaft to a gearbox designed for increasing the angular velocity of the rotor and transmit it through a high speed shaft to a generator, there are many generators available in the industry for wind applications, however the DFIG have undoubtedly arisen as one of the leading technologies for wind turbine manufacturing, demonstrating that is a cost effective, efficient and reliable solution (Abad et al., 2011).

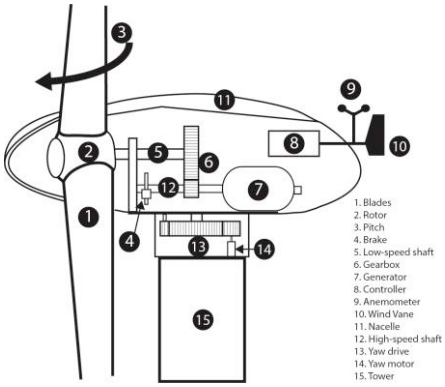

Fig. 1. General structure of a HAWT.

In this work the yaw mechanism was not considered since only the normal to the blades horizontal component of the wind is used for calculations.

In summary, we are considering an ideal normal component of wind which gives mechanical energy to the blades attached to an inertial mass (rotor), torsional spring and damper (low speed shaft), then an ideal gearbox and another inertial mass (generator shaft) as the transmission medium for the mechanical power of the DFIG. In the next sub-section the mathematical model of the described components is presented.

2.2 Mechanical power extraction from the wind and (blades model)

The power that can be extracted from the wind depends on its kinetic energy of it and can be obtained from:

$$P = \frac{1}{2} C_P(\lambda, \theta) \rho A V^3 \quad (1)$$

Where:

- Cp is the power coefficient (maximum achievable is 0.593 because of Betz limit) and is a function of the tip speed ratio λ and the pitch angle θ.
- ρ is the density of the fluid.
- A is the transversal area of the turbine.
- V is the normal component of the speed.

As can be seen the velocity has a great impact, and it is the most important issue for choosing the location of the turbine (Burton et al., 2011).

The power coefficient Cp represents the efficiency of the turbine and this factor depends only on the aerodynamical properties of the blades. The power coefficient is a function of the tip speed ratio (λ) and pitch angle θ. The tip speed ratio is the relation between the tangential component of the tip of the blades and the normal component of the wind speed, it is defined as follow:

$$\lambda = \frac{\omega R}{V} \quad (2)$$

Where ω is the rotational speed of the blades, R is the rotor's radium and V is the normal component of the wind speed. Figure 2 shows the Cp-λ characteristics of the modeled airfoil, it can be seen that there is a specific λ where the turbine extracts the maximum energy from wind, so it is important maintaining constant the factor ω/V. The angle θ is modified in some fixed speed wind turbines in order to maintain the energy production below the maximum power capacity of the system in case of high wind periods, otherwise it will result in damage to the electric generator.

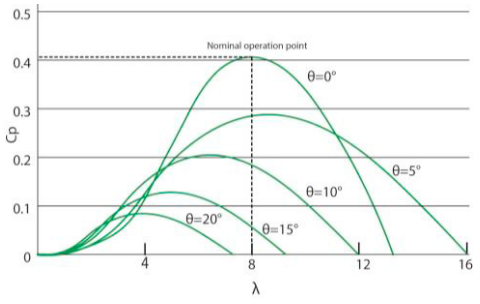

Fig. 2. Cp-λ Characteristic of the simulated airfoil for different values of pitch angle.

According to (Lubosny, 2003) a wind turbine can be modelled with the following polynomial form:

$$\boldsymbol{Cp = c_1[c_2/\Lambda - c_3\theta - c_4\theta^x - c_5]e^{-c6/\Lambda}} \quad (3)$$

$$\frac{\mathbf{1}}{\boldsymbol{\Lambda}} = \frac{\mathbf{1}}{\boldsymbol{\lambda + 0.08\,\theta}} - \frac{\mathbf{0.035}}{\mathbf{1+\theta^3}} \quad (4)$$

Where C1-C6 and x are coefficients obtained from experimental results of the blades. λ is the tip speed ratio defined by equation 2.
The next table summarizes the coefficients used for obtaining the Cp-λ curves shown in figure 2, those values are based on experimental results of a WKA-60 wind turbine(Lubosny, 2003).

Table 1. Parameters used in the simulation for the blade's model

Coefficient	Value
C1	0.5
C2	116
C3	0.4
C4	0

2.3 Drive train model

The drive train consist on the element that transmit the mechanical power from the blades to the electric machine, which are the low speed shaft, the gearbox and the high speed shaft. Those elements can be seen in figure 1, numbered 5, 6 and 12 respectively.

The drive train was modeled as an inertial mass which represents the rotor with the blades and the inertia of the low speed shaft. The low speed shaft was modeled as a damper and a rotational spring, the damp coefficient and spring constant of the high speed shaft were neglected since is considered as a very short shaft with negligible friction losses and rigid material. The gears are considered ideal and for the generation is considered the rotational inertia. Figure 3 shows all the components of the drive train which are modeled.

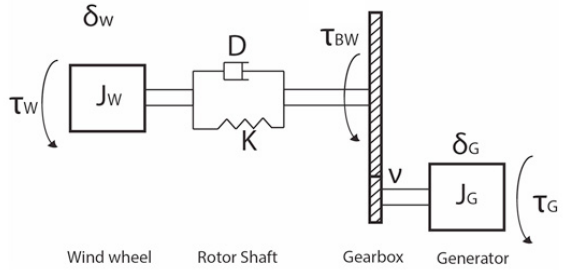

Fig. 3. Drive train model for the wind turbine simulation.

Taking into account all the assumptions made before the equations that describe the drive train are:

$$J_W \frac{d^2\delta_W}{dt} = \tau_W - \tau_{BW} \quad (5)$$

$$J_G \frac{d^2\delta_W}{dt} = \tau_G - \frac{\tau_{BW}}{\nu} \quad (6)$$

$$\tau_{BW} = K\left(\delta_W - \frac{\delta_G}{\nu}\right) + D\left(\frac{d\delta_W}{dt} - \frac{d\delta_G}{dt}\frac{1}{\nu}\right) \quad (7)$$

Where τ_W is the torque extracted from the wind, δ_W is the angle position of the rotor, J_W is the inertia of the wind wheel, D is the damper coefficient of the low speed shaft, K is the torsional spring constant of the low speed shaft, τ_{BW} is the torque at the low speed side of the gearbox, ν is the gearbox ratio defined as:

$$\nu = \frac{rotational\ speed\ at\ high\ speed\ shaft}{rotational\ speed\ at\ low\ speed\ shaft} \quad (8)$$

δ_G is the angular position at the generator side, worth mentioning that the angular position at the left side of the gearbox is $\frac{\delta_G}{\nu}$ because the high speed shaft is considered as a rigid body and the angle do not vary in the entire body. J_G is the rotational inertia of the generator and τ_G is the torque at the generator shaft. In the next table are shown the constant values used for modelling the drive train used in the simulation.

Table 2. Drive train model parameters used in the simulation.

Coefficient	Value
J_W	0.089 kg.m^2
J_G	0.089 kg.m^2
ν	6.25
K	1453 N.m/deg
D	0.015 N.m.s

2.4 DFIG model

In order to control the rotational speed of the electric machine and obtain the best efficiency at a wide range of operation, many electric machines equipped with power converters has been proved in industrial applications. The DFIG has been widely used because it has the advantage of implementing a reduced size power converter. The typical scheme implemented is shown in figure 4. The rotor can be accessed through slip rings and two PWM power converters are installed in a back-to-back configuration, the voltage frequency and amplitude can be controlled by adjusting the switching of the transistors.

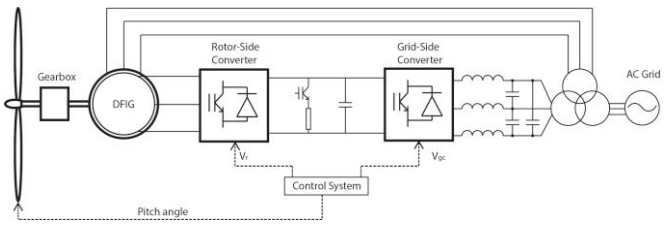

Fig. 4. DFIG wind turbine scheme.

The frequency of the stator can be determine by the following equation:

$$f_{stator} = \frac{n_{rotor} \times P}{120} \pm f_{rotor} \quad (9)$$

Where *nrotor* is the rpm speed of the rotor, *P* is the number of poles of the machine and *frotor* is the electrical frequency of the current that flows in the rotor. Of course the stator frequency is fixed since it is connected directly to the electric grid, therefore in order to modify the speed of the rotor it is necessary to control the electric frequency of the rotor's power source.

The DFIG can be modeled as a traditional induction machine, with the only difference that the voltage at the rotor side is different to zero. The voltage equations of the stator and rotor referred to the stator side at any reference frame with angular speed ω can be written as follows (Ong, 1998):

$$v_{qs} = p\lambda_{qs} + \omega\lambda_{ds} + R_s i_{qs} \quad (10)$$
$$v_{ds} = p\lambda_{ds} + \omega\lambda_{qs} + R_s i_{ds} \quad (11)$$
$$v'_{qr} = p\lambda'_{qs} + (\omega - \omega_r)\lambda'_{ds} + R'_r i'_{qs} \quad (12)$$
$$v'_{dr} = p\lambda'_{dr} - (\omega - \omega_r)\lambda'_{qr} + R'_r i'_{dr} \quad (13)$$

Where p represent a differential operator. λ is magnetic linkage flux and the subscript $_d$ and $_q$ are the corresponding component in the d-q reference frame and $_s$ and $_r$ are the subscripts of stator and rotor respectively. ω is the angular speed of the reference frame with respect to an stationary reference frame, ω_r is the speed of the rotor with respect to an stationary reference frame, R is the resistance value and i is the current value. $'$ means that the quantity is related to the stator's voltage base.

The stator and rotor flux linkage can be expressed in matrix form as follows:

$$\begin{bmatrix}\lambda_{qs}\\ \lambda_{ds}\\ \lambda'_{qs}\\ \lambda'_{ds}\end{bmatrix} = \begin{bmatrix} L_{ls}+L_m & 0 & L_m & 0 \\ 0 & L_{ls}+L_m & 0 & L_m \\ L_m & 0 & L'_{lr}+L_m & 0 \\ 0 & L_m & 0 & L'_{lr}+L_m \end{bmatrix} \begin{bmatrix} i_{qs}\\ i_{ds}\\ i'_{qr}\\ i'_{ds}\end{bmatrix} \quad (14)$$

Where L_{ls} is the linkage inductance of the stator L_m is the magnetizing inductance on the stator side and L'_{lr} is the linkage inductance of the rotor referred to the stator side.

The electromagnetic torque can be obtained by:

$$T_G = \frac{3P}{4} * L_m(i'_{dr}i_{qs} - i'_{qr}i_{ds}) \quad (15)$$

If the equations are represented in an equivalent circuit form the resulting circuit will looks as follow:

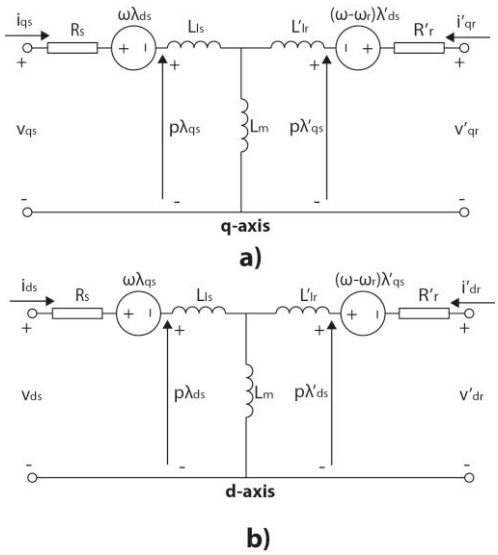

Fig. 5. Equivalent circuit of the dynamic model of a DFIG in an arbitrary reference frame. a) q axis circuit, b) d axis circuit.

Table 2. DFIG simulation parameters.

Coefficient	Value
R_s	0.003007 pu
R'_r	0.00608 pu
L_{ls}	0.05783 pu
L_m	1.85068 pu
L'_{lr}	0.05783 pu
F_{base}	60 Hz
S_{base}	1.6E+6 W

The main reason of using a DFIG is the possibility of modifying the rotor speed. Variable speed wind energy conversion systems (WECS) can provide greater efficiency that fixed ones, in a large period of time, it is economically viable to implement a variable speed control for obtaining maximum wind energy. The speed control strategy consist on obtaining the maximum power point of the Cp- λ curve at any time, as shown in figure 6, once the power has reached it nominal value, the control strategy must change trying to maintain the power generation at its limit value for avoiding endangering the electric machine:

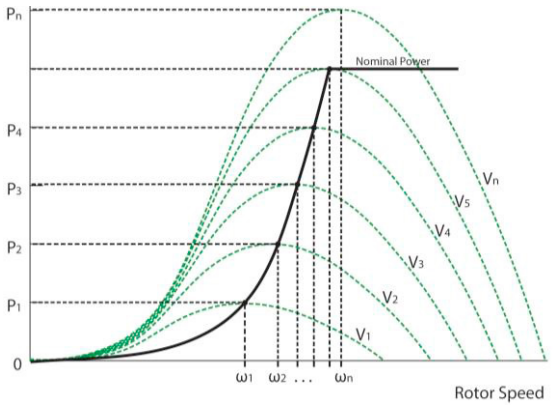

Fig. 6. WECS maximum power extraction.

2.5 Pitch actuator

A pitch actuator is needed for the active-pitch control. Where the power limitation in high winds is achieved by modifying the attack angle of the blades, this inducing blade feathering effect. The range of blade pitch is angles required is from 0° to about 35° according to (Munteanu et al., 2008). In order to meet the requirements for the power limitation in a real system, the pitch actuator needs to acts rapidly with changes rates of about 5°/s. Most actuators are made of mechanical components since the precision of the actuator is crucial, typically they are based on ball screws or rack-pinion driven by electric servo-motors. The pitch actuator can be approximated to a second order transfer function:

$$H(s) = \frac{\theta}{\theta_{ref}} = \frac{K\omega_n^2}{s^2+2\zeta\omega_n * s+\omega_n^2} \quad (16)$$

Where θ is the pitch angle of the turbine, θ_{ref} is the desired pitch angle, ζ is the critical damping coefficient (typically about 80%), ω_n is the natural frequency (4 rad/s were used in (Fadaeinedjad et al., 2008)) and K is a constant gain.

3. INTERVAL TYPE 2 FUZZY SETS

In 1975 Lofti Zadeh proposed the the bases of T2FS (Zadeh, 1975). But it was not until the weaknesses of T1FS came to light that the mathematical bases of the operators of T2FS were developed.

Mizumoto and Tanaka (Mizumoto and Tanaka, 1976) studied and presented the basic algebraic structures for fuzzy sets for the joint, meet and negation operation employing the principles of fuzzy sets defined by Zadeh, after that Karnik and Mendel (Karnik et al., 1999) developed the mathematical bases for the implementation of type 2 fuzzy logic sets. In (Karnik et al., 1999) is defined the concept of footprint of uncertainty, the mathematical bases for the T-norm and T-conorm and three type reducer techniques for implementing the defuzzification: centroid, height and center of sets.

Once the bases of type 2 were published, Gorzalczany (Gorzałczany, 1987) published the first interval type 2 technique and many other authors start implementing it and continue researching (Schwartz, 1985, Türkşen, 1995, Klir and Folger, 1988). In 2000 Liang and Mendel published the theory and design of the interval type 2 fuzzy sets (Liang and Mendel, 2000) and introduce the concept of upper and lower membership functions, this paper presented an application for performing time series forecasting with the input signal corrupted by additive noise.

Interval type 2 fuzzy logic has developed quickly due to the fast computation respect to the general case where the secondary set has a non-interval shape making the computation much more difficult. The fast success of interval type 2 fuzzy logic is proved by the raise in the number of publications since 1999 and until present. Interval type 2 fuzzy logic provides good applications performance and there are many comparisons with type 1 fuzzy logic, however, the great potential of the general case gets limited when interval is used for defining the secondary membership function. As shown in figure 8, IT2FS is a special case of T2FS where one dimension of the membership function is constant. $\mu_{\tilde{A}}(x,u) = 1$.

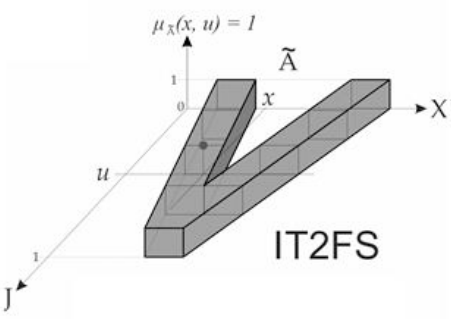

Fig. 8. 3D representation of IT2FS.

The definition of IT2FS can be written in integral form as:

$$\tilde{A} = \int_{x\in X} \int_{u\in J_x} \frac{1}{(x,u)} \qquad J_x \subseteq [0,1] \quad (17)$$

Where the ∫ operator means union of all the elements within the rank of x and u.

3.1 Interval type 2 PI fuzzy controller design.

In figure 8 is shown the scheme implemented for the PI fuzzy controllers, when the wind speed is superior to the nominal wind speed and the power extracted by the blades could damage the electric generator, the controller modifies the pitch angle of the blades. The inputs for the fuzzy controller are the error and the derivate of error. The output of the fuzzy controller is integrated and that value is sent to the pitch actuator. Once the pitch angle is obtained is used in combination with the wind speed and the rotational speed of the electric machine for the estimation of the generation power. Then the actual power error is calculated and used to evaluate the performance of the controller.

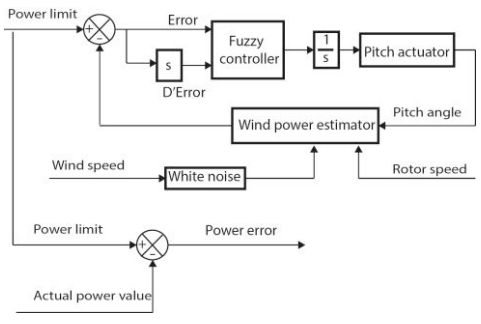

Fig. 9. PI fuzzy control scheme for power limitation.

To control the electric machine a field oriented control was used, where the active and the reactive power were controlled separately. The vector of stator magnetic flux was aligned to the direct axis. Under this orientation the active, reactive power of the stator and rotor currents may be related as (Abad et al., 2011):

$$P_s = -\frac{3}{2} V_g \frac{L_m}{L_{ls}} i_{qr} \quad (18)$$

$$Q_s = \frac{3\,V_g^2}{2\omega_s L_{ls}} - \frac{3}{2} V_g \frac{L_m}{L l_s} i_{dr} \quad (19)$$

Where P_s is the active power of the stator, Q_s is the reactive power of the stator, V_g is the voltage of the grid, ω_s is the angular speed of the stator flux, L_m is the mutual inductance, L_{ls} the stator inductance and i_{dr} and i_{qr} are the direct and quadrant components of the current respectively. In figure 10 can be seen the strategy followed in order to control the DFIG

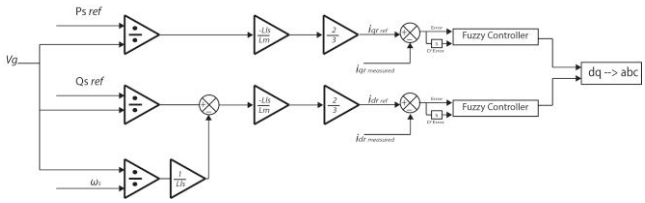

Fig. 10. Vector control diagram implemented.

The fuzzy controller has as inputs the error and the derivate of the error (D'Error), the used rules were obtained from (Ponce Cruz, 2011) and are summarized in the following table:

Table 3. Rules for the fuzzy controller

Error/D'Error	**N**	**Z**	**P**
N	N	N	N
Z	N	Z	P
P	P	P	P

In order to evaluate the performance of the controller, the quadratic error criteria was used, defined as:

$$ISE = \int_0^\infty e(t)^2 dt \quad (18)$$

Where e is the error with respect to time. The type 1 fuzzy set shape used for terms of comparison can be seen in figure 10:

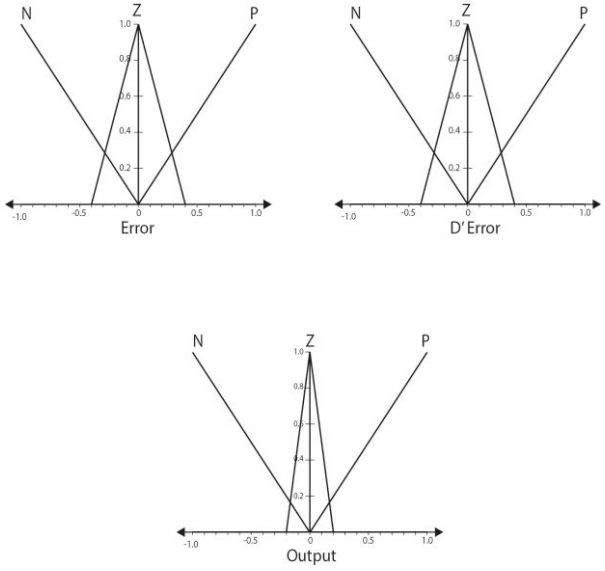

Fig. 11. Type 1 fuzzy sets used.

Then three Type 2 fuzzy sets were proposed with different ranges of footprint of uncertainty (FOU). The proposed controllers were evaluated with different amount of amplitude for the white noise. The width of the FOU was changed for obtaining the shape that can handle more white noise. The shapes of the evaluated IT2FS are showed below:

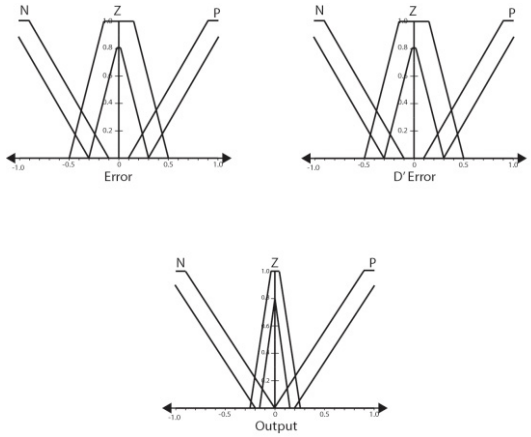

Fig. 12. Type 2 fuzzy sets used for controller 1.

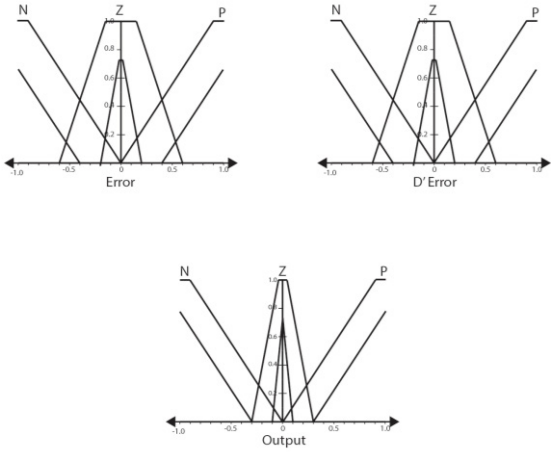

Fig. 13. Type 2 fuzzy sets used for controller 2.

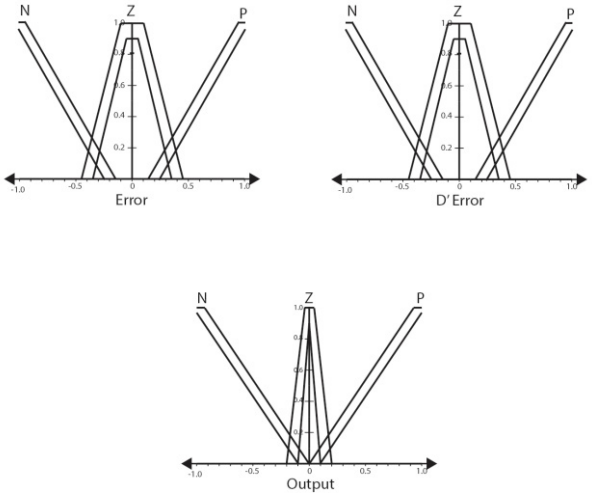

Fig. 14. Type 2 fuzzy sets used for controller 3.

4. RESULTS

The wind used for the performance test were signals with no noise, 0.833 % of amplitude of the nominal wind speed (12 m/s), 4.167 % of amplitude of the nominal wind speed and 6.667 of amplitude of the nominal wind speed. The input signal is shown in the next figure:

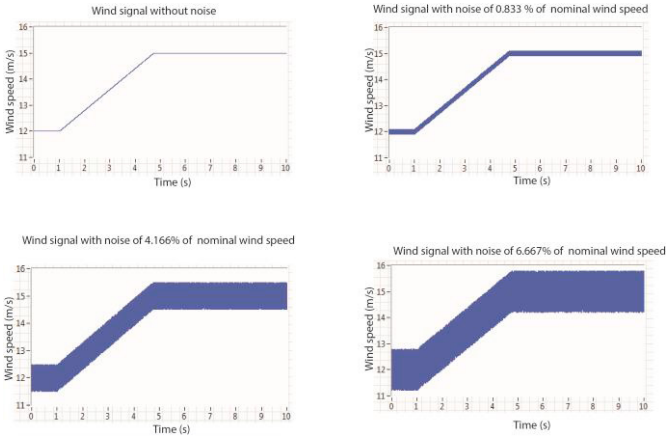

Fig. 15. Input wind signals for the power limit controllers.

The results of the integral of quadratic error after 10 seconds of simulation are summarized in the next table:

Table 4. Integral square error of the inputs

Percentage of noise	T1 controller	IT2 controller 1	IT2 controller 2	IT2 controller 3	PI traditional controller
0 %	0.1258	0.1154	0.1298	0.1110	0.1524
0.833 %	0.3129	0.3055	0.3094	0.2928	0.4456
4.167 %	0.3274	0.3226	0.3452	0.3059	0.4673
6.667 %	0.3346	0.3248	0.3584	0.3160	0.4901

Also in graphical form, the integral the quadratic error for the different controllers is:

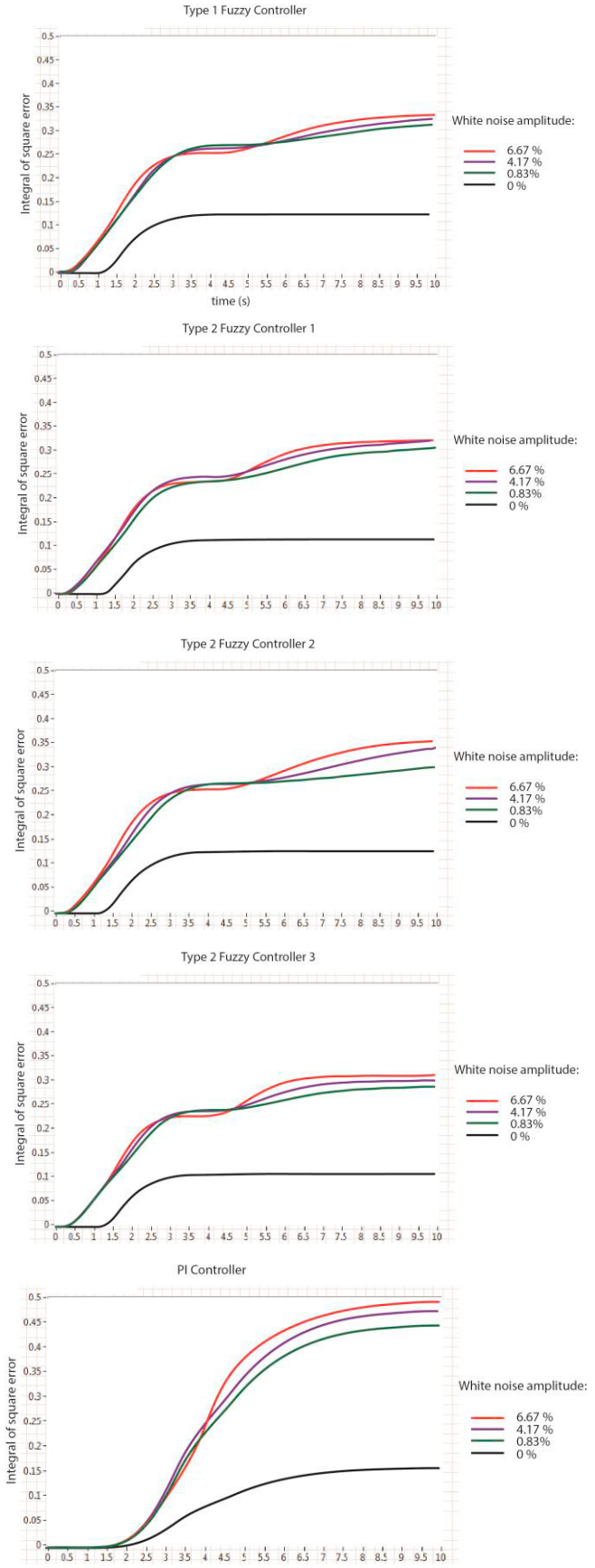

Fig. 16. Integral square error for power limit controllers used.

5. CONCLUSIONS

The performance of the designed inputs could not be observed by simple graphic observation of the limited output power since the graphics where very similar between them, therefore, a criteria of evaluation was used. The PI controller, however had a very poor performance when white noise was added and in some points the output power was superior to the nominal power which means overheating of the electric generator and possible permanent damage.

As can be seen in the table the best performance obtained was using the type 2 controller design 3, the criteria used to evaluate the performance was the integral square error which do not consider the speed of convergence to the desired output, however, this last criteria could be severe affected by the white noise used since the actuator is much more slow than the input noise signal.

The design of the type 2 fuzzy sets were subjective and by the method used it is not possible to find the best performance of the type 2 fuzzy controller since there are infinite possibilities of design. Therefore as a future work an ANFIS system is planned to be implemented for obtaining not only a better performance of the controller but also to diminish the number of rules used.

REFERENCES

Abad, G., López, J., Rodriguez, M., Maeeoyo, L. & Iwanski, G. (2011). *Doubly fed induction machine: modeling and control for wind energy generation*, John Wiley & Sons.

Biglarbegian, M., Melek, W. & Mendel, J. M. (2011). Design of novel interval type-2 fuzzy controllers for modular and reconfigurable robots: theory and experiments. *Industrial Electronics, IEEE Transactions on,* 58**,** 1371-1384.

Boukhezzar, B. & Siguerdidjane, H. (2005). Nonlinear control of variable speed wind turbines without wind speed measurement. Decision and Control, 2005 and 2005 European Control Conference. CDC-ECC'05. 44th IEEE Conference on, 2005. IEEE, 3456-3461.

Burton, T., Jenkins, N., Sharpe, D. & Bossanyi, E. (2011). *Wind energy handbook*, John Wiley & Sons.

Fadaeinedjad, R., Moallem, M. & Moschopoulos, G. (2008). Simulation of a wind turbine with doubly fed induction generator by FAST and Simulink. *Energy Conversion, IEEE Transactions on,* 23**,** 690-700.

Gorzałczany, M. B. (1987). A method of inference in approximate reasoning based on interval-valued fuzzy sets. *Fuzzy sets and systems,* 21**,** 1-17.

Hand, M. M. & Balas, M. J. (1999). *Non-linear and linear model based controller design for variable-speed wind turbines*, National Renewable Energy Laboratory.

Jammeh, E. A., Fleury, M., Wagner, C., Hagras, H. & Ghanbari, M. (2009). Interval type-2 fuzzy logic congestion control for video streaming across IP networks. *Fuzzy Systems, IEEE Transactions on,* 17**,** 1123-1142.

Karnik, N. N., Mendel, J. M. & Liang, Q. (1999). Type-2 fuzzy logic systems. *Fuzzy Systems, IEEE Transactions on,* 7**,** 643-658.

Klir, G. J. & Folger, T. A. (1988). Fuzzy sets, uncertainty, and information.

Liang, Q. & Mendel, J. M. (2000). Interval type-2 fuzzy logic systems: theory and design. *Fuzzy Systems, IEEE Transactions on,* 8**,** 535-550.

Lubosny, Z. (2003). *Wind turbine operation in electric power systems: advanced modeling*, Springer Berlin.

Mizumoto, M. & Tanaka, K. (1976). Some properties of fuzzy sets of type 2. *Information and control,* 31**,** 312-340.

Munteanu, I., Bratcu, A. I., Cutululis, N.-A. & Ceanga, E. (2008). *Optimal control of wind energy systems: towards a global approach*, Springer.

ONG, C.-M. (1998). *Dynamic simulation of electric machinery: using MATLAB/SIMULINK*, Prentice Hall PTR Upper Saddle River, NJ.

Ponce Cruz, P. (2011). *Inteligencia artificial con aplicaciones a la ingeniería*, Alfaomega.

Schwartz, D. G. (1985). The case for an interval-based representation of linguistic truth. *Fuzzy Sets and Systems,* 17**,** 153-165.

Türkşen, I. (1995). Fuzzy normal forms. *Fuzzy Sets and Systems,* 69**,** 319-346.

Wu, H. & Mendel, J. M. (2002). Uncertainty bounds and their use in the design of interval type-2 fuzzy logic systems. *Fuzzy Systems, IEEE Transactions on,* 10**,** 622-639.

Xu, L. & Cartwright, P. (2006). Direct active and reactive power control of DFIG for wind energy generation. *Energy Conversion, IEEE Transactions on,* 21**,** 750-758.

Zadeh, L. A. (1975). The concept of a linguistic variable and its application to approximate reasoning—I. *Information sciences,* 8**,** 199-249.

3.3 Thermal cycling and life-time estimation of GSC

Villanueva, I., Ponce, P., Molina, A., & MacCleery, B. (2016). **Grid-side inverter thermal cycling analysis of 1.6 MW Doubly-Fed Induction Generation wind turbine and life-time estimation**. In *Power Electronics (CIEP), 2016 13th International Conference on* (pp. 329-334). IEEE.

This paper has been presented in the IEEE 13th International Conference on Power Electronics (CIEP) in Guanajuato, Mexico.

A simulation of the thermal loses due to switching and conduction is presented, a life-time estimation method known as "Coffin-Manson" law is evaluated to calculate the life-time expectancy of the power electronic devices for different operational zones of the machine.

2016 13th International Conference on Power Electronics (CIEP)

Grid-Side Inverter Thermal Cycling Analysis of 1.6 MW Doubly-Fed Induction Generation Wind Turbine and Life-Time Estimation

Iván Villanueva
Pedro Ponce
Arturo Molina
School of Engineering and Sciences
Tecnologico de Monterrey
Mexico City, Mexico

Brian MacCleery
National Instruments
Austin, Texas

***Abstract*—This paper presents a simulation of wind turbine driven by a Doubly-Fed Induction Generator (DFIG), the rotor is fed through a two level inverter using Space Vectors Pulse Width Modulation (SVM). LabVIEW and Multisim are used to co-simulate the control and power electronics steps respectively. The thermal models of Multisim are used in order to analyze the thermal performance of IGBTs under different zones of operation of the electric machine. After that, the lifetime of the power electronics devices is estimated using the modified Coffin-Manson law of the LESIT project. The work demonstrate that the most demanding conditions are at nominal power of the converter while for underrated condition the damage due to thermal loading is minimum. This could be exploit increasing the switching frequency in order to enhance power output to the electric grid.**

***Index Terms*—Wind energy, thermal analysis, power inverter.**

I. Introduction

Wind energy is currently the most used renewable source not considering hydro power. In 2014 the total installed capacity worldwide was approximately 369,553 MW [1], increasing about 15 % with respect to 2013. Furthermore, the installed capacity of renewable energy sources (chiefly solar and wind) will continuously increase during the upcoming years [2], [3].

Installation and maintenance are ones of the most expensive factors in the total cost of offshore wind turbines. For offshore projects, foundation, installation and interconnection to the grid are typically 47 % the cost of the total project because of the intricate environment, in contrast to onshore projects where it is about 27 %, therefore, maintenance schedule needs to be prolongated much more compared with other generation technologies.

Power electronics step is essential for ensuring safe and efficient operation of a wind turbine. The most common generator topology is the DFIG because it drives only the rotor power (about 25-30 % of the rated machine power) and the allowable speed range is enough for maintaining the tip-speed ratio at its optimal value [4].

Thermal behavior is one of the most important factors concerning lifetime and reliability of power converters. According to [5] about 21 % of the failures of the converters are related with semiconductor devices, 26 % with the circuit board and 13 % with solder joints. Moreover, the mentioned faults are strongly related to thermal cycling [6].

Thermal modeling and life-time calculation of wind turbines has been of great interest in resent years due to reliability concerns of full-size power converters [7], [8], [9] and reduced-size power converters [6], [10], [11], [12]

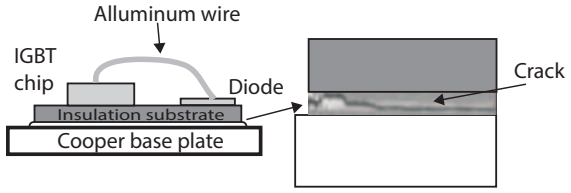

Fig. 1. Crack in IGBT union due to thermal stress, modified from [13]

When temperature of the semiconductor layers reaches certain value, the mechanical stress due to different thermal expansion of the components of the device leads to appearance of cracks mainly in the solder union and the bottom of the device, deteriorating the heat transfer with the board. If the operation continues under these conditions the device will fail after some cycles (see Figure 1). Some manufacturers provide curves of number of commutation cycles against difference in temperature between power electronic joint with the base and the case of the device. Other commonly used approach is the Coffin-Manson law (and some modifications) which is valid for plastic fracture modeling. This law has been extensively used in IGBT lifetime calculation [14], [15], [16], [17], [10], [18].

978-1-5090-1775-1/16/$31.00

In this paper a 1.6 MW wind turbine is simulated and controlled using a stator-flux-oriented vector controller, the reference rotor voltage is regulated using a SVM algorithm [19], the wind speed was taken from the Department of Wind Energy, Denmark [20]. Besides the grid-side power electronics step is simulated and evaluated in NI Multisim, a thermal model based on Foster networks was parameterized with data from the FF450R12KT4 Infineon module datasheet [15]. Results section presents power losses by switching and conduction and thermal performances of IGBT modules and their corresponding freewheeling diodes. With the information obtained it is possible to estimate the life time of the inverter, although more information is needed to in order to validate the model.

II. DFIG Model and Control

The most common configuration of commercial variable speed wind turbines is the DFIG, this type of electric machine allows a reduced size power converter (typically about 30 % of the nominal power) reducing system cost and allowing an operational speed about 30 % around the synchronous speed.

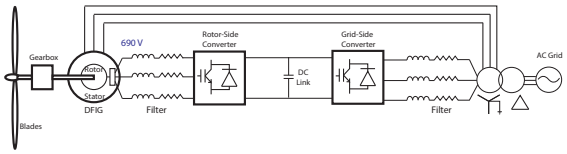

Fig. 2. DFIG Model

The simulated system is based on a 1.6 MW wind turbine. The stator is connected to the AC grid through a step up transformer while the rotor is connected through a back-to-back two levels inverter. The inverter's nominal power is 480 kW, which is 30 % of the nominal power of the turbine.

The blades, gearbox and pitch control models of the simulated turbine can be found in [21]. The electric machine model used does not consider magnetic saturation nor changes in machine parameters due to thermal effects, the dynamic equations can be found in [22].

The parameters (in per unit) used for the simulation are displayed in figure 3. The equivalent circuit of the electric machine model used in this work with a reference frame rotating at the rotor speed is the following:

A. Controller

A stator-flux-oriented reference frame was selected, equations 1 and 2 were used to compute the reference currents. The complete procedure for obtaining those equations can be found in [23].

$$i_{dr}^{*} = \frac{2Q_s L_m}{3\omega_{sf} L_m^2 i_{ms}} + i_{ms} \tag{1}$$

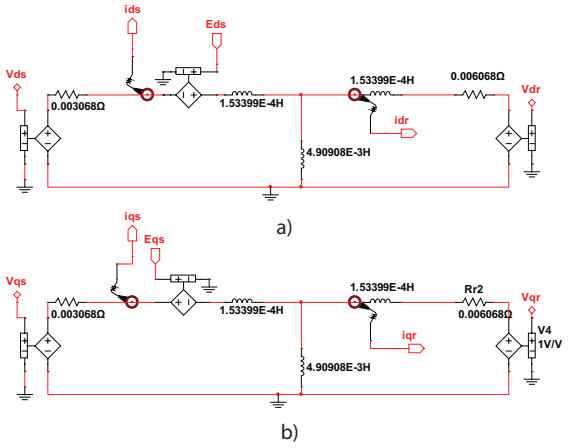

Fig. 3. DFIG equivalent circuit in per unit: a) direct reference frame, b) quadrature reference frame

TABLE I
Power Inverter Parameters

Inverter parameter
DC link voltage = 1200 V
Nominal current = 400 A
Nominal power = 480 kW
Commutation frequency = 2000 Hz
Grid frequency = 60 Hz
Grid-side filter = 0.01 + j 0.5655 Ω

$$i_{qr}^{*} = \frac{-2P_s\left(L_{ls} + L_m\right)}{3\omega_{sf} L_m^2 i_{ms}} \tag{2}$$

where:

$$i_{ms} = \frac{v_{qr} - r_s i_{qs}}{\omega_{sf} L_m} \tag{3}$$

III. Thermal Model

Many important properties of power electronics devices are highly dependent on the temperature. Insulated gate bipolar transistors (IGBTs) are nowadays suitable for medium power range at high switching frequency. The main advantages of those devices are low switching and conduction losses, high short-circuit capability and easiness to connect devices in parallel [24].

Thermal behavior of semiconductors are commonly described using Foster model, since the computation is much simpler than Cauer model and can be easily adjusted using real measurements of the temperature of interest. For many statistical models the only temperature using in life-time calculation is the solder joint one [14], [15], [16], [10], [25].

Solder joint temperature has been considered to be crucial in empirical lifetime models since there is a close interaction between different failure mechanism. For example, solder fatigue results in higher thermal resistance of the power module, that leads to higher stress in both chip base and bond wires [26]. Therefore, joint temperature is a good indicator for general degradation of the power module.

A. Foster Model or Ladder Network

The Foster model, unlike Cauer model, does not have any physical analogy, moreover, node voltages do not represent temperatures at each layer of the model, however,the solution is much more straightforward than using Cauer model and normally the manufacturers provide thermal models based on Foster networks.

The Foster model can be represented in a circuit as a set of resistance and capacitances in parallel connected one after another. This model is convenient when it is not necessary to know the temperature inside the power electronics device but the temperature at one specific point, the most recurrent one is the joint temperature of the base of the device with the substrate. The number of elements in the network depends on the complexity of the thermal behavior of the device and the degree of precision with respect to a finite element method model or real measurements of the temperature.

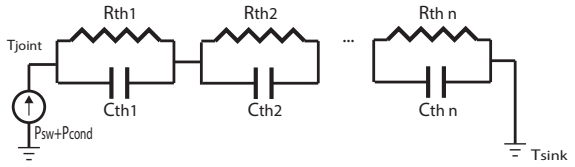

Fig. 4. Foster thermal network

The main advantage of the Foster model is that the computation is much simpler since the temperature change can be expressed as the sum of exponentially decaying terms:

$$\Delta T_j(t) = (P_{sw} + P_{cond}) Z_{th}(T) \tag{4}$$

$$Z_{th}(t) = \sum_{i=1}^{n} R_{th_i}(1 - e^{-\frac{t}{\tau_i}}) \tag{5}$$

where P_{sw} and P_{cond} are switching and conduction power losses respectively, R_{th_i} are the resistances of the Foster network, τ_i are the time constants of each resistance-capacitance pair, that is:

$$\tau = R_{th} C_{th} \tag{6}$$

B. Loses Calculation

Conduction Loses: The conduction loses are simply calculated as the current flowing throw the device multiplied by the voltage between its terminals, for an IGBT transistor the mathematical expression is the following:

$$P_{cond} = V_{ce}(I_c, T_j) I_C \tag{7}$$

where V_{ce} is the colector-emissor voltage dependent on the current flowing through the collector and the joint temperature of the device. The manufacturers provide curves with diferent temperatures [13] and this data can be entered in Multisim as piecewise linear function in order to compute those losses.

Switching : For IGBT and other transistors the dissipation of energy due to switching can be modeled with the following equation:

$$P_{sw} = \frac{E_{on}(Ic, Tj) + E_{off}(Ic, Tj)}{1000} f_{sw} \frac{V_{dc,real}}{V_{dc,nominal}} \tag{8}$$

where E_{on} and E_{off} are the energy dissipated in average during one switching cycle and are dependent on the current flowing immediately before or after switching the device and the temperature of the joint. Datasheet information can be entered in piecewise functions and then interpolated by Multisim. f_{sw} is the switching frequency, $V_{dc,real}$ is the operating collector emitter voltage and $V_{dcnominal}$ is the collector emitter voltage in which the manufacturer's tests were made.

The thermal model used in this work has the next values and shape, with a heat sink temperature of 40 C:

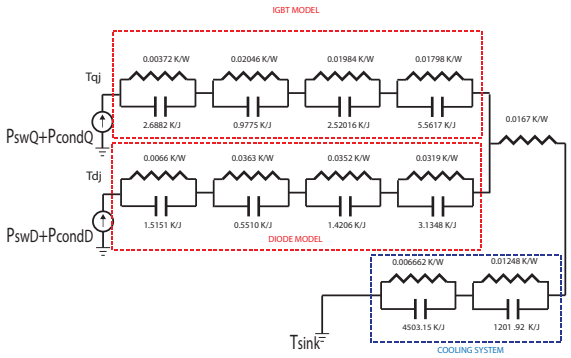

Fig. 5. Foster network used in this work

IV. Life-time estimation model

In this work we are considering that the main failure mechanism is the chip joint failure and that the failure is due to plastic strain fatigue. In 1954 Coffin and Manson presented a model of for plastic strain fatigue crank-growth of materials under thermal stress [27]. The modified equation commonly used for power electronics failure calculation is the following [25]:

$$N_{failure} = A(\Delta T_j)^{\alpha} \exp\left(\frac{E_a}{k_b T_{jm}}\right) \tag{9}$$

where $N_{failure}$ is the number of cycles in which a failure is expected to occur, A is an adjustment constant, α is a constant obtained by experiments, Δ_{tj} is the joint temperature fluctuation, E_a is the activation energy, k_b is the Boltzmann constant (1.38066 e-23 [J/K]) and T_{jm} is the average joint temperature [15].

The parameter A was adjusted for a lifetime expectancy of 20 years at nominal power of the converter with an operation factor of 66 %, the parameters A, α and E_a were taken from a previous work [15]:

TABLE II
PARAMETERS USED FOR LIFE-TIME EXPECTANCY CALCULATION

Parameter
A = 33.2346 e+4 [K]
α = -5.039
E_a = 9.89 e-20 [J]
K_b = 1.38066 e-23 [J/K]

The total damage expression can be calculated with the following equation:

$$D = \sum_{i=1}^{j} \frac{n(i)}{N_{failure}} \tag{10}$$

V. METHODOLOGY

The steps followed in this work are illustrated in figure 6. First a wind profile is set, in this work measurements from the Department of Wind Energy, Denmark taken at San Georgino, California where used. Then the mathematical model of the turbine blades and the gearbox are used in order to obtain a mechanical torque and speed of the machine shaft, after that the generator controller computes the signals of the power converter, next the power loses are calculated and used in the Foster network to obtain the thermal profile, subsequently thermal cycles are counted using an efficient on-line rainflow counting algorithm [28] and finally the remaining life-time is calculated.

Additionally to the real wind profile, constant wind speed values were studied in order to obtain a wear factor according to the operational speed and then extrapolate the results for a determined wind speed distribution chart (although that approach neglects transient loses)

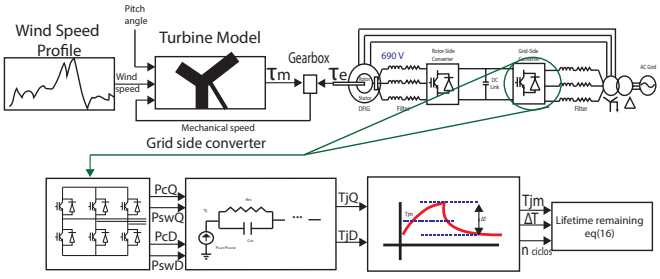

Fig. 6. Remaining life-time calculation methodology

For the grid side controller, a regulator is used to maintain the DC voltage at the rated value and unity power factor. Since the grid side converter thermal loading has a constant frequency, we are only focusing on the thermal loading of this step, as further work.

VI. RESULTS

The life-time estimation for the range of speed of the generator are summarized in table III. Measurements were obtained at steady estate.

TABLE III
LIFE-TIME EXPECTANCY FOR DIFFERENT WIND SPEEDS

Wind Speed (m/s)	Life-time expectancy IGBT (years)	Life-time expectancy Diode (years)	Rotor power (pu)
6	277.71	4567	-0.09011
7	254.68	7912	-0.0924
8	240.65	24630	-0.0812
9	236.57	37744	-0.0527
10	471.29	33088	-0.0031
11	100.76	38186	0.0741
12	23.71	39577	0.19
13	8.74	35942	0.325
14	8.62	28406	0.327

The results displayed in table III could be used for long-term life time estimation extrapolating the life-time expectancy calculation to a speed distribution chart of certain region. A recent relevant work presents extrapolation of wear calculation for average constant wind profiles into a one year-time interval [9].

The next plots were captured from the steady state using 12 m/s wind speed.

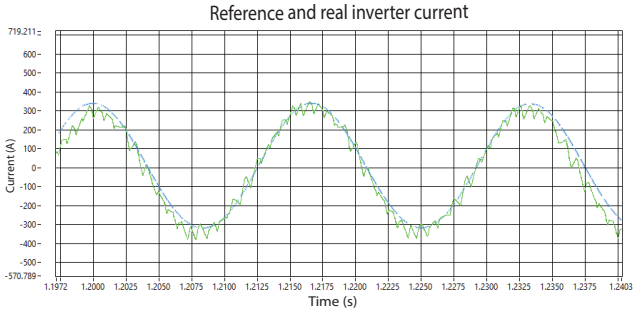

Fig. 7. Reference and real inverter current

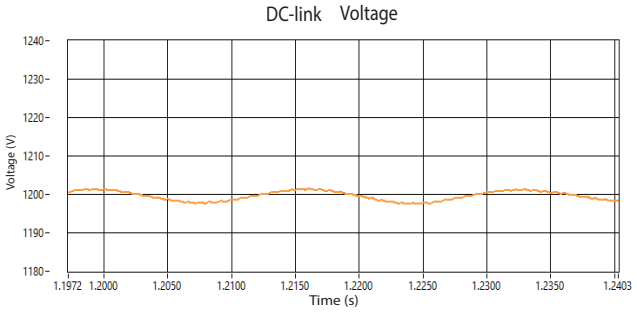

Fig. 8. DC link voltage

In figure 7, the current delivered to the power grid is shown, it can be seen large swings and low power quality due to the low switching frequency of the inverter. Switching frequency is maintained low for large wind-generation systems in order to ensure low loses and safe operation. figure 8 display how the DC-link voltage is regulated maintained within an acceptable range. The IGBT and diode temperature (figure 9)

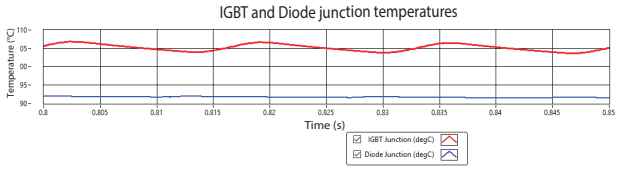

Fig. 9. IGBT and diode junction temperatures at 12m/s wind speed

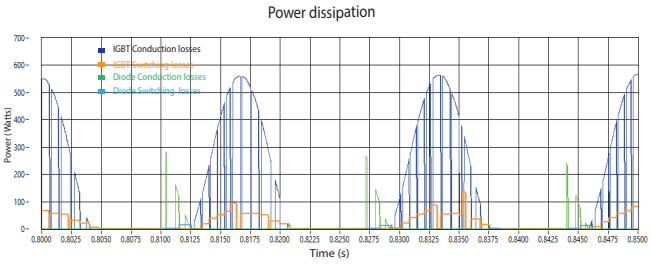

Fig. 10. IGBT and diode power dissipation at 12 m/s wind speed

present low thermal cycling, the IGBT clearly wears faster for this particular operation point. Figure 10 displays the conduction and switching loses considered in this work, it can be seen that switching loses are in a very low range and the dominant loses are because of current conduction.

The following figures are a sample of the thermal behavior under the wind profile shown in figure 11:

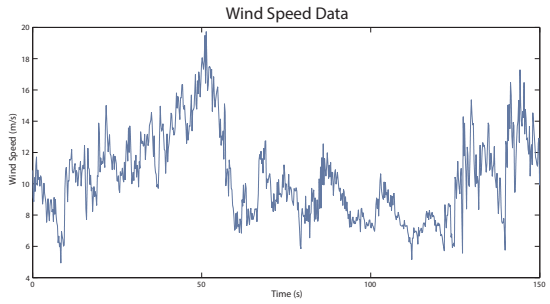

Fig. 11. Wind speed profile used for the simulation

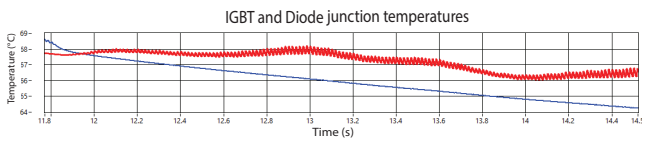

Fig. 12. IGBT and diode junction temperatures

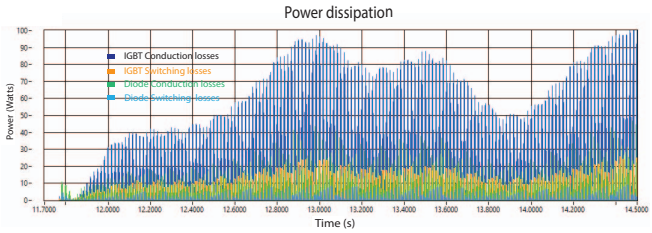

Fig. 13. Power dissipation of power electronic devices

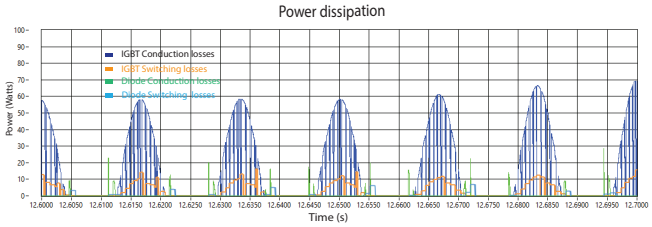

Fig. 14. Detal of power dissipation

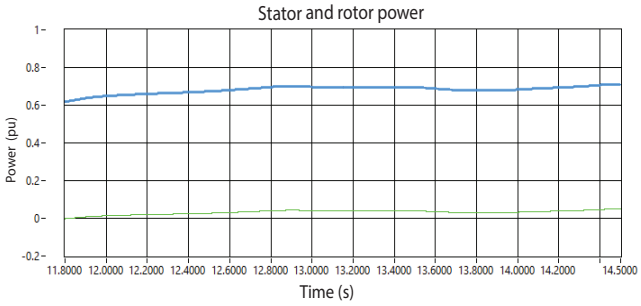

Fig. 15. Stator and Rotor power of DFIG

Figure 12 displays the variation of the power electronics joint temperature, rainflow method is necessary in order to obtain valid cycle counting. Figure 13 shows that power loses are again mainly due to conduction loses, as the calculated cycling wearing is minimal, it suggests the possibility of increasing switching frequency. The rotor power is positive indicating super-synchronous rotor speed.

VII. Conclusion

A straightforward lifetime estimation method has been proposed for wind generation and simulated under different wind speed conditions. The method was used for life-time estimation of the grid-side converter. Foster networks were used in order to calculate the joint temperature with respect to time for a determined model of IGBT and then Coffin Manson Law was used. Real measurements of wind speed were used to calculate the total damage of the power electronics devices during a simulation run.

The presented method can be used to determine thermal behavior under different wind speed and switching conditions

to determine possible hazardous conditions. This can be specially useful in the design step of a power converter system.

This work has the following limitations: Only the grid-side part of the converter was analyzed. There is not a consensus of which is the most important failure mechanism of power electronic devices and this methodology do not consider case temperature which is used by many models to calculate base solder failures. Thermal failures are just one little part of the total failures that could occur in a power converter and there are not many information of the causes and types of failures in the device in order to define a complete and valid formulation of thermal deterioration failures.

VIII. Further Work

Due to time limitations and constant advances in power electronics technology, manufacturers cannot provide empirical models for low ΔT_j thermal cycles (less than 10 Celsius degrees) and high cycling frequency (more than 1 Hz). Those tests are very important in order to obtain a reliable life-time for wind applications, however, the opinion of the authors is that with the rough approximations as the one presented in this work, it is possible to develop a switching frequency controller that enhances output power quality at not harmfully operation conditions while maintaining the temperature within safe ranges throughout operational range of the turbine.

The present work has only considered the grid-side part of the inverter, the rotor-side is slightly more complex due to the constant change in thermal cycling frequency, as further work the rotor side will be considered and a novel controller for life-time optimization will be proposed.

References

[1] GWEC, "Global wind statistics 2015," Global Wind Energy Council, Tech. Rep., Feb 2016.

[2] A. McCrone and B. N. E. Finance, *Global trends in renewable energy investment 2015*. Frankfurt School of Finance and Management Frankfurt, 2015.

[3] J. L. Sawin, C. Lins, E. Musolino, K. Petrichenko, W. Richerson, K. Seyboth, J. Skeen, B. Sovacool, F. Sverrisson, and L. E. Williamson, "Renewables 2015-global status report," REN21 Secretariat, Paris, France, Tech. Rep., 2015.

[4] M. H. Ali, *Wind energy systems: solutions for power quality and stabilization*. CRC Press, 2012.

[5] T. Orowska-Kowalska, F. Blaabjerg, and J. Rodrguez, *Advanced and intelligent control in power electronics and drives*. Springer, 2014, vol. 531.

[6] M. Ikonen, "Power cycling lifetime estimation of IGBT power modules based on chip temperature modeling," *Acta Universitatis Lappeenrantaensis*, 2012.

[7] S. D'Arco, T. M. Undeland, M. Bohlländer, and J. Lutz, "A simplified algorithm for predicting power cycling lifetime in direct drive wind power systems," in *Systems, Signals and Devices (SSD), 2012 9th International Multi-Conference on*. IEEE, 2012, pp. 1–6.

[8] R. Pittini, S. D'Arco, M. Hernes, and A. Petterteig, "Thermal stress analysis of IGBT modules in VSCs for PMSG in large offshore wind energy conversion systems," in *Power Electronics and Applications (EPE 2011), Proceedings of the 2011-14th European Conference on*. IEEE, 2011, pp. 1–10.

[9] K. Ma, M. Liserre, F. Blaabjerg, and T. Kerekes, "Thermal loading and lifetime estimation for power device considering mission profiles in wind power converter," *Power Electronics, IEEE Transactions on*, vol. 30, no. 2, pp. 590–602, 2015.

[10] M. Bartram, I. Von Bloh, and R. W. De Doncker, "Doubly-fed-machines in wind-turbine systems: Is this application limiting the lifetime of IGBT-frequency-converters?" in *Power Electronics Specialists Conference, 2004. PESC 04. 2004 IEEE 35th Annual*, vol. 4. IEEE, 2004, Conference Proceedings, pp. 2583–2587.

[11] K. Ma, M. Liserre, and F. Blaabjerg, "Reactive power influence on the thermal cycling of multi-MW wind power inverter," *Industry Applications, IEEE Transactions on*, vol. 49, no. 2, pp. 922–930, 2013.

[12] L. Wei, R. J. Kerkman, R. A. Lukaszewski, H. Lu, and Z. Yuan, "Analysis of IGBT power cycling capabilities used in doubly fed induction generator wind power system," *Industry Applications, IEEE Transactions on*, vol. 47, no. 4, pp. 1794–1801, 2011.

[13] Mitsubishi Electric. (2013) Reliability of power modules.

[14] R. Bayerer, T. Herrmann, T. Licht, J. Lutz, and M. Feller, "Model for power cycling lifetime of IGBT modules - various factors influencing lifetime," in *Integrated Power Systems (CIPS), 2008 5th International Conference on*. VDE, 2008, Conference Proceedings, pp. 1–6.

[15] J. Due, S. Munk-Nielsen, and R. Nielsen, "Lifetime investigation of high power IGBT modules," in *Power Electronics and Applications (EPE 2011), Proceedings of the 2011-14th European Conference on*. IEEE, 2011, Conference Proceedings, pp. 1–8.

[16] M. Ciappa and W. Fichtner, "Lifetime prediction of IGBT modules for traction applications," in *Reliability Physics Symposium, 2000. Proceedings. 38th Annual 2000 IEEE International*. IEEE, 2000, Conference Proceedings, pp. 210–216.

[17] M. Ciappa, F. Carbognani, and W. Fichtner, "Lifetime prediction and design of reliability tests for high-power devices in automotive applications," *Device and Materials Reliability, IEEE Transactions on*, vol. 3, no. 4, pp. 191–196, 2003.

[18] M. Ciappa, P. Malberti, W. Fichtner, P. Cova, L. Cattani, and F. Fantini, "Lifetime extrapolation for IGBT modules under realistic operation conditions," *Microelectronics Reliability*, vol. 39, no. 6, pp. 1131–1136, 1999.

[19] N. Celanovic and D. Boroyevich, "A fast space-vector modulation algorithm for multilevel three-phase converters," *Industry Applications, IEEE Transactions on*, vol. 37, no. 2, pp. 637–641, 2001.

[20] (2002) Database on wind characteristics. [Online]. Available: http://www.winddata.com/

[21] I. Villanueva, P. Ponce, and A. Molina, "Interval type 2 fuzzy logic controller for rotor voltage of a doubly-fed induction generator and pitch angle of wind turbine blades," *IFAC-PapersOnLine*, vol. 48, no. 3, pp. 2195–2202, 2015.

[22] C.-M. Ong, *Dynamic simulation of electric machinery: using MATLAB/SIMULINK*. Prentice Hall PTR Upper Saddle River, NJ, 1998, vol. 5.

[23] W. Qiao, "Dynamic modeling and control of doubly fed induction generators driven by wind turbines," in *Power Systems Conference and Exposition, 2009. PSCE'09. IEEE/PES*. IEEE, 2009, pp. 1–8.

[24] Z. Luo, H. Ahn, and M. Nokali, "A thermal model for insulated gate bipolar transistor module," *Power Electronics, IEEE Transactions on*, vol. 19, no. 4, pp. 902–907, 2004.

[25] M. Held, P. Jacob, G. Nicoletti, P. Scacco, and M.-H. Poech, "Fast power cycling test of IGBT modules in traction application," in *Power Electronics and Drive Systems, 1997. Proceedings., 1997 International Conference on*, vol. 1. IEEE, 1997, pp. 425–430.

[26] I. F. Kovacevic-Badstuebner, J. W. Kolar, and U. Schilling, "Modelling for the lifetime prediction of power semiconductor modules," in *Reliability of Power Electronic Converter Systems*, H. S. Chung, H. Wang, F. Blaabjerg, and M. Pecht, Eds. IET Publishing, 2015, ch. 5, pp. 103–140.

[27] S. Manson, "Behaviour of materials under conditions of thermal stress," *Transactions of the ASME*, vol. 76, p. 931, 1954.

[28] M. Musallam and C. M. Johnson, "An efficient implementation of the rainflow counting algorithm for life consumption estimation," *Reliability, IEEE Transactions on*, vol. 61, no. 4, pp. 978–986, 2012.

Chapter 4

Sliding Mode Control for DFIG

This chapter conforms the main body of the thesis and it is focused on the internal control loop of the DFIG, considering the control references given. The main proposal is a Grid-Voltage-Oriented (GVO) controller able to work under unbalanced grid conditions. Grid voltage orientation allows to decouple active and reactive power and ensures stability of the system without dependence on the operational conditions. The controller is robust against bounded disturbances and not-dependent on system parameters. A demagnetizing current is injected to enhance the transient behavior of DFIG in presence of voltage faults.

To reduce the switching frequency of SMC, a hysteresis-based comparator is included and characterized in both, time and frequency domains. In the time domain, the equivalent control is used to estimate the dynamics of the system and an adaptable hysteresis is proposed. In the frequency domain a fixed hysteresis that ensures a maximum switching frequency of the converter is presented.

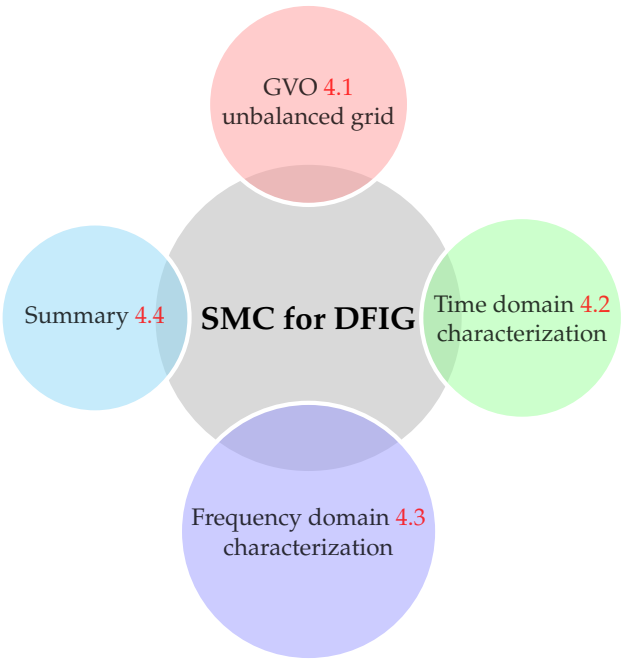

FIGURE 4.1: SMC for DFIG scientific production.

The manuscripts that conform the main contributions of this thesis are presented below. The result is a controller able to work under unbalanced gird conditions with enhanced transient behavior and limited switching frequency. In Figure 4.1 the

scientific production is organized in a diagram, starting with the main contribution in section 4.1, then the limit switching strategies in sections 4.2 and 4.3. Finally a book chapter that summarizes the work is presented in section 4.4.

4.1 Sliding mode control for DFIG under unbalanced conditions

Villanueva, I., Rosales, A., Ponce, P., & Molina, A. (2017).**Grid-Voltage-Oriented Sliding Mode Control for DFIG Under Balanced and Unbalanced Grid Faults**. *IEEE Transactions on Sustainable Energy*.

In this paper, SMC is oriented in the voltage grid reference frame, which ensures stability of the control system without dependence on the operational condition of the machine. The presented controller is robust against voltage disturbances in the grid, furthermore, a demagnetization control strategy is implemented for enhancing the transient operation of the DFIG under voltage dips.

This article has been accepted for publication in a future issue of this journal, but has not been fully edited. Content may change prior to final publication. Citation information: DOI 10.1109/TSTE.2017.2769062, IEEE Transactions on Sustainable Energy

Grid-Voltage-Oriented Sliding Mode Control for DFIG Under Balanced and Unbalanced Grid Faults

Iván Villanueva, *Student Member, IEEE,* Antonio Rosales, *Member, IEEE,* Pedro Ponce and Arturo Molina

***Abstract*—Doubly Fed Induction Generators (DFIGs) are widely used in variable-speed wind turbines. Despite the well-accepted performance of DFIGs, these generators are highly sensible to grid faults. Hence, the presence of grid faults must be considered in the design of any control system to be deployed on DFIGs. Sliding Mode Control (SMC) is a useful alternative for electric machinery control since SMC offers fast dynamic response and less sensitivity to parameter variations and disturbances. Additionally, the natural outputs of SMC are discontinuous signals allowing direct switching of power electronic devices. In this work, a grid-voltage-oriented sliding mode control is proposed and tested under low voltage grid faults. Unlike other non-modulated techniques like direct torque control (DTC) there is not a necessity of modifying the controller structure for withstanding low depth voltage dips. For stator natural flux cancellation, the torque and reactive power references are modified to inject a demagnetizing current. Simulation results demonstrate the demagnetization of the natural flux component as well as a robust tracking control under balanced and unbalanced voltage dips.**

***Index Terms*—Doubly Fed Induction Generator, Sliding Mode Control, Low Voltage Ride-Through**

NOMENCLATURE

$\vec{v}$	Voltage vector
$\vec{\lambda}$	Flux vector
$\vec{i}$	Current vector
^{v}	Virtual quantity superscript
$_{s}$ $(_{r})$	Stator (rotor) index
$_{d,q}$	Synchronous reference frame index
$_{\alpha,\beta}$	Stationary reference frame index
θ_{sf}	Stator flux angle
θ_{mec}	Rotor angle
θ_{g}	Grid voltage angle
θ_{d}	Reference frame orientation angle
ω_{s}	Synchronous angular speed
ω_{m}	Rotor angular speed
ω_{r}	Rotor current angular speed $[\omega_r = \omega_s - \omega_m]$
L_{m}	Linkage inductance
L_{s}	Stator inductance $[L_s = L_m + L_{sleakage}]$
L_{r}	Rotor inductance $[L_r = L_m + L_{rleakage}]$
P	Number of pole pairs
τ_{e}	Electromagnetic torque
P_s (Q_s)	Stator active (reactive) power
V_{dc}	DC link voltage.

I. INTRODUCTION

DFIG is the most commonly used electric machine in wind generation. It provides excellent performance in limited-range speed applications with the main advantage of partially rated power converter, however this machine is particularly sensitive to voltage variations since the stator is connected directly to the electric grid. When mutual flux is altered, torque oscillations may appear severely affecting blades shaft and transmission system. If the rotor-side controller is not suitable for working under disturbances, the stator currents may become non-sinusoidal compromising stability of the electric grid.

In several countries, fault ride-through capability has become mandatory in the interconnection of new generation units. The higher the penetration of wind generators the stricter the technical standards for turbines interconnection must be. These requirements, known as *grid codes*, cover voltage operating range, power factor regulation, frequency operating range, grid support capability and low fault ride-through capability [1], [2].

Modern *grid codes* require the generator to stay connected during voltage dips and inject reactive power to restore the electric grid [1], [2]. Furthermore, after clearance of the fault, active power injection is required for electric frequency support [3]. For DFIG, an abrupt voltage variation causes a natural flux in the stator that may induce over-voltages in the rotor windings that could affect or even destroy the power converter [4], [5]. Therefore, the use of crowbar or another protection device is necessary for severe voltage dips. However, once the current has decreased, the injection of demagnetizing current can be used for restoring faster the stator flux to its central position and continue with reactive power contribution to the grid, improving transient response of the generator under natural flux [4].

Feedback control is a useful alternative to improve the performance of DFIG generators in presence of electric faults since it is possible to face low depth faults without disconnecting the generator from the grid [6], [7]. SMC is a robust control technique capable of providing insensitivity against bounded disturbance/uncertainties and finite-time convergence [8]. Furthermore, the discontinuous nature of SMC fits with the direct control of power electronics (inverters) used on DFIG avoiding modulation of the control signal, see [9]. In [10], [11] it is presented a strategy based on continuous SMC for DFIG, however these proposals require modulation to be implementable and the fault considered do not present an abrupt change in the stator voltage, mitigating the natural flux effects. In [12], [13] it is presented a stator-oriented SMC for DFIG which is tested under unbalanced and harmonic distorted grid, the controller can regulate the references even during such disturbances, however, the natural flux is ignored. Natural flux may induce a very large voltage to the rotor windings, which can saturate the power converter causing loss of the rotor current control, moreover, if natural flux is not

This article has been accepted for publication in a future issue of this journal, but has not been fully edited. Content may change prior to final publication. Citation information: DOI 10.1109/TSTE.2017.2769062, IEEE Transactions on Sustainable Energy

eliminated, the DFIG may inject distorted current to the grid after the clearance of the grid fault, therefore, it is important to mitigate the effect of natural flux [14].

Due to the limited voltage and power of rotor converter, no control strategy can completely fulfill the requirements of *grid codes* specially at high rotor speed [3], therefore in this study only low voltage dips that can be controlled using the rotor inverter are simulated. The proposed SMC can regulate the desired torque and reactive power even under unbalanced faults. In comparison with other proposals based on vector control [15], [16], [17], [18], [19], [7], [20], [21], [22], [23] and direct-control methods [24], [25], [26], [27], the proposed controller does not require modification of the controller structure for compensating torque and reactive power oscillations, nor rotor current sequence components separation, although the stator voltage sequence decomposition is required to estimate the natural flux. From symmetrical components point of view, to satisfy non-oscillating torque and reactive power is equivalent to compensate the negative sequence components in the stator circuit, reducing unbalanced current exchange with the grid and enhancing fault ride through capability [22].

In this paper, it is proposed a grid-voltage oriented SMC controlling directly torque and stator reactive power. The "q" reference frame axis is aligned with the stator voltage for maintaining the same nomenclature and mathematical derivation used in stator-flux oriented SMC [28]. The "virtual stator flux" is 90 degrees apart from the grid voltage and the terms due to the actual misalignment are incorporated as perturbations in the controller design. The grid-voltage orientation is selected because it has been demonstrated by [29], [30] that the system oriented to the grid voltage direction is stable independently of the rotor current in contrast to stator-flux orientation, which may become unstable for large values of i_{rd} [29], [31]. i_{rd} is used to control the stator reactive power, which a requirement for grid interconnection of new wind generators[1], [2]. Despite newer SMC algorithms as Second Order Sliding Mode (SOSM) and Higher Order Sliding Mode (HOSM) controllers, have been applied in DFIG [10], [11], the DFIG dynamics are relative degree one, then classical SMC works for this type of generator. Furthermore, the performance of SOSM/HOSM is not better, and the implementation of these algorithms is more complicated, compared with classical SMC, see [9].

The proposed SMC is validated via simulations considering balanced and unbalanced voltage dips faults. Depending on the voltage dip type and the dip starting time, a transient natural flux may appear in the stator, therefore the torque and reactive power references are modified to inject a demagnetizing current for restoring stator flux. The controller offers fast dynamic response, non-dependence on system parameters, direct control of torque and reactive power without sequence decomposition of the rotor current and direct switching power electronic devices.

The structure of the paper is as follows: Section II has the mathematical model of the DFIG wind turbine generation system; the control design is presented in section III; demagnetizing current strategy is shown in section IV; the simulations results are reported in section V; and section VI contains the conclusions.

II. System Modeling

The basic scheme of the system is display in Figure 1, the stator is directly connected to the electric grid, while the rotor needs a bidirectional power flow between the grid and electric machine, therefore, back-to-back power converter is used. Typically, the nominal power of the back-to-back converter is 30% of the generator nominal power.

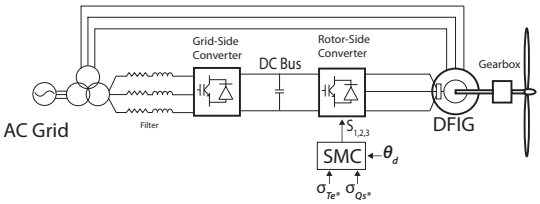

Fig. 1: Wind turbine scheme with DFIG.

A. DFIG model

The electric machine model refereed to a synchronous rotating reference frame can be summarized using the following set of equations in vector form [32]:

$$\vec{v_s} = \frac{d\vec{\lambda_s}}{dt} + R_s\vec{i_s} + j\omega_s\vec{\lambda_s} \tag{1}$$

$$\vec{v_r} = \frac{d\vec{\lambda_r}}{dt} + R_r\vec{i_r} + j\omega_r\vec{\lambda_r} \tag{2}$$

$$\vec{\lambda_s} = L_s\vec{i_s} + L_m\vec{i_r} \tag{3}$$

$$\vec{\lambda_r} = L_r\vec{i_r} + L_m\vec{i_s} \tag{4}$$

where $\vec{v_s}, \vec{i_s}, \vec{v_r}, \vec{i_r}$ are the stator and rotor voltage and current vectors, R, L are resistance and inductance respectively and the subscripts "s" "r" are stator and rotor. L_m is the linkage inductance, ω_s is the synchronous angular speed, ω_r is the rotor current angular speed and $\vec{\lambda_s}, \vec{\lambda_r}$ are stator and rotor fluxes respectively.

For DFIG it is convenient to orient the machine model in a synchronous speed rotating reference frame. Neglecting voltage drop due to stator resistance, the stator voltage phasor will lead the stator flux phasor by 90 degrees under normal operation, therefore orienting the d axis in the stator flux vector direction will decouple active and reactive power ($\lambda_{sq} = 0$ and $v_{sd} = 0$):

$$\tau_e = \frac{3PL_m}{2L_s}(i_{rd}\lambda_{sq} - i_{rq}\lambda_{sd}) \tag{5}$$

$$\tau_{e,normal} = \frac{-3PL_m}{2L_s}(i_{rq}\lambda_{sd}) \tag{6}$$

$$Q_s = \frac{3L_m}{2L_s}(v_{sd}i_{rq} - v_{sq}i_{rd}) + \frac{3}{2L_s}(\lambda_{sd}v_{sq} - \lambda_{sq}v_{sd}) \tag{7}$$

$$Q_{s,normal} = \frac{-3L_m}{2L_s}(v_{sq}i_{rd}) + \frac{3}{2L_s}(\lambda_{sd}v_{sq}) \tag{8}$$

where P is the number of pole pairs of the electric machine. The torque is controlled by the quadrature axis rotor current, while the reactive power is controlled by the direct axis rotor current.

This article has been accepted for publication in a future issue of this journal, but has not been fully edited. Content may change prior to final publication. Citation information: DOI 10.1109/TSTE.2017.2769062, IEEE Transactions on Sustainable Energy

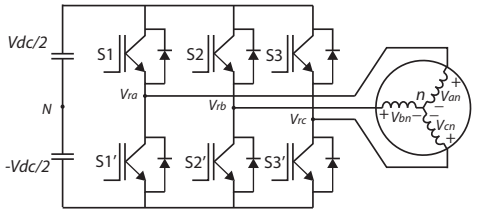

Fig. 2: Two level inverter.

B. Rotor-side power converter model

The output voltage of a power converter seen from the neutral of the DFIG rotor (see Figure 2) is:

$$\begin{bmatrix} V_{an} \\ V_{bn} \\ V_{cn} \end{bmatrix} = \frac{V_{dc}}{3} \begin{bmatrix} 2 & -1 & -1 \\ -1 & 2 & -1 \\ -1 & -1 & 2 \end{bmatrix} \begin{bmatrix} S_1 \\ S_2 \\ S_3 \end{bmatrix} \tag{9}$$

where V_{dc} is the DC link voltage, S_1, S_2 and S_3 are the switch states of each leg of the power converter. Each leg can only have two valid switching states (zero or one).

The voltage can be measured with respect to an imaginary reference point in the middle of the DC link (see Figure 2), the output voltage will be in that case a sign function with a gain equal to $V_{dc}/2$. Since the basic output of SMC is a sign function, it can be used for direct switching of power electronic devices if a relationship between d, q and a, b, c quantities is established.

$$\begin{bmatrix} V_{aN} \\ V_{bN} \\ V_{cN} \end{bmatrix} = \frac{V_{dc}}{2} \begin{bmatrix} 1 & 0 & 0 \\ 0 & 1 & 0 \\ 0 & 0 & 1 \end{bmatrix} \overbrace{\begin{bmatrix} \text{sign}(S_1 - 0.5) \\ \text{sign}(S_2 - 0.5) \\ \text{sign}(S_3 - 0.5) \end{bmatrix}}^{S_{1,2,3}} \tag{10}$$

The sign function is defined as follows:

$$\text{sign}(x) := \begin{cases} -1 \text{ if } x < 0, \\ 1 \text{ if } x > 0. \end{cases} \tag{11}$$

III. Grid-voltage-oriented controller design

For decoupling active and reactive power, a synchronous-speed reference frame is used. There are two options: stator flux and grid voltage orientation.

Stator-flux orientation may cause the DFIG to be an unstable system when $i_{rd} > \frac{2\|\vec{v_s}\|}{\omega_s L_m}$ [29], [31]. It is convenient to select the grid voltage orientation since i_{rd} is directly related with reactive power. Therefore, the presented controller is oriented in the grid-voltage direction for ensuring stability independently on operational conditions. In Figure 3 it is displayed the comparison between stator flux and grid voltage orientation. Where $\vec{\lambda}_s^v$ is the virtual stator flux defined as:

$$\vec{\lambda}_s^v = \frac{\vec{v_s}}{j\omega_s} \tag{12}$$

Grid-voltage orientation will ensure that $v_{sd} = 0$ and a constant change in the evolution of the reference frame rotational angle ($d\theta_{sf}^v/dt = \omega_s$), however, the stator flux will have components in both reference axis direction, for unbalanced conditions λ_{sq} will have a sinusoidal behavior centered in zero while λ_{sd} will be sinusoidal as well with an offset. The dynamics of the rotor current are obtained from Equations (2) to (4):

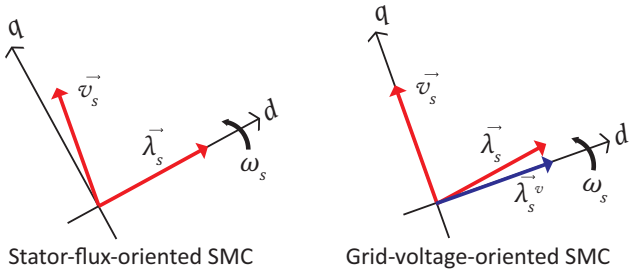

Fig. 3: Comparison between reference frame orientation.

$$\frac{di_{rd}}{dt} = \frac{1}{L_r'}(v_{rd} - R_r i_{rd} - \frac{L_m}{L_s}\frac{d\lambda_{sd}}{dt} + \omega_r L_r' i_{rq} + \frac{L_m}{L_s}\omega_r \lambda_{sq}) \tag{13}$$

$$\frac{di_{rq}}{dt} = \frac{1}{L_r'}(v_{rq} - R_r i_{rq} - \frac{L_m}{L_s}\frac{d\lambda_{sq}}{dt} - \omega_r L_r' i_{rd} - \frac{L_m}{L_s}\omega_r \lambda_{sd}) \tag{14}$$

where $L_r' = L_r - L_m^2/L_s$.

The main control objective of variable-speed turbines is to maintain the power coefficient of the turbine at the optimal value, that can be achieved indirectly by controlling the electromagnetic torque of the machine. On the other hand, reactive power control is required for fault recovery support, therefore, the following sliding surfaces are selected:

$$\sigma_{\tau_e} = \tau_e - \tau_e^* \tag{15}$$

$$\sigma_{Q_s} = Q_s - Q_s^* \tag{16}$$

The dynamics of the sliding surfaces are:

$$\dot{\sigma}_{\tau_e} = \dot{\tau}_e - \dot{\tau}_e^* \tag{17}$$

$$\dot{\sigma}_{Q_s} = \dot{Q}_s - \dot{Q}_s^* \tag{18}$$

where derivative of equations (5) and (7) results:

$$\dot{\tau}_e = \frac{-3PL_m}{2L_s}(\dot{i}_{rq}\lambda_{sd} + i_{rq}\dot{\lambda}_{sd} - \dot{i}_{rd}\lambda_{sq} - i_{rd}\dot{\lambda}_{sq}) \tag{19}$$

$$\dot{Q}_s = \frac{-3L_m}{2L_s}(\dot{v}_{sq} i_{rd} + v_{sq}\dot{i}_{rd}) + \frac{3}{2L_s}(\dot{\lambda}_{sd} v_{sq} + \lambda_{sd}\dot{v}_{sq}) \tag{20}$$

Under normal conditions the terms $\dot{v}_{sq}$, λ_{sq} and $\dot{\lambda}_{sq}$ are equal to zero, however when a fault in the stator voltage occurs, the mathematical expressions depending on the mentioned can be seen as perturbations (P_{τ_e} and P_{Q_s}). On the other hand, let's consider that the torque and reactive power references are much slower than the rest of system dynamics ($\dot{\tau}_e^* = 0$ and $\dot{Q}_s^* = 0$):

$$\dot{\sigma}_{\tau_e} = \overbrace{k\lambda_{sd}(R_r i_{rq} + \frac{L_m}{L_s}\omega_r \lambda_{sd} + \omega_r L_r' i_{rd})}^{F_{\tau_e}} \underbrace{-k\lambda_{sd}}_{d_{\tau_e}} v_{rq} + P_{\tau_e} \tag{21}$$

This article has been accepted for publication in a future issue of this journal, but has not been fully edited. Content may change prior to final publication. Citation information: DOI 10.1109/TSTE.2017.2769062, IEEE Transactions on Sustainable Energy

$$\dot{\sigma}_{Q_s} = \overbrace{\frac{k}{P} v_{sq}(R_r i_{rd} - \omega_r L'_r i_{rq})}^{F_{Q_s}} \underbrace{-\frac{k}{P} v_{sq}}_{d_{Q_s}} v_{rd} + P_{Q_s} \quad (22)$$

where $k = \frac{3PL_m}{2L_s L'_r}$, $P_{\tau_e} = kL'_r(\dot{i}_{rd}\lambda_{sq} + i_{rd}\dot{\lambda}_{sq} - i_{rq}\dot{\lambda}_{sd}) + k\lambda_{sd}\frac{L_m}{L_s}\dot{\lambda_{sq}}$ and $P_{Q_s} = \frac{k}{P} v_{sq}[\frac{L_m}{L_s}(\dot{\lambda}_{sd} - \omega_r\lambda_{sq}) - \frac{L'_r}{v_{sq}}\dot{v}_{sq} i_{rd}] + \frac{3}{2L_s}(\dot{\lambda}_{sd} v_{sq} + \lambda_{sd}\dot{v}_{sq})$.

The rotor voltage can be oriented to the virtual stator flux reference frame using the Clarke transform and then a reference frame rotation:

$$\begin{bmatrix} v_{rd} \\ v_{rq} \end{bmatrix} = \overbrace{\begin{bmatrix} \cos\theta_d & -\sin\theta_d \\ \sin\theta_d & \cos\theta_d \end{bmatrix} \frac{2}{3} \begin{bmatrix} 1 & -1/2 & -1/2 \\ 0 & \sqrt{3}/2 & -\sqrt{3}/2 \end{bmatrix}}^{\mathrm{T}} \begin{bmatrix} V_{an} \\ V_{bn} \\ V_{cn} \end{bmatrix} \quad (23)$$

where θ_d is the angle of the direct axis orientation. For orientation of rotor voltage in the stator flux direction, the reference frame angle is the rotor mechanical angle minus the virtual stator flux angle ($\theta_d = \theta_{mec} - \theta^v_{sf}$).

Expressing the dynamics of the system in equations (21) and (22) as matrix form:

$$\begin{bmatrix} \dot{\sigma_{\tau_e}} \\ \dot{\sigma Q_s} \end{bmatrix} = \begin{bmatrix} F_{\tau_e} \\ F_{Q_s} \end{bmatrix} + \begin{bmatrix} 0 & d_{\tau_e} \\ d_{Q_s} & 0 \end{bmatrix} \begin{bmatrix} v_{rd} \\ v_{rq} \end{bmatrix} + \begin{bmatrix} P_{\tau_e} \\ P_{Q_s} \end{bmatrix} \quad (24)$$

the control signals (v_{rd} and v_{rq}) appear in the first derivate of the sliding surface. Then, the relative degree of the system is one, therefore it is possible to control the system with a first order SMC. It is worth mentioning that both control objectives are decoupled since they are seen from a virtual stator flux reference frame. The used controller is a sign function:

$$\begin{bmatrix} v_{rd} \\ v_{rq} \end{bmatrix} = \begin{bmatrix} -M_d \operatorname{sign}(\sigma_{Q_s}) \\ -M_q \operatorname{sign}(\sigma_{\tau_e}) \end{bmatrix} \quad (25)$$

The relationship between a, b, c quantities and dq reference-frame quantities is:

$$\underbrace{\begin{bmatrix} \sigma_{\tau_e} \\ \sigma_{Q_s} \end{bmatrix}}_{\sigma_{\tau_e, Q_s}} = \overbrace{\begin{bmatrix} 0 & d_{\tau_e} \\ d_{Q_s} & 0 \end{bmatrix}}^{D} T \underbrace{\begin{bmatrix} \sigma_a \\ \sigma_b \\ \sigma_c \end{bmatrix}}_{\sigma_{a,b,c}} \quad (26)$$

where D matrix is not square, therefore in order to obtain the relationship between $\sigma_{a,b,c}$ and σ_{τ_e, Q_s} the Moore-Penrose pseudo-inverse is used:

$$\sigma_{a,b,c} = \overbrace{D^T(DD^T)^{-1}}^{D^+} \sigma_{\tau_e, Q_s} \quad (27)$$

$$D^+ = -\frac{2L_s L'_r}{3L_m} \begin{bmatrix} \frac{1}{P\lambda^v_{sd}} \sin\theta_d & \frac{1}{v_{sq}} \cos\theta_d \\ \frac{1}{P\lambda^v_{sd}} \sin(\theta_d + \frac{2\pi}{3}) & \frac{1}{v_{sq}} \cos(\theta_d + \frac{2\pi}{3}) \\ \frac{1}{P\lambda^v_{sd}} \sin(\theta_d - \frac{2\pi}{3}) & \frac{1}{v_{sq}} \cos(\theta_d - \frac{2\pi}{3}) \end{bmatrix} \quad (28)$$

Since the sign of the mathematical operation $D^T\sigma_{\tau_e, Q_s}$ is independent on the constant term $\frac{2L_s L'_r}{3L_m}$, the matrix D^+ can be simplified as follows:

$$D_2 = -\begin{bmatrix} \frac{1}{P\lambda^v_{sd}} \sin\theta_d & \frac{1}{v_{sq}} \cos\theta_d \\ \frac{1}{P\lambda^v_{sd}} \sin(\theta_d + \frac{2\pi}{3}) & \frac{1}{v_{sq}} \cos(\theta_d + \frac{2\pi}{3}) \\ \frac{1}{P\lambda^v_{sd}} \sin(\theta_d - \frac{2\pi}{3}) & \frac{1}{v_{sq}} \cos(\theta_d - \frac{2\pi}{3}) \end{bmatrix} \quad (29)$$

Then, the controller is insensitive to parameter variations if grid-voltage vector and mechanical angle are properly measured or estimated.

The controller scheme is shown in Figure 4, the SMC consists on the transformation matrix D_2 which transforms the error in torque and reactive power into three phases error, then a hysteresis loop is used for directly sending the desired switching state $S_{1,2,3}$ to the rotor-side power converter. A hysteresis loop (width=Δ) is used for decreasing the switching frequency of an ideal sign function.

A. Sliding mode existence condition

Considering a relative degree one system:

$$\dot{\sigma} = F(x) + d(x)u \quad (x \in \mathbb{R}^n) \quad (30)$$

with a scalar control

$$u = -M \operatorname{sign}(\sigma) \quad (31)$$

then the condition for satisfy the existence of sliding mode is [33]:

$$d(x)M > |F(x)| \quad (32)$$

Therefore for the torque loop, the minimum controller gain is (see equation (21)):

$$M_{\tau_e,\min} > |R_r i_{rq} + \frac{L_m}{L_s}\omega_r\lambda_{sd} + \omega_r L'_r i_{rd}| \quad (33)$$

When the stator flux is disturbed, which is the case of unbalanced voltage dips and natural flux in symmetrical faults, the stator flux magnitude is variable in time and it will not be perfectly aligned to the d axis therefore:

$$\dot{\sigma_{\tau_e}} = F_{\tau_e} + d_{\tau_e} v_{rq} + P_{\tau_e} \quad (34)$$

The minimum gain in case of perturbed system is:

$$M_{\tau_e,\min} > |(F_{\tau_e} + P_{\tau_e})/d_{\tau_e}| \quad (35)$$

For the reactive power loop, the procedure is very similar. From equation (22),

$$M_{Q_s,\min} > |R_r i_{rd} - \omega_r L'_r i_{rq}| \quad (36)$$

in case of perturbation in the voltage grid, the stator flux and stator voltage magnitude are variable in time:

$$\dot{\sigma}_{Q_s} = F_{Q_s} + d_{Q_s} v_{rd} + P_{Q_s} \quad (37)$$

The minimum gain in case of perturbed system is:

$$M_{Q_s,\min} > |(F_{Q_s} + P_{Q_s})/d_{Q_s}| \quad (38)$$

According to the two level converter model (equation (9)), the phase voltage can only be $\pm 2V_{dc}/3$, $\pm V_{dc}/3$ and 0. For an ideal sliding mode controller, the inverter zero vectors (000 or 111) are not valid states, therefore the minimum phase voltage is $\pm V_{dc}/3$.

This article has been accepted for publication in a future issue of this journal, but has not been fully edited. Content may change prior to final publication. Citation information: DOI 10.1109/TSTE.2017.2769062, IEEE Transactions on Sustainable Energy

IV. Natural flux and demagnetizing current

In [34] the dynamic behavior of DFIG under voltage dips is studied in detail. The natural flux is a component appearing due to instantaneous voltage dips, since the stator flux cannot change abruptly. The natural flux induces a large voltage in the rotor and may cause lost of control of the electric machine. Therefore, the concept of demagnetizing current [35], [4], [36] is used in order to counteract the natural flux and return the electric machine to a stable state, preventing further deformation of stator and rotor currents.

The stator flux derivative seen in a stationary reference frame can be obtained with equations (1) and (3), considering that the stator volage is faulted, $\vec{v_s} = \vec{v_{sfault}}$:

$$\frac{d\vec{\lambda_s}}{dt} = \vec{v_{sfault}} - \frac{R_s}{L_s}\vec{\lambda_s} + \frac{L_m}{L_s}R_s\vec{i_r} \tag{39}$$

Neglecting rotor current and considering that the fault voltage can be decoupled in symmetrical components $\vec{v_{sfault}} = \vec{v_s^+} + \vec{v_s^-}$. The stator flux has the following dynamic behavior [37]:

$$\vec{\lambda_s}(t) = \vec{\lambda_{sn}}(0)e^{-\frac{R_s}{L_s}t} + \frac{\vec{v_s^+}}{j\omega_s}e^{j\omega_s t} - \frac{\vec{v_s^-}}{j\omega_s}e^{-j\omega_s t} \tag{40}$$

The first term is the natural flux which decays exponentially if the rotor current is neglected. On the other hand, the forced flux due to the remaining voltage applied to the stator has two components, one rotating in synchronous speed due to the positive sequence component of the faulted voltage and the other one rotating in the opposite direction due to the negative sequence component of voltage.

A rotor current could be applied to eliminate natural flux [4]:

$$\vec{i_{rn}} = -\frac{L_m}{L_s L_r'}k_d\vec{\lambda_{sn}} \tag{41}$$

where $\vec{i_{rn}}$ is the demagnetizing current, $\vec{\lambda_{sn}}$ is the stator natural flux and k_d is a constant term used to modify the demagnetization (natural flux clearance) time.

Since the controller directly regulates torque and reactive power, the reference in those terms can be calculated substituting the components of the demagnetizing current ($\vec{i_{rn}} = i_{rn\alpha} + j\ i_{rn\beta}$) in equations (5) and (7):

$$\tau_{e,dm} = G_\tau\left[\frac{3PL_m}{2L_s}(i_{rn\alpha}\lambda_{s\beta} - i_{rn\beta}\lambda_{s\alpha})\right] \tag{42}$$

$$Q_{s,dm} = G_Q\left[\frac{3L_m}{2L_s}(v_{s\alpha}i_{rn\beta} - v_{s\beta}i_{rn\alpha})\right] \tag{43}$$

$$k_d = \frac{G_\tau + G_Q}{2}; \tag{44}$$

where G_τ and G_Q are the corresponding part of k_d to torque and reactive power demagnetization components, the larger the demagnetizing reference gains, the faster the natural flux elimination, nevertheless, a faster natural flux clearance implies larger torque and reactive power oscillations and higher power requirements for the rotor side power converter.

The demagnetizing torque and reactive power references are added to the original references (see Figure 4) to eliminate natural flux. A saturation block is included in order to limit the demagnetizing current. The selection of the saturation limit should be done considering a maximum allowable demagnetizing current, since it will be added to the normal references the total current must not exceed the maximum current value of power electronic devices.

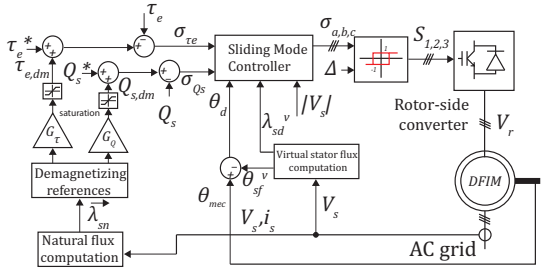

Fig. 4: Sliding mode control with demagnetizing current injection.

The main disadvantage of demagnetizing current strategy is the need of natural flux calculation. Typically band pass filters are used for decoupling positive, negative and natural fluxes [36], [4]. Since the stator resistance is negligible specially for large electric machines, the natural flux can be easily computed if the voltage sequence components are known. In this paper a fast convergence delayed signal cancellation method [38] is used for stator voltage sequence decomposition, then the symmetrical components are subtracted from the total stator flux and the natural flux component is obtained (see Figure 5).

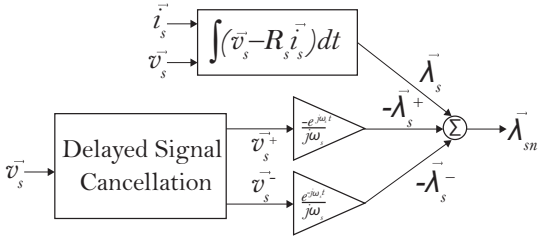

Fig. 5: Natural flux estimation using delayed signal cancellation.

A. Evolution of natural flux in time

Let's consider a 100% voltage dip in the stator, the forced flux will be zero and the stator flux evolution in time will be only due to natural flux. The stator voltage dynamic equation in a stationary reference is:

$$\vec{v_s} = \frac{d\vec{\lambda}_{sn}}{dt} + R_s\vec{i_s} = 0 \tag{45}$$

Solving for stator current from equation (3):

$$\vec{i_s} = \frac{\vec{\lambda}_{sn}}{L_s} - \frac{L_m}{L_s}\vec{i_r} \tag{46}$$

Substituting equations (46) and (41) in equation (45):

$$\frac{d\vec{\lambda}_{sn}}{dt} = -\left(\frac{R_s}{L_s} + \frac{L_m^2 R_s}{L_s^2 L_r'}k_d\right)\vec{\lambda}_{sn} \tag{47}$$

This article has been accepted for publication in a future issue of this journal, but has not been fully edited. Content may change prior to final publication. Citation information: DOI 10.1109/TSTE.2017.2769062, IEEE Transactions on Sustainable Energy

Finally, it is easy to obtain the time response of equation (47):

$$\vec{\lambda}_{sn}(t) = \vec{\lambda}_{sn}(0)e^{-t/\tau_d} \tag{48}$$

where $\tau_d = \frac{L'_r L_s^2}{0.5(G_\tau+G_Q)L_m^2 R_s + L'_r L_s R_s}$.
It should be noted that equation (48) is valid while the demagnetizing references are not saturated.

V. Results

In order to prove the SMC with demagnetizing current strategy, a simulation was done for a $2\ \mathrm{MW}$ DFIG with the characteristics shown in table I. The simulation time step is $0.00001\ \mathrm{s}$ using Euler method for solving ODEs. The DFIG has a constant mechanical torque of $7500\ \mathrm{N\,m}$ at the shaft.

TABLE I: Electric machine parameters used in simulation

Nominal power $= 2$ MW
Nominal voltage $= 690$ V rms
Poles $= 4$
Nominal Frequency $= 50$ Hz
$R_s = 2.6 \times 10^{-3}\ \Omega$
$R_r = 2.9 \times 10^{-3}\ \Omega$
$L_s = 2.577 \times 10^{-3}$ H
$L_r = 2.583 \times 10^{-3}$ H
$L_m = 2.5 \times 10^{-3}$ H
DC-link voltage $= 500$ V
inverter nominal power $= 600$ kW

The simulation consist on a voltage dip starting at $0.1\ \mathrm{s}$ and ending at $0.605\ \mathrm{s}$, therefore the fault starts at $t_0 = 0(T)$ and ends at $t_1 = T/4$ (where T is the period of the stator voltage.

The reactive power reference is increased from zero to $1.5\ \mathrm{MVAr}$, while the electromagnetic torque reference is decreased from $-1000\ \mathrm{N\,m}$ to $-5000\ \mathrm{N\,m}$ (the negative sign is due to the generator operation of the machine). According to grid codes, the generator must supply reactive power in case of contingency for grid recovery supporting [1], [2]. For limiting the current carried out by the rotor side converter the saturation block of the demagnetizing references is set to $\pm 5000\ \mathrm{N\,m}$ for the torque and $\pm 1.5 \times 10^6\ \mathrm{VAr}$ for the reactive power. Figures 6a to 6c display the evolution of the stator flux in time under different faults and demagnetizing conditions, where the time covered by *normal operation* is $t = [0 - 0.1\mathrm{s})$, *fault start* $t = [0.1 - 0.605\mathrm{s})$ and *fault end* $t = [0.605 - 1\mathrm{s}]$. As shown in Figure 6a, the fault starts at $3\pi/2\ \mathrm{rad}$ when the stator voltage is at $0\ \mathrm{rad}$, then the natural flux is cleared and the flux returns to the central position. After that, the stator voltage recovers when the stator flux is at $0\ \mathrm{rad}$ and the voltage vector is at $\pi/2\ \mathrm{rad}$, this is equivalent to a second perturbation, the natural flux is again eliminated and the stator flux return to the normal operation zone.

The next simulation consists on a 20 % type E voltage dip (phases B and C voltage dip) from 0.1 to 0.605 seconds. For this type of fault, the largest possible natural flux component appears if the voltage dip starts at $t_0 = nT/2$ or $t_0 = nT$ (where T is the period of the stator voltage and $n \in \mathbb{N}$), that is the case for a fault starting at $0,1\ \mathrm{s}$. The controller is able to follow torque and reactive power references even under unbalanced conditions (see Figure 8b II and IV). The stator and rotor fluxes maintain the ratio $\frac{\lambda_{sd}}{\lambda_{sq}} = \frac{\lambda_{rd}}{\lambda_{rq}}$(Figure 8b III), which is necessary for sinusoidal current exchange with the electric grid at an imposed electromagnetic torque [14]. The stator active power oscillates since it is not possible to maintain constant torque and active power as demonstrated by [15]. The filtered rotor voltage (see Figure 8b VII) shows a negative sequence voltage injection which is necessary to achieve the desired references tracking.

As shown in Figure 6b the stator flux natural component is eliminated. The electromagnetic torque necessary for demagnetizing current injection is shown in Figure 8b II, once the natural flux has been eliminated the torque and reactive powers are constant, the active power oscillates and the rotor voltage injects negative sequence components for achieving the desired references. Neither the rotor converter maximum current (3000 A) nor nominal power (600 kW) are surpassed, these limitations do not allow faster elimination of natural flux component.

If the demagnetizing current injection is avoided, the zero sequence component elimination is much slower (Figure 6c) affecting the current sent to the grid, stator active power and rotor current harmonics components (see Figure 8c V, IV and VI). Furthermore, when the grid fault the stator flux remains perturbed which causes a negative sequence voltage injection of the rotor converter and deforms the sinusoidal current of the stator (Figure 6c V).

Torque oscillations can be very harmful for mechanical system of the wind turbine, therefore, the demagnetizing current can be performed only by means of the reactive power, avoiding torque oscillations, however, demagnetization is slower than using both components of demagnetizing current. The results of the pure reactive power demagnetization are displayed in Figure 6d. The natural flux clearance time is increased due to the absence of demagnetizing torque component.

The evolution of the natural flux for a 20% three phase voltage dip is shown in Figure 7. A comparison is made between the theoretical value using equation (48) and the values obtained in the simulation with different gains for the demagnetizing torque and reactive power. The predicted value is accurate for values in which the saturation functions shown in Figure 4 do not affect the result, on the other hand for $G_\tau = G_Q = 1$ the saturation blocks are activated for avoiding over-current in the converter slowing down the natural flux clearance. It is worth mentioning that the oscillations of the flux are due to the errors generated in the natural flux estimation method which neglects voltage drop due to the stator resistance in the sequence components. The natural flux dynamics are also affected by the rotor current used to control torque and reactive power, however the demagnetizing current is dominant because it is in an orientation contrary to the natural flux, consequently, equation (48) can be used to obtain an approximation of natural flux clearance time.

This article has been accepted for publication in a future issue of this journal, but has not been fully edited. Content may change prior to final publication. Citation information: DOI 10.1109/TSTE.2017.2769062, IEEE Transactions on Sustainable Energy

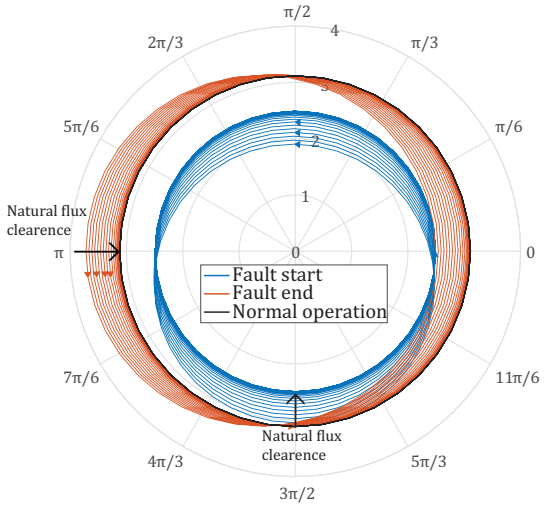

(a) 20 % fault type A ($G_\tau = G_Q = 1$).

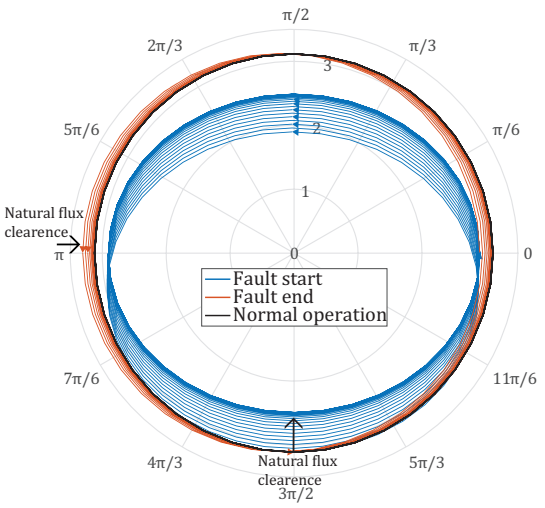

(b) 20 % fault type E ($G_\tau = G_Q = 1$).

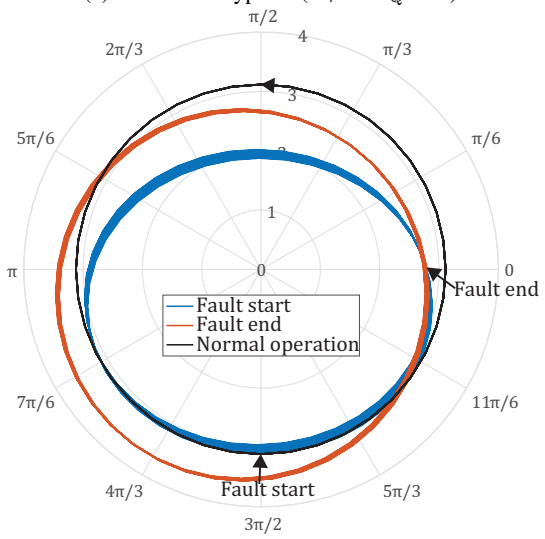

(c) 20 % fault type E ($G_\tau = G_Q = 0$).

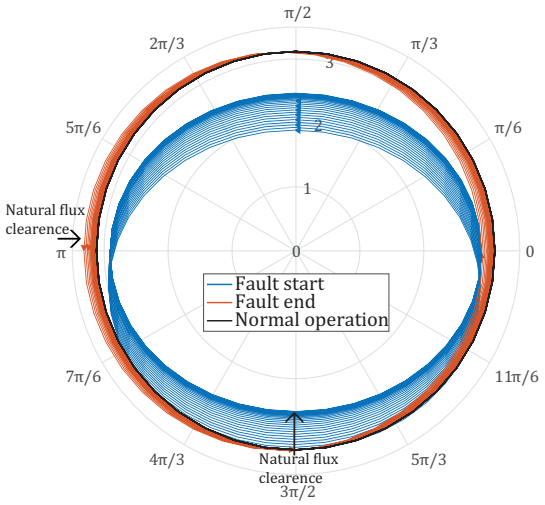

(d) 20 % fault type E ($G_\tau = 0,\ G_Q = 1$).

Fig. 6: Stator flux

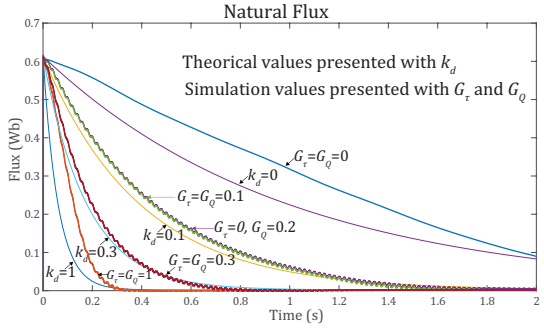

Fig. 7: Natural flux evolution for different values of demagnetizing gains.

VI. Conclusion

A grid-voltage-oriented sliding mode control for DFIG is presented and tested under voltage dips. The controller has the main advantages of simple structure, no dependence on system parameters and switching of power electronic devices directly from the controller output signals.

The controller is able to track torque and stator reactive power even under voltage distortion of the grid without sequence decomposition of rotor current nor further modification of the original controller. However, the natural stator flux component may affect stator current and active power oscillations, therefore a transient demagnetizing reference is included to the original scheme in order to eliminate natural flux component enhancing fault ride through capability of the controller. Different simulations are reported for testing the controller under balanced and unbalanced grid conditions,

This article has been accepted for publication in a future issue of this journal, but has not been fully edited. Content may change prior to final publication. Citation information: DOI 10.1109/TSTE.2017.2769062, IEEE Transactions on Sustainable Energy

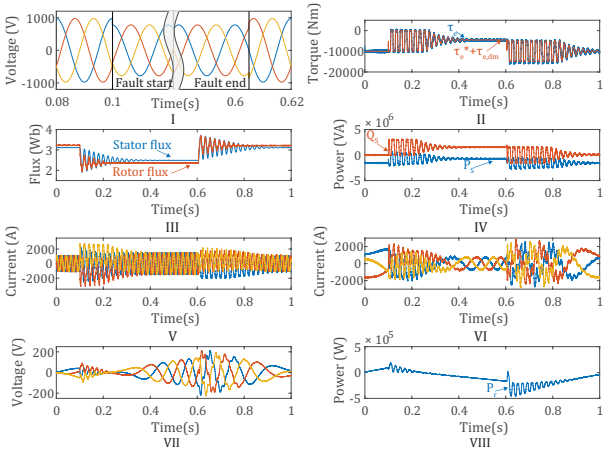

(a) Three phase fault ($G_\tau = G_Q = 1$).

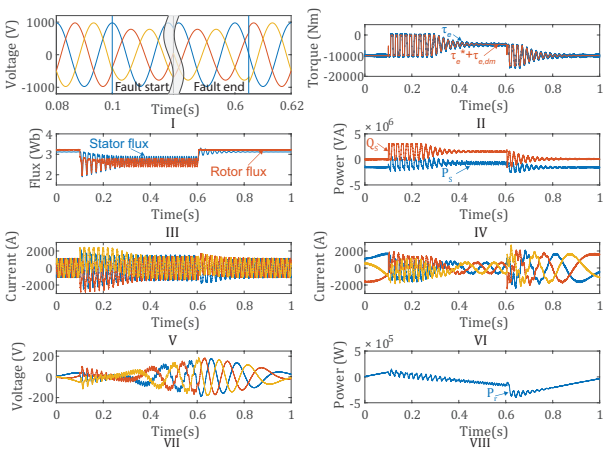

(b) Type E fault ($G_\tau = G_Q = 1$).

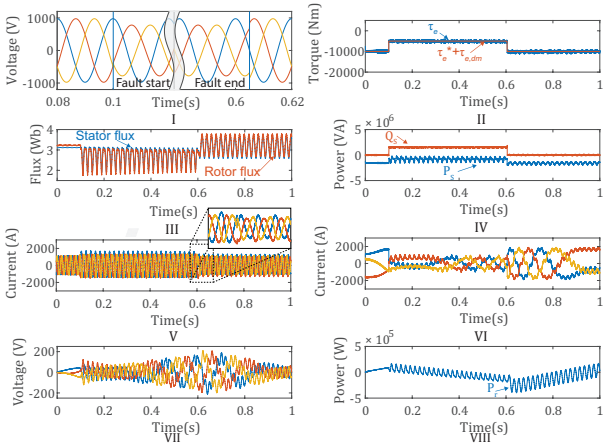

(c) Type E fault ($G_\tau = G_Q = 0$).

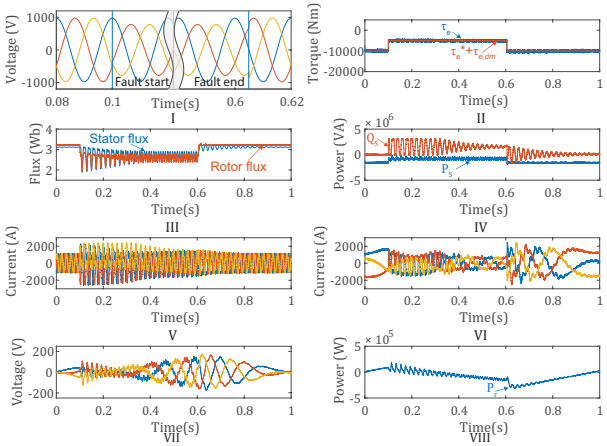

(d) Type E fault ($G_\tau = 0,\ G_Q = 1$).

Fig. 8: Results for 20 % symmetrical and asymmetrical faults: I stator voltage, II electromagnetic torque, III stator and rotor fluxes, IV stator active and reactive power, V stator current, VI rotor current, VII filtered rotor voltage, VIII rotor active power.

the results demonstrate the demagnetization strategy and the reference tracking even under unbalanced conditions, which is equivalent to negative sequence rotor current injection for compensating torque and reactive power oscillations.

Since torque oscillation may be very dangerous for the mechanical components, the natural flux elimination strategy was presented injecting only demagnetizing reactive power. As expected the natural flux is eliminated without torque oscillations. The clearance time is limited by the maximum current of the rotor-side power converter.

REFERENCES

[1] M. Benbouzid, S. Muyeen, and F. Khoucha, "An up-to-date review of low-voltage ride-through techniques for doubly-fed induction generator-based wind turbines," *International Journal on Energy Conversion*, vol. 3, no. 1, pp. 1–9, 2015.

[2] M. Mohseni and S. M. Islam, "Review of international grid codes for wind power integration: Diversity, technology and a case for global standard," *Renewable and Sustainable Energy Reviews*, vol. 16, no. 6, pp. 3876–3890, 2012.

[3] S. Tohidi and M.-i. Behnam, "A comprehensive review of low voltage ride through of doubly fed induction wind generators," *Renewable and Sustainable Energy Reviews*, vol. 57, pp. 412–419, 2016.

[4] J. López, E. Gubía, E. Olea, J. Ruiz, and L. Marroyo, "Ride through of wind turbines with doubly fed induction generator under symmetrical voltage dips," *IEEE Transactions on Industrial Electronics*, vol. 56, no. 10, pp. 4246–4254, 2009.

[5] J. Morren and S. W. De Haan, "Ridethrough of wind turbines with doubly-fed induction generator during a voltage dip," *IEEE Transactions on energy conversion*, vol. 20, no. 2, pp. 435–441, 2005.

[6] R. Cárdenas, R. Peña, S. Alepus, and G. Asher, "Overview of control systems for the operation of DFIGs in wind energy applications," *IEEE Transactions on Industrial Electronics*, vol. 60, no. 7, pp. 2776–2798, 2013.

[7] J. Hu, Y. He, L. Xu, and B. W. Williams, "Improved control of DFIG systems during network unbalance using PI–R current regulators," *IEEE Transactions on Industrial Electronics*, vol. 56, no. 2, pp. 439–451, 2009.

[8] Y. Shtessel, C. Edwars, L. Fridman, and A. Levant, *Sliding Mode Control and Observation*. New York: Springer, 2014.

[9] V. Utkin, "Discussion aspects of high-order sliding mode control," *IEEE Transactions on Automatic Control*, vol. 61, no. 3, pp. 829–833, 2016.

[10] M. Benbouzid, B. Beltran, Y. Amirat, G. Yao, J. Han, and H. Mangel, "Second-order sliding mode control for DFIG-based wind turbines fault ride-through capability enhancement," *ISA transactions*, vol. 53, no. 3, pp. 827–833, 2014.

[11] B. Beltran, M. Benbouzid, and T. Ahmed-Ali, "High-order sliding mode control of a DFIG-based wind turbine for power maximization and grid fault tolerance," in *Electric Machines and Drives Conference, 2009. IEMDC'09. IEEE International*. IEEE, 2009, pp. 183–189.

[12] M. I. Martinez, G. Tapia, A. Susperregui, and H. Camblong, "Sliding-mode control for dfig rotor-and grid-side converters under unbalanced and harmonically distorted grid voltage," *IEEE Transactions on Energy Conversion*, vol. 27, no. 2, pp. 328–339, 2012.

[13] M. Martinez, A. Susperregui, G. Tapia, and L. Xu, "Sliding-mode control of a wind turbine-driven double-fed induction generator under non-ideal grid voltages," *IET Renewable Power Generation*, vol. 7, no. 4, pp. 370–379, 2013.

[14] G. Abad, J. Lopez, M. Rodríguez, L. Marroyo, and G. Iwanski, *Doubly fed induction machine: modeling and control for wind energy generation*. John Wiley & Sons, 2011, vol. 85.

[15] L. Xu and Y. Wang, "Dynamic modeling and control of DFIG-based wind turbines under unbalanced network conditions," *IEEE Transactions on Power Systems*, vol. 22, no. 1, pp. 314–323, 2007.

[16] Y. Zhou, P. Bauer, J. A. Ferreira, and J. Pierik, "Operation of grid-connected dfig under unbalanced grid voltage condition," *IEEE Transactions on Energy Conversion*, vol. 24, no. 1, pp. 240–246, 2009.

[17] P. S. Flannery and G. Venkataramanan, "Unbalanced voltage sag ride-through of a doubly fed induction generator wind turbine with series grid-side converter," *IEEE Transactions on Industry Applications*, vol. 45, no. 5, pp. 1879–1887, 2009.

[18] O. Gomis-Bellmunt, A. Junyent-Ferre, A. Sumper, and J. Bergas-Jane, "Ride-through control of a doubly fed induction generator under unbalanced voltage sags," *IEEE Transactions on Energy Conversion*, vol. 23, no. 4, pp. 1036–1045, 2008.

[19] L. Xu, "Coordinated control of dfig's rotor and grid side converters during network unbalance," *IEEE Transactions on Power Electronics*, vol. 23, no. 3, pp. 1041–1049, 2008.

[20] L. Trilla, O. Gomis-Bellmunt, A. Junyent-Ferre, M. Mata, J. S. Navarro, and A. Sudria-Andreu, "Modeling and validation of DFIG 3-MW wind turbine using field test data of balanced and unbalanced voltage sags," *IEEE Transactions on sustainable energy*, vol. 2, no. 4, pp. 509–519, 2011.

[21] Y. Wang, L. Xu, and B. Williams, "Compensation of network voltage unbalance using doubly fed induction generator-based wind farms," *IET Renewable Power Generation*, vol. 3, no. 1, pp. 12–22, 2009.

[22] T. Brekken, N. Mohan, and T. Undeland, "Control of a doubly-fed induction wind generator under unbalanced grid voltage conditions," in *Power Electronics and Applications, 2005 European Conference on*. IEEE, 2005, pp. 10–pp.

[23] H. Nian, Y. Song, P. Zhou, and Y. He, "Improved direct power control of a wind turbine driven doubly fed induction generator during transient grid voltage unbalance," *IEEE Transactions on Energy Conversion*, vol. 26, no. 3, pp. 976–986, 2011.

[24] D. Santos-Martin, J. L. Rodriguez-Amenedo, and S. Arnalte, "Direct power control applied to doubly fed induction generator under unbalanced grid voltage conditions," *IEEE Transactions on Power Electronics*, vol. 23, no. 5, pp. 2328–2336, 2008.

[25] D. Santos-Martin, J. L. Rodriguez-Amenedo, and S. Arnaltes, "Providing ride-through capability to a doubly fed induction generator under unbalanced voltage dips," *IEEE Transactions on Power Electronics*, vol. 24, no. 7, pp. 1747–1757, 2009.

[26] G. Abad, M. A. Rodriguez, G. Iwanski, and J. Poza, "Direct power control of doubly-fed-induction-generator-based wind turbines under unbalanced grid voltage," *IEEE Transactions on Power Electronics*, vol. 25, no. 2, pp. 442–452, 2010.

[27] G. Abad, M. Rodriguez, J. Poza, and J. Canales, "Direct torque control for doubly fed induction machine-based wind turbines under voltage dips and without crowbar protection," *IEEE Transactions on Energy Conversion*, vol. 25, no. 2, pp. 586–588, 2010.

[28] I. Villanueva, A. Rosales, P. Ponce, and A. Molina, "Stator-flux-oriented sliding mode controller for DFIG with variable hysteresis loop for limiting switch frequency of rotor-side power converter," in *Industrial Technology (ICIT), 2017 IEEE International Conference on*. IEEE, 2017.

[29] A. Petersson, L. Harnefors, and T. Thiringer, "Comparison between stator-flux and grid-flux-oriented rotor current control of doubly-fed induction generators," in *Power Electronics Specialists Conference, 2004. PESC 04. 2004 IEEE 35th Annual*, vol. 1. IEEE, 2004, pp. 482–486.

[30] S. Peresada, A. Tilli, and A. Tonielli, "Indirect stator flux-oriented output feedback control of a doubly fed induction machine," *IEEE Transactions on Control Systems Technology*, vol. 11, no. 6, pp. 875–888, 2003.

[31] L. Congwei, W. Haiqing, S. Xudong, and L. Fahai, "Research of stability of double fed induction motor vector control system," in *Electrical Machines and Systems, 2001. ICEMS 2001. Proceedings of the Fifth International Conference on*, vol. 2. IEEE, 2001, pp. 1203–1206.

[32] S. N. Vukosavic, *Electrical machines*. Springer Science & Business Media, 2012.

[33] V. Utkin, J. Guldner, and J. Shi, *Sliding mode control in electro-mechanical systems*. CRC press, 2009, vol. 34.

[34] J. Lopez, P. Sanchis, X. Roboam, and L. Marroyo, "Dynamic behavior of the doubly fed induction generator during three-phase voltage dips," *IEEE Transactions on Energy conversion*, vol. 22, no. 3, pp. 709–717, 2007.

[35] J. López, P. Sanchis, E. Gubía, A. Ursúa, L. Marroyo, and X. Roboam, "Control of doubly fed induction generator under symmetrical voltage dips," in *Industrial Electronics, 2008. ISIE 2008. IEEE International Symposium on*. IEEE, 2008, pp. 2456–2462.

[36] D. Xiang, L. Ran, P. J. Tavner, and S. Yang, "Control of a doubly fed induction generator in a wind turbine during grid fault ride-through," *IEEE Transactions on Energy Conversion*, vol. 21, no. 3, pp. 652–662, 2006.

[37] J. Lopez, E. Gubia, P. Sanchis, X. Roboam, and L. Marroyo, "Wind turbines based on doubly fed induction generator under asymmetrical voltage dips," *IEEE Transactions on Energy Conversion*, vol. 23, no. 1, pp. 321–330, 2008.

[38] R. Cárdenas, F. Rojas, J. Clare *et al.*, "Fast convergence delayed signal cancellation method for sequence component separation," *IEEE Transactions on Power Delivery*, vol. 30, no. 4, pp. 2055–2057, 2015.

4.2 Variable hysteresis in the time domain

Villanueva, I., Rosales, A., Ponce, P., & Molina, A. (2017). **Stator-flux-oriented sliding mode controller for DFIG with variable hysteresis loop for limiting switch frequency of rotor-side power converter**. *In Industrial Technology (ICIT), 2017 IEEE International Conference on* (pp. 213-218). IEEE.

This paper has been presented in the 2016 IEEE 18th International Conference on Industrial Technology (ICIT 2017) in Toronto, Canada.

In this paper, the proposed controller scheme is presented by the first time. The stator-flux oriented SMC switching frequency is limited by an adaptive hysteresis width which is adjusted according with the operational state of the machine. The presented controller has the main advantages of simple structure, robustness and direct switching of power converter.

Stator-Flux-Oriented Sliding Mode Controller for DFIG with Variable Hysteresis Loop for Limiting Switch Frequency of Rotor-Side Power Converter

Iván Villanueva, Antonio Rosales, Pedro Ponce and Arturo Molina
Tecnologico de Monterrey
School of Engineering and Sciences
Calle del Puente 222 Col. Ejidos de Huipulco, Tlalpan 14380, Mexico City

***Abstract*—Doubly fed induction generator (DFIG) is the most implemented electric machine in wind energy conversion systems (WECS) due to reduced size converter, active and reactive power control and economic factors. However, the power electronic stage needs an accurate controller that allows to follow the stator power regulation. As a result, Sliding-Mode Control (SMC) has been successfully implemented in DFIG because the natural discontinuous control signals arising from the controller can be used for direct switching of power electronic devices. Yet, switching frequency of SMC depends on the sample rate, controller parameters and electric machine dynamics; this conditions produce a control signal with a variable switching frequency hindering implementation. In this paper a stator-flux-Oriented sliding-mode controller with a hysteresis band that limits the switching frequency of power electronic devices to a set value is presented. This methodology improves previous proposals by limiting switching frequency making implementation more feasible. Simulation results are presented to validate the control methodology.**

I. Introduction

Wind energy has been continuously increasing the contribution of total electric generation in several European, Asian and American countries. Recently, the European Union has considered a 100% renewable generation scenario for 2050 [1]. Furthermore, some nations have already achieve 100% renewable generation during short periods of time. Then, maintain safe turbine operation, maximize power, mitigate damage and detect faults are very important challenges for wind energy systems [2]. The key to address these challenges is the design of control algorithms.

Sliding Mode Control (SMC) is a nonlinear control technique known for providing insensitivity to bounded disturbance/uncertainties and finite convergence of the sliding variable to zero [3]. SMC can be used for direct switching of power electronics instead of giving a reference signal to a Pulse Width Modulation (PWM) algorithm. In the literature there are several examples that replace PWM with SMC, mainly on DC-DC converters [4], [5]; grid-connected inverters [6], [7] and electric machines controllers [8]. The idea is to exploit the discontinuous nature of SMC since the control signals are governed by the sign function (two states). Then, the switching states are injected directly to a two level power inverter.

Voltage source inverters are restricted in terms of switching frequency and commutation power losses. Wind turbine power converters use IGBT devices switching at frequencies between 1 and 5 kHz [9]. In SMC, the most commonly used solution to reduce switching frequency of the control signal is the implementation of a hysteresis function instead of the ideally infinite-switching-frequency sign function. The nonideality of hysteresis in the comparator makes, in the real sliding control, the switching frequency to be finite [10]. Other typical solutions are sliding-mode PWM [11], adding disturbing signals to the comparator in order to force a switching frequency [12] and zero average dynamics [13]. The main advantages of hysteresis-based methods are the relationship between hysteresis width and system dynamics as well as simplicity of implementation.

DFIG is currently the most implemented electric machine in wind generation. SMC has been recently proposed for controlling mechanical torque and stator reactive power on DFIG, the controller is stable and fault tolerant [14]. In [8], a SMC approach, robust even during unbalanced grid conditions and parameters variation, commuting directly the inverter is developed for a stator reference frame controller. However, no solution is presented for controlling the switching frequency of the inverter.

In this work, a stator-flux-oriented sliding mode controller, which ensures a set frequency of commutation, is presented. The reference frame orientation decouples the control, therefore the direct axis rotor voltage controls the reactive power, while the active power is controlled by the quadrature axis rotor voltage. This allows to control the switching frequency of the power converter since the hysteresis can be calculated for either torque or reactive power loops. Additionally, the implemented methodology has the following advantages in contrast to PWM algorithms: 1) easy computation; and 2) the controller does not depend on DFIG electric parameters.

II. DFIG Modeling and Control

General scheme of DFIG-based wind turbine is displayed in figure 1. In this paper only the rotor-side converter is considered and the DC-link is maintain at constant voltage.

978-1-5090-5320-9/17/$31.00 ©2017 IEEE

The electric machine model refereed to a synchronous rotating reference frame (stator flux or stator voltage) can be summarized using the following set of equations [15]:

$$\vec{v_s} = \frac{d\vec{\lambda}_s}{dt} + R_s\vec{i_s} + j\omega_s\vec{\lambda_s} \tag{1}$$

$$\vec{v_r} = \frac{d\vec{\lambda}_r}{dt} + R_r\vec{i_r} + j\omega_r\vec{\lambda_r} \tag{2}$$

$$\vec{\lambda_s} = L_s\vec{i_s} + L_m\vec{i_r} \tag{3}$$

$$\vec{\lambda_r} = L_r\vec{i_r} + L_m\vec{i_s} \tag{4}$$

where $\vec{v_s}, \vec{i_s}, \vec{v_r}, \vec{i_r}$ are the stator and rotor voltage and current vectors, R, L represent resistance and inductance and the subscripts "s" "r" are stator and rotor respectively, L_m is the magnetization inductance, ω_s is the synchronous angular speed, ω_r is the electrical angular speed of the rotor current and $\vec{\lambda_s}, \vec{\lambda_r}$ are the stator and rotor fluxes.

The stator and rotor fluxes must rotate at the same speed in order to meet the condition for delivering power and torque with nonzero average values [15], therefore the rotor electrical angular speed can be calculated using: $\omega_r = \omega_s - \omega_{mec}$ where ω_{mec} is the mechanical speed.

In steady state, the stator flux is proportional to the grid voltage, if the voltage drop due to the stator resistance is neglected, the stator voltage phasor will lead the stator flux phasor by 90 degrees. Aligning voltages and currents with the stator-flux reference frame, the torque can be controlled by means of the quadrature-axis current,

$$\tau_e = \frac{3PL_m}{2L_s}(i_{rd}\lambda_{sq} - i_{rq}\lambda_{sd}) = \frac{-3PL_m}{2L_s}(i_{rq}\lambda_{sd}) \tag{5}$$

where P is the number of pole pairs of the electric machine. On the other hand, the stator reactive power can be controlled regulating the direct-axis rotor current,

$$\begin{aligned} Q_s &= \frac{3L_m}{2L_s}(v_{sd}i_{rq} - v_{sq}i_{rd}) + \frac{3}{2L_s}(\lambda_{sd}v_{sq} - \lambda_{sq}v_{sd}) \\ &= \frac{-3L_m}{2L_s}(v_{sq}i_{rd}) + \frac{3}{2L_s}(\lambda_{sd}v_{sq}) \end{aligned} \tag{6}$$

where the second term of equation (6) can be interpreted as the reactive power needed for magnetizing the electric machine.

Equations (1) to (4) can be used for obtaining dynamic equations of the rotor current, aligning the system with the stator flux reference frame ($\lambda_{sq} = 0$ and $v_{sd} = 0$):

$$\frac{di_{rd}}{dt} = \frac{1}{L'_r}(v_{rd} - R_r i_{rd} - \frac{L_m}{L_s}\frac{d\lambda_{sd}}{dt} + \omega_r L'_r i_{rq}) \tag{7}$$

$$\frac{di_{rq}}{dt} = \frac{1}{L'_r}(v_{rq} - R_r i_{rq} - \frac{L_m}{L_s}\omega_r\lambda_{sd} - \omega_r L'_r i_{rd}) \tag{8}$$

where $L'_r = L_r + L_m^2/L_s$.

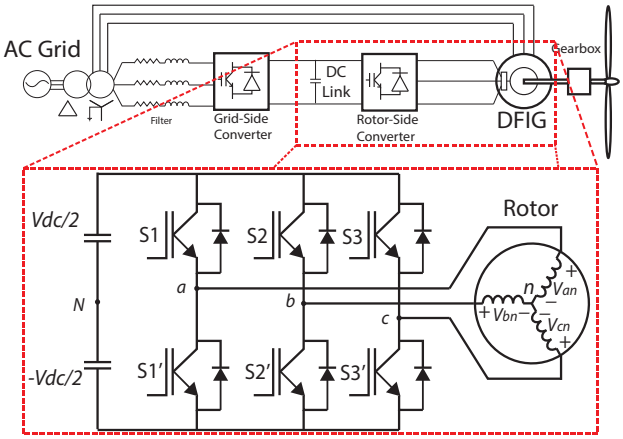

Fig. 1: Two level inverter

In case of wind-speed under the rated value for a turbine, the control objective of most DFIG-based turbines is to maintain the power coefficient of the turbine at the optimal value, that can be achieved indirectly by controlling the electromagnetic torque of the electric machine [8]. Additionally, the stator reactive power is regulated by the controller. Therefore, the following sliding surfaces are selected:

$$\sigma_{\tau_e} = \tau_e - \tau_e^* \tag{9}$$

$$\sigma_{Q_s} = Q_s - Q_s^* \tag{10}$$

The dynamics of the sliding surfaces are:

$$\dot{\sigma}_{\tau_e} = \dot{\tau_e} - \dot{\tau_e^*} \tag{11}$$

$$\dot{\sigma}_{Q_s} = \dot{Q_s} - \dot{Q_s^*} \tag{12}$$

where derivative of equations (5) and (6) results:

$$\dot{\tau_e} = \frac{-3PL_m}{2L_s}(\dot{i_{rq}}\lambda_{sd} + i_{rq}\dot{\lambda_{sd}}) \tag{13}$$

$$\dot{Q_s} = \frac{-3L_m}{2L_s}(\dot{v_{sq}}i_{rd} + v_{sq}\dot{i_{rd}}) + \frac{3}{2L_s}(\dot{\lambda_{sd}}v_{sq} + \lambda_{sd}\dot{v_{sq}}) \tag{14}$$

If the system is considered to operate under normal conditions, the stator voltage and stator flux do not variate in time leading to:

$$\dot{\sigma}_{\tau_e} = \overbrace{k_{\tau_e}\lambda_{sd}(R_r i_{rq} + \frac{L_m}{L_s}\omega_r\lambda_{sd} + \omega_r L'_r i_{rd}) - \dot{\tau_e^*}}^{F_{\tau_e}} \underbrace{-k_{\tau_e}\lambda_{sd}}_{d_{\tau_e}} v_{rq} \tag{15}$$

$$\dot{\sigma}_{Q_s} = \overbrace{k_{Q_s}v_{sq}(R_r i_{rd} - \omega_r L'_r i_{rq}) - \dot{Q_s^*}}^{F_{Q_s}} \underbrace{-k_{Q_s}v_{sq}}_{d_{Q_s}} v_{rd} \tag{16}$$

where $k_{\tau_e} = \frac{3PL_m}{2L_s L'_r}$ and $k_{Q_s} = \frac{3L_m}{2L_s L'_r}$

On a two level power converter, the relationship between

switch states and output voltage can be determined using the following operation:

$$\begin{bmatrix} V_{an} \\ V_{bn} \\ V_{cn} \end{bmatrix} = \frac{V_{dc}}{3} \begin{bmatrix} 2 & -1 & -1 \\ -1 & 2 & -1 \\ -1 & -1 & 2 \end{bmatrix} \begin{bmatrix} S_1 \\ S_2 \\ S_3 \end{bmatrix} \tag{17}$$

where V_{dc} is the DC link voltage, S_1, S_2 and S_3 are the switch states of each leg of the power converter. Since the devices of each legs cannot be commuted simultaneously, each leg can only has two valid switching states (zero or one).

If the output voltage is measured with respect a neutral point in the middle of the DC link (see figure 1), the voltage output can be expressed as a sign function, therefore the system can be easily controlled using SMC having as possible states only -1 and 1. The output of the inverter can be either $V_{dc}/2$ or $-V_{dc}/2$ for each phase.

$$\begin{bmatrix} V_{aN} \\ V_{bN} \\ V_{cN} \end{bmatrix} = \frac{V_{dc}}{2} \begin{bmatrix} 1 & 0 & 0 \\ 0 & 1 & 0 \\ 0 & 0 & 1 \end{bmatrix} \overbrace{\begin{bmatrix} \text{sign}(S_1 - 0.5) \\ \text{sign}(S_2 - 0.5) \\ \text{sign}(S_3 - 0.5) \end{bmatrix}}^{S_{123}} \tag{18}$$

The rotor voltage can be oriented to the stator flux reference frame using the Clarke transform and then a reference frame rotation:

$$\begin{bmatrix} v_{rd} \\ v_{rq} \end{bmatrix} = \overbrace{\begin{bmatrix} \cos\theta_d & -\sin\theta_d \\ \sin\theta_d & \cos\theta_d \end{bmatrix} \frac{2}{3} \begin{bmatrix} 1 & -1/2 & -1/2 \\ 0 & \sqrt{3}/2 & -\sqrt{3}/2 \end{bmatrix}}^{\text{T}} \begin{bmatrix} V_{an} \\ V_{bn} \\ V_{cn} \end{bmatrix} \tag{19}$$

where θ_d is the angle of the direct axis orientation. In this case, as we want to orientate the voltage quantities with the stator flux, the angle will be the rotor mechanical angle minus the stator flux angle, $\theta_d = \theta_{mec} - \theta_{sf}$.

Expressing the dynamics of the system in equations (15) and (16) as matrix form:

$$\begin{bmatrix} \dot{\sigma_{\tau_e}} \\ \dot{\sigma_{Q_s}} \end{bmatrix} = \begin{bmatrix} F_{\tau_e} \\ F_{Q_s} \end{bmatrix} + \begin{bmatrix} 0 & d_{\tau_e} \\ d_{Q_s} & 0 \end{bmatrix} \begin{bmatrix} v_{rd} \\ v_{rq} \end{bmatrix}, \tag{20}$$

the control signals (v_{rd} and v_{rq}) appear in the first derivate of the sliding surface. Then, the relative degree of the system is one, therefore it is possible to control the system with a first order SMC. It is worth mentioning that both control objectives are decoupled since they are seen from a stator flux reference frame. The used controller is a sign function:

$$\begin{bmatrix} v_{rd} \\ v_{rq} \end{bmatrix} = \begin{bmatrix} -M\,\text{sign}(\sigma_{Q_s}) \\ -M\,\text{sign}(\sigma_{\tau_e}) \end{bmatrix} \tag{21}$$

The relationship between phase quantities and dq reference-frame quantities is [8]:

$$\underbrace{\begin{bmatrix} \sigma_{\tau_e} \\ \sigma_{Q_s} \end{bmatrix}}_{\sigma_{\tau_e,Q_s}} = \overbrace{\begin{bmatrix} 0 & d_{\tau_e} \\ d_{Q_s} & 0 \end{bmatrix} T}^{D} \underbrace{\begin{bmatrix} \sigma_a \\ \sigma_b \\ \sigma_c \end{bmatrix}}_{\sigma_{abc}} \tag{22}$$

where D matrix is not square, therefore in order to obtain the relationship between σ_{abc} and σ_{τ_e,Q_s} the Moore-Penrose pseudo-inverse is used:

$$\sigma_{abc} = \overbrace{D^T(DD^T)^{-1}}^{D^+} \sigma_{\tau_e,Q_s} \tag{23}$$

$$D^+ = -\begin{bmatrix} \frac{1}{k_{\tau_e}\lambda_{sd}}\sin\theta_d & \frac{1}{k_{Q_s}v_{sq}}\cos\theta_d \\ \frac{1}{k_{\tau_e}\lambda_{sd}}\sin(\theta_d + \frac{2\pi}{3}) & \frac{1}{k_{Q_s}v_{sq}}\cos(\theta_d + \frac{2\pi}{3}) \\ \frac{1}{k_{\tau_e}\lambda_{sd}}\sin(\theta_d - \frac{2\pi}{3}) & \frac{1}{k_{Q_s}v_{sq}}\cos(\theta_d - \frac{2\pi}{3}) \end{bmatrix} \tag{24}$$

Since the transformation matrix T in equation (22) does not change the magnitude of the resulting phasors, it can be concluded from equations (18) and (21) that: $M = V_{dc}/2$.

Matrix D^+ apparently depends on system parameters L_m, L_s and L'_r which may be impractical to consider to be known, however since the sign of the resulting operation is not affected by parameters variation, the matrix D^+ can be simplified as follows:

$$D_2 = -\begin{bmatrix} \frac{1}{P\lambda_{sd}}\sin\theta_d & \frac{1}{v_{sq}}\cos\theta_d \\ \frac{1}{P\lambda_{sd}}\sin(\theta_d + \frac{2\pi}{3}) & \frac{1}{v_{sq}}\cos(\theta_d + \frac{2\pi}{3}) \\ \frac{1}{P\lambda_{sd}}\sin(\theta_d - \frac{2\pi}{3}) & \frac{1}{v_{sq}}\cos(\theta_d - \frac{2\pi}{3}) \end{bmatrix} \tag{25}$$

Then, the controller is insensitive to parameter variations if stator flux vector and mechanical angle are properly measured or estimated.

III. Hysteresis-Loop for switch-frequency regulation

Given the dynamics,

$$\dot{\sigma} = F(x) + d(x)u, \tag{26}$$

where $u = M\,\text{sign}(\sigma)$, $d(x) > 0$, $d(x)M > F(x)$ and $x \in R^n$. A hysteresis loop in the switching function u can be implemented as [16],

$$\Delta = d(x)\frac{M^2 - (F(x)/d(x))^2}{2M}\frac{1}{f_{des}} \tag{27}$$

where f_{des} is the desired switching frequency. Note that dynamics in eq. (26) are similar to equations (16) and (15). Then, applying equation (27) to electromagnetic torque and stator reactive power dynamics, the controllers v_{rd} and v_{rq} in eq. (21) that ensure the desired switching frequency can be implemented.

The width of the hysteresis depends completely on the dynamics of the system, as can be observed in eq. (27). However, this issue can be solved using the equivalent control, where the parameter $(F(x)/d(x))$ can be easily computed using a low-pass filter [16]. As can be seen from equations (15) and (16), the parameters d_{τ_e} and d_{q_s} depend on measuring (or estimating) only the stator flux magnitude or the stator voltage magnitude and a constant, making this methodology feasible to implement.

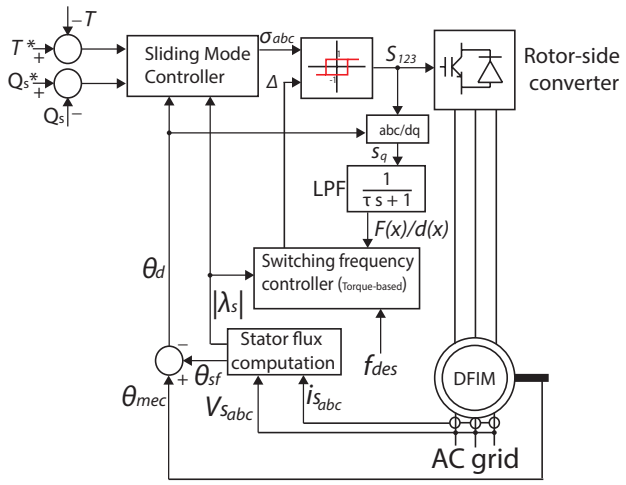

Fig. 2: Sliding mode controller with switching frequency control

TABLE I: Electric machine parameters used in simulation

Nominal power $= 2\ MW$
Nominal voltage $= 690\ Vrms$
Poles $= 4$
Nominal Frequency $= 50Hz$
$R_s = 2.6 \times 10^{-3}\ \Omega$
$R_r = 2.9 \times 10^{-3}\ \Omega$
$L_s = 2.58 \times 10^{-3}\ H$
$L_r = 2.58 \times 10^{-3}\ H$
DC-link voltage $= 400\ V$

The controller scheme is shown in figure 2. The SMC has as inputs the torque and stator reactive power error, the stator flux magnitude and direct axis angle. If the voltage drop due to stator resistance is neglected, v_{sq} can be computed using $v_{sq} = 2\pi f_{grid}\lambda_{sd}$, where f_{grid} is the stator voltage frequency. Stator flux vector can be calculated from equation (1) using a stationary reference frame: $\vec{\lambda}_s = \int (\vec{v}_s - R_s\vec{i}_s)dt$. The use of a low-pass filter allows to obtain an equivalent control (s_q) for the quadrature axis rotor voltage (v_{rd}). If the equivalent control and the stator flux magnitude are known, it is possible to calculate a hysteresis width Δ which will maintain a desired switching frequency f_{des}. It is important to highlight that the vector σ_{abc} must have the same magnitude of vector σ_{τ_e,Q_s}.

IV. Results

In order to prove the switching frequency regulation, a DFIG is simulated with a constant mechanical torque at the shaft of $10000\ Nm$, see DFIG parameters at Table I. The reference torque oscillates between the applied value at the machine shaft for accelerating and decelerating the DFIG rotor within the speed range of the machine ($\pm 30\ \%$ of the synchronous speed). Simulation demonstrates the tracking capability of the controller as can be seen in figure 3. Additionally, the reactive power reference was moved from zero (unity power factor operation) to 2 MVAr, the controller is able to follow the reference almost instantaneously, see figure 4. Reactive power tracking is an important requirement for grid support, specially in case of contingencies.

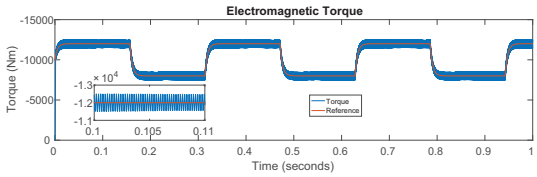

Fig. 3: Reference and real torque

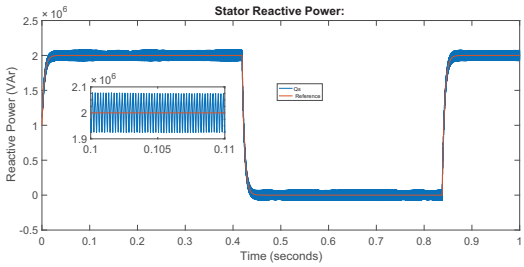

Fig. 4: Reference and real reactive power

The stator current and voltage of phase "a" of the simulated machine is displayed in figure 5, the units are in amperes and volts respectively. A zoom of the current from 0.4 to 0.5 s is also presented (figure 6) in order to see the distortion of the current due to the non-sinusoidal voltage of the rotor inverter. In that time interval, reactive power changes from 2 MVA to 0 MV, while the generator electromagnetic torque changes from 12000 to 8000 Nm, therefore current magnitude and phase angle between current and voltage are reduced.

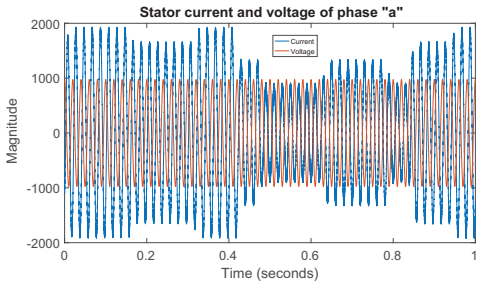

Fig. 5: Stator current and voltage of phase "a"

On the other hand, the switching frequency is regulated by the hysteresis loop as demonstrated by figure 7. The switching frequency is limited to the nominal value of the power inverter, $5000\ Hz$ (see [9]). A zoom of the switching state of leg "a" transistor proves that the desired frequency is ensured since there are 10 cycles in 0.002 seconds.

Simulation test presented in figures 3 and 4, where the operation point of reactive power and torque changes, is performed using the proposed approach (variable hysteresis value) to regulate commutation frequency. Then, a comparison between the classical approach (fixed hysteresis value) and

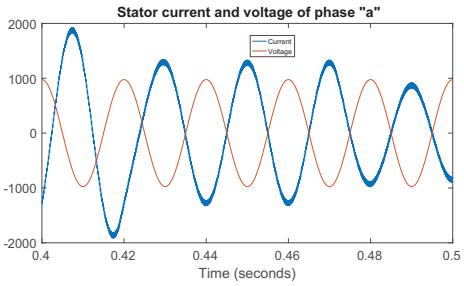

Fig. 6: Zoom of stator current and voltage of phase "a"

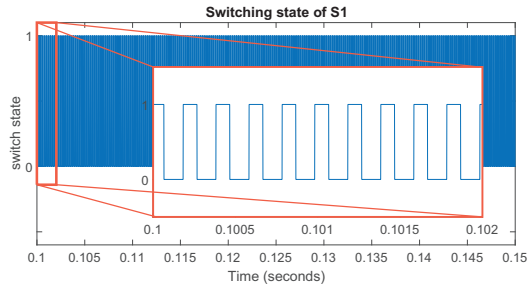

Fig. 7: Switching state of leg "a" of power inverter

the proposed variable hysteresis, at different operation points, is presented in figure 8. From 8(a), it can be observed that the switching frequency is maintained fixed at the desired value independently of the operation point. On the other hand, when a fixed hysteresis value is used, see figure 8(b), the switching frequency varies depending on the operation point of the generator since the switching frequency at 0.05 seconds is different to the switching frequency at 0.5 seconds.

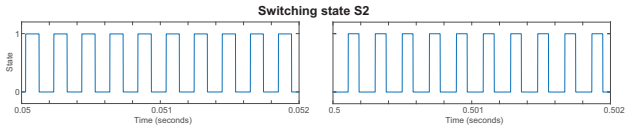

(a) Variable hysteresis

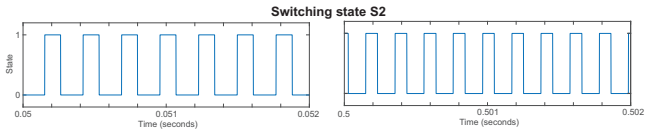

(b) Fixed hysteresis

Fig. 8: Switching state comparison between variable hysteresis-loop and fixed-value hysteresis loop

V. Conclusion

A rotor-side converter control based on stator-flux reference frame is presented. The proposal has the advantage of avoiding PWM algorithms by virtue of switching power electronic devices directly from a SMC algorithm.

The proposed SMC do not present infinite switching frequency thanks to a hysteresis loop, that ensures a desired switching frequency. The controller is applied separately to torque and reactive power loops since it is decoupled by means of a reference frame orientation. The direct axis rotor voltage controls the reactive power and the quadrature axis rotor voltage controls the active power. Furthermore, it is not necessary to known the system dynamics since the use of SMC makes possible to obtain the equivalent control of the system by means of a low pass filter for the voltages, v_{rd} or v_{rq}, relaxing the dependency of the systems parameters.

The methodology has been validated via simulations. The switching frequency is maintained within a limit which may ensure reliable operation of the power inverter. The main advantages of the proposed methodology compared with PWM-based algorithms are easy computation and independence of the system parameters.

VI. Further Work

This work presents a novel control proposal of a non-modulated strategy based on sliding mode control. Like DTC, control signals arise directly from the controller. The next step is to test the proposal in real-time simulations and proceed to hardware-in-the-loop implementation in order to validate the output controller's signals.

Acknowledgment

The authors would like to thank the support from grant 266632 "Bi-national Laboratory on Smart Sustainable Energy Management and Technology Training" from CONACYT.

References

[1] D. Connolly, H. Lund, and B. Mathiesen, "Smart energy Europe: The technical and economic impact of one potential 100% renewable energy scenario for the European Union," *Renewable and Sustainable Energy Reviews*, vol. 60, pp. 1634–1653, 2016.

[2] J. Aho, A. Buckspan, J. Laks, Y. Jeong, F. Dunne, and L. Pao, "Tutorial of wind turbine control for supporting grid frequency through active power control," in *Industrial Electronics, 1996. ISIE'96., Proceedings of the IEEE International Symposium on*. IEEE, 2012, pp. 3120–3131.

[3] V. Utkin, J. Guldner, and J. Shi, *Sliding Modes in Electromechanical Systems*, 2nd ed. USA: CRC Press, 2009.

[4] F. Ciccarelli and D. Lauria, "Sliding-mode control of bidirectional dc-dc converter for supercapacitor energy storage applications," in *SPEEDAM 2010*. IEEE, 2010, pp. 1119–1122.

[5] A. El Aroudi, B. Robert, and R. Leyva, "Sliding mode control of a high voltage dc-dc buck converter," in *Proceedings of the 2005 European Conference on Circuit Theory and Design, 2005.*, vol. 3. IEEE, 2005, pp. III–55.

[6] J. Hu, L. Shang, Y. He, and Z. Zhu, "Direct active and reactive power regulation of grid-connected dc/ac converters using sliding mode control approach," *IEEE transactions on power electronics*, vol. 26, no. 1, pp. 210–222, 2011.

[7] L. Shang and J. Hu, "Sliding-mode-based direct power control of grid-connected wind-turbine-driven doubly fed induction generators under unbalanced grid voltage conditions," *IEEE Transactions on Energy Conversion*, vol. 27, no. 2, pp. 362–373, 2012.

[8] M. I. Martinez, G. Tapia, A. Susperregui, and H. Camblong, "Sliding-mode control for DFIG rotor-and grid-side converters under unbalanced and harmonically distorted grid voltage," *IEEE Transactions on Energy Conversion*, vol. 27, no. 2, pp. 328–339, 2012.

[9] T. Green, J. Barria, A. J. Ferre, Y. Pipelzadeh, M. Merlin, and N. Bottrell., "Electrical models of new network technologies and devices including power electronics and supporting ICT infrastructures," The Institution of Engineering and Technology, Tech. Rep., March 2015.

[10] R. Venkataramanan, "Sliding mode control of power converters," Ph.D. dissertation, California Institute of Technology, 1986.
[11] A. Abrishamifar, A. Ahmad, and M. Mohamadian, "Fixed switching frequency sliding mode control for single-phase unipolar inverters," *IEEE Transactions on Power Electronics*, vol. 27, no. 5, pp. 2507–2514, 2012.
[12] B. Nicolas, M. Fadel, and Y. Chéron, "Fixed-frequency sliding mode control of a single-phase voltage source inverter with input filter," in *Industrial Electronics, 1996. ISIE'96., Proceedings of the IEEE International Symposium on*, vol. 1. IEEE, 1996, pp. 470–475.
[13] E. Fossas, R. Grinó, and D. Biel, "Quasi-sliding control based on pulse width modulation, zero averaged dynamics and the l2 norm," *Advances in Variable Structure System, Analysis, Integration and Applications*, pp. 335–344, 2001.
[14] B. Beltran, M. Benbouzid, and T. Ahmed-Ali, "High-order sliding mode control of a dfig-based wind turbine for power maximization and grid fault tolerance," in *Electric Machines and Drives Conference, 2009. IEMDC'09. IEEE International*. IEEE, 2009, pp. 183–189.
[15] S. N. Vukosavic, *Electrical machines*. Springer Science & Business Media, 2012.
[16] H. Lee and V. Utkin, "Chattering suppression methods in sliding mode control systems," *Annual Reviews in Control*, vol. 31, pp. 179–188, 2007.

4.3 Hysteresis width calculation in the frequency domain

Villanueva, I., Rosales, A., Ponce, P., & Molina, A. (2017). **Frequency domain characterization of statator-flux-oriented SMC for DFIG using Tsypkin's Method**. *Electrical Engineering, Computer Science and Automatic Control (CCE), 2017 IEEE International Conference on* (pp. ???-???). IEEE. **Accepted, unpublished.**

This paper has been accepted for presentation in the IEEE 14th International Conference on Electrical Engineering, Computing Science and Automatic Control (CCE 2017) in Mexico City.

As a continuation of the research work, a frequency domain characterization is done for the SMC proposed controller using Tsypkin's locus to calculate limit cycles and switching frequency of the power converter. The proposed methodology has the advantage of ensuring safe range of operation by using a static value of hysteresis, which ensures a desired maximum switching frequency without using extra sensors.

2017 14th International Conference on Electrical Engineering, Computing Science and Automatic Control (CCE)
Mexico City, Mexico. September 20-22, 2017

Frequency Domain Characterization of Stator-Flux-Oriented SMC for DFIG using Tsypkin's Method

Ivan Villanueva
Esc. de Ingenieria y Ciencias
Tecnologico de Monterrey
Mexico City, Mexico
A01212854@itesm.mx

Antonio Rosales
Esc. de Ingenieria y Ciencias
Tecnologico de Monterrey
Mexico City, Mexico
antonio.rosales@itesm.mx

Pedro Ponce
Esc. de Ingenieria y Ciencias
Tecnologico de Monterrey
Mexico City, Mexico
pedro.ponce@itesm.mx

Arturo Molina
Esc. de Ingenieria y Ciencias
Tecnologico de Monterrey
Mexico City, Mexico
armolina@itesm.mx

***Abstract*—Sliding Mode Control (SMC) has been successfully implemented in power converters applications since the discontinuous nature of the controller output allows direct switching of power electronic devices. However, due to physical limitations of power converter, the switching frequency must be maintained at low levels in order to prevent overheating and hazardous conditions of the semiconductors, therefore, hysteresis loops are typically included in the switching logic. In this work, a the Doubly Fed Induction Generator (DFIG) controlled by a stator flux oriented SMC is analyzed in the frequency domain using Tsypkin's method in order to obtain the hysteresis width that ensures a maximum switching frequency value covering all the operational conditions of the electric machine. The results are tested and evaluated by means of simulation studies of a DFIG controlled by a two level power converter.**

***Index Terms*—DFIG, Sliding Mode Control, frequency-domain analysis.**

I. Introduction

Doubly Fed Induction Generator (DFIG) is the most important electric machine used in wind generation, in onshore generation DFIG-based turbines cover about 50% of the new installed capacity in Europe and more than 70% in North America, Asia and the rest of the world [1]. The DFIG success lies in the reduced-size of power converter and excellent rotor speed control which covers a wide range of wind speed values.

It is well known that power converters of high-power applications require low switching frequency values for avoiding overheating of power electronic devices which may result in premature failures and hazardous conditions [2], [3]. Therefore hysteresis bands are typically implemented in direct control techniques, for example in hysteresis-band current PWM, Direct Torque Control (DTC), Direct Power Control (DPC) and Sliding Mode Control (SMC), however hysteresis widths are commonly selected based on trial and error procedures or other subjective methods.

SMC has been successfully implemented in control of DFIG with direct switching of power electronic devices, achieving good performance on torque and reactive power tracking with the main advantages of non-dependency on system parameters, fast dynamic response and robustness against external disturbances [4], [5]. Seen from a stator-flux-oriented reference frame, stator active and reactive power can be controlled independently by means of quadrature and direct axis rotor current components, unfortunately, due to the nature of power converters, the rotor voltage gain magnitude is variable in time depending on the vector selected by the controller and the reference frame orientation angle, which makes difficult to maintain switching frequency at a constant value. Common solutions for switching frequency regulation include carrier based modulation to force the switching frequency at a determined value [6], [7], closed loop control to regulate hysteresis width [8], [9], space vector modulation inclusion [10] and measuring system variables to calculate hysteresis width [11], [12]. All those solutions require additional signal acquisition and processing or sacrificing direct switching by including modulation which directly affects the simplicity of hysteresis-based relay control systems.

In this work, SMC is used to control direct and quadrature rotor current, which are directly related with stator reactive and active power (or electromagnetic torque) respectively. Tsypkin's method [13] is used to determine the oscillation of the limit cycle of the relay control system which is used to calculate the commutation frequency of the power converter ensuring safe operational range of switching frequencies during all the operational zones of the electric machine. The proposed solution do not require additional sensors giving a well-founded selection of the hysteresis width of the control system.

II. Dynamic Modeling of DFIG in Stator Flux Reference Frame

DFIG is a special type of wound rotor induction machine with the stator directly connected to the electrical grid while the rotor is fed through a back-to-back power converter. DFIG-based wind turbines use a transmission system in order to increase the shaft speed, the electric generators are high speed machines typically up to 6 poles. In Figure 1 the basic scheme of the DFIG is displayed, since the voltage levels of the stator

978-1-5386-3406-6/17/$31.00

and rotor are normally different, a three winding transformer is used to couple the DFIG with the electric grid.

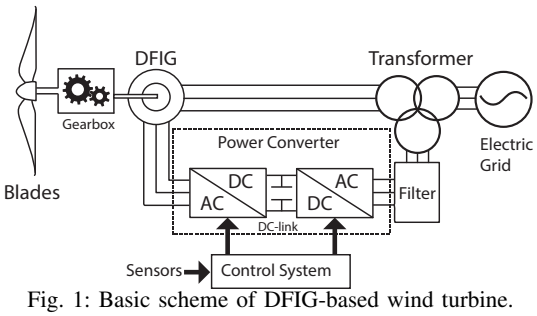

Fig. 1: Basic scheme of DFIG-based wind turbine.

Equations (1) to (8) summarize the dynamic model of the electric machine seen from a synchronous speed (ω_s) rotating reference frame. The model does not consider neither saturation of the ferromagnetic core nor machine parameter changes due to temperature variation [14]:

$$v_{sd} = R_s i_{sd} + \frac{d\lambda_{sd}}{dt} - \omega_s \lambda_{sq} \tag{1}$$

$$v_{sq} = R_s i_{sq} + \frac{d\lambda_{sq}}{dt} + \omega_s \lambda_{sd} \tag{2}$$

$$v_{rd} = R_r i_{rd} + \frac{d\lambda_{rd}}{dt} - \omega_r \lambda_{rq} \tag{3}$$

$$v_{qr} = R_r i_{rq} + \frac{d\lambda_{rq}}{dt} + \omega_r \lambda_{rd} \tag{4}$$

$$\lambda_{sd} = L_s i_{sd} + L_m i_{rd} \tag{5}$$

$$\lambda_{sq} = L_s i_{sq} + L_m i_{rq} \tag{6}$$

$$\lambda_{rd} = L_r i_{rd} + L_m i_s d \tag{7}$$

$$\lambda_{rq} = L_r i_{rq} + L_m i_s q \tag{8}$$

where $\omega_r = \omega_s - \omega_m$ is the synchronous speed minus the mechanical speed, λ is the magnetic flux and the subscripts $_s$ and $_r$ mean stator and rotor quantities respectively while $_d$ and $_q$ are the corresponding component in the $d-q$ reference frame.

The electromagnetic torque produced by the interaction between magnetic flux and current can be expressed as:

$$\tau_e = \frac{3}{2} P \frac{L_m}{L_s} \operatorname{Im}(\lambda_{sq} i_{rd} - \lambda_{sd} i_{rq}) \tag{9}$$

where P is the number of pole pairs. A simple mechanical model which does not consider shaft torsion and is seen at the electric machine shaft can be modeled with the following equation:

$$\tau_e - \tau_{load} - k_{fl}\omega_m = J\frac{d\omega_m}{dt} \tag{10}$$

where J is the equivalent inertia at the electric machine shaft and k_{fl} is a constant term related with friction loses.

From Equations (1) to (8) it is possible to obtain a state-space representation of the current magnitudes (for further details see [14]):

$$\dot{x} = Ax + Bu; \quad y = Cx \tag{11}$$

where $x = [i_{sd}\ i_{sq}\ i_{rd}\ i_{rq}]^T$, $u = [v_{sd}\ v_{sq}\ v_{rd}\ v_{rq}]^T$

$$A = \left(\frac{1}{\sigma L_s L_r}\right) \begin{bmatrix} -R_s L_r & \omega_m L_m^2 + \omega_s \sigma L_s L_r & R_r L_m & \omega_m L_m L_r \\ -\omega_m L_m^2 - \omega_s \sigma L_s L_r & -R_s L_r & -\omega_m L_m L_r & R_r L_m \\ R_s L_m & -\omega_m L_s L_m & -R_r L_s & -\omega_m L_r L_s + \omega_s \sigma L_s L_r \\ \omega_m L_s L_m & R_s L_m & \omega_m L_r L_s - \omega_s \sigma L_s L_r & -R_r L_s \end{bmatrix}$$

$$B = \left(\frac{1}{\sigma L_s L_r}\right) \begin{bmatrix} L_r & 0 & -L_m & 0 \\ 0 & L_r & 0 & -L_m \\ -L_m & 0 & L_s & 0 \\ 0 & -L_m & 0 & L_s \end{bmatrix}$$

$$C = \begin{bmatrix} 0 & 0 & 1 & 0 \\ 0 & 0 & 0 & 1 \end{bmatrix}$$

where $\sigma = 1 - L_m^2/(L_s L_r)$, commonly known as leakage coefficient. The typical power loses due to mechanical components of a wind turbine are about 0.035 pu at maximum rotational speed [15].

Singular perturbation methods have been applied to analyse time-scale properties in nonlinear systems [16] and wind turbines [17]. The condition for decoupling a system in different time scales is $\epsilon = \tau_{el}/\tau_{mec} << 1$ [17], where ϵ is a dimensionless parameter, τ_{el} and τ_{mec}, are the electrical and mechanical time constants, respectively. Then, the wind turbine analysed in this paper with parameters $k_{fl} = \frac{0.035*2e^6 W}{(1.3*157\ rad/s)^2} = 1.6804\ N \cdot m \cdot s$, inertia $J = 30\ kg \cdot m^2$, $\tau_{mec} = J/k_{fl} = 17.8528\ s$, and $\tau_{el} = L_s/R_s = 0.9923\ s$ [14], can be considered as a decoupled system since $\epsilon = 0.055 << 1$.

From the state space representation (Equation (11)) we can see that the system nonlinearity is due to the mechanical speed present in matrix A, taking advantage of the two-time-scales property, the system can be linearized at different points considering that the operational range of the generator speed is $\pm 30\%$ of the synchronous speed. The transfer function matrix can be obtained using the following equation:

$$G(s) = C(sI - A)^{-1}B + D \tag{12}$$

where I is a 4×4 identity matrix and s is the complex frequency variable. The diagonal components of the $G(s)$ matrix are:

$$H(s) = \frac{I_{rd}(s)}{V_{rd}(s)} = \frac{I_{rq}(s)}{V_{rq}(s)} = \frac{a_3 s^3 + a_2 s^2 + a_1 s + a_0}{d_4 s^4 + d_3 s^3 + d_2 s^2 + d_1 s + d_0} \tag{13}$$

with the following coefficients:

$a_3 = -L_m L_r^3 L_s^3 \sigma^3$; $a_2 = -L_m R_s L_r^3 L_s^2 \sigma^2 - L_m R_r L_r^2 L_s^3 \sigma^2$;

$a_1 = -L_m^5 L_r L_s \omega_m^2 \sigma + 2L_m^3 L_r^2 L_s^2 \omega_m^2 \sigma - 2L_m^3 L_r^2 L_s^2 \omega_m \omega_s \sigma^2 + R_r R_s L_m^3 L_r L_s \sigma - L_m L_r^3 L_s^3 \omega_m^2 \sigma + 2L_m L_r^3 L_s^3 \omega_m \omega_s \sigma^2 - L_m L_r^3 L_s^3 \omega_s^2 \sigma^3 - R_r R_s L_m L_r^2 L_s^2 \sigma$;

$a_0 = -R_s L_m^5 L_r \omega_m^2 + 2R_s L_m^3 L_r^2 L_s \omega_m^2 - 2R_s L_m^3 L_r^2 L_s \omega_m \omega_s \sigma - R_r L_m^3 L_r L^2 \omega_m \omega_s \sigma - R_s L_m L_r^3 L_s^2 \omega_m^2 + 2R_s L_m L_r^3 L_s^2 \omega_m \omega_s \sigma - R_s L_m L_r^3 L_s^2 \omega_s^2 \sigma^2 + R_r L_m L_r^2 L_s^3 \omega_m \omega_s \sigma - R_r L_m L_r^2 L_s^3 \omega_s^2 \sigma^2$;

$d_4 = L_r^4 L_s^4 \sigma^4$; $d_3 = 2R_s L_r^4 L_s^3 \sigma^3 + 2R_r L_r^3 L_s^4 \sigma^3$

$d_2 = L_m^4 L_r^2 L_s^2 \omega_m^2 \sigma^2 - 2L_m^2 L_r^3 L_s^3 \omega_m^2 \sigma^2 + 2L_m^2 L_r^3 L_s^3 \omega_m \omega_s \sigma^3 - 2L_m^2 L_r^2 L_s^2 R_r R_s \sigma^2 + L_r^4 L^4 \omega_m^2 \sigma^2 - 2L_r^4 L - s^4 \omega_m \omega_s \sigma^3 + 2L_r^4 L_s^4 \omega_s^2 \sigma^4 + L_r^4 L_s^2 R_s^2 \sigma^2 + 4L_r^3 L_s^3 R_r R_s \sigma^2 + L_r^2 L_s^4 R_r^2 \sigma^2)$

$d_1 = 2L_m^4 L_r^2 L_s R_s \omega_m^2 \sigma - 4L_m^2 L_r^3 L_s^2 R_s \omega_m^2 \sigma + 4L_m^2 L_r^3 L_s^2 R_s \omega_m \omega_s \sigma^2 - 2L_m^2 L_r^2 L_s R_r R_s^2 \sigma - 2L_m^2 L_r L_s^2 R_r^2 R_s \sigma + 2L_r^4 L_s^3 R_s \omega_m^2 \sigma - 4L_r^4 L_s^3 R_s \omega_m \omega_s \sigma^2 +$

$2L_r^4L_s^3R_s\omega_s^2\sigma^3 + 2L_r^3L_s^4R_r\omega_s^2\sigma^3 + 2L_r^3L_s^2R_rR_s^2\sigma + 2L_r^2L_s^3R_r^2R_s\sigma)$

$d_0 = L_m^4L_r^2L_s^2\omega_m^2\omega_s^2\sigma^2 + L_m^4L_r^2R_s^2\omega_m^2 + 2L_m^4L_rL_sR_rR_s\omega_m\omega_s\sigma + L_m^4R_r^2R_s^2 - 2L_m^2L_r^3L_s^3\omega_m^2\omega_s^2\sigma^2 + 2L_m^2L_r^3L_s^2\omega_m\omega_s^3\sigma^3 - 2L_m^2L_r^2L_s^3R_s\omega_m^2\omega_s^2 + 2L_m^2L_r^3L_s^2R_s\omega_m\omega_s\sigma - 2L_m^2L_r^2L_s^3R_rR_s\omega_m\omega_s\sigma + 2L_m^2L_r^2L_s^2R_rR_s\omega_s^2\sigma^2 - 2L_m^2L_rL_s^2R_r^2R_s^2 + L_r^4L_s^4\omega_m^2\omega_s^2\sigma^2 - 2L_r^4L_s^4\omega_m\omega_s^3\sigma^3 + L_r^4L_s^4\omega_s^4\sigma^4 + L_r^4L_s^2R_s^2\omega_m^2 - 2L_r^4L_s^3R_s^2\omega_m\omega_s\sigma + L_r^4L_s^2R_s^2\omega_s^2\sigma^2 + L_r^2L_s^4R_r^2\omega_s^2\sigma^2 + L_r^2L_s^3R_r^2R_s^2$

III. Sliding Mode Control Design

A commonly used method for decoupling active and reactive power is reference frame orientation, in case of DFIG, the stator flux orientation allows independent stator active and reactive power control by means of rotor current regulation. If the voltage drop due to the stator resistance is neglected, the stator voltage phasor lead the stator flux phasor by 90 degrees ($\lambda_{sq} = 0$ and $v_{sd} = 0$), therefore is easy to see that the active and reactive power can be controlled independently by q and d components of the rotor current respectively:

$$\tau_e = \frac{3PL_m}{2L_s}(\cancelto{0}{i_{rd}\lambda_{sq}} - i_{rq}\lambda_{sd}) = \frac{-3PL_m}{2L_s}(\lambda_{sd}\boldsymbol{i_{rq}}) \quad (14)$$

$$P_s = \frac{3}{2}(\cancelto{0}{v_{sd}i_{sd}} + v_{sq}i_{sq}) = \frac{-3L_m}{2L_s}(v_{sq}\boldsymbol{i_{rq}}) \quad (15)$$

$$\begin{aligned} Q_s &= \frac{3L_m}{2L_s}(\cancelto{0}{v_{sd}i_{rq}} - v_{sq}i_{rd}) + \frac{3}{2L_s}(\lambda_{sd}v_{sq} - \cancelto{0}{\lambda_{sq}v_{sd}}) \\ &= \frac{-3L_m}{2L_s}(v_{sq}\boldsymbol{i_{rd}}) + \frac{3}{2L_s}(\lambda_{sd}v_{sq}) \end{aligned} \quad (16)$$

The active power or torque can be controlled by the quadrature axis rotor current, while the reactive power can be controlled by the direct axis rotor current. In order to regulate the rotor current, the following sliding surfaces are selected:

$$S_{i_{rd}} = i_{rd} - i_{rd}^*; \quad S_{i_{rq}} = i_{rq} - i_{rq}^* \quad (17)$$

Considering that the rotor reference current (i_{rd}^* and i_{rd}^*) is much slower than the dynamics of the current, the dynamics of the sliding surfaces are:

$$\dot{S_{i_{rd}}} = \frac{di_{rd}}{dt} - \cancelto{0}{\frac{di_{rd}^*}{dt}} = \frac{1}{L_r'}(v_{rd} - R_ri_{rd} - \cancelto{0}{\frac{L_m}{L_s}\frac{d\lambda_{sd}}{dt}} + \omega_rL_r'i_{rq}) \quad (18)$$

$$\dot{S_{i_{rq}}} = \frac{di_{rq}}{dt} - \cancelto{0}{\frac{di_{rq}^*}{dt}} = \frac{1}{L_r'}(v_{rq} - R_ri_{rq} - \frac{L_m}{L_s}\omega_r\lambda_{sd} - \omega_rL_r'i_{rd}) \quad (19)$$

where $L_r' = \sigma L_r$.

Representing Equations (18) and (19) in matrix form:

$$\begin{bmatrix}\dot{S_{i_{rd}}} \\ \dot{S_{i_{rq}}}\end{bmatrix} = \overbrace{\frac{1}{L_r'}\begin{bmatrix}-R_ri_{rd} + \omega_rL_r'i_{rq} \\ -R_ri_{rq} - \frac{L_m}{L_s}\omega_r\lambda_{sd} - \omega_rL_r'i_{rd}\end{bmatrix}}^{F_S} + \underbrace{\begin{bmatrix}1/L_r' & 0 \\ 0 & 1/L_r'\end{bmatrix}}_{d_S}\begin{bmatrix}v_{rd} \\ v_{rq}\end{bmatrix} \quad (20)$$

Since the control signals (v_{rd} and v_{rq}) appear in the first derivative of the sliding surface, the relative degree of the system is one, therefore, it is possible to achieve finite time convergence to the sliding surface and robustness against parameters variations and system disturbances using the controllers:

$$\begin{bmatrix}v_{rd} \\ v_{rq}\end{bmatrix} = \begin{bmatrix}-M_d\,\mathrm{sign}(S_{i_{rd}}) \\ -M_q\,\mathrm{sign}(S_{i_{rq}})\end{bmatrix} \quad (21)$$

where the gains $M_{d,q}$ are computed as $M_{d,q} > |F_M|/|d_M|$, considering Equation (20) with the bounds $F_s = F_M$ and $d_s = D_M$, [18].

SMC in Equation (21) cannot be directly applied to the power converter, a relationship between dq and abc quantities is necessary. The relation $dq - abc$ is established considering the output rotor phase voltage in Equation (22) seen from the neutral point of the rotor (see Figure 2):

$$\begin{bmatrix}V_{an} \\ V_{bn} \\ V_{cn}\end{bmatrix} = \overbrace{\frac{V_{DC}}{3}\begin{bmatrix}2 & -1 & -1 \\ -1 & 2 & -1 \\ -1 & -1 & 2\end{bmatrix}}^{C}\overbrace{\begin{bmatrix}Sw_1 \\ Sw_2 \\ Sw_3\end{bmatrix}}^{Sw_{1,2,3}} \quad (22)$$

where V_{DC} is the DC-link voltage, Sw_1, Sw_2 and Sw_3 are the switch states of each leg of the rotor-side power converter (zero or one); and the Park transform in Equation (23):

$$\begin{bmatrix}v_{rd} \\ v_{rq}\end{bmatrix} = \overbrace{\begin{bmatrix}\cos\theta_d & -\sin\theta_d \\ \sin\theta_d & \cos\theta_d\end{bmatrix}\frac{2}{3}\begin{bmatrix}1 & -1/2 & -1/2 \\ 0 & \sqrt{3}/2 & -\sqrt{3}/2\end{bmatrix}}^{T}\begin{bmatrix}V_{an} \\ V_{bn} \\ V_{cn}\end{bmatrix} \quad (23)$$

where θ_d is the angle of the direct axis orientation ($\theta_d = \theta_{mec} - \theta_{sf}$).

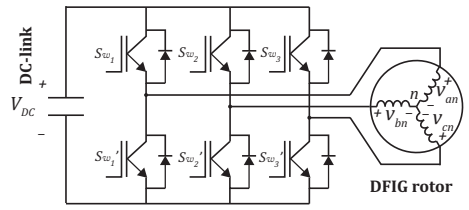

Fig. 2: Two level inverter connected to the rotor

Then, the $dq - abc$ relation is:

$$\begin{bmatrix}S_{i_{rd}} \\ S_{i_{rq}}\end{bmatrix} = \overbrace{-d_STC}^{D}\begin{bmatrix}S_a \\ S_b \\ S_c\end{bmatrix} \quad (24)$$

Since the resulting matrix D is not square, the Moore-Penrose pseudoinverse is used to calculate the relationship between abc and dq quantities, [4]:

$$D^+ = D^T(DD^T)^{-1} \quad (25)$$

$$\overbrace{\begin{bmatrix}S_a \\ S_b \\ S_c\end{bmatrix}}^{S_{a,b,c}} = \underbrace{-\frac{L_r'}{V_{DC}}\begin{bmatrix}\cos(\theta_d) & \sin(\theta_d) \\ \cos(\theta_d + \frac{2\pi}{3}) & \sin(\theta_d + \frac{2\pi}{3}) \\ \cos(\theta_d - \frac{2\pi}{3}) & \sin(\theta_d - \frac{2\pi}{3})\end{bmatrix}}_{D^+}\begin{bmatrix}S_{i_{rd}} \\ S_{i_{rq}}\end{bmatrix} \quad (26)$$

TABLE I: SMC switching vectors

$S_{i_{rd}}$	$S_{i_{rq}}$	D Sector	Q Sector
+	+	$sector-2$	$sector+2$
	−	$sector+2$	$sector+1$
−	+	$sector-1$	$sector-2$
	−	$sector+1$	$sector-1$

The controller scheme is displayed in Figure 3, the control system consist on the transformation matrix D^+ and an offset sign function at the output in order to send the pulses to the rotor-side converter where the state 1 means that the upper leg of the inverter is on while 0 means that the lower leg of the inverter is on. A hysteresis loop is added in the current regulation to reduce the theoretically infinite switching frequency of an ideal sign function, the design of hysteresis is provided in section IV.

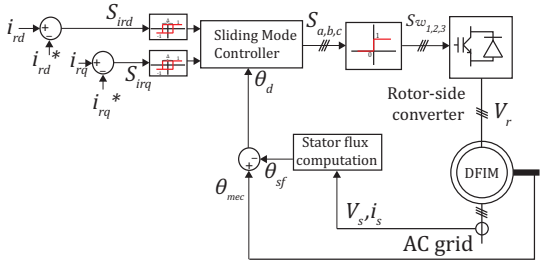

Fig. 3: Sliding mode control block diagram

The output of the SMC block of figure 3 is limited by the number of vectors of the two level inverter, therefore it is easy to implement the proposed control scheme using a table, like the controllers used in the industry as DTC and DPC. The resulting control system has 12 sectors which are required to avoid full orientation of a voltage vector in neither the reference frame direct axis direction nor the quadrature axis direction. The resulting sectors are shown in Figure 4 which are divided in six D and six Q sectors for convenience, then the voltage vectors summarized in Table I are injected to the electric machine rotor in order to regulate the rotor current. When the rotor is rotating at super-synchronous speed, θ_d rotates in clockwise direction.

Despite the operation principle of the SMC is very simple, the rotor voltage seen from the stator flux reference frame is variable and depends on the orientation angle θ_d and the inverter voltage vector as described by Equations (23) and (22). As shown in Figure 5 when the angle lies in a Q vector, v_q has a low gain (between 0.4713 and 0.1725) and v_d has a high gain (between 0.6440 and 0.4713) when the angle lies in a D vector, the opposite happens.

The design of the proposed SMC is summarized as follows: (a) Chose sliding mode surfaces in Equation (17); (b) Select the control gains using Equation (21); and (c) Compute the inverter inputs $S_{a,b,c}$ with the transformation in Equation (26) and the switching vectors described in Table I.

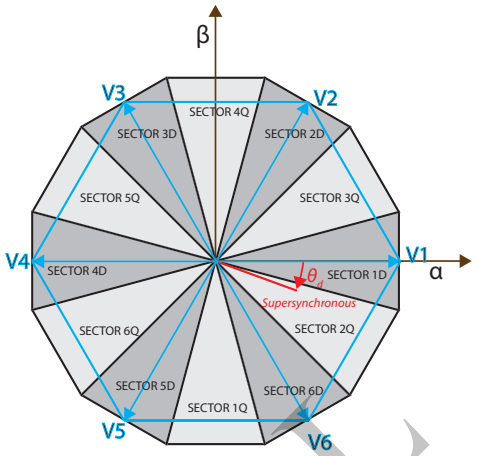

Fig. 4: 12 sectors of SMC

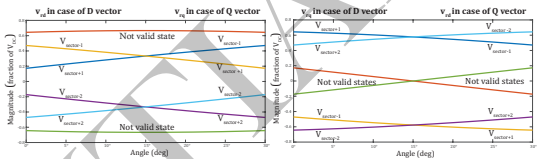

Fig. 5: Variable rotor voltage gain seen from the stator flux reference frame: a) low gain, b) high gain.

IV. Frequency Domain Characterization

Sinusoidal input Describing Function (DF) is an useful method to identify limit cycles (oscillations) in non-linear systems, where a segmentation of the system in a linear part L and a non-linear part is possible [19], see Figure 6. Low-pass filter characteristic of linear part L is the main assumption to apply DF since it is a first harmonic approximation of the non-linear part [19]. On the other hand, the theoretically exact Tsypkin's method provides more accurate identification of limit cycles in non-linear systems because it considers all the harmonics for quasi-linearization of the non-linearity, see [13] and [19].

Another important difference between DF and Tsypkin's method lies in the analysis of relay control systems where the linear part is relative degree 1. DF function analysis of hysteresis can not identify limit cycles in systems with relative 1 while Tsypkin's method analysis can do it, see [19]. The dynamics of DFIG analysed in this work are represented by a transfer function of relative degree one (see Figure 7), then it is necessary to apply Tsypkin's method in order to estimate the switching frequency.

Tsypkin's Method allows to determine the frequency of a limit cycle to any desired accuracy depending on the number of harmonics considered. The Tsypkin's locus is defined as [19]:

$$T(j\omega) = \sum_{k\ odd}^{\infty} \mathrm{Re}[L_1(jk\omega)] + j \sum_{kodd}^{\infty} \frac{1}{k} \mathrm{Im}[L_1(jk\omega)] \quad (27)$$

a limit cycle oscillating at a frequency ω_0 is predicted if the

TABLE II: Electric machine parameters used in simulation

Nominal power $= 2\ MW$
Nominal voltage $= 690\ Vrms$
Poles $= 4$
Nominal Frequency $= 50Hz$
$R_s = 2.6 \times 10^{-3}\ \Omega$
$R_r = 2.9 \times 10^{-3}\ \Omega$
$L_s = 2.58 \times 10^{-3}\ H$
$L_r = 2.58 \times 10^{-3}\ H$
$L_m = 2.5 \times 10^{-3}\ H$
DC-link voltage $= 400\ V$

following conditions are met:

$$\mathrm{Im}[T(j\omega_0)] = \frac{\pi}{4}\left[L(\infty) - \frac{\delta_h}{M}\right] \tag{28}$$

$$\mathrm{Re}[T(j\omega_0)] < \frac{\pi}{4\omega_0}\lim_{s\to\infty}[sL_1(s)] \tag{29}$$

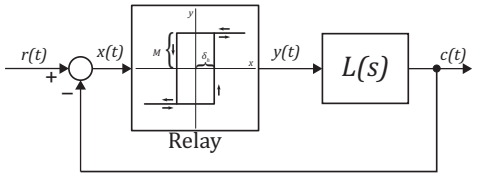

Fig. 6: Closed loop relay-based control system

The parameters shown in Table II are substituted in Equation (13) for different values of ω_m, considering that the operational speed of the DFIG is $\pm 30\%$ of the synchronous speed (314 rad/s). Then the Nyquist diagram was plotted (Figure 7), at very high switching frequencies the phase shift of the system is -90 degrees, therefore using DF will predict no oscillation. On the other hand, since the closed loop transfer function has all its poles in the left half-plane, the system is stable and can be analyzed using Tsypkin's method. At high switching frequencies, the Tsypkin locus of the different ω_m values are seen as superimposed lines (see Figure 8), therefore it is concluded that the rotor speed has a minimum influence in the switching frequency of the rotor-side power converter. In Figure 8 is displayed the graphical solution using Tsypkin locus for a mechanical speed of 220 rad/s, considering up to the 100^{th} harmonic. Since condition of Equation (29) is met, the ratio δ_h/M can be calculated for different values of switching frequencies, in this case, the frequencies were selected from 1000 to 5000 Hz in 1000 Hz increments.

V. Results

A DFIG with the characteristics shown in Table II was simulated, the rotor-stator turns ratio is considered to be 1. A constant mechanical torque or 10000 $N \cdot m$ is simulated at the shaft and the equivalent inertia of the machine $J = 30\ kg{\cdot}m^2$.

From the results reported in figure 8, considering that the maximum allowable switching frequency of the power converter is 3000 Hz, the ratio $\frac{\delta_h}{M} = \frac{4(0.4125)}{\pi} = 0.5252$, since the maximum gain M of the controller is 0.644 V_{DC} the hysteresis value that will ensure maximum switching frequency

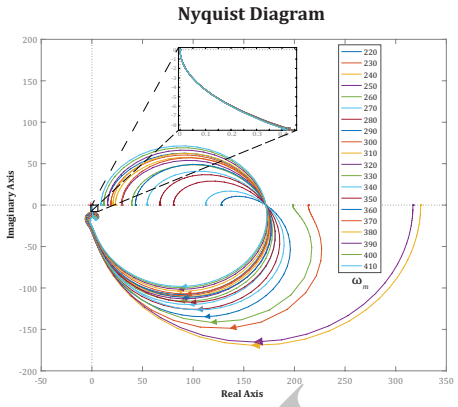

Fig. 7: Nyquist plot at different mechanical speeds

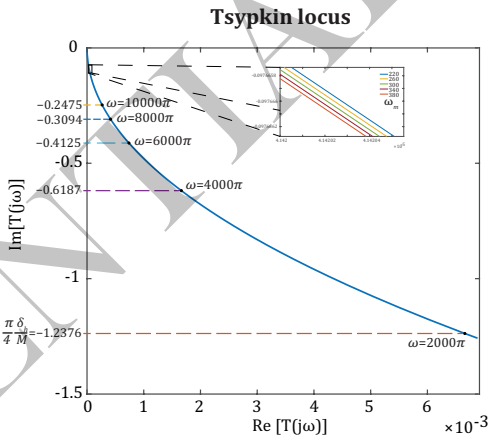

Fig. 8: Graphical limit cycle solution at different frequencies

of 3000 Hz is $\delta_h = (0.5252)(0.644)(400) = 135.29$. Using the same logic, the hysteresis values for different maximum desired switching frequencies are presented in Table III.

In Figure 9 is displayed the regulation of current with a fixed hysteresis band of $\Delta = 2\delta_h = 270.58$, as can be seen in the current error. The current regulation correspond to acceleration and deceleration of the electric machine rotor and reactive power injection or unity power factor operation of the stator.

Depending on the sector in which the controller lies, the current regulator will have low switching frequency or high switching zones, as displayed in Figure 10, in Q sectors the switching frequency of d component of rotor current is high because it has high voltage gain. The switching frequency average is close to 2600 Hz while for the low gain zone, the

TABLE III: Hysteresis width for a desired maximum switching frequency

f_{sw}, max	δ_h
1000 Hz	405.92
2000 Hz	202.925
3000 Hz	135.29
4000 Hz	101.48
5000 Hz	81.18

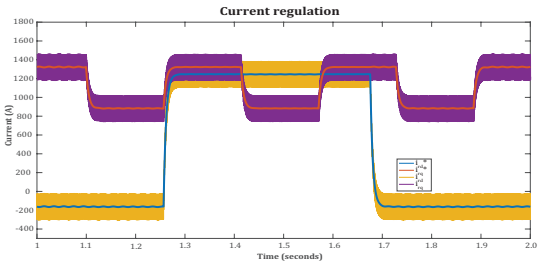

Fig. 9: Rotor dq current regulation

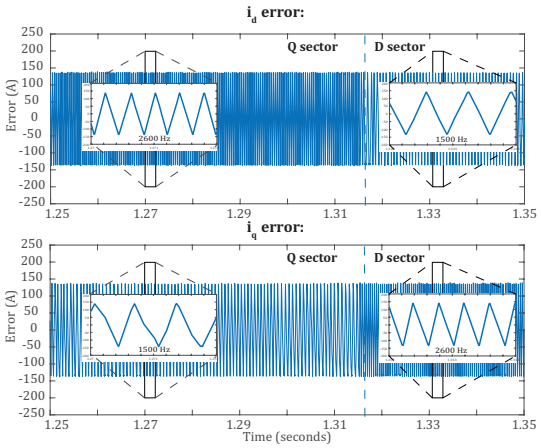

Fig. 10: Sliding surfaces $S_{i_{rd}}$ and $S_{i_{rq}}$

switching frequency is reduced to approximately $1500\ Hz$.

VI. Conclusion

A simple stator-flux-oriented SMC is presented and characterized in the frequency domain, the controller has the main advantages of non-parameter dependence, direct switching of power converter without modulation and simple structure. The controller is oriented in the stator flux direction for decoupling active and reactive power, comparator outputs are send to the sliding mode controller which can operate either as a transformation matrix or a table which dictates the switching state of the rotor-side converter.

A hysteresis loop is included in the current regulator in order to reduce the switching frequency of the power converter. The hysteresis width is calculated by means of limit cycle estimation using Tsypkin's method. The proposed methodology gives a guide to select the hysteresis width based on the maximum allowable switching frequency. The methodology could be used for hysteresis selection in other popular direct control techniques like DTC and DPC.

The Tsypkin's Locus demonstrate that the mechanical speed of the rotor is not significant in the switching frequency of the system. However, due to the nature of power converter and reference frame orientation the voltage gain of the SMC has variable magnitude, which makes difficult to maintain the switching frequency constant, therefore the larger voltage gain value is selected in order to ensure a desired maximum switching frequency.

This work presents a recent control proposal of a non-modulated strategy based on sliding mode control limited by a hysteresis band which up to now has only been tested via simulations. The next step is to test the proposal in real-time implementation and corroborate the results reported in this work.

Acknowledgment

The authors would like to thank the support from grant 266632 "Bi-national Laboratory on Smart Sustainable Energy Management and Technology Training" from CONACYT.

References

[1] C. V. Hernández, T. Telsnig, and A. V. Pradas, "JRC wind energy status report 2016 edition," 2017.

[2] F. Blaabjerg, M. Liserre, and K. Ma, "Power electronics converters for wind turbine systems," *IEEE Transactions on Industry Applications*, vol. 48, no. 2, pp. 708–719, 2012.

[3] S. Yang, A. Bryant, P. Mawby, D. Xiang, L. Ran, and P. Tavner, "An industry-based survey of reliability in power electronic converters," *IEEE Transactions on Industry Applications*, vol. 47, no. 3, pp. 1441–1451, 2011.

[4] M. I. Martinez, G. Tapia, A. Susperregui, and H. Camblong, "Sliding-mode control for DFIG rotor-and grid-side converters under unbalanced and harmonically distorted grid voltage," *IEEE Transactions on Energy Conversion*, vol. 27, no. 2, pp. 328–339, 2012.

[5] I. Villanueva, A. Rosales, P. Ponce, and A. Molina, "Stator-flux-oriented sliding mode controller for DFIG with variable hysteresis loop for limiting switch frequency of rotor-side power converter," in *Industrial Technology (ICIT), 2017 IEEE International Conference on*. IEEE, 2017, pp. 213–218.

[6] R. Gupta and A. Ghosh, "Frequency-domain characterization of sliding mode control of an inverter used in DSTATCOM application," *IEEE Transactions on Circuits and Systems I: Regular Papers*, vol. 53, no. 3, pp. 662–676, 2006.

[7] B. Kang and C. Liaw, "Robust hysteresis current-controlled PWM scheme with fixed switching frequency," *IEE Proceedings-Electric Power Applications*, vol. 148, no. 6, pp. 503–512, 2001.

[8] V. Repecho, D. Biel, and E. Fossas, "Fixed switching frequency sliding mode control using an hysteresis band controller," in *Variable Structure Systems (VSS), 2014 13th International Workshop on*. IEEE, 2014, pp. 1–6.

[9] V. Repecho, D. Biel, J. M. Olm, and E. F. Colet, "Switching frequency regulation in sliding mode control by a hysteresis band controller," *IEEE Transactions on Power Electronics*, vol. 32, no. 2, pp. 1557–1569, 2017.

[10] J. Hu, H. Nian, B. Hu, Y. He, and Z. Zhu, "Direct active and reactive power regulation of DFIG using sliding-mode control approach," *IEEE Transactions on energy conversion*, vol. 25, no. 4, pp. 1028–1039, 2010.

[11] B. K. Bose, "An adaptive hysteresis-band current control technique of a voltage-fed PWM inverter for machine drive system," *IEEE Transactions on industrial electronics*, vol. 37, no. 5, pp. 402–408, 1990.

[12] H. Lee and V. I. Utkin, "Chattering suppression methods in sliding mode control systems," *Annual reviews in control*, vol. 31, no. 2, pp. 179–188, 2007.

[13] I. Z. TSypkin, *Relay control systems*. CUP Archive, 1984.

[14] G. Abad, J. Lopez, M. Rodríguez, L. Marroyo, and G. Iwanski, *Doubly fed induction machine: modeling and control for wind energy generation*. John Wiley & Sons, 2011, vol. 85.

[15] M. G. Simões, F. A. Farret, and F. Blaabjerg, "Small wind energy systems," *Electric Power Components and Systems*, vol. 43, no. 12, pp. 1388–1405, 2015.

[16] H. K. Khalil, "Noninear systems," *Prentice-Hall, New Jersey*, vol. 2, no. 5, pp. 5–1, 1996.

[17] H. M. Nguyen and D. S. Naidu, "Time scale analysis and control of wind energy conversion systems," in *Resilient Control Systems (ISRCS), 2012 5th International Symposium on*. IEEE, 2012, pp. 149–154.

[18] V. Utkin, J. Guldner, and J. Shi, *Sliding mode control in electro-mechanical systems*. CRC press, 2009, vol. 34.

[19] W. E. Vander Velde, *Multiple-input describing functions and nonlinear system design*. McGraw-Hill, New York, 1968.

4.4 Sliding mode control for DFIG

Villanueva, I., Rosales, A., Ponce, P., & Molina, A. (2017). **Stator Flux Oriented Sliding Mode Control for Doubly Fed Induction Generator**. In *Adaptive Robust Control and its Application*. InTech. **Chapter accepted, unpublished.**

This work has been accepted for publication in the Intech open book "Robust control and its Applications" to be published on January 2018.

The article presents the proposed controller and the frequency domain characterization, the system is tested under a real wind profile obtained from [74].

Stator Flux Oriented Sliding Mode Control for Doubly Fed Induction Generator

Ivan Villanueva, ivan.villanueva@itesm.mx

Antonio Rosales

Pedro Ponce

Arturo Molina

Tecnologico de Monterrey, Mexico

Abstract: Doubly fed induction generator (DFIG) is the most implemented electric machine in wind energy conversion systems (WECS) due to reduced size converter, active and reactive power control and economic factors. However, the power electronic stage needs an accurate controller that allows to follow the stator power regulation despite the presence of disturbances. On the other hand, Sliding-Mode Control (SMC) offers a fast-dynamic response and provides insensitivity to matched and bounded disturbance/uncertainties, and its natural discontinuous control signals can be used for direct switching of power electronic devices. Switching frequency must be maintained inside acceptable values to avoid exceeding the maximum admissible switching frequency of semiconductors. The contribution of this chapter is a stator-flux- oriented SMC with a hysteresis band that limits the switching frequency of power electronic devices to a set value. Furthermore, the proposed SMC ensure robustness against bounded low voltage grid faults. Unlike other non-modulated techniques like direct torque control (DTC) there is not necessity of modifying the controller structure for withstanding low depth voltage dips. The controller injects negative sequence voltage/currents to compensate the unbalanced conditions. The advantages of the proposed SMC control are validated via simulations.

Keywords: Doubly-Fed Induction Generator, Sliding Mode Control.

Nomenclature

v	Voltage [V]
i	Current [A]
λ	Magnetic flux [Wb]
s, r	Stator, rotor sub index
d, q	Direct, quadrature reference frame axis component
α, β	Alpha, beta reference frame axis component
L_m	Magnetic inductance [H]
L_s	Stator inductance [H]
L_r	Rotor inductance [H]
P	Number of pole pairs.
P_s, Q_s	Stator active, reactive power [W, VA]
T_{em}	Electromagnetic torque [N·m]
V_{DC}	DC-link voltage [V]
ω_s	Synchronous speed [rad/s]
θ_{sf}	Stator flux angular position [rad]
ω_m	Rotor speed [rad/s]
θ_m	Rotor mechanical angle [rad]
ω_r	Rotor electrical speed [rad/s]
s	Slip
P_{wind}	Aerodynamic power [W]
C_P	Power coefficient
γ	Pitch angle [deg]
Λ	Tip-speed ratio
ρ	Air density [kg/m^3]
A	Turbine transverse area [m^2]
r	Turbine radius [m]
V	Wind speed [m/s]
η	Gearbox ratio
$\mathcal{s}$	Complex frequency variable

1. Introduction

In recent years wind energy has been established as the fastest-growing energy source among renewables. From a global perspective, more than 90 countries have been involved in the installation of new renewable wind power plants [1]. In 2015 the new global installed capacity hit the record for an increase of approximately 64 GW. During 2016 more than 54 GW were installed for a total of approximately 487 GW by the end of 2016. Conservative prognoses forecast an increment of 60 GW in 2017 with a continuous annual grow of about 75 GW by 2021. With the continued improvement in wind turbines technology and ecological concerns, the wind power is now a serious competitor against heavily subsidized energy industries [1][2].

Doubly Fed Induction Generator (DFIG) is a wound-rotor induction machine with voltage injection in the rotor winding. This allows a limited speed control of the electric machine which is sufficient to implement maximum aerodynamic efficiency by maintaining the tip-speed ratio at the nominal value at most operational conditions of the turbine.

The success of DFIG in wind energy applications lies in the reduced power converter, which is typically about 25-30% of the nominal power of the electric machine, furthermore, by current injection in the rotor, it is possible to control the reactive power injected to the electric grid, which is very important for minimizing cooper loses or reactive power compensation[3]. More than 70 % of the installed wind turbines use DFIG. However, this machine is very sensitive to voltage variations in the grid because the stator is directly connected to the grid [4], in contrast to other variable-speed machines which are connected through a full-size power converter.

Sliding Mode Control (SMC) is a non-linear control technique that ensures finite-time convergence of the sliding surface to zero guarantying robustness against bounded disturbances and parameter variations [9]. The main disadvantage of SMC is the chattering effect (high frequency oscillations with finite amplitude) caused by un-modelled dynamics and discretization [9]. On the other hand, power electronics are controlled by means of the injection of discontinuous signals matching with the discontinuous nature of conventional SMC, therefore conventional SMC can be used for direct switching of power electronics on DFIG applications, avoiding modulation. SMC has been successfully implemented in DFIG control and tested under unbalanced conditions and harmonics [15]-[18]. However, the proposals given in [16][17] requires modulation, and the tested faults are moderate since these do not represent a brusque variation in the stator voltage. The SMC presented in [15][18] works under unbalanced conditions but implementation of the SMC regarding with the commutation of the power electronics is not discussed.

In this chapter, it is presented a SMC with the following advantages: a) do not required modulation; b) do not require modifications of the controller structure to withstand stator voltage perturbances (compared with classical control approach as Direct-Torque-Control (DTC), see [5]); and c) the controller can regulate torque and reactive power even under unbalanced conditions, which is equivalent to negative current regulation. Therefore, the proposed SMC offers a very simple alternative that do not require symmetrical decomposition nor pulse width modulation and is not affected by parameter variation. Furthermore, the DFIG system with SMC is characterized in the frequency domain for estimating the commutation frequency of power electronics. A maximum switching frequency value is ensured by means of the addition of hysteresis in the sign function. The hysteresis value is computed applying the Tsypkin's method, a theoretically exact technique to analysed nonlinear systems [12],[14]. Due to the nature of the power converter, the voltage gain seen by the controller is variable in time, which makes difficult to maintain the switching frequency constant. However, it is possible to compute a maximum switching frequency value (minimum hysteresis value), which provides a commutation frequency inside of the acceptable values given in the datasheet of the power electronics.

The chapter presents the dynamic modelling of the electric machine and the wind turbine, the controller design, frequency domain characterisation and finally fault-ride through capability is evaluated analysing the regulated current from a sequence components point of view.

2. Aerodynamic model of wind turbine:

Horizontal axis wind turbines are used to extract mechanical power from the wind resource based on the lifting force of the rotor blades. The mechanical power is a function of the kinematic energy of the wind and the power coefficient:

$$P_{wind} = \frac{1}{2} C_P(\Lambda, \gamma) \rho A V^3 \tag{1}$$

The power coefficient is a function of the tip speed ratio and the pitch angle. Since very complex aerodynamic analyses are required to characterize turbine blades, the power coefficient is usually approximated using mathematical expressions such as [7]:

$$C_P = c_1(c_2\kappa - c_3\gamma - c_4\gamma^{c_5} - c_6)\mathrm{e}^{-c7\kappa} \tag{2}$$

where $\kappa = \frac{1}{\Lambda + 0.06\,\gamma} - \frac{0.035}{1+\gamma^3}$ and c_1 to c_7 are coefficients dependent on the blades geometry.

The tip speed ratio is the relationship between the tangential speed of the blades tip and the wind speed if it is expressed using the DFIG mechanical speed and the gearbox ratio we obtain:

$$\Lambda = \frac{\omega_m r}{\eta V} \tag{3}$$

Pitch angle is normally used for aerodynamically reduce power extraction when the wind speed is above the nominal value. For normal operation, it is maintained constant, while the rotor speed is controlled by the DFIG to maintain the tip speed ratio constant, for the blades model shown in Figure 1 the nominal pitch angle is zero and the nominal tip speed ratio is 8 for a maximum power coefficient of approximately 0.41. The parameters used to generate the displayed function are $c_1 = 0.5; c_2 = 116; c_3 = 0.4; c_4 = 0; c_6 = 5; c_7 = 21$:

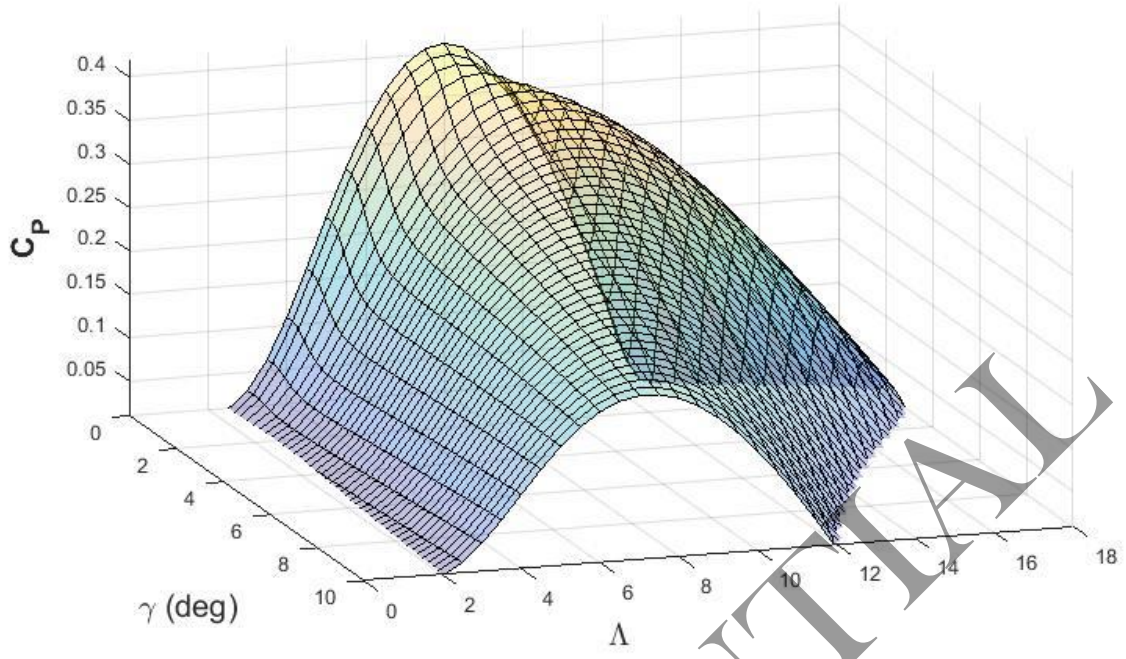

Figure 1. Power coefficient as a function of tip speed ratio and pitch angle.

3. Dynamic modelling of the DFIG

The dynamic equivalent circuit of DFIG can be expressed in an arbitrary reference frame rotating at a speed equal to ω [8]:

$$v_{sd} = \frac{d\lambda_{sd}}{dt} - \omega\lambda_{sq} + R_s i_{sd} \quad (4)$$

$$v_{sq} = \frac{d\lambda_{sq}}{dt} + \omega\lambda_{sd} + R_s i_{sq} \quad (5)$$

$$v_{rd} = \frac{d\lambda_{rd}}{dt} - (\omega - \omega_m)\lambda_{rq} + R_r i_{rd} \quad (6)$$

$$v_{rq} = \frac{d\lambda_{rq}}{dt} + (\omega - \omega_m)\lambda_{rd} + R_r i_{rq} \quad (7)$$

$$\lambda_{sd} = L_s i_{sd} + L_m i_{rd} \quad (8)$$

$$\lambda_{sq} = L_s i_{sq} + L_m i_{rq} \quad (9)$$

$$\lambda_{rd} = L_r i_{rd} + L_m i_{sd} \quad (10)$$

$$\lambda_{rq} = L_r i_{rq} + L_m i_{sq} \quad (11)$$

The electromagnetic torque can be expressed as an interaction between rotor current and stator magnetic flux:

$$T_{em} = \frac{3PL_m}{2L_s}\left(i_{rd}\lambda_{sq} - i_{rq}\lambda_{sd}\right) \quad (12)$$

A common expression of the stator reactive power in terms of the stator voltage and rotor current is:

$$Q_s = \frac{3L_m}{2L_s}\left(v_{sd}i_{rq} - v_{sq}i_{rd}\right) + \frac{3}{2L_s}\left(\lambda_{sd}v_{sq} - \lambda_{sq}v_{sd}\right) \quad (13)$$

The second term of equation (13) is the reactive power required to magnetize the electric machine.

The basic scheme of a wind turbine is shown in Figure 2, a back-to-back power converter is necessary to send the required voltage to the rotor. In the grid side, it is also necessary a converter since the power flow must be bidirectional, from the electric machine to the grid at super-synchronous operation of the machine and from the electric grid to the machine at sub-synchronous operation. Grid side converter is usually controlled by cascade controller which maintains DC-link voltage constant by regulating the grid current. The reactive power can also be controlled; hence, the wind turbine operates at unitary power factor or it can inject reactive power to the grid similarly to an electrically excited synchronous generator. For porpoises of this work, let's consider than the DC-link voltage is maintain constant by the grid-side controller.

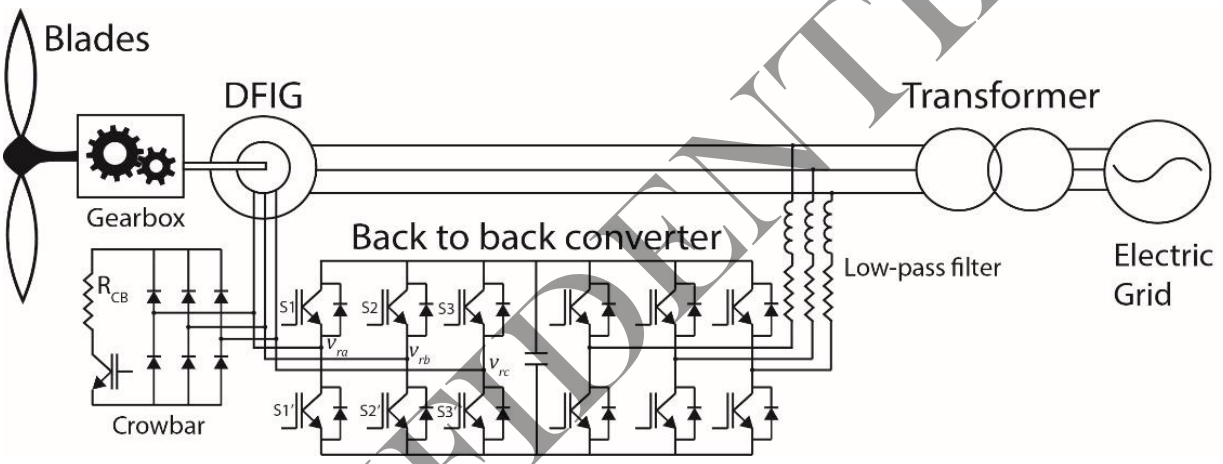

Figure 2. Basic scheme of DFIG-based wind turbine

3.1. Rotor-side power converter model

DFIG rotors are typically connected in star with the neutral connection isolated, the voltage if measured from phase a to the neutral point of the rotor star will be a combination of the phases voltages which can be summarised using the following matrix equation:

$$\begin{bmatrix} v_{an} \\ v_{bn} \\ v_{cn} \end{bmatrix} = \frac{V_{DC}}{3}\begin{bmatrix} 2 & -1 & -1 \\ -1 & 2 & -1 \\ -1 & -1 & 2 \end{bmatrix}\overbrace{\begin{bmatrix} S_1 \\ S_2 \\ S_3 \end{bmatrix}}^{S_{123}} \quad (14)$$

Each component of the vector $S_{1,2,3}$ has only two valid states, 0 or 1. Then each phase voltage has 6 different possible values: $\pm\frac{2}{3}V_{DC}, \pm\frac{1}{3}V_{DC}, 0$. The rotor side converter can be analysed as a discontinuous sign function with variable gain.

4. Sliding Mode Controller Design

It is well known from vector control that orienting the machine model presented in section 3 in the stator flux reference frame is an effective way for decoupling active power (or torque) and reactive power control by means of rotor current regulation. In normal operation, the stator voltage vector will lead the stator flux by approximately 90 degrees neglecting voltage drop due to the stator resistance. From equations (12) and (13) oriented at the stator flux direction i.e., $\lambda_{sq} = 0$ and $v_{sd} = 0$, we obtain a decoupled control system: $T_{em} = -\frac{3PL_m}{2L_s}\lambda_{sd}\boldsymbol{i_{rq}}$ and $Q_s = -\frac{3L_m}{2L_s}v_{sq}\boldsymbol{i_{rd}} + \frac{3}{2L_s}\lambda_{sd}v_{sq}$. However, under unbalanced conditions the phase shift between voltage and flux will not be constant, therefore robust control is necessary to withstand this perturbation.

From equation (8) the direct axis component of stator current can be expressed as:

$$i_{sd} = \frac{\lambda_{sd} - L_m i_{rd}}{L_s} \tag{15}$$

Substituting equation (15) in equation (10):

$$\lambda_{rd} = L'_r i_{rd} + \frac{L_m}{L_s}\lambda_{sd} \tag{16}$$

where $L'_r = L_r - \frac{L_m^2}{L_s}$.

The quadrature component of rotor flux can be obtained in a similar way:

$$\lambda_{rq} = L'_r i_{rq} + \frac{L_m}{L_s}\lambda_{sq} \tag{17}$$

Substituting equations (16) and (17) in (6) and (7) and solving for $\frac{di_{rd}}{dt}$ and $\frac{di_{rq}}{dt}$:

$$\frac{di_{rd}}{dt} = \frac{1}{L'_r}\left(v_{rd} - R_r i_{rd} - \frac{L_m}{L_s}\frac{d\lambda_{sd}}{dt} + \omega_r L'_r i_{rq} + \frac{L_m}{L_s}\omega_r \lambda_{sq}\right) \tag{18}$$

$$\frac{di_{rq}}{dt} = \frac{1}{L'_r}\left(v_{rq} - R_r i_{rq} - \frac{L_m}{L_s}\frac{d\lambda_{sq}}{dt} - \omega_r L'_r i_{rd} - \frac{L_m}{L_s}\omega_r \lambda_{sd}\right) \tag{19}$$

where $\omega_r = \omega_s - \omega_m$. Since the reference frame selected rotate at a synchronous speed, ω_r is equivalent to the rotor current angular speed and the slip angular frequency.

In Figure 3 the equivalent system for current regulation is shown. Under normal operation, the stator flux induces a voltage in the quadrature axis loop. The induced voltage is proportional to the slip and affects only the active power (or torque) regulation loop. Under a grid fault the stator flux is directly affected and can be analysed as another perturbation affecting the current regulation. Analysing the flux in positive, negative, and natural fluxes we can see the influence of the induced voltage (perturbation) to the current regulation loop. The positive sequence flux has an induced voltage proportional to $s\omega_s$, the slip is less than 0.3 for this type of machine therefore the induced voltage is low. The natural flux does not rotate;

therefore, the induced voltage is proportional to the mechanical speed of the machine and the negative flux rotates opposite to the reference frame orientation, the induced voltage is very large, proportional to near twice the synchronous speed $(2-s)\omega_s$ [8]. If the grid fault is very large, no control strategy could withstand this kind of perturbation, since the induced voltage may be larger than the rotor voltage. For that reason, external protection devices are required, the simplest one is the crowbar.

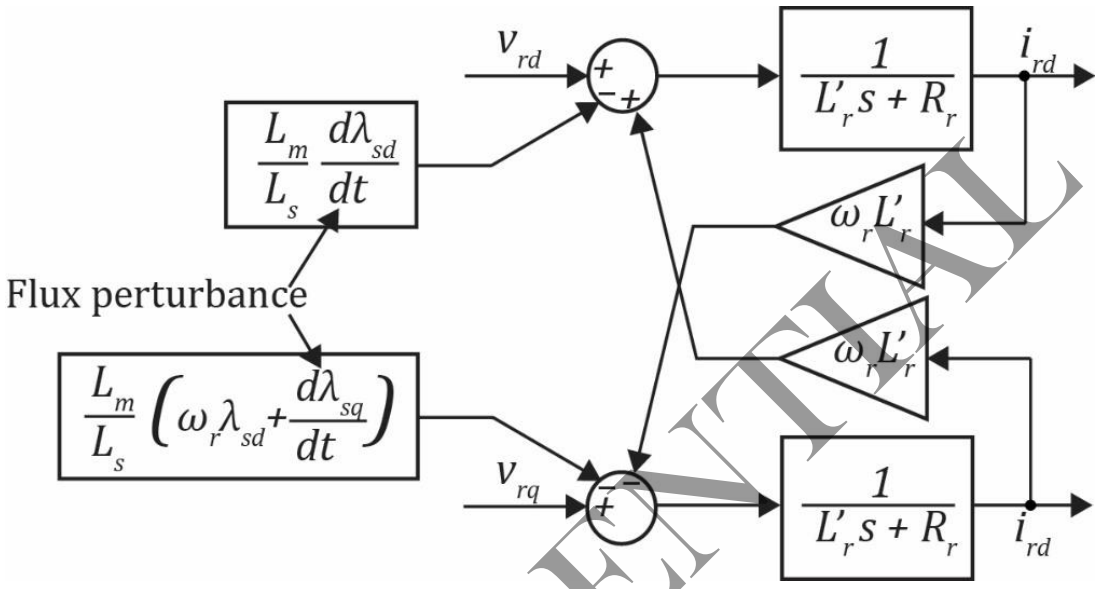

Figure 3. Equivalent current plant including stator flux perturbation

SMC is robust against bounded disturbances and parameter variations; hence it is a good alternative to control perturbed plants as the DFIG model shown in Figure 3. As we want to control the torque and reactive power, the following sliding surfaces are selected:

$$\sigma_{T_{em}} = T_{em} - T_{em}^*; \qquad \sigma_{Q_s} = Q_s - Q_s^* \tag{20}$$

where T_{em}^* and Q_s^* are the desired (reference) value of torque and reactive power, considering that the reference values are much slower than the dynamics of the system and that the stator flux is perfectly aligned with the reference frame d axis:

$$\dot{\sigma}_{T_{em}} = \dot{T}_{em} = -\frac{3PL_m}{2L_s}\left(\dot{i}_{rq}\lambda_{sd} + i_{rq}\dot{\lambda_{sd}}\right) \tag{21}$$

On the other hand, the voltage vector may have a d component due to voltage perturbation:

$$\dot{\sigma}_{Q_s} = \dot{Q}_s = \frac{3L_m}{2L_s}\left(\dot{v}_{sd}i_{rq} + v_{sd}\dot{i}_{rq} - \dot{v_{sq}}i_{rd} - v_{sq}\dot{i}_{rd}\right) + \frac{3}{2L_s}\left(\dot{\lambda}_{sd}v_{sq} + \lambda_{sd}\dot{v}_{sq}\right) \tag{22}$$

Substituting equations (18) and (19) in (22) and (23):

$$\dot{\sigma}_{T_{em}} = \overbrace{kP\lambda_{sd}\left(R_r i_{rq} + \frac{L_m}{L_s}\omega_r\lambda_{sd} + \omega_r L'_r i_{rd}\right)}^{F_{T_{em}}} \overbrace{-kP\lambda_{sd}v_{rq}}^{d_{T_{em}}} \overbrace{-kPL'_r i_{rq}\dot{\lambda}_{sd}}^{P_{T_{em}}} \tag{23}$$

$$\dot{\sigma}_{Q_s} = \overbrace{kv_{sq}\left(R_r i_{rq} - \omega_r L'_r i_{rq}\right)}^{F_{Q_s}} \overbrace{-kv_{sq}v_{rd}}^{d_{Q_s}}$$

$$\underbrace{+kv_{sq}\left[\frac{L_m}{L_s}\dot{\lambda_{sd}} + \frac{L'_r}{v_{sq}}(\dot{v}_{sd}i_{rq} + v_{sd}\dot{i}_{rq} - \dot{v_{sq}}i_{rd})\right] + \frac{3}{2L_s}(\dot{\lambda}_{sd}v_{sq} + \lambda_{sd}\dot{v}_{sq})}_{P_{Q_s}} \quad (24)$$

where $k = \frac{3L_m}{2L_s L'_r}$, expressing equations (23) and (24) in matrix form:

$$\begin{bmatrix}\dot{\sigma}_{T_{em}} \\ \dot{\sigma}_{Q_s}\end{bmatrix} = \begin{bmatrix}F_{T_{em}} \\ F_{Q_s}\end{bmatrix} - k\begin{bmatrix}0 & P\lambda_{sd} \\ v_{sq} & 0\end{bmatrix}\begin{bmatrix}v_{rd} \\ v_{rq}\end{bmatrix} + \begin{bmatrix}P_{T_{em}} \\ P_{Q_s}\end{bmatrix} \quad (25)$$

Under normal conditions, all the terms dependent on $v_{sd}, \dot{v}_{sd}, \dot{v}_{sq}$ and $\dot{\lambda}_{sd}$ are equal to zero. Under abnormal conditions those terms can be analysed as perturbations $P_{T_{em}}$ and P_{Q_s}. The control signals v_{rd} and v_{rq} appears in the first derivate of the sliding surface, thus the relative degree of the control system is one. Then, finite time convergence to the sliding surface and robustness against bounded disturbance/uncertainties can be achieved using the control signal:

$$\begin{bmatrix}v_{rd} \\ v_{rq}\end{bmatrix} = \begin{bmatrix}-M_d \operatorname{sgn}(\sigma_{Q_s}) \\ -M_q \operatorname{sgn}(\sigma_{T_{em}})\end{bmatrix} \quad (26)$$

where $M_d, M_q > 0$. A detailed description of M_d and M_q computation is given in section 4.1.

Remark: A discontinuous function is intentionally selected because the nature of the rotor-side power converter is discontinuous as well, therefore the control signal can be easily used directly from the controller algorithm to the power converter without modulation. On the contrary, any continuous control; e.g. saturation, sigmoid function, etc. employed to smooth the discontinuous control in equation (26) must be modulated to be implementable in a power converter, therefore chattering will be present no matter the control strategy used.

The desired voltage need to be send through the rotor-side power converter. The voltage seen from the stator flux reference frame is obtained using park transform:

$$\begin{bmatrix}v_{rd} \\ v_{rq}\end{bmatrix} = \overbrace{\begin{bmatrix}\cos\theta_d & -\sin\theta_d \\ \sin\theta_d & \cos\theta_d\end{bmatrix}\frac{2}{3}\begin{bmatrix}1 & -1/2 & -1/2 \\ 0 & \sqrt{3}/2 & -\sqrt{3}/2\end{bmatrix}}^{T}\begin{bmatrix}v_{an} \\ v_{bn} \\ v_{cn}\end{bmatrix} \quad (27)$$

where the reference frame angle is $\theta_d = \theta_m - \theta_{sf}$.

Using equations (14) (25) and (27) it is possible to establish a relationship between *dq* and *abc* quantities:

$$\begin{bmatrix}\sigma_{T_{em}} \\ \sigma_{Q_s}\end{bmatrix} = \overbrace{-k\begin{bmatrix}0 & P\lambda_{sd} \\ v_{sq} & 0\end{bmatrix}T\frac{V_{DC}}{3}\begin{bmatrix}2 & -1 & -1 \\ -1 & 2 & -1 \\ -1 & -1 & 2\end{bmatrix}}^{D}\begin{bmatrix}\sigma_a \\ \sigma_b \\ \sigma_c\end{bmatrix} \quad (28)$$

Since the matrix D is not square, the Moore-Penrose pseudo-inverse is used:

$$\overbrace{\begin{bmatrix}\sigma_a\\ \sigma_b\\ \sigma_c\end{bmatrix}}^{\sigma_{abc}} = D^{+}\begin{bmatrix}\sigma_{T_{em}}\\ \sigma_{Q_s}\end{bmatrix} \tag{29}$$

where:

$$D^{+} = D^{T}(DD^{T})^{-1} = -\frac{3}{kV_{DC}}\begin{bmatrix}\frac{1}{P\lambda_{sd}}\sin\theta_d & \frac{1}{v_{sq}}\cos\theta_d\\ \frac{1}{P\lambda_{sd}}\sin(\theta_d + 2\pi/3\,) & \frac{1}{v_{sq}}\cos(\theta_d + 2\pi/3)\\ \frac{1}{P\lambda_{sd}}\sin(\theta_d - 2\pi/3\,) & \frac{1}{v_{sq}}\cos(\theta_d - 2\pi/3)\end{bmatrix}$$

The constant term $\frac{3}{kV_{DC}}$, which contains parameters of the electric machine, can be removed from the transformation matrix since the controller will only evaluate the sign of σ_{abc}, thus the controller is robust against parametric uncertainties, under normal conditions the stator flux direct component (λ_{sd}) and stator voltage quadrature component (v_{sq}) are constant. In Figure 4 is shown the basic scheme of the presented controller. The output of equation (29) is the equivalent *abc* sliding surface, then a function similar to sign is used to evaluate the switch state (0 means lower leg activated and 1 means upper leg activated). The resulting control system do not require modulation since the switching state is determined directly from the control system.

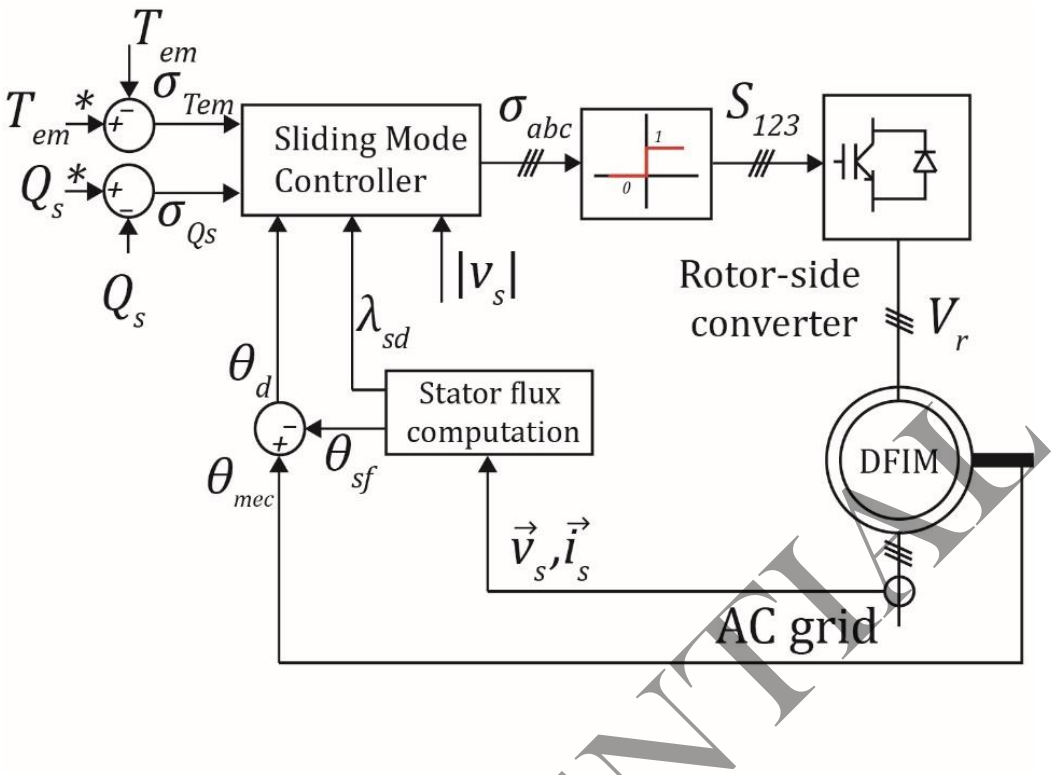

Figure 4. Basic scheme of SMC

4.1. Sliding mode existence condition

For a relative degree one system

$$\dot{\sigma} = F(x) + d(x)u \qquad (x \in \mathbb{R}^n) \tag{30}$$

With a scalar control

$$u = -M\text{sgn}(\sigma) \tag{31}$$

The condition for satisfying the existence of the sliding mode is [9]:

$$d(x)M > |F(x)| \tag{32}$$

The stator flux oriented SMC has a very similar form of system of equation (30). Then, existence of SMC is ensured if the following conditions are met:

$$M_{q,min} > \left|(F_{T_{em}} + P_{T_{em}})/d_{T_{em}}\right|; \qquad M_{d,min} > |(F_{Q_s} + P_{Q_s})/d_{Q_s}| \tag{33}$$

Therefore, choosing M_d and M_q using equation (33) ensures finite convergence to the sliding variable and insensitivity to bounded disturbance/uncertainties. The only requirement to compute the gains M_d and M_q is the knowledge of the bounds of the system and the disturbance/uncertainties, $|F_{Q_s,T_{em}}|$, $|d_{Q_s,T_{em}}|$ and $|P_{Q_s,T_{em}}|$. Note that real implementation of control gains in equations (33) depends of DC-link voltage V_{DC}, which is variable in practice

and it must be ensured that V_{DC} is regulated correctly to ensure a robust performance of the rotor side of the DFIG system.

4.2. Switching frequency limitation.

In Figure 4 it is shown the scheme of an ideal sliding mode controller, however, it requires infinite switching frequency which is not possible in real physical systems, therefore, the most common solution for this issue is to include a hysteresis loop to the ideal sign function [10] since hysteresis makes the switching frequency finite. Note that sigmoid functions and saturation can be implemented to reduce switching frequency as well as attenuate chattering. However, these functions are continuous and/or contain linear parts requiring modulation for its application to power electronics while a sign function with hysteresis can be injected without modulation.

A widely used method to determine limit cycles and the oscillation frequency is the sinusoidal Describing Function (DF) which can be used for segmented non-linear system composed by a linear system and a non-linear part [12], that is the case of a linear plant controlled by a relay-based control system (see Figure 5). A requirement for applying DF is that the linear system $L(s)$ must have a low-pass filter behaviour. Furthermore, only the first harmonic is considered in the analysis. However, for relative degree-one systems as the one presented in this chapter this technique is not suitable [12]. DF will predict no oscillations because it ignores the contribution of the harmonics. On the other hand, Tsypkin's method is an exact method in which one can select the number of harmonics to be considered and it can be applied to estimate oscillations in relative degree one systems. Therefore, the DFIG system with SMC presented in this chapter is analysed in the frequency domain using Tsypkin's method.

Expressing equations (4-11) in matrix form:

$$\dot{x} = Ax + Bu; \qquad y = Cx \tag{34}$$

where:

$$x = [i_{sd} \quad i_{sq} \quad i_{rd} \quad i_{rq}]^T; \qquad u = [v_{sd} \quad v_{sq} \quad v_{rd} \quad v_{rq}]^T;$$

$$A = \frac{1}{L'_r L_s}\begin{bmatrix} -R_s L_r & \omega_m L_m^2 + \omega_s L'_r L_s & R_r L_m & \omega_m L_m L_r \\ -\omega_m L_m^2 - \omega_s L'_r L_s & -R_s L_r & -\omega_m L_m L_r & R_r L_m \\ R_s L_m & -\omega_m L_s L_m & -R_r L_s & -\omega_m L_r L_s + \omega_s L'_r L_s \\ \omega_m L_s L_m & R_s L_m & \omega_m L_r L_s - \omega_s L'_r L_s & -R_r L_s \end{bmatrix};$$

$$B = \frac{1}{L'_r L_s}\begin{bmatrix} L_r & 0 & -L_m & 0 \\ 0 & L_r & 0 & -L_r \\ -L_m & 0 & L_s & 0 \\ 0 & -L_m & 0 & L_s \end{bmatrix}; \qquad C = \begin{bmatrix} 0 & 0 & 1 & 0 \\ 0 & 0 & 0 & 1 \end{bmatrix}.$$

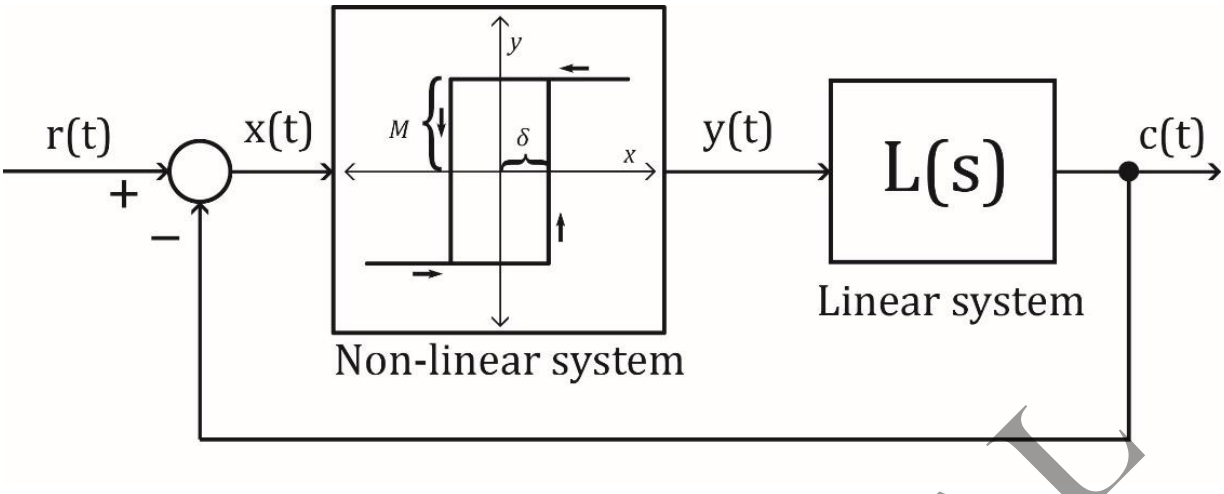

Figure 5. Relay-based control of a linear system

The system presents a non-linearity due to the mechanical speed ω_m, which is dependent on the electromagnetic torque and the mechanical equation, however since the time scales of the electrical quantities is much smaller than the time scale of the mechanical system we are going to study system of equation (34) as a set of linear systems varying the mechanical speed in a range of $\pm 30\%$ about the synchronous speed. Other supposition is that the system is fully decoupled, that is v_{rd} controls i_{rd} and v_{rq} controls i_{rq}. So, we can obtain both transfer functions from the diagonal elements of the following matrix equation:

$$G(s) = C(sI - A)^{-1}B + D \tag{35}$$

where I is a 4x4 identity matrix. The diagonal transfer functions will be relative degree one systems with 4 poles and 3 zeros:

$$L(s) = \frac{I_{rd}(s)}{V_{rd}(s)} = \frac{I_{rq}(s)}{V_{rq}(s)} = \frac{a_3 s^3 + a_2 s^2 + a_1 s + a_0}{d_4 s^4 + d_3 s^3 + d_2 s^2 + d_1 s + d_0} \tag{36}$$

Tsypkin's locus is defined as [12]:

$$T(j\omega) = \sum_{n\,\text{odd}}^{\infty} \text{Re}[L_1(jn\omega)] + j \sum_{n\,\text{odd}}^{\infty} \frac{1}{\text{n}} \text{Im}[L_1(jn\omega)] \tag{37}$$

The conditions required to predict a limit cycle oscillating at an angular frequency ω_0 are [12]:

$$\text{Im}[T(j\omega_0)] = \frac{\pi}{4}\left[L(\infty) - \frac{\delta}{M}\right] \tag{38}$$

$$\text{Re}[T(j\omega_0)] < \frac{\pi}{4\omega_0} \lim_{s \to \infty} [sL_1(s)] \tag{39}$$

In Figure 6 it is shown the graphical solution for a DFIG with the characteristics shown in Table 1, the mechanical speed has minor influence at high frequencies, therefore, it is valid to consider the DFIG as a linear system (note that the number of pole pairs is not considered in (34), therefore the mechanical speed reported is the one of an equivalent two pole machine). Supposing that the power inverter has a maximum switching frequency of $f_{max} = 4000$ Hz →

$\omega_0 = 8000\pi \frac{\text{rad}}{\text{s}}$, from equation (38) we can calculate the hysteresis width. We know that the maximum gain the system can have is $M_{max} = \frac{2}{3}V_{dc}$, then the hysteresis loop that will ensure a maximum switching frequency of 4000 Hz is:

$$\delta = \frac{(0.3094)(4)}{\pi} * \frac{2}{3}600 = 157.57\ A$$

However, the control system was designed to direct control torque and reactive power, so we need to calculate the hysteresis width of those quantities, which can be easily done since the control system is decoupled, and the current direct and quadrature components are directly related with reactive power and torque respectively.

$$\delta_{Q_s} = \frac{3L_m v_{sq}}{2L_s}\delta; \qquad \delta_{T_{em}} = \frac{3PL_m\lambda_{sd}}{2L_s}\delta \tag{40}$$

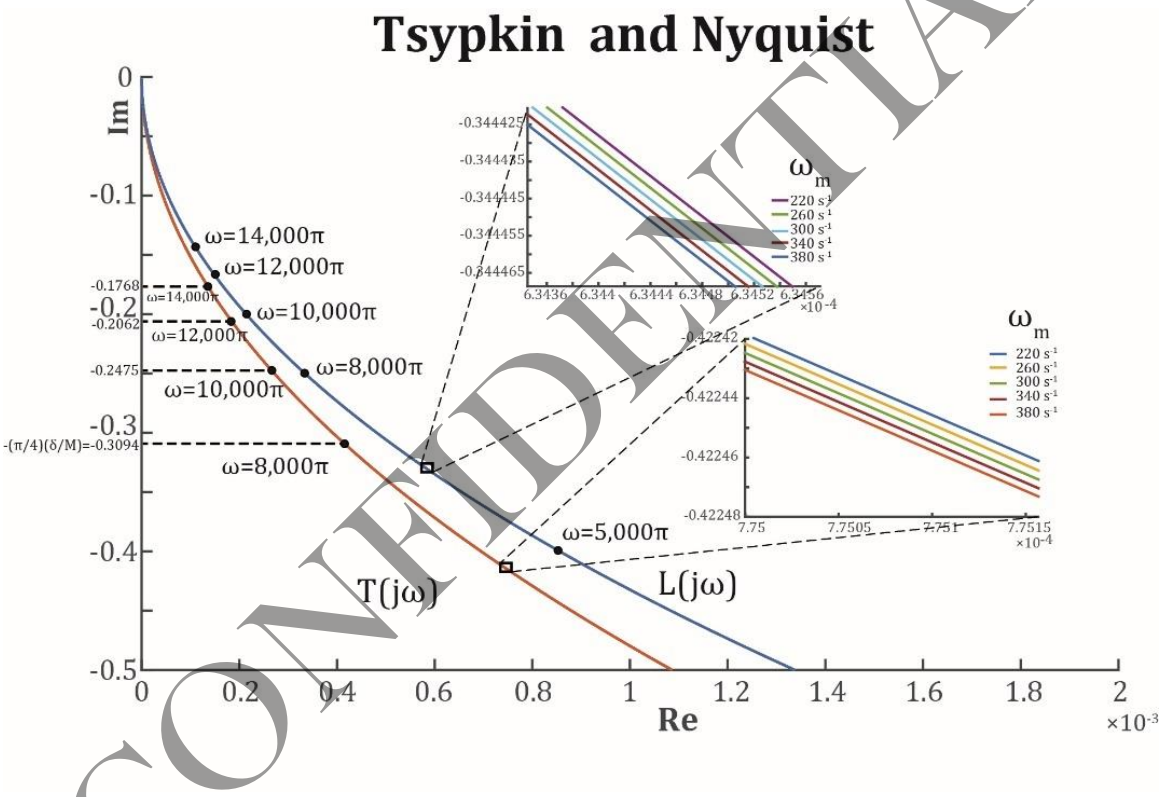

Figure 6. Graphical solution using Tsypkin's method

Moreover, as can be seen from Figure 6 and equations (38-39), the addition of hysteresis can be used to attenuated chattering since the hysteresis width is directly proportional to amplitude of chattering while it is inversely proportional to the frequency.

4.3. Step-by-step design

The design of the SMC proposed in this section, can be summarized in the next step-by-step algorithm:

1. Select the sliding mode surfaces for torque and reactive power using equation (20)

2. Choose the gains, M_d and M_q, of the controller in equation (26) using the conditions given in equation (33) to guarantying robustness.

3. Compute a hysteresis value for the torque and reactive power controllers (sign functions) using equations (40) to ensure an acceptable switching frequency in the power electronics.

Then, following the step-by-step process described in this subsection, a robust SMC for regulate torque and reactive power in DFIG systems can be designed. Furthermore, practical implementation is considered in the design since a method to compute a hysteresis value, limiting undesired high frequency commutation in power electronics, is provided.

5. Complex power and torque under unbalanced conditions

The active and reactive power can be obtained from electrical quantities seen from a stationary reference frame:

$$P_s = \frac{3}{2}\mathrm{Re}(\overrightarrow{v_s}\,\overline{\overrightarrow{i_s}}) = \frac{3}{2}(v_{s\alpha}i_{s\alpha} + v_{s\beta}i_{s\beta}) \tag{41}$$

$$Q_s = \frac{3}{2}\mathrm{Im}(\overrightarrow{v_s}\,\overline{\overrightarrow{i_s}}) = \frac{3}{2}(v_{s\beta}i_{s\alpha} - v_{s\alpha}i_{s\beta}) \tag{42}$$

where the operator $\overline{\vec{x}}$ is the complex conjugate.

In case of unbalanced conditions, the symmetrical components methods can be used for simplifying analysis, since zero sequence do not produce complex power, only positive and negative sequences are analysed:

$$\overrightarrow{v_s} = \vec{v}_{s_1} + \vec{v}_{s_2} = v_{s\alpha 1} + v_{s\alpha 2} + j(v_{s\beta 1} + v_{s\beta 2}) \tag{43}$$

$$\overrightarrow{i_s} = \vec{i}_{s_1} + \vec{i}_{s_2} = i_{s\alpha 1} + i_{s\alpha 2} + j(i_{s\beta 1} + i_{s\beta 2}) \tag{44}$$

Substituting (43) and (44) in equations (41) and (42) yields:

$$P_s = \overbrace{\tfrac{3}{2}(v_{s\alpha 1}i_{s\alpha 1} + v_{s\beta 1}i_{s\beta 1})}^{P_{s11}} + \overbrace{\tfrac{3}{2}(v_{s\alpha 1}i_{s\alpha 2} + v_{s\beta 1}i_{s\beta 2})}^{P_{s12}} + \overbrace{\tfrac{3}{2}(v_{s\alpha 2}i_{s\alpha 1} + v_{s\beta 2}i_{s\beta 1})}^{P_{s21}} + \overbrace{\tfrac{3}{2}(v_{s\alpha 2}i_{s\alpha 2} + v_{s\beta 2}i_{s\beta 2})}^{P_{s22}} \tag{45}$$

$$Q_s = \overbrace{\tfrac{3}{2}(v_{s\beta 1}i_{s\alpha 1} - v_{s\alpha 1}i_{s\beta 1})}^{Q_{s11}} + \overbrace{\tfrac{3}{2}(v_{s\beta 1}i_{s\alpha 2} - v_{s\alpha 1}i_{s\beta 2})}^{Q_{s12}} + \overbrace{\tfrac{3}{2}(v_{s\beta 2}i_{s\alpha 1} - v_{s\alpha 2}i_{s\beta 1})}^{Q_{s21}} + \overbrace{\tfrac{3}{2}(v_{s\beta 2}i_{s\alpha 2} - v_{s\alpha 2}i_{s\beta 2})}^{Q_{s22}} \tag{46}$$

On the other hand, electromagnetic torque can be obtained using the well-known equation:

$$T_{em} = \frac{3P}{2}\mathrm{Im}(\overrightarrow{\lambda_s}\,\overline{\overrightarrow{i_s}}) \tag{47}$$

Using the symmetrical components theory, an unbalance condition can be modelled with invariant positive and negative sequence components, therefore at steady state the derivate

term of equations (4) and equation (5) are zero leading to the following positive and negative stator flux components:

$$\vec{\lambda}_{s1} = \frac{\vec{v}_{s1} - R_s \vec{i}_{s1}}{j\omega_s}; \qquad \vec{\lambda}_{s2} = \frac{\vec{v}_{s2} - R_s \vec{i}_{s2}}{-j\omega_s} \tag{48}$$

Substituting equations (43,44) and (48) in (47):

$$T_{em} = \frac{3P}{2\omega_s} \mathrm{Re}[\vec{v}_{s1}\overline{\vec{i}_{s1}} + \vec{v}_{s1}\overline{\vec{i}_{s2}} - \vec{v}_{s2}\overline{\vec{i}_{s1}} - \vec{v}_{s2}\vec{i}_{s2} - R_s(|\vec{i}_{s1}|^2 - |\vec{i}_{s2}|^2)] \tag{49}$$

Comparing equation (50) with equation (45) it is easy to see that the same terms appear in both equations:

$$T_{em} = \frac{P}{\omega_s}[P_{s11} + P_{s12} - P_{s21} - P_{s22} + \frac{3R_s}{2}(|\vec{i}_{s2}|^2 - |\vec{i}_{s1}|^2)] \tag{50}$$

The terms P_{s12} and P_{s21} are the cause of oscillation in torque and power when an unbalanced dip occurs. Since the condition for cancelling torque oscillations ($P_{s12} = P_{s21}$) is opposite to the condition for cancelling active power oscillations ($P_{s12} = -P_{s21}$) it is not possible to cancel both at the same time. It is preferable to cancel torque oscillations, otherwise the mechanical components may be severely damaged. On the other hand, to cancel reactive power oscillations, the following condition must be met $Q_{s12} = -Q_{s21}$.

6. Simulation results

To test the controller a DFIG was simulated using the parameters displayed in table 1. The blades model surface is shown in Figure 1 with: gearbox ratio ($\eta = 85.8$) rotor radius ($r =$ 40 m) and air density ($\rho = 1.25$ kg\m^3). The nominal wind speed of 12 m/s, the nominal tip speed ratio $\Lambda_{opt} = 7.9533$ and the maximum power coefficient is $C_{p,max} = 0.4109$. The pitch controller is ideal chopping the extracted aerodynamic power to the nominal power (2MW) for wind speed above the nominal value. Considering that the maximum switching frequency of the converter is 7000 Hz, from Figure 6 the desired hysteresis width is $\delta = 90.04A$, therefore, $\delta_{Q_s} = 128\times10^3$ and $\delta_{T_{em}} = 811$.

The following electromagnetic torque reference is used for maintaining the tip-speed ratio at the optimal value without measuring wind speed:

$$T_{ref} = -\frac{\frac{1}{2}\pi\rho R^5 C_{p,max}}{\Lambda_{opt}^2 \eta^3}\omega_m^2 \tag{51}$$

on the other hand, the reactive power reference is maintained at zero.

Nominal power = 2 MW
Voltage=690 V / 50 Hz
DC-link voltage= 1200 V
Stator/rotor turns ratio = 1/2

Mutual inductance (L_m)=2.5 mH
Stator inductance (L_s)=2.58 mH
Rotor inductance (L_r)=2.58 mH
Stator resistance (R_s)=2.6 mΩ
Rotor resistance (R_r)=2.9 mΩ
Pole pairs (P)=2

Table 1: Machine parameters used in simulation.

The wind speed profile is shown in Figure 7 II, the wind speed was taken from real measurements reported by the Department of Wind Energy, Technical University of Denmark [19]. With values oscillating in all the operational range of the wind speed.

The power extracted by the blades is shown in Figure 7 III, during the high wind speed periods the ideal pitch controller maintain the extracted power at the nominal value of 2MW, while the mechanical speed is controlled during the rest of the time to optimize power extraction as shown in Figure 7 IV. The rotor converter nominal power limits the operational speed of the wind turbine $P_r \approx sP_s$.

The references are followed even under unbalanced grid conditions, a two-phase voltage dip is simulated at the terminals of the electric machine, the voltage dip is 20% of the nominal value. In Figure 7 I, it is displayed the detail of the voltage dip. The voltage dip starts at 95 seconds and ends at 98 seconds of the simulation, the time axis in Figure 7 I is chopped from 95.05-97.95 seconds, in order to better see the stator voltage waveform during the fault. As demonstrated in section 5, it is not possible to maintain both torque and reactive power constant during unbalanced conditions, therefore the stator reactive power is affected (see Figure 7 VI) since the controller forces the electromagnetic torque to be constant. As a result the controller injects a negative sequence current to the rotor in order to cancel torque oscillations out (see Figure 7 VII), it is worth mention that other control strategies as vector control requires a double control loop for controlling positive and negative sequence separated [13], which not only complicates the current regulation algorithm but also requires sequence decoupling of rotor current, a very complex issue that is avoided by using a robust control strategy.

Finally, the filtered rotor voltage is displayed in Figure 7 VIII. The controller does not require modulation and automatically injects negative sequence voltage to regulate torque and reactive power under unbalanced conditions.

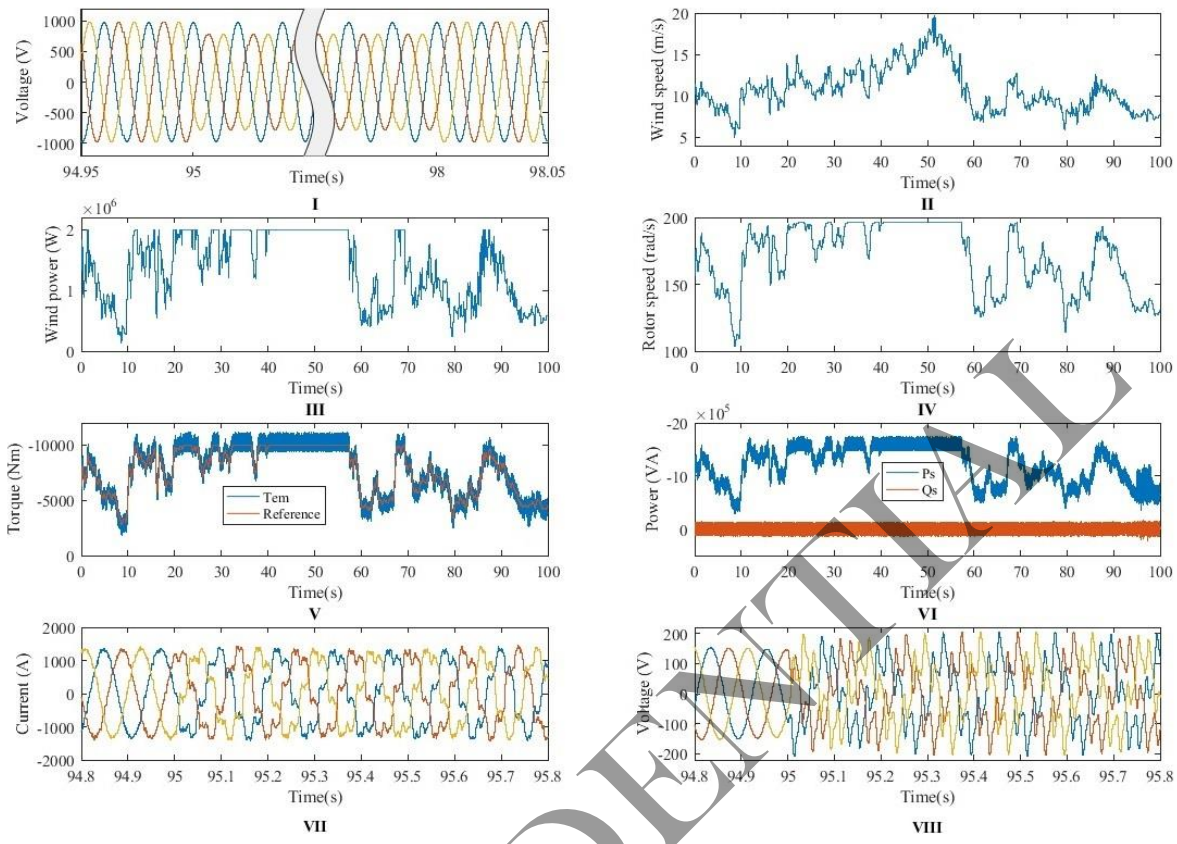

Figure 7. Simulation results: I Stator voltage, II Wind speed profile, III Extracted aerodynamic wind power, IV Rotor speed, V Electromagnetic torque, VI Stator active and Reactive Power, VII Rotor current, VIII Rotor filtered voltage

7. Conclusions

A stator flux oriented Sliding Mode Control, which regulate torque and reactive power in DFIG, is presented. The controller is not dependent on electric machine parameters and do not require modulation, injecting the desired voltage vector directly to a two-level power converter. Despite the proposed SMC controller has a variable switching frequency, which is not desired in practical applications, the switching frequency is limited by a hysteresis loop in the torque and reactive power controllers. The hysteresis value is calculated by means of the frequency domain characterization of the DFIG system with SMC, via Tsypkin's method. Then, the safe operation of the power converter regarding commutation frequency is ensured. Furthermore, the proposed SMC is capable to reject stator flux variations providing a desired operation even under unbalanced grid conditions. Compared with classical control techniques as DTC, the presented SMC do not require the modification of the control loop. The equations for compute the control gains that ensure robustness and existence of SMC are given. Simulations validating the advantages of the proposed SMC are shown.

8. References

[1] GWEC. Global Wind Report 2016 [Internet]. 2017. Available from: http://www.gwec.net/publications/global-wind-report-2/global-wind-report-2016/# [Accessed: 07/17/2017]

[2] European Commission . JRC Wind Energy Status Report: 2016 Edition [Internet]. March 2017 . Available from: https://ec.europa.eu/jrc/en/news/jrc-wind-energy-status-report-2016-edition [Accessed: 07/17/2017]

[3] Tapia, A, Tapia, G, Ostaloza, JX, Saenz JR. Modeling and control of a wind turbine driven doubly fed induction generator. IEEE Transactions on energy conversion . 2003;**18**(2):194-204.

[4] Xu L, Wang Y. Dynamic modeling and control of DFIG-based wind turbine under unbalanced network conditions. IEEE Transactions on Power Systems . 2007;**22**(1):314-323.

[5] Abad G, Rodriguez MA, Poza J, Canales M. Direct torque control of doubly fed induction machine-based wind turbines under voltage dips and without crowbar protection. IEEE Transactions on Energy Conversion . 2012;**25**(2):586-588.

[6] Ong CM. Dynamic Simulation of Electric Machinery using Matlab/Simulink. Upper Saddle River, New Jersey: Prentice Hall; 1998. 626 p.

[7] Lubosny Z. Wind Turbine Operation in Electric Power Systems. Springer; 2003. 262 p.

[8] Abad G, Lopez J, Rodriguez M, Marroyo L, Iwanski G. Doubly Fed Induction Machine: Modeling and Control for Wind Energy Generation. Hoboken, New Jersey: John Willey & Sons; 2011. 625 p.

[9] Utkin V, Guldner J, Shi J. Sliding Mode Control in Electro-Mechanical Systems. 2nd ed. CRC Press; 2009. 503 p.

[10] Venkataramanan R. Sliding mode control of power converters [dissertation]. California Institute of Technology; 1986.

[11] Villanueva I, Rosales A, Ponce P, Molina A. Stator-flux-oriented sliding mode controller for DFIG with variable hysteresis loop for limiting switch frequency of rotor-side power converter. In: IEEE, editor. Industrial Technology (ICIT), 2017 IEEE International Conference on; 2017.

[12] Gelb A, Vander Velde WE. Multiple-input describing functions and nonlinear system design . New York,: McGraw-Hill; 1968. 655 p.

[13] Xu L. Coordinated control of DFIG's rotor and grid side converters during network unbalance. IEEE Transactionss on Power Electronics. 2008;**23** (3):1041-1049.

[14] Gupta G, Gosh A. Frequency-domain characterization of sliding mode control of an inverter used in DSTATCOM application. IEEE Transactions on Circuits and Systems. 2006;**53**(3):662-672.

[15] Martinez MI, Tapia G, Susperregui A, Camblong H. Sliding mode control for DFIG rotor and grid side converters under unbalanced and harmonically distorted grid voltage . IEEE Transactions on Energy Conversions. 2012;**27**(2):328-339.

[16] Beltran B, Benbouzid M, Ahmed-Ali. High-order sliding mode control of a DFIG-based wind turbine for power maximization and grid fault tolerance. In: Electric Machines and Drives Conference; IEEE ; 2009. p. 183-189.
[17] Benbouzid M, Beltran B, Amirat Y, Yao G, Han J, Mangel H. Second order sliding mode control of DFIG-based wind turbines fault ride through capability enhancement. ISA transactions . 2014;**53**(3):827-833.
[18] Martinez M, Susperregui A, Tapia G, Xu L . Sliding mode control of a wind turbine driven double-fed induction generator under non-ideal grid voltages . IET Renewable Power Generation . 2013;**7**(4):370-379.
[19] Hansen KS, Larsen GC . Database of Wind Characteristics [Internet]. Available from: http://www.winddata.com/ [Accessed: January 2016]

Chapter 5

Contributions and conclusion

5.1 Contributions

The main scientific contributions to the state of art of DFIG control are:

5.1.1 Supervisory controller using short-term ahead prediction

1. A new fuzzy logic supervisory controller for smoothing power fluctuation of WECS using a FESS.

5.1.2 Pitch angle control using type 2 fuzzy logic

2. Evaluation of a type 2 fuzzy logic controller in the pitch angle control and current regulation loop of vector control.

5.1.3 Thermal cycling and life-time estimation of GSC

3. Methodology for evaluate the remaining life-time of GSC IGBT's.

5.1.4 Sliding mode control for DFIG under unbalanced conditions

4. Development of a new grid-voltage-oriented SMC stable under any operational condition of the DFIG

5. Enhancement of transient behavior of DFIG by means of "demagnetizing torque" and "demagnetizing reactive power".

5.1.5 Variable hysteresis in the time domain

6. Development of an strategy for switching frequency limitation based on an estimation of the system dynamics by means of a low-pass filter and rotor current measurement.

5.1.6 Hysteresis width calculation in the frequency domain

7. Characterization of the proposed SMC in the frequency domain for the selection of fixed hysteresis width with well-founded bases.

5.2 Conclusion

In this thesis, sliding mode control for the doubly fed induction machine, for wind energy application has been studied. The main contributions of this work have been summarized. It can be concluded that SMC offers a simple, fast-dynamic response alternative with robustness against parameter variations of the electric machine. The controller do not require modulation to be implemented since it is based on discontinuous control which are directly sent to the inverter state. The controller is robust against disturbances which make it suitable for operation even under unbalanced grid conditions.

Unlike other not-modulated techniques like DTC which uses subjective methods for hysteresis width selection, the presented controller is characterized in the frequency and time domain for the selection of the hysteresis width based on the switching frequency of the power converter.

When operating under unbalanced conditions the controller present remarkable advantages, its robustness allows to control torque and reactive power without modification of the control system or rotor current sequence separation. In contrast to traditional vector control which requires decouple rotor current and implement dual control techniques to achieve torque and reactive power control under unbalanced conditions.

With the implementation of demagnetization control strategies it is possible to enhance the transient behavior of DFIG under voltage dips, which is important for grid support in fault conditions. The grid-voltage orientation is selected since it provides stability under all the operational conditions of the machine, in contrast to stator-flux orientation which may become unstable for large values of i_{rd}.

The main drawbacks of the controller are:

- The controller presents high ripple in the response due to the limited switching frequency and the high gain needed for robustness against disturbances.
- The voltage gain seen by the controller is variable, therefore an exact value of switching frequency is not possible.
- The controller cannot be easily expanded to multilevel converters like space-vector-modulated controllers.
- Although the controller is robust against parameter variation, it relies in the correct estimation of stator flux or stator voltage vectors.

The presented publications demonstrate that SMC could be an alternative solution to classical control methods implemented in DFIG specially for fault ride-trough capability enhancement.

5.3 Future Research

Flux oriented SMC for DFIG has been proposed, the following challenges are considered to be suitable for further research:

The controller has been extendedly proved in simulation models, however, the real-life experimentation is needed. The controller can be easily adapted in a test bench with a programed vector controller or DTC. In section 4.2 SMC has been presented in table form in a similar way that DTC.

Another important research area is to develop a variable-gain using multilevel power converters. Due to the limited states that a two level converter can supply, the controller injects the larger possible gain to control both active and reactive power at the same time. However, in some situation the gain needed by each control loop will be much lower. Using an adaptive gain strategy combined with a multilevel power converter will greatly reduce the chattering of the proposed controller maintaining the robustness. One solution is the use of multi-band hysteresis loops to expand the controller to multi-level converter topologies.

Appendix A

Simulation parameters

System	Parameter	Value
Wind Turbine	$\rho(km/m^3)$	1.25
	$A(m^2)$	3848.45
	$\Lambda_{optimal}$	12
Blades Model	c_1	0.5
	c_2	116
	c_3	0.4
	c_4	0
	c_5	5
	c_6	21
DFIG	$R_s(pu)$	0.006014
	$R'_r(pu)$	0.01216
	$L_{ls}(pu)$	0.05783
	$L'_{lr}(pu)$	0.05783
	$L_m(pu)$	1.85083
	$S_{base}(MVA)$	2.4
Gearbox	$J_W(kg.m^2)$	3
	$J_G(kg.m^2)$	0.089
	ν	6.25
	$K(N.m/deg)$	1435
	$D(N.m.s)$	0.015
Grid-Side Control	$L_f(pu)$	0.0015
	$V^*_{DC}(V)$	1200
	V_{DC} regulator parameter	Kp=5,Ki=0.1;
	Current regulator parameters	Kp=100,Ki=1;

Appendix B

Three-phase transformations

In electric machinery studies, the mathematical transformation of three-phase machine are often used to decouple variables, refer all the variables to a common reference frame or simplify the analysis. In this appendix are presented useful transformations that were used in this work.

B.0.1 Clarke's transform

Three-phase electric machines can be simplified to an equivalent two phase machine, when the two-phase variables are refereed to stationary reference frame denoted as "α, β" plane the transformation is known as Clarke's transform [67]:

$$\begin{bmatrix} f_\alpha \\ f_\beta \end{bmatrix} = \overbrace{\begin{bmatrix} 1 & -\frac{1}{2} & -\frac{1}{2} \\ 0 & \frac{\sqrt{3}}{2} & \frac{\sqrt{3}}{2} \end{bmatrix}}^{[T_{\alpha\beta}]} \begin{bmatrix} f_a \\ f_b \\ f_c \end{bmatrix} \tag{B.1}$$

The inverse transformation is:

$$\begin{bmatrix} f_a \\ f_b \\ f_c \end{bmatrix} = \overbrace{\begin{bmatrix} 1 & 0 \\ -\frac{1}{2} & \frac{\sqrt{3}}{2} \\ -\frac{1}{2} & -\frac{\sqrt{3}}{2} \end{bmatrix}}^{[T_{\alpha\beta}]^{-1}} \begin{bmatrix} f_\alpha \\ f_\beta \end{bmatrix} \tag{B.2}$$

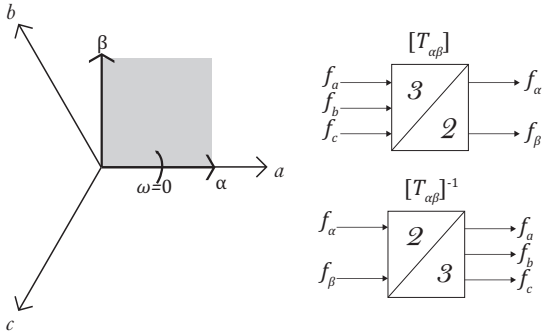

FIGURE B.1: Clarke transform orientation and diagram

B.0.2 Park's transform

When the equivalent two phase system is oriented in a desired direction it is called Park's transform. Park's transform can be obtained by multiplying the Clark's transform by $e^{j\theta_d}$ where θ_d is the angle of orientation and j is the complex variable. For rotating reference frames usually the axis are denoted as direct "d" and quadrature "q" [67]:

$$\begin{bmatrix} f_d \\ f_q \end{bmatrix} = \overbrace{\begin{bmatrix} \cos\theta_d & \sin\theta_d \\ -\sin\theta_d & \cos\theta_d \end{bmatrix} \frac{2}{3} \begin{bmatrix} 1 & -1/2 & -1/2 \\ 0 & \sqrt{3}/2 & -\sqrt{3}/2 \end{bmatrix}}^{[T_{dq}]} \begin{bmatrix} f_a \\ f_b \\ f_c \end{bmatrix} \tag{B.3}$$

The transform can be further simplified [67]:

$$[T_{dq}] = \frac{2}{3} \begin{bmatrix} \cos\theta_d & \cos\left(\theta_d - \frac{2\pi}{3}\right) & \cos\left(\theta_d + \frac{2\pi}{3}\right) \\ -\sin\theta_d & -\sin\left(\theta_d - \frac{2\pi}{3}\right) & -\sin\left(\theta_d + \frac{2\pi}{3}\right) \end{bmatrix} \tag{B.4}$$

With the inverse operation:

$$\begin{bmatrix} f_a \\ f_b \\ f_c \end{bmatrix} = \overbrace{\begin{bmatrix} \cos\theta_d & -\sin\theta_d \\ \cos\left(\theta_d - \frac{2\pi}{3}\right) & -\sin\left(\theta_d - \frac{2\pi}{3}\right) \\ \cos\left(\theta_d + \frac{2\pi}{3}\right) & -\sin\left(\theta_d + \frac{2\pi}{3}\right) \end{bmatrix}}^{[T_{dq}]^{-1}} \begin{bmatrix} f_d \\ f_q \end{bmatrix} \tag{B.5}$$

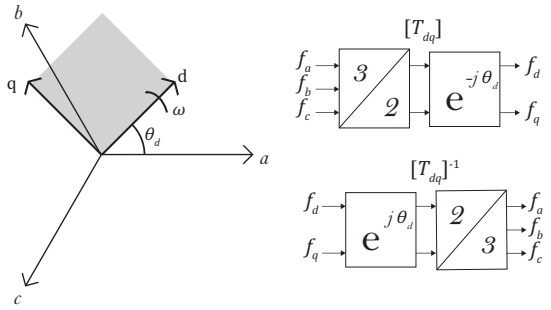

FIGURE B.2: Parke transform orientation and diagram

B.0.3 Fortescue's transformation

Also known as symmetrical components, it is a method used to simplify the analysis of unbalanced three-phase systems, representing them as a sum of three balanced systems, one of positive sequence, other of negative sequence and a non-rotating element known as zero sequence.

$$\begin{bmatrix} f_0 \\ f_1 \\ f_2 \end{bmatrix} = \overbrace{\frac{1}{3} \begin{bmatrix} 1 & 1 & 1 \\ 1 & a & a^2 \\ 1 & a^2 & a \end{bmatrix}}^{[T_{012}]} \begin{bmatrix} f_a \\ f_b \\ f_c \end{bmatrix} \tag{B.6}$$

where a is a complex number of unitary magnitude and angle equal to 120 degrees ($a = e^{j\frac{2\pi}{3}}$). The transform inverse is:

$$\begin{bmatrix} f_a \\ f_b \\ f_c \end{bmatrix} = \overbrace{\begin{bmatrix} 1 & 1 & 1 \\ 1 & a^2 & a \\ 1 & a & a^2 \end{bmatrix}}^{[T_{012}]^-1} \begin{bmatrix} f_0 \\ f_1 \\ f_2 \end{bmatrix} \tag{B.7}$$

Bibliography

[1] C. V. Hernández, T. Telsnig, and A. V. Pradas, "JRC wind energy status report 2016 edition", 2017.

[2] GWEC, "Global wind report 2016", *Brussels, Belgium*, 2017.

[3] PRODESEN, *Programa de desarrollo del sistema eléctrico nacional 2016-2030*, 2016.

[4] *Inventario Nacional de Energías Renovables*, http://dgel.energia.gob.mx/inere/, Accessed: 2017-08-30.

[5] Cámara de diputados, *Ley de transición energética*, 2015.

[6] Secretaría de Energía, *Programa especial para el aprovechamiento de energías renovables*, 2014.

[7] J. C. Miranda, *Aumentó 43% subsidio a tarifas eléctricas: CFE*, [Online; posted 01-February-2017], 2017. [Online]. Available: http://www.jornada.unam.mx/ultimas/2017/02/01/aumento-43-subsidio-a-tarifas-electricas-cfe.

[8] E. Pérez-Denicia, F. Fernández-Luqueño, D. Vilariño-Ayala, L. M. Montaño-Zetina, and L. A. Maldonado-López, "Renewable energy sources for electricity generation in Mexico: A review", *Renewable and Sustainable Energy Reviews*, vol. 78, pp. 597–613, 2017.

[9] M. Mohseni and S. M. Islam, "Review of international grid codes for wind power integration: Diversity, technology and a case for global standard", *Renewable and Sustainable Energy Reviews*, vol. 16, no. 6, pp. 3876–3890, 2012.

[10] M. Benbouzid, S. Muyeen, and F. Khoucha, "An up-to-date review of low-voltage ride-through techniques for doubly-fed induction generator-based wind turbines", *International Journal on Energy Conversion*, vol. 3, no. 1, pp. 1–9, 2015.

[11] J. L. Sawin *et al.*, "Renewables 2017-global status report", Tech. Rep., 2017.

[12] T. Burton, N. Jenkins, D. Sharpe, and E. Bossanyi, *Wind energy handbook*. John Wiley & Sons, 2011.

[13] S. Tohidi and M.-i. Behnam, "A comprehensive review of low voltage ride through of doubly fed induction wind generators", *Renewable and Sustainable Energy Reviews*, vol. 57, pp. 412–419, 2016.

[14] J. Morren and S. W. De Haan, "Ridethrough of wind turbines with doubly-fed induction generator during a voltage dip", *IEEE Transactions on energy conversion*, vol. 20, no. 2, pp. 435–441, 2005.

[15] L. Xu and Y. Wang, "Dynamic modeling and control of DFIG-based wind turbines under unbalanced network conditions", *IEEE Transactions on Power Systems*, vol. 22, no. 1, pp. 314–323, 2007.

[16] J. Lopez, P. Sanchis, X. Roboam, and L. Marroyo, "Dynamic behavior of the doubly fed induction generator during three-phase voltage dips", *IEEE Transactions on Energy conversion*, vol. 22, no. 3, pp. 709–717, 2007.

[17] R. Cárdenas, R. Peña, S. Alepus, and G. Asher, "Overview of control systems for the operation of DFIGs in wind energy applications", *IEEE Transactions on Industrial Electronics*, vol. 60, no. 7, pp. 2776–2798, 2013.

[18] J. Hu, Y. He, L. Xu, and B. W. Williams, "Improved control of DFIG systems during network unbalance using PI–R current regulators", *IEEE Transactions on Industrial Electronics*, vol. 56, no. 2, pp. 439–451, 2009.

[19] Y. Shtessel, C. Edwards, L. Fridman, and A. Levant, *Sliding mode control and observation*. Springer, 2014, vol. 10.

[20] Y Djeriri, A Meroufel, A Massoum, and Z Boudjema, "A comparative study between field oriented control strategy and direct power control strategy for DFIG", *Journal of Electrical Engineering*, vol. 14, no. 2, pp. 159–167, 2014.

[21] T. Noguchi and I. Takahashi, "Quick torque response control of an induction motor based on a new concept", in *IEEJ Tech. Meeting Rotating Mach*, 1984, pp. 61–70.

[22] I. Takahashi and T. Noguchi, "A new quick-response and high-efficiency control strategy of an induction motor", *IEEE Transactions on Industry applications*, no. 5, pp. 820–827, 1986.

[23] M Depenbrock, "Direct self control for high dynamics performance of inverter feed ac machines", *ETZ Arch*, vol. 7, no. 7, pp. 211–218, 1985.

[24] T. Noguchi, H. Tomiki, S. Kondo, and I. Takahashi, "Direct power control of PWM converter without power-source voltage sensors", *IEEE Transactions on Industry Applications*, vol. 34, no. 3, pp. 473–479, 1998.

[25] L. Xu and P. Cartwright, "Direct active and reactive power control of DFIG for wind energy generation", *IEEE Transactions on energy conversion*, vol. 21, no. 3, pp. 750–758, 2006.

[26] G. Abad, J. Lopez, M. Rodríguez, L. Marroyo, and G. Iwanski, *Doubly fed induction machine: modeling and control for wind energy generation*. John Wiley & Sons, 2011, vol. 85.

[27] Y. Zhou, P. Bauer, J. A. Ferreira, and J. Pierik, "Operation of grid-connected dfig under unbalanced grid voltage condition", *IEEE Transactions on Energy Conversion*, vol. 24, no. 1, pp. 240–246, 2009.

[28] O. Gomis-Bellmunt, A. Junyent-Ferre, A. Sumper, and J. Bergas-Jane, "Ride-through control of a doubly fed induction generator under unbalanced voltage sags", *IEEE Transactions on Energy Conversion*, vol. 23, no. 4, pp. 1036–1045, 2008.

[29] L. Xu, "Coordinated control of DFIG's rotor and grid side converters during network unbalance", *IEEE Transactions on Power Electronics*, vol. 23, no. 3, pp. 1041–1049, 2008.

[30] L. Trilla, O. Gomis-Bellmunt, A. Junyent-Ferre, M. Mata, J. S. Navarro, and A. Sudria-Andreu, "Modeling and validation of DFIG 3-MW wind turbine using field test data of balanced and unbalanced voltage sags", *IEEE Transactions on sustainable energy*, vol. 2, no. 4, pp. 509–519, 2011.

[31] Y. Wang, L Xu, and B. Williams, "Compensation of network voltage unbalance using doubly fed induction generator-based wind farms", *IET Renewable Power Generation*, vol. 3, no. 1, pp. 12–22, 2009.

[32] H. Nian, Y. Song, P. Zhou, and Y. He, "Improved direct power control of a wind turbine driven doubly fed induction generator during transient grid voltage unbalance", *IEEE Transactions on Energy Conversion*, vol. 26, no. 3, pp. 976–986, 2011.

[33] S. Alepuz, S. Busquets-Monge, J. Bordonau, J. A. Martinez-Velasco, C. A. Silva, J. Pontt, and J. Rodriguez, "Control strategies based on symmetrical components for grid-connected converters under voltage dips", *IEEE Transactions on Industrial Electronics*, vol. 56, no. 6, pp. 2162–2173, Jun. 2009, ISSN: 0278-0046. DOI: 10.1109/TIE.2009.2017102.

[34] M. J. Hossain, T. K. Saha, N. Mithulananthan, and H. R. Pota, "Control strategies for augmenting LVRT capability of DFIGs in interconnected power systems", *IEEE Transactions on Industrial Electronics*, vol. 60, no. 6, pp. 2510–2522, Jun. 2013, ISSN: 0278-0046. DOI: 10.1109/TIE.2012.2228141.

[35] H. Xu, J. Hu, and Y. He, "Integrated modeling and enhanced control of DFIG under unbalanced and distorted grid voltage conditions", *IEEE Transactions on Energy Conversion*, vol. 27, no. 3, pp. 725–736, Sep. 2012, ISSN: 0885-8969. DOI: 10.1109/TEC.2012.2199495.

[36] D. Campos-Gaona, E. L. Moreno-Goytia, and O. Anaya-Lara, "Fault Ride-Through Improvement of DFIG-WT by Integrating a Two-Degrees-of-Freedom Internal Model Control", *IEEE Transactions on Industrial Electronics*, vol. 60, no. 3, pp. 1133–1145, Mar. 2013, ISSN: 0278-0046. DOI: 10.1109/TIE.2012.2216234.

[37] N. Amuthan, "Direct model reference adaptive internal model controller for DFIG wind farms with dither injection", in *2009 International Conference on Power Systems*, Dec. 2009, pp. 1–6. DOI: 10.1109/ICPWS.2009.5442663.

[38] S. Q. Bu, W. Du, H. F. Wang, and S. Gao, "Power angle control of grid-connected doubly fed induction generator wind turbines for fault ride-through", *IET Renewable Power Generation*, vol. 7, no. 1, pp. 18–27, Feb. 2013, ISSN: 1752-1416. DOI: 10.1049/iet-rpg.2012.0130.

[39] S. Xiao, G. Yang, H. Zhou, and H. Geng, "An LVRT control strategy based on flux linkage tracking for DFIG-based WECS", *IEEE Transactions on Industrial Electronics*, vol. 60, no. 7, pp. 2820–2832, Jul. 2013, ISSN: 0278-0046. DOI: 10.1109/TIE.2012.2205354.

[40] G Abad, M. Rodriguez, J Poza, and J. Canales, "Direct torque control for doubly fed induction machine-based wind turbines under voltage dips and without crowbar protection", *IEEE Transactions on Energy Conversion*, vol. 25, no. 2, pp. 586–588, 2010.

[41] G. Abad, M. A. Rodriguez, G. Iwanski, and J. Poza, "Direct power control of doubly-fed-induction-generator-based wind turbines under unbalanced grid voltage", *IEEE Transactions on Power Electronics*, vol. 25, no. 2, pp. 442–452, 2010.

[42] D. Santos-Martin, J. L. Rodriguez-Amenedo, and S. Arnalte, "Direct power control applied to doubly fed induction generator under unbalanced grid voltage conditions", *IEEE Transactions on Power Electronics*, vol. 23, no. 5, pp. 2328–2336, 2008.

[43] D. Santos-Martin, J. L. Rodriguez-Amenedo, and S. Arnaltes, "Providing ride-through capability to a doubly fed induction generator under unbalanced voltage dips", *IEEE Transactions on Power Electronics*, vol. 24, no. 7, pp. 1747–1757, 2009.

[44] M. Benbouzid, B. Beltran, Y. Amirat, G. Yao, J. Han, and H. Mangel, "Second-order sliding mode control for DFIG-based wind turbines fault ride-through capability enhancement", *ISA transactions*, vol. 53, no. 3, pp. 827–833, 2014.

[45] B. Beltran, T. Ahmed-Ali, and M. E. H. Benbouzid, "Sliding mode power control of variable-speed wind energy conversion systems", *IEEE Transactions on Energy Conversion*, vol. 23, no. 2, pp. 551–558, 2008, ISSN: 0885-8969.

[46] B. Beltran, M. Benbouzid, and T. Ahmed-Ali, "High-order sliding mode control of a DFIG-based wind turbine for power maximization and grid fault tolerance", in *Electric Machines and Drives Conference, 2009. IEMDC'09. IEEE International*, IEEE, 2009, pp. 183–189.

[47] M. I. Martinez, G. Tapia, A. Susperregui, and H. Camblong, "Sliding-mode control for DFIG rotor-and grid-side converters under unbalanced and harmonically distorted grid voltage", *IEEE Transactions on Energy Conversion*, vol. 27, no. 2, pp. 328–339, 2012.

[48] M. Martinez, A. Susperregui, G. Tapia, and L. Xu, "Sliding-mode control of a wind turbine-driven double-fed induction generator under non-ideal grid voltages", *IET Renewable Power Generation*, vol. 7, no. 4, pp. 370–379, 2013.

[49] T. Sun, Z. Chen, and F. Blaabjerg, "Transient stability of DFIG wind turbines at an external short-circuit fault", en, *Wind Energy*, vol. 8, no. 3, pp. 345–360, Jul. 2005, ISSN: 1099-1824. DOI: 10.1002/we.164. [Online]. Available: http://onlinelibrary.wiley.com/doi/10.1002/we.164/abstract.

[50] T. Brekken, N. Mohan, and T. Undeland, "Control of a doubly-fed induction wind generator under unbalanced grid voltage conditions", in *Power Electronics and Applications, 2005 European Conference on*, IEEE, 2005, 10–pp.

[51] M. Rahimi and M. Parniani, "Grid-fault ride-through analysis and control of wind turbines with doubly fed induction generators", *Electric Power Systems Research*, vol. 80, no. 2, pp. 184–195, Feb. 2010, ISSN: 0378-7796. DOI: 10.1016/j.epsr.2009.08.019. [Online]. Available: http://www.sciencedirect.com/science/article/pii/S037877960900203X.

[52] T. D. Vrionis, X. I. Koutiva, and N. A. Vovos, "A genetic algorithm-based low voltage ride-through control strategy for grid connected doubly fed induction wind generators", *IEEE Transactions on Power Systems*, vol. 29, no. 3, pp. 1325–1334, 2014.

[53] M. Mohseni, M. A. S. Masoum, and S. M. Islam, "Low and high voltage ride-through of DFIG wind turbines using hybrid current controlled converters", *Electric Power Systems Research*, vol. 81, no. 7, pp. 1456–1465, Jul. 2011, ISSN: 0378-7796. DOI: 10.1016/j.epsr.2011.02.010. [Online]. Available: http://www.sciencedirect.com/science/article/pii/S0378779611000538.

[54] "Transient control of DFIG-based wind power plants in compliance with the australian grid code",

[55] V. F. Mendes, C. V. de Sousa, S. R. Silva, B. C. Rabelo Jr, and W. Hofmann, "Modeling and ride-through control of doubly fed induction generators during symmetrical voltage sags", *IEEE Transactions on energy conversion*, vol. 26, no. 4, pp. 1161–1171, 2011.

[56] J. López, E. Gubía, E. Olea, J. Ruiz, and L. Marroyo, "Ride through of wind turbines with doubly fed induction generator under symmetrical voltage dips", *IEEE Transactions on Industrial Electronics*, vol. 56, no. 10, pp. 4246–4254, 2009.

[57] D. Xiang, L. Ran, P. J. Tavner, and S. Yang, "Control of a doubly fed induction generator in a wind turbine during grid fault ride-through", *IEEE Transactions on Energy Conversion*, vol. 21, no. 3, pp. 652–662, 2006.

[58] J. López, P. Sanchis, E. Gubía, A. Ursúa, L. Marroyo, and X. Roboam, "Control of doubly fed induction generator under symmetrical voltage dips", in *Industrial Electronics, 2008. ISIE 2008. IEEE International Symposium on*, IEEE, 2008, pp. 2456–2462.

[59] S. Hu, X. Lin, Y. Kang, and X. Zou, "An improved low-voltage ride-through control strategy of doubly fed induction generator during grid faults", *IEEE transactions on power electronics*, vol. 26, no. 12, pp. 3653–3665, 2011.

[60] Z. Sorchini and P. T. Krein, "Formal derivation of direct torque control for induction machines", *IEEE transactions on Power Electronics*, vol. 21, no. 5, pp. 1428–1436, 2006.

[61] V. Utkin, J. Guldner, and J. Shi, *Sliding mode control in electro-mechanical systems*. CRC press, 2009, vol. 34.

[62] K. Bergey, "The Lanchester-Betz limit", *Journal of Energy*, vol. 3, pp. 382–384, 1979.

[63] I. E. Commission *et al.*, *Iec 61400-1: Wind turbines part 1: Design requirements*, 2005.

[64] G. L. Johnson, *Wind energy systems*. Prentice-Hall Englewood Cliffs (NJ), 1985.

[65] Z. Lubosny and Z Lubosny, *Wind turbine operation in electric power systems: advanced modeling*. Springer Berlin, 2003.

[66] I. Munteanu, A. I. Bratcu, N Cutululis, and E Ceanga, *Optimal control of wind energy systems: towards a global approach*. Springer, 2008.

[67] C.-M. Ong, *Dynamic simulation of electric machinery using Matlab/Simulink*. Prentice-Hall PTR, 1998.

[68] R. G. De Almeida and J. P. Lopes, "Participation of doubly fed induction wind generators in system frequency regulation", *IEEE transactions on power systems*, vol. 22, no. 3, pp. 944–950, 2007.

[69] M. Kayikçi and J. V. Milanovic, "Dynamic contribution of dfig-based wind plants to system frequency disturbances", *IEEE Transactions on Power Systems*, vol. 24, no. 2, pp. 859–867, 2009.

[70] I. D. Margaris, S. A. Papathanassiou, N. D. Hatziargyriou, A. D. Hansen, and P. Sorensen, "Frequency control in autonomous power systems with high wind power penetration", *IEEE Transactions on Sustainable Energy*, vol. 3, no. 2, pp. 189–199, 2012.

[71] X.-j. Yao, L. Tian, Z.-x. Xing, and X.-b. Su, "Dynamic model and simulation of doubly feed induction generator wind turbine", in *Automation and Logistics, 2009. ICAL'09. IEEE International Conference on*, IEEE, 2009, pp. 1667–1671.

[72] W. Qiao, "Dynamic modeling and control of doubly fed induction generators driven by wind turbines", in *Power Systems Conference and Exposition, 2009. PSCE'09. IEEE/PES*, IEEE, 2009, pp. 1–8.

[73] J. Lopez, E. Gubia, P. Sanchis, X. Roboam, and L. Marroyo, "Wind turbines based on doubly fed induction generator under asymmetrical voltage dips", *IEEE Transactions on Energy Conversion*, vol. 23, no. 1, pp. 321–330, 2008.

[74] K. Hansen and G. Larsen, *Database of Wind Characteristics*, http://winddata.com/, [Online; accessed January-2016].